Étude de l'interface sang-vaisseaux : rôles cellulaires des facteurs de la coagulation et implication de l'immunothrombose, du glycocalyx et des globules rouges.

Jeremy Lagrange

École Doctorale BioSE (Biologie, Santé, Environnement)

Laboratoire UMR_S1116 (DCAC)

Mémoire

Présenté pour la candidature au diplôme

D'HABILITATION À DIRIGER DES RECHERCHES

par

Jérémy LAGRANGE

Le 25 novembre 2021

Étude de l'interface sang-vaisseaux : rôles cellulaires des facteurs de la coagulation et implication de l'immunothrombose, du glycocalyx et des globules rouges.

(Discipline CNU 65)

Membres du jury :

Jean-François Arnal (DR INSERM)	**Rapporteur**
Marie-Luce Bochaton-Piallat (Pr.)	**Rapporteur**
Florence Pinet (DR INSERM)	**Rapporteur**
Patrick Lacolley (DR INSERM)	**Examinateur**
Jean-Baptiste Michel (DR INSERM)	**Examinateur**
Michel Neunlist (DR INSERM)	**Examinateur**
Laurent Peyrin-Biroulet (PU-PH)	**Examinateur**
Véronique Regnault (DR INSERM)	**Examinateur**
Luc Hittinger (PU-PH)	**Invité**

Table des matières

Liste des abréviations 4

Liste des figures 6

I. Curriculum vitae synthétique. 7

II. Responsabilités administratives et activités enseignements. 8

A. Responsabilités administratives scientifiques. 8

B. Responsabilités pédagogiques. 8

III. Bilan des activités de recherche. 9

IV. Résumé des activités de recherche. 9

A. Doctorat. 9

B. Postdoctorat. 13

V. Encadrements. 18

VI. Publications et rayonnement scientifique. 20

A. Travaux originaux. 20

B. Revues et chapitres de livres. 21

C. Selection de présentations en congrès internationaux (sélection). 22

D. Communications affichées (sélection). 23

E. Liste des revues d'articles et de demandes de financements. 24

F. Contrats de recherche et financements. 25

G. Autres responsabilités. 26

VII. Projet de recherche : Étude de l'interface sang-vaisseaux : rôles cellulaires des facteurs de la coagulation et implication de l'immunothrombose, du glycocalyx et des globules rouges. 27

A. Introduction Générale. 27

B. Etat de l'art. 28

1. L'interface sang-vaisseaux : exemple des facteurs de la coagulation. 28

2. Implication des facteurs de la coagulation sur la fonction vasculaire. 30

3. Le rôle central de la thrombine dans le couplage sang-vaisseaux. 32

4. Conclusion sur les fonctions cellulaires des facteurs de coagulation. 34

C. Rôle du glycocalyx des cellules endothéliales et des cellules musculaires lisses dans l'interface sang-vaisseaux. 35

1. Glycocalyx endothélial et interface sang-vaisseaux. 35

2. Rôles du glycocalyx des cellules musculaires lisses vasculaires. 36

D. Altération de l'interface sang-vaisseaux : exemple de l'immunothrombose dans les maladies inflammatoires chronique de l'intestin. 37

1. Les MICI et le risque de thrombose. 37

2. Implication des plaquettes dans les MICI. 38

3. Les altérations de la coagulation dans les MICI. 39

4. Formation du caillot et altération de la fibrinolyse au cours des MICI. 41

5. Endothélium vasculaire. 42

E. Implication des globules rouges dans les MICI. 43

1. Les globules rouges dans les thromboses. 43

2. Les globules rouges dans les maladies inflammatoires chroniques de l'intestin 44

F. Rôles des globules rouges dans la dysfonction vasculaire et implications possibles dans l'immunothrombose. 45

***L'importance de l'interface sang-vaisseaux et des fonctions cellulaires des facteurs de la coagulation* 47**

***La dégradation du glycocalyx endothélial, première étape du déséquilibre de l'interface sang-vaisseaux.* 48**

G. Hypothèses générales de travail et objectifs. 50

I. Axes de recherche. 52

1. Axe de recherche 1 : Rôle des cellules circulantes dans l'immunothrombose au cours des MICI. 52

2. Axe de recherche 2 : Implication du VWF et de l'A2M dans l'immunothrombose et sa dérégulation au cours des MICI 53

3. Axe de recherche 3 : Altération du glycocalyx endothelial et répercutions sur l'interface sang-vaisseaux. 54

4. Axe de recherche 4 : Implication des globules rouges dans la dysfonction vasculaire. 55

Les avancées de ce projet pourront être applicables à d'autres maladies inflammatoires chroniques qui touchent au total un Français sur 10. 56

J. Activités de direction et collaborations. 56

VIII. References. 59

Liste des abréviations

ACE : Enzyme de conversion de l'angiotensine
AngI : Angiotenine I
Angiotensine II (AngII)
Ang 1-7 : Angiotensine (1-7)
AR : Récepteur beta-2-adrénergique
AT: Antithrombine
AT2R : Recepteur 2 de l'angiotensine
B2R : Récepteur 2 de la bradykinine
C1inh : C1-inhibiteur
CAT : *Calibrated automated thrombography*
CCM: chromatographie sur couche mince
CE : Cellule endothéliale
CMLV : Cellule musculaire lisse vasculaire
CTH: *Center for Thrombosis and Hemostasis*
DLS : Microrhéologie par diffusion dynamique de la lumière
DSS : Dextran sulfate de sodium
EGFR : Facteur de croissance de l'épithélium
EPCR : Récepteur endothélial de la protéine C
F : Facteur
FII : Prothrombine
FIIa : Thrombine
FAK : *Focal adhesion kinase*
FFC : Fédération française de cardiologie
FID : Détecteur à ionisation de flamme
F1+2 : Fragments 1+2 de la prothrombine
FT : Facteur tissulaire
GAG : Glycosaminoglycanes
GPx1 : Glutathion peroxydase 1
HK : Kininogène de haut poids moléculaire
HO-1: Heme oxygenase-1
IC : Insuffisance Cardiaque
IT: Immunothrombose
IDR : Indice de distribution des globules rouges
IL-6 : Interleukine 6
MICI : Maladies inflammatoires chroniques de l'intestin
MMP : Métalloprotéinase
MAC-1 : Antigène des macrophages
MC : Maladie de Crohn
MCP-1 (CCL2) : Monocyte chemoattractant protein 1
Mac-1 (intégrine $\alpha_M\beta_2$l) : Antigène macrophage-1
NETs : Pièges extracellulaires de neutrophiles
PAI-1, PAI-2 : Inhibiteurs de l'activateur du plasminogène
PAR : Récepteur activé par les protéases
PC : Protéine C
PDF : Produits de dégradation du fibrinogène
PPP : Plasma pauvre en plaquettes
PRP : Plasma Riche en Plaquettes

PS : Protéine S
P-VEL : Vésicules extracellulaires larges dérivées des plaquettes
RCH : Rectocolite hémorragique
RM : Récepteur minéralocorticoïde
SHR : Rat spontanément hypertendu
SOD1 : Superoxyde-dismutase-1
SPMs : Médiateurs lipidiques pro-résolutifs spécifiques
SRAA : Système rénine angiotensine aldostérone
STEMI : Infarctus du myocarde avec segment ST élevé
RvD2 : Résolvine D2
TAFI : Inhibiteur de la fibrinolyse activable par la thrombine
TAT: Complexes thrombine-antithrombine
TFPI : Inhibiteur de la voie du FT
TM : Thrombomoduline
t-PA : Activateur tissulaire de la plasmine
UL : Université de Lorraine
uPA : Urokinase
VEL : Vésicules extracellulaires larges
VOP : Vitesse de l'onde de pouls carotido-fémorale
VS : Vitesse de sédimentation
VWF : Facteur von Willebrand

Liste des figures

Figure 1. Modification de la capacité thrombotique des cellules musculaires lisses vasculaire chez le rat spontanément hypertendu (SHR). 10
Figure 2. Modifications vasculaires et de l'hémostase au cours du vieillissement chez le rat Zucker. 11
Figure 3. Implication du récepteur minéralocorticoïde (RM) dans la thrombose. 12
Figure 4. Exemple de courbes de génération de thrombine altérées chez les patients traitées avec des anti-FXa. 13
Figure 5. Implication du facteur XI dans le développement de l'inflammation vasculaire et de l'hypertension. 14
Figure 6. Schema de l'implication du facteur XI dans le developpement de l'inflammation vasculaire et de l'hypertension. 15
Figure 7. Modification de la réactivité vasculaire chez les souris déficiantes the HO-1 et infusée avec de l'angiotensine II. 16
Figure 8. Effet du VWF sur la prolifération des cellules musculaires lisses vasculaires (CMLVs)..... 17
Figure 9 Résumé du rôle du facteur von Willebrand (VWF) sur les cellules musculaires lisses vasculaires (CMLVs). 18
Figure 10. Vue générale des échanges entre les compartiments sanguin et parietal. 28
Figure 11. Vue Générale de la cascade de coagulation. 29
Figure 12 Implication des facteurs de la coagulation dans le développement de la dysfonction vasculaire. 31
Figure 13. Rôle des contraintes pulsatiles sur la synthèse de l'inhibiteur de la voie du facteur tissulaire (TFPI) par les cellules musculaires lisses vasculaires (CMLVs). 31
Figure 14. Effets cellulaires des facteurs de la coagulation via les récepteurs activés par les protéases (PARs). 33
Figure 15. Glycocalyx des cellules endothéliales en microscopie électronique. 35
Figure 16. Altération plaquettaire chez les patients atteints de MICI. 38
Figure 17. Modification de la fibrinolyse chez les patients atteints de MICI. 42
Figure 18. Implication des globules rouges dans la modification du temps de coagulation en sang total. 48
Figure 19. Modification de marqueurs liés à la nétose chez les patients atteints de MICI. 48
Figure 20. L'augmentation des concentrations circulantes de syndécane-1 indique une dégradation du glycocalyx endothélial..... 49
Figure 21. Implication du thrombus intraluminal dans les anevrysmes aortiques abdominaux (AAA). 49
Figure 22. Résumé des hypothèses de travail et axes de recherche. 50
Figure 23 Résumé de l'environnement de recherche et des collaborations 57

I. Curriculum vitae synthétique.

2021-	Chargé de recherche INSERM	UMR_S 1116
	Doctorat et Post-doctorats	
2010-2013	Doctorat Biologie-Santé. Titre: Changements hémostatiques du syndrome métabolique, de l'hypertension artérielle, et de l'insuffisance cardiaque : approches physiologique et physiopathologique	UMR_S 1116
2014-2019	Chercheur postdoctorant (Mobilité Allemagne)	Center for Thrombosis and Hemostasis Mainz
2019-2020	Chercheur postdoctorant (Retour France)	UMR_S 1116
	Production scientifique	
Articles	18 articles dont 9 en premier auteur et 2 en dernier auteur	IF<5 : 5 5<IF<15 : 10 IF>15 : 3
Revues et Chapitres de livres	6 revues 2 chapitres	
	Contrats de recherche	
Depuis 2018	7 contrats obtenus pour un total de 470 k€	
	Communications scientifique	
Invités	3	
Orales	15	
Posters	27	
	Activités de révisions	
Articles	23 depuis 2018	
Demandes de financements	4 depuis 2017	
	Enseignements	
2012	72h de TD/TP	Licence 1 (UL)
2020	1h de cours magistral	Master 2 (UL)
	Encadrements	
2012	C.Docq, co-encadrant V.Regnault	SIR
2014-2017	Y.Weihert, co-encadrant P.Wenzel	Doctorat
2019-	M.Bardin, co-encadrant M.Bäck (ACT 23/10/19)	Doctorat
2020	J.Martin	M2
2021	A.Thomas, co-encadrant S.Toupance	M1
2021-	V Dufrost, co-encadrant D. Wahl (ACT en cours)	Doctorat
2021-	M. Jahangiri, co-encadrant N.Mercier	Doctorat
	Autres	
2012-2013	Président/Fondateur de l'association des doctorants en biologie santé de l'UL	
2012-2013	Elu au conseil du pôle biologie/santé/médecine de l'UL	
2019-	Membre du comité d'éthique de Lorraine	
2021-	*Topic editor* pour *Journal of Clinical Medicine*	
Depuis 2013	6 prix et distinctions	

II. Responsabilités administratives et activités enseignements.

A. Responsabilités administratives scientifiques.

Lors de mon doctorat j'ai été élu pendant près de deux ans au conseil scientifique du pôle BMS (biologie/médecine/santé) de l'université de Lorraine postes.

J'ai également mis en place en 2012 l'association des doctorants en biologie de l'université de Lorraine. Cette association a regroupé plus de 50 membres dès la première année et continue de fonctionner encore actuellement. Elle a été organisée autour d'un bureau comprenant un président, un vice-président, un trésorier et un secrétaire mais également des membres actifs investi à différents niveaux. Les missions de cette association sont les suivantes :

- Organiser des évènements scientifiques comme par exemple des présentations des projets de thèse de doctorant des différentes écoles doctorales de l'‘université,
- Préparer les étudiants au concours de l'école doctorale,
- Rédiger un journal de l'association deux fois par an et distribué à la journée de rentrée et la journée annuelle de l'école doctorale,
- Contribuer à la journée scientifique et journée de rentrée de l'école doctorale,
- Constituer des dossiers de demande de financement d'évènements auprès de l'Université pour organiser quelques sorties (visites d'entreprises, week-end de randonnée).

Durant mon postdoctorat j'ai mis en place pendant 1 an les séminaires hebdomadaires du centre de recherche. Depuis mon retour en France en septembre 2019 j'ai intégré le Comité d'Ethique Lorrain en Matière d'Expérimentation Animale de Lorraine (CELMEA 66) (suppléant du Pr Thornton). Depuis début 2021 je suis topic editor pour le *journal of clinical medicine* ou mon rôle sera de proposer des sujets pour des numéros spéciaux et rechercher des éditeurs dédiés à ces sujets.

B. Responsabilités pédagogiques.

Durant mon doctorat j'ai effectué 72 h de vacations dans l'EU 2.05 de première année de licence sciences du vivant intitulé « plans d'organisations des invertébrés ». Chaque séance de 2 h était découpée en deux parties, la moitié en TD et l'autre en TP. La séance précédant l'examen final était organisée au musée aquarium de Nancy où les étudiants ont pu observer des spécimens vivants.

En janvier 2020 j'ai également participé à la Journée de la Recherche du Master du vivant ou j'ai présenté les laboratoires INSERM a des étudiants en licence et master de la faculté des sciences et technologies. En octobre 2020 j'ai réalisé 1h de cours magistrales pour le M2 « Recherches cardiovasculaires ». Le titre de ce cours était : Des nouveaux anticoagulants aux fonctions cellulaires des facteurs de la coagulation.

III. Bilan des activités de recherche.

Résumé du parcours.

Biologiste cellulaire et moléculaire de formation, mes activités de recherche ont commencé en Master 2 lors de mon arrivée au laboratoire UMR_S 1116 (Défaillance cardiovasculaire aiguë et chronique) à Nancy (Université de Lorraine) sous la direction de P Lacolley et V Regnault (2010). Le titre de mon projet de M2 était : Caractérisation de l'état prothrombotique et de la fonction endothéliale dans le syndrome métabolique. Le laboratoire de Nancy possède une notoriété internationale dans l'étude de l'insuffisance cardiaque (IC), du récepteur minéralocorticoïde, (RM), de l'hypertension, du vieillissement, de la rigidité artérielle (mécanotransduction) et des thrombophilies acquises (syndrome des anti-phospholipides), le tout avec des approches allant des modèles animaux aux cohortes. Mon sujet de thèse a porté sur l'étude des modifications de l'hémostase dans des modèles animaux de d'hypertension ou modifiés génétiquement (rat spontanément hypertendu SHR, rat Zucker obèse, souris surexprimant le RM au niveau endothélial) prédisposant au développement de l'IC.

J'ai ensuite réalisé mon postdoctorat en Allemagne entre juillet 2014 et aout 2019 dans l'équipe de recherche du Pr P Wenzel au centre de recherche sur la thrombose et l'hémostase (CTH) de la faculté de médecine de Mayence, l'un des 6 centres d'excellence de recherche en santé d'Allemagne. L'équipe dispose d'une solide expérience en immunologie et en biologie vasculaire notamment dans la biologie des monocytes. Ma thématique de recherche a porté sur l'étude du rôle de l'activation par les facteurs de la coagulation des monocytes dans l'inflammation vasculaire, sa résolution, et la thrombose.

Je suis revenu en France à l'UMR_S 1116 en septembre 2019 où j'ai poursuivi mon objectif d'étudier les rôles cellulaires des facteurs de la coagulation. J'ai plus particulièrement travaillé sur le rôle du facteur von Willebrand sur la prolifération des CMLVs qui a été publié dans *Cardiovascular Reseach* début 2021. Parallèlement j'ai mis en place un projet de recherche pour comprendre les causes de l'augmentation du risque de thrombose dans les maladies inflammatoire chronique de l'intestin. Ce projet a été proposé au concours de chargé de recherche INSERM.

IV. Résumé des activités de recherche.

A. Doctorat.

Les mécanismes vasculaires et de l'hémostase (autres que coronariens) sont généralement mis au second plan par les spécialistes de l'IC. L'unité est l'auteur de travaux reconnus sur le vieillissement et l'IC diastolique. Sur le versant de l'hémostase, nos études fondamentales et cliniques sur le RM endothélial et la génération de thrombine dans l'IC aiguë s'inscrivent dans une démarche translationnelle avec l'essai clinique COMMANDER (NEJM 2018[1]) étudiant les effets d'un anticoagulant oral direct.

Une originalité du travail du laboratoire est de s'intéresser aux mécanismes périphériques de l'IC ce qui constitue une approche « décalée » : le fait d'intégrer l'artère et la coagulation est inédit par rapport à l'approche traditionnelle « cardiocentrique ». Sur le plan clinique, nous avons montré que la mesure de la vitesse de l'onde de pouls carotido-

fémorale (VOP) reste un paramètre prédictif des anomalies des grosses artères chez le patient porteur d'une IC sévère à l'inverse de la pression pulsée (différentielle systole-diastolique) fortement dépendante de la fonction ventriculaire gauche (étude ancillaire d'EPHESUS, co-premier auteur, *Hypertension* 2014[1]).

Chez le rat SHR, porteur d'une hypertrophie cardiaque et vasculaire, nous avons observé une accélération de l'occlusion carotidienne *in vivo* dans un modèle d'application de chlorure de fer. Le mécanisme résultait d'une plus grande capacité des cellules musculaires lisses vasculaires (CMLVs) à servir de support cellulaire pour la génération de thrombine *via* une augmentation de l'exposition des phospholipides membranaires procoagulants **(Figure 1)** (co-premier auteur, *Arterioscler Thromb Vasc Biol* 2015. Le groupe de Nancy (V Regnault) en collaboration avec le groupe de Maastricht (HC Hemker) a été pionnier en France dans les années 2000 dans le développement du suivi complet de la concentration en thrombine active dans le plasma avec ou sans plaquettes. Cette technique a été adaptée pour ce travail aux modèles murins et aux CMLVs. Elle a depuis été élargie au sang total pour prendre en compte la contribution des globules rouges (GRs) et des cellules immunitaires dans les processus thrombotiques.

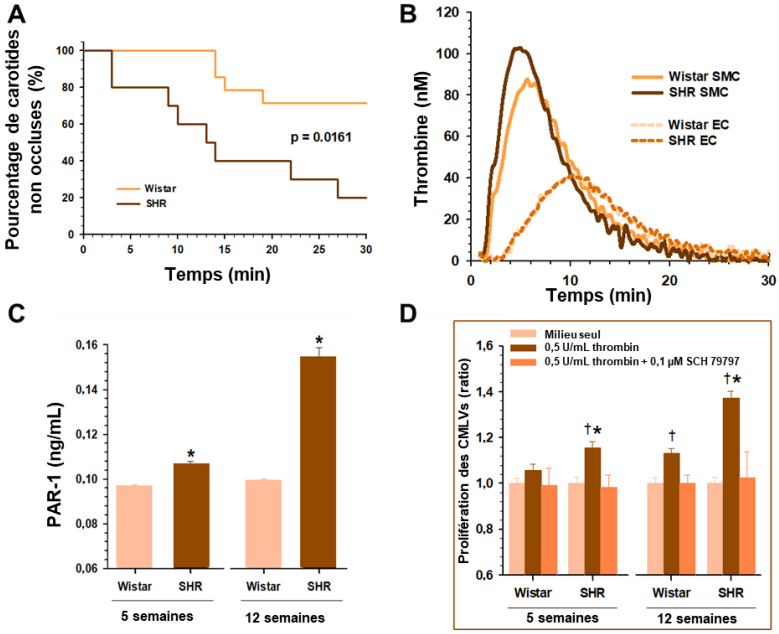

Figure 1. Modification de la capacité thrombotique des cellules musculaires lisses vasculaire chez le rat spontanément hypertendu (SHR).

*La vitesse d'occlusion de la carotide dans un modèle de thrombose au chlorure ferrique est augmentée chez le rat SHR (**A**). La génération de thrombine à la surface des CMLVs des rats SHR est plus importantes que chez les rats contrôles alors qu'elle est similaire à la surface des CEs (**B**). Le récepteur à la thrombine PAR-1 est augmenté chez le rat SHR ce qui participe à expliquer l'augmentation de génération de thrombine(**C**). De plus, l'inhibition de PAR-1 diminue la capacité proliférative des CMLVs (**D**). * p < 0,05 vs rats Wistar au même âge.*

Dans un modèle combinant une hypertension spontanée et une obésité (rat Zucker), nous avons montré pour la première fois une association entre une hypertension et un phénotype pro-thrombotique due à des anomalies conjointes des cellules endothéliales

(CEs) et des CMLVs indépendamment des plaquettes (premier auteur, *Front Physiol* 2017) **(Figure 2).** Ce travail a bénéficié d'une collaboration avec une entreprise privée Lorraine (SD innovation, Frouard) qui a mis à ma disposition des appareils d'évaluation plaquettaire à visée « recherche » que nous n'avions pas à l'époque au laboratoire et que j'ai utilisé dans plusieurs de mes travaux.

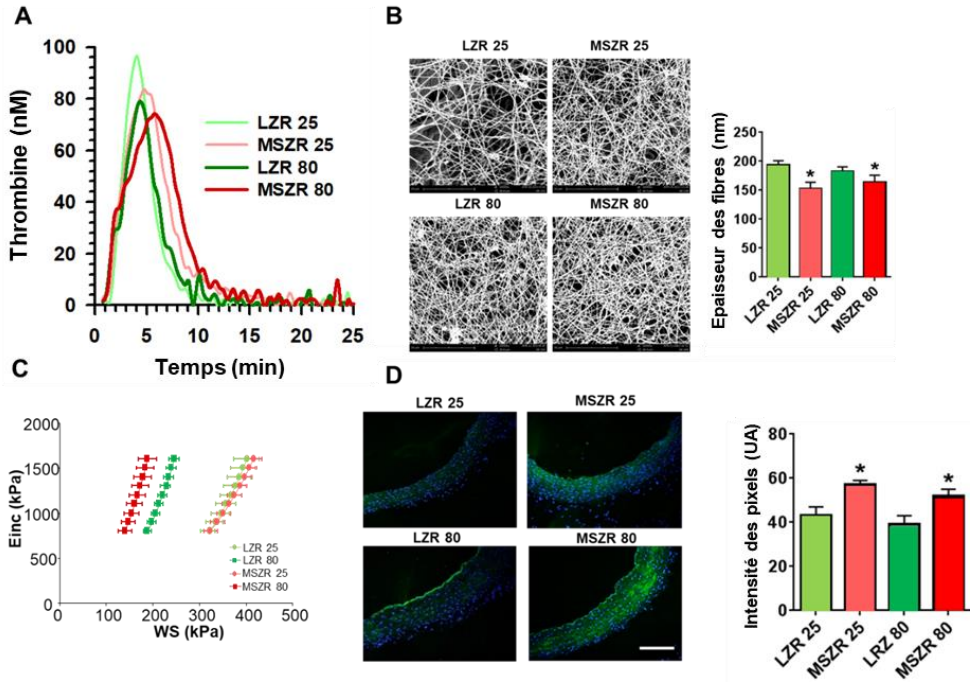

Figure 2. Modifications vasculaires et de l'hémostase au cours du vieillissement chez le rat Zucker.

*La génération de thrombine est augmentée dès l'âge adulte (25 semaines) chez le rat Zucker obèse et reste augmentée chez le rat âgé (80 semaines) (**A**). Le diamètre des fibres de fibrine est diminué chez les rats Zucker adultes obèses (MSZR) et âgés par rapport aux rats contrôles (LZR) ce qui indique une vitesse de formation du caillot augmentée (**B**). La rigidification des artères augmente uniquement avec le vieillissement chez les rats Zucker MSZR par rapport aux rats contrôles (**C**). L'activité des métalloprotéinases (MMPs) (activité gélatinolytique indiquant les MMP-2 et MMP-9) est augmentée dès l'âge adulte chez les rats Zucker par rapport aux rats contrôles et reste augmentée avec le vieillissement (**D**). * < 0,05 vs rats contrôles au même âge.*

A un niveau plus moléculaire et faisant suite aux travaux du laboratoire sur le RM dans l'IC, nous avons montré dans un modèle de souris surexprimant le RM au niveau endothélial, que de façon paradoxale ce récepteur jouait un rôle anticoagulant en situation physiologique mais délétère en présence d'une IC. Ce phénotype était expliqué par la capacité du RM à induire la synthèse du récepteur endothélial de la protéine C (EPCR) *via* le facteur de transcription SP1 (*specificity protein 1*). En participant à l'activation de la protéine C, l'EPCR stimule l'un des principaux systèmes anticoagulants vasculaires. (**Figure 3**). Cet effet protecteur n'existe pas dans des pathologies comme l'IC où la dysfonction endothéliale favorise le contact direct des facteurs de coagulation plasmatiques avec les CMLVs qui exercent ainsi un rôle procoagulant majeur (premier auteur, *FASEB J 2014*) [2].

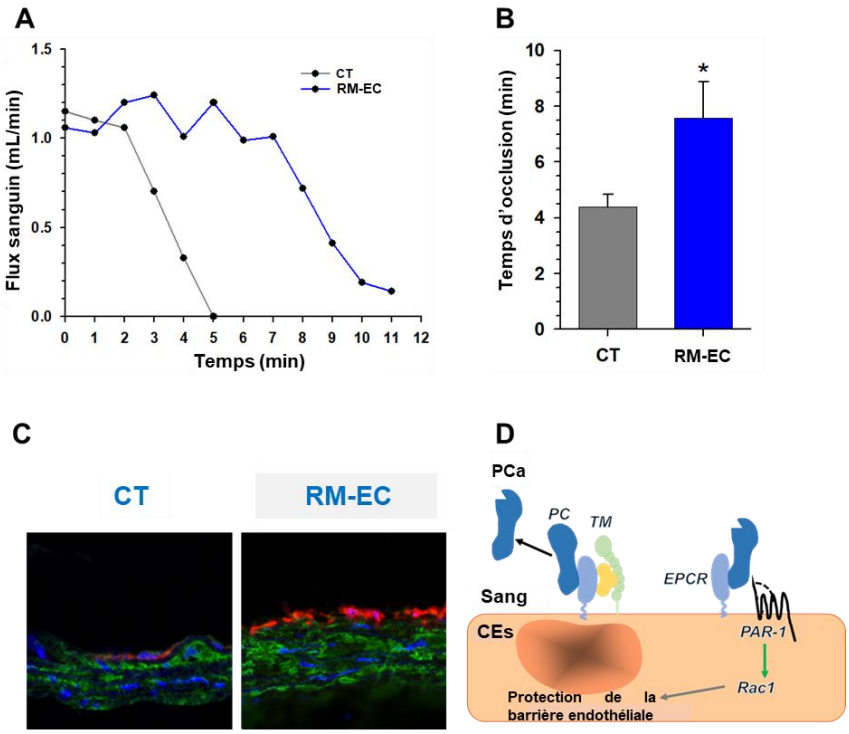

***Figure 3**. **Implication du récepteur minéralocorticoïde (RM) dans la thrombose.** Dans un modèle de thrombose chez la souris surexprimant le RM dans l'endothélium (RM-EC) le temps d'occlusion de la carotide est augmenté par rapport aux souris contrôles (CT) (**A, B**). L'activation du RM dans l'endothélium induit la synthèse du récepteur endothéliale à la proteine C (EPCR), en rouge (marquage de noyaux en bleu et autofluorescence des cartotides en vert) (**C**). L'augmentation de la synthèse d'EPCR limite la formation du caillot en inhibant la thrombine (**D**). * < 0,05 vs souris contrôles.*

En parallèle, ma thèse a comporté un travail de développement technique pour améliorer la pertinence du test de génération de thrombine *in vitro* par rapport aux tests cliniques qui n'explorent que partiellement la coagulation. Cette mesure est faite majoritairement en plasma avec ou sans plaquettes et dans le cas où elles sont présentes, elles ne sont pas dans un état « activé » et ne correspondent donc pas à leur phénotype observé en hémostase primaire. Pour pallier cette limitation majeure, j'ai imaginé un protocole qui a montré que les plaquettes agrégées modifiaient bien les paramètres cinétiques de la génération de thrombine en relarguant des microvésicules. Ce travail réalisé par une étudiante de médecine en stage d'initiation à la recherche (C Docq, 2013) que j'ai encadré s'est traduit par une publication (dernier auteur, *Platelets* 2018) [3] et une invitation personnelle à donner une présentation aux Hôpitaux Universitaires de Genève (6/11/2018).

J'ai publié un deuxième travail fondamental réalisé à Mayence sur les modifications des courbes de génération de thrombine en présence de plaquettes activées et de rivaroxaban (un inhibiteur du facteur X activé) chez des patients avec maladie thromboembolique veineuse (dernier auteur, *J Clin Med* 2019) [4]. Ce travail se poursuit pour évaluer plus précisément l'effet conjoint des anticoagulants oraux directs et des antiplaquettaires chez des patients issus de deux cohortes à Mayence (patients avec embolie pulmonaire (FOCUS) et patients avec thromboses veineuses profondes (VTEVAL). Le suivi des patients aura lieu pour encore 2 ans mais un premier article sur ce sujet a été publié à l'automne 2020 (***Figure 4***) (premier auteur *J Clin Med* 2020) [5].

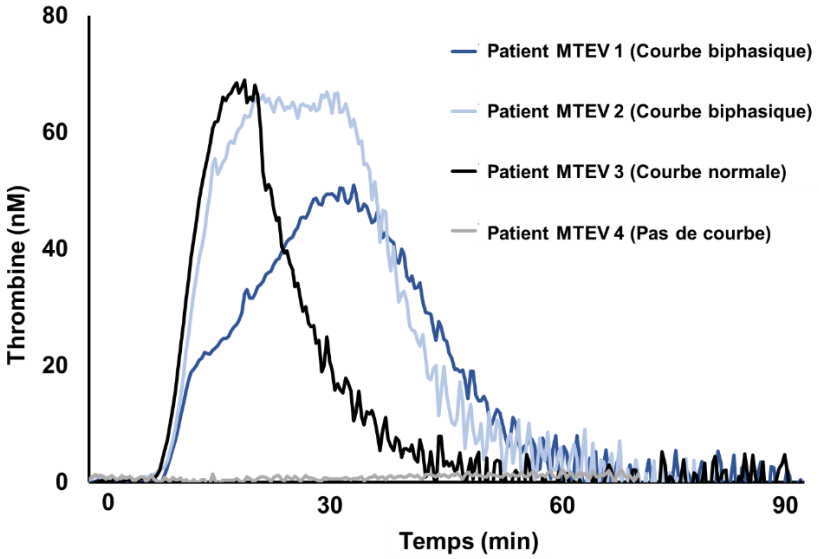

Figure 4. Exemple de courbes de génération de thrombine altérées chez les patients traitées avec des anti-FXa.

Les courbes de génération de thrombines ont habituellement une forme de courbe en cloche avec un maximum (pic) court (courbe 1). Ces courbes peuvent être altérées dans certaines conditions et à la suite de certains traitements (courbe 2-4). MTEV : Maladie thrombo-embolique veineuse

Au total, mes travaux de Master 2 et thèse m'ont permis de faire des avancées significatives dans l'axe novateur développé dans l'unité sur les interactions entre les facteurs de la coagulation et la rigidité artérielle. Les principaux résultats débouchant sur des perspectives cliniques encourageantes concernent les effets opposés du RM endothélial en physiologie (anticoagulant) et pathologie (procoagulant) et la contribution majeure des CMLVs dans le phénotype thrombotique associé à l'hypertension artérielle, à l'obésité, au vieillissement et à l'insuffisance cardiaque.

Le bilan est de 4 articles originaux en premier ou co-premier auteur (Hypertension 2014, FASEB J 2014, Arterioscler Thromb Vasc Biol 2015, et Front Physiol 2017) et un article en dernier auteur dans Platelets 2018 qui s'est accompagné d'une conférence invitée aux Hôpitaux Universitaires de Genève.

B. Postdoctorat.

Le postdoctorat a comporté 3 versants spécifiques dont le démarrage s'est étalé dans la durée du postdoctorat.

Versant 1 : A mon arrivée au centre, mon sujet d'étude portait sur l'implication des cellules LysM^{+}, en particulier les monocytes, dans le développement de l'hypertension. Le travail portait sur le rôle du facteur XI (FXI) dans le développement de l'hypertension artérielle *via* sa capacité à activer la thrombine, elle-même responsable de l'activation des plaquettes et monocytes selon une boucle d'auto-amplification dans un contexte inflammatoire conduisant à l'exacerbation de l'hypertension. Des souris invalidées pour le gène du FXI n'ont pas de modification de la relaxation endothélium-dépendante après traitement à l'angiotensine II (AngII) alors que des souris invalidées pour le FXII (activateur du facteur XI) perdent cette propriété de relaxation. La microscopie intravitale

montre que l'inhibition du FXI (à l'aide d'un oligonucléotide antisens) conjointe à un traitement par AngII diminue le roulement et l'adhésion des monocytes à l'endothélium. L'adhésion leucocytaire qui est régulée positivement par un circuit pro-inflammatoire impliquant facteur tissulaire (FT), thrombine et GPIbα plaquettaire est restaurée par l'injection d'un FXI recombinant (**Figure 5**). De plus, une des parties de ce projet a permis le recrutement d'une cohorte de patients hypertendus pour étudier la génération de thrombine en présence de plaquettes. Avec l'aide d'une doctorante en médecine que j'ai encadrée (Yvonne Weihert), nous avons recruté 71 patients pour la cohorte « *interaction of coagulation FACtors, Thrombocyes and leukOcytes in patients with aRterial hypeRtension study (FACTO-RR study, DRKS00011232*). Nous avons réalisé des tests de génération de thrombine dans plusieurs conditions : (i) avec et sans plaquettes, (ii) en inhibant l'activation du FXI dépendante de la la thrombine et (iii) en resuspendant les plaquettes dans du plasma contrôle. Nous avons montré que les variations de génération de thrombine en présence de plasma riche en plaquettes étaient dépendantes de l'activation du FXI par la thrombine **(co-premier auteur, *Science Trans Med 2017***). Les résultats de ces travaux sont résumés **figure 6**. La suite de ce projet est l'étude du rôle du facteur von Willebrand (VWF) (qui se lie à GPIbα) dans les interactions entre plaquettes, leucocytes et endothélium.

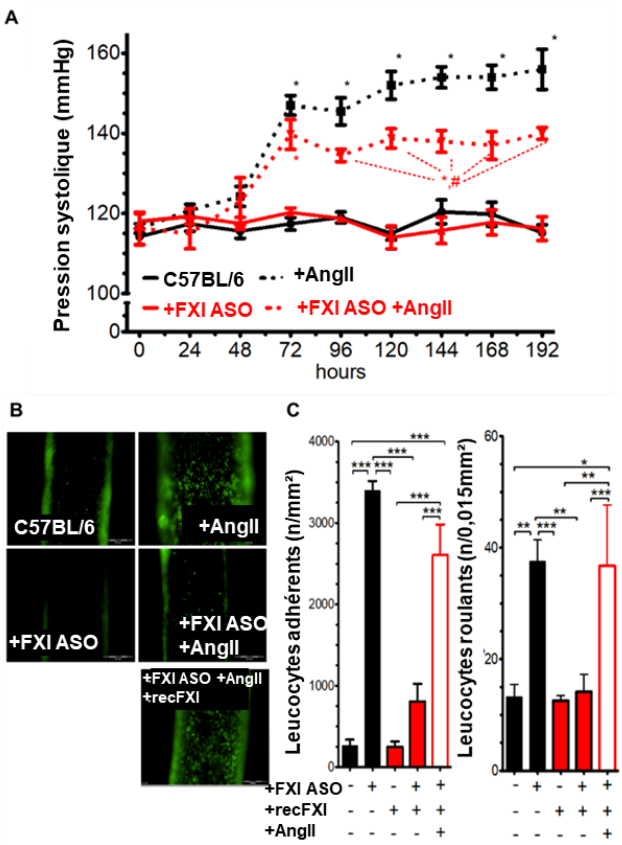

Figure 5. Implication du facteur XI dans le développement de l'inflammation vasculaire et de l'hypertension.

*L'augmentation de la pression artérielle consécutive à l'infusion d'angiotensine II (AngII) est limitée chez les souris traitées avec un oligonucléotide antisens (ASO) dirigé contre le FXI (**A**). L'inflammation et l'activation de la coagulation induite par l'AngII provoque le roulement et l'adhésion des cellules immunitaires à l'endothélium tandis que l'inhibition du FXI aboli l'activation des cellules immunitaires. L'injection de FXI recombinant (recFXI) restaure le roulement et l'adhésion des cellules immunitaires (**B-C**). * p < 0,05 ** p < 0,01 *** p < 0,001.*

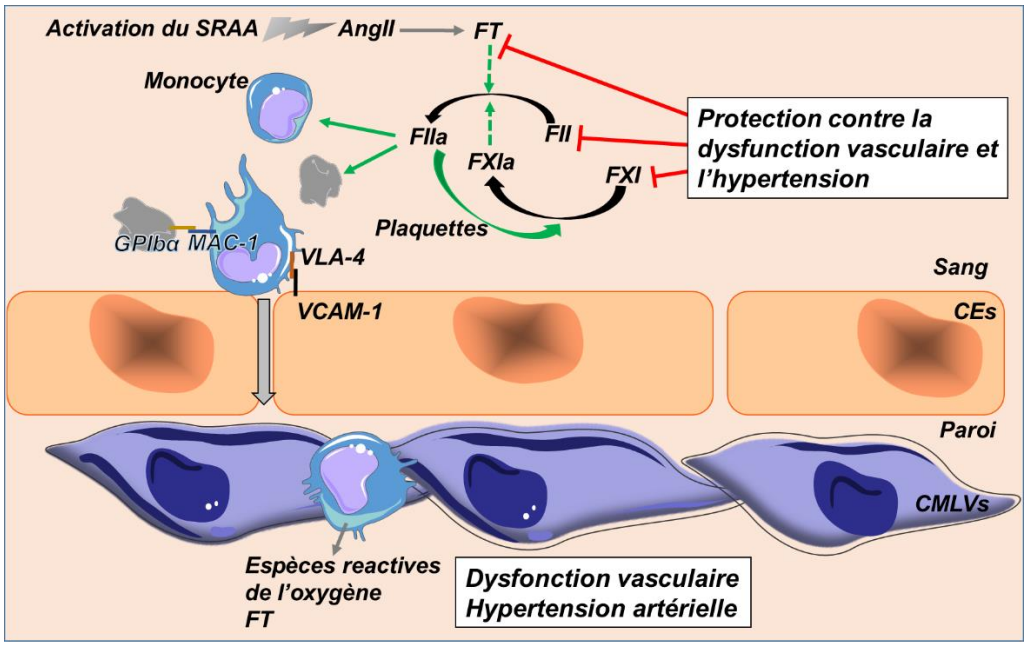

Figure 6. Schema de l'implication du facteur XI dans le developpement de l'inflammation vasculaire et de l'hypertension.

L'activation du système rénine angiotensine aldostérone (SRAA) augmente la synthèse d'angiotensine II (AngII) dont l'effet proinflammatoire augmente la synthèse de facteur tissulaire (FT). La stimulation de la voie extrinsèque et l'amplification de conversion de la prothrombine (FII) en thrombine (FIIa) par l'activation du facteur XI (FXIa) à la surface des plaquettes. Les plaquettes et les monocytes activés peuvent adhérer entre eux par l'intermédiaire de la glycoprotéine Ibα (GPIbα) et du macrophage antigen-1 (MAC-1) puis adhérer à l'endothélium à l'aide du very Late Antigen-4 ou intégrine α4β1 (VLA-4) et du vascular cell adhesion protein 1 (VCAM-1). La transmigration dans la paroi des monocytes activés permet leurs effets dans le développement de la dysfonction vasculaire. L'inhibition de l'amplification de la génération de thrombine via l'inhibition du FXI limite le développement de la dysfonction vasculaire. Les flèches noires courbées indiquent une conversion, les flèches vertes une activation, les flèches bleue, l'activation d'un récepteur, les bars en T une inhibition, et les flèches grises des effets pléiotropies. CEs : cellules endothéliales ; CMLVs: cellules musculaires lisses vasculaires.

Versant 2 : Mon objectif a porté sur les cellules LysM$^+$ mais dans un contexte de protection contre l'inflammation puisque l'heme oxygenase-1 (HO-1) des monocytes diminue le stress oxydatif induit par Nox2 et réduit la polarisation des monocytes vers un phénotype inflammatoire (**Eur Heart J)**.
Pour ce projet, j'ai obtenu un financement de 40 k€ (fonctionnement et financement d'un technicien) pour 'jeune investigateur' (Deutsche Stiftung für Herzforschung DSHF-F/24/18). Les financements sont détaillés pages 25-26.
J'ai étudié comment la modulation de l'HO-1 dans les cellules LysM$^+$ module le trafic des monocytes dans la paroi vasculaire **(Figure 7)**.

Ce travail est actuellement poursuivi par une doctorante ayant débuté sa thèse en novembre 2019 (je ne co-encadre pas cette doctorante mais l'aide sur le plan technique).

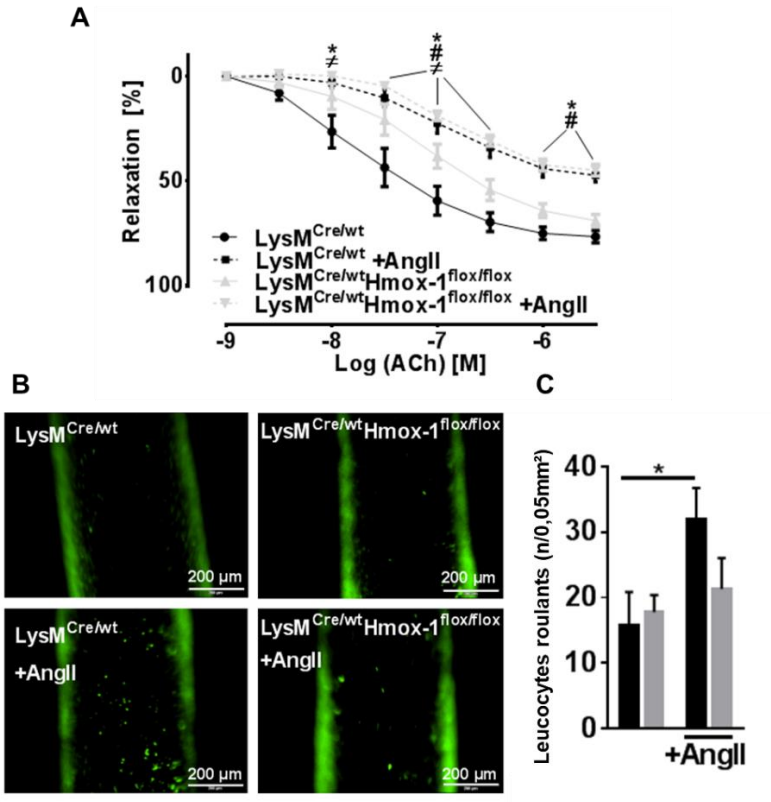

Figure 7. Modification de la réactivité vasculaire chez les souris déficiantes the HO-1 et infusées avec de l'angiotensine II.

Des souris spécifiquement déficientes pour l'hémoxygenase 1 dans les monocytes et les neutrophiles (LysM$^{cre/wt}$ Hmox-1$^{flox/flox}$) montrent une tendance à l'altération de leur relaxation vasculaire basale (A). Il n'y a en revanche pas de modification de la relaxation après un traitement à l'angiotensine II (AngII). Pourtant les leucocytes de souris déficientes en HO-1 roulent moins sur l'endothélium par rapport aux leucocytes de souris contrôles (B-C).

Versant 3 : L'objectif de cette partie visait à mieux comprendre la relation entre thrombose et inflammation. J'ai utilisé un modèle de souris surexprimant l'interleukine 6 (IL-6) dans les cellules LysM$^+$ de manière Cre spécifique. De manière inattendue les souris surexprimant l'IL-6 ne forment pas de thrombus dans un modèle de sténose de la veine cave. Un phénotypage complet des facteurs de la coagulation réalisé en collaboration avec H Spronk (Maastricht) n'a pas permis de mettre en évidence une modification significative d'un facteur en particulier. Cependant l'IL-6 augmente beaucoup la synthèse de l'alpha-2-macroglobuline (A2M) qui est un inhibiteur puissant de la thrombine. Parallèlement l'A2M provoque l'agglutination des GRs ayant pour effet de limiter le développement du thrombus. Ce travail constitue un pont entre mon postdoctorat et mon sujet de retour en France car l'IL-6 est la cytokine majoritairement augmentée dans les maladies inflammatoires chroniques de l'intestin (MICI). Ainsi avant la fin de mon postdoctorat j'ai obtenu des résultats préliminaires mettant en évidence une modification de l'hémostase provoquée par l'agglutination des GRs chez ces patients et récapitulant le phénotype observé chez les souris surexprimant l'IL-6. Ce sont des résultats forts dans la mesure où des variations inattendues et inexpliquées de l'A2M plasmatique sont décrites depuis plus de 40 ans dans certaines maladies inflammatoires sans que ni leur l'origine ni leurs répercussions sur l'hémostase ne soient comprises.

Parallèlement, j'ai obtenu un contrat de recherche du ministère de la recherche allemande de 50 k€ pour mettre en place une collaboration entre les laboratoires de Mayence et de Nancy sur le rôle du glycocalyx endothélial dans les modifications de la balance hémostatique pendant le vieillissement.

En résumé, les résultats sur le rôle direct du facteur XI dans l'inflammation vasculaire et l'hypertension viennent en appui des travaux cliniques utilisant une stratégie anti-sens pour inhiber le facteur XI. Le résumé de cette littérature sur le rôle du facteur XI et des autres facteurs de la coagulation dans la thromboinflammation et la dysfonction vasculaire a fait l'objet de 2 revues récentes sur lesquelles je suis premier et deuxième auteur. J'ai exploré les modifications du phénotype vasculaire dans un contexte inflammatoire via l'HO-1 des cellules LysM⁺ (soutenu par un contrat jeune chercheur). J'ai acquis durant ces années une capacité d'approche transversale d'une pathologie en intégrant le rôle primordial des cellules immunitaires en lien avec l'hémostase et leur retentissement sur la fonction vasculaire. J'ai démontré le rôle de l'IL-6 dans la thrombose via sa capacité à induire l'A2M qui inhibe la thrombine et promeut l'agglutination des GRs. Cette découverte nourrit notre hypothèse que le risque augmenté de thrombose au cours des MICI ne dépend pas des facteurs habituels de thrombose observés dans la population générale.
Mon postdoctorat au sein du centre CTH à Mayence a permis la publication de 8 articles dont 3 en premier auteur et un en dernier auteur, de 3 revues, l'invitation à des conférences et laboratoires internationaux et l'obtention de deux contrats de recherche.

Mon retour en France a eu lieu en septembre 2019 où j'ai été financé par un RHU (FIGHT-HF). J'ai travaillé sur le rôle du VWF dans la prolifération des CMLVs. Au plan moléculaire, nous avons montré que le domaine A2 du VWF induisait la prolifération des CMLVs par un mécanisme impliquant 2 récepteurs, LRP4 comme ligand du domaine A2 et l'intégrine $\alpha_v\beta_3$ pour la signalisation (co-premier auteur, *Cardiovasc Res 2021*) [6] (**Figure 8 et 9**). La prolifération des CMLVs induite par le VWF se traduit par un épaississement de l'intima dans un modèle de ligature carotidienne tandis que des souris invalidées pour le VWF ne présentent pas d'épaississement. Enfin, nous avons observé une colocalisation du VWF et des CMLVs dans des pathologies vasculaires liés au développement de l'athérosclérose.

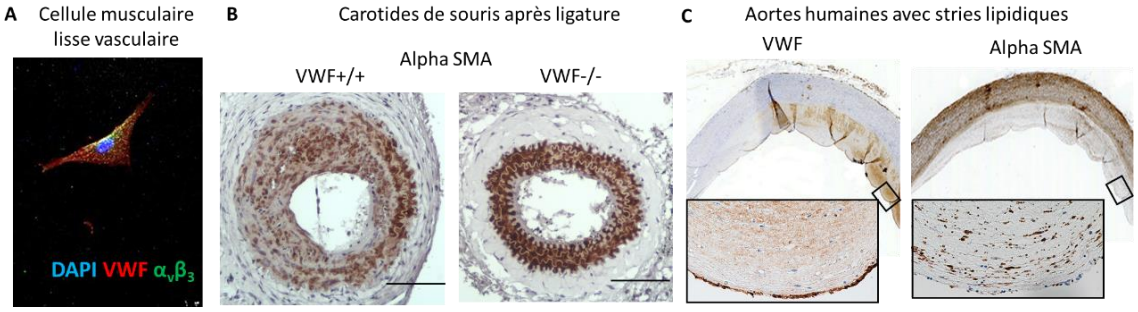

Figure 8. **Effet du VWF sur la prolifération des cellules musculaires lisses vasculaires (CMLVs).**
Le VWF est colocalisé avec l'intégrine $\alpha_v\beta_3$ à la surface des CMLVs (**A**). Les souris déficientes en VWF sont protégées de la prolifération néointimale consécutive à la ligature carotidienne (**B**). Le VWF est présent au niveau des CMLVs de la néointima chez l'homme (**C**).

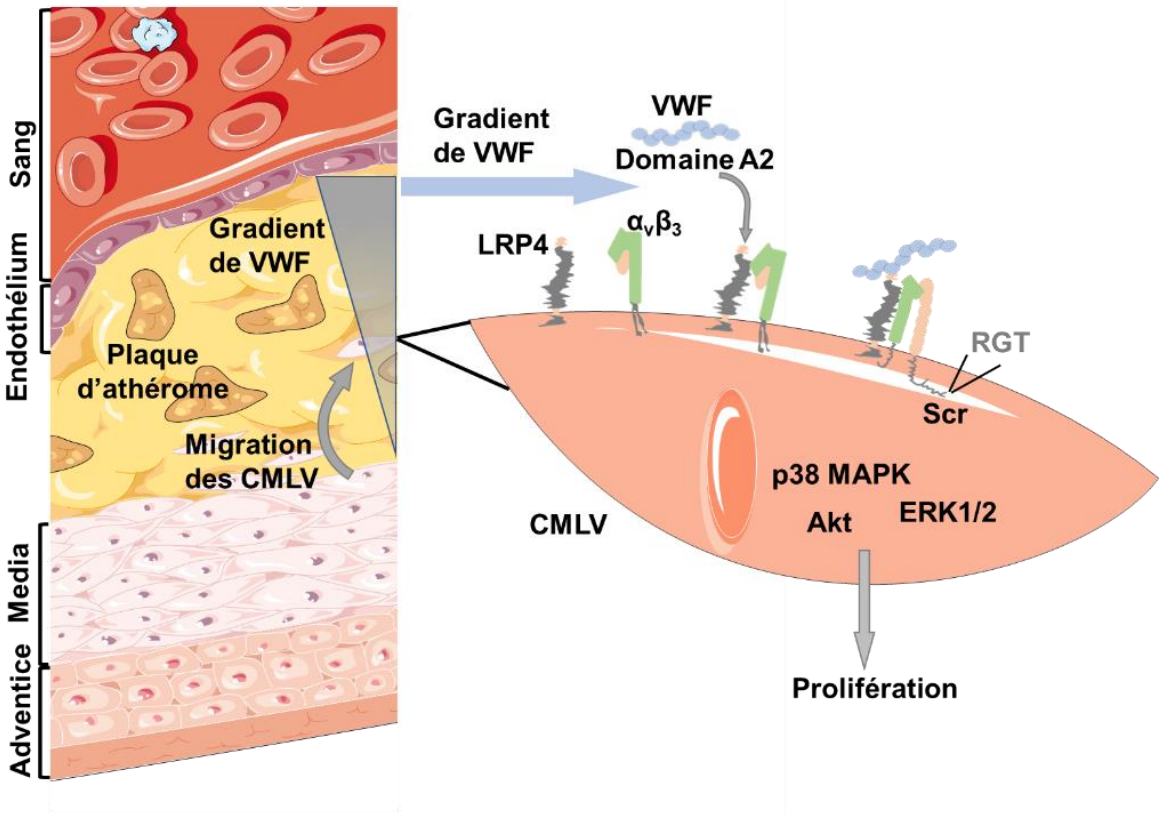

Figure 9 Résumé du rôle du facteur von Willebrand (VWF) sur les cellules musculaires lisses vasculaires (CMLVs).

Le VWF peut induire la prolifération des CMLVs en se liant au recepteur LRP4. Le recepteur LRP4 va ensuite intératir avec l'intégrine $\alpha_v\beta_3$. L'intégrine $\alpha_v\beta_3$ va activer la voie de signalisation Src aboutissant à la proliferation des CMLVs (4).

Dans le même temps j'ai obtenu un financement pour 2 ans de la FRM (fondation pour la recherche médicale) et un financement de la FFC (fédération française de cardiologie) pour commencer mon projet.

V. Encadrements.

Dès mon doctorat j'ai participé à l'encadrement et la formation d'étudiants. Pendant mon postdoctorat j'ai co-encadré une doctorante réalisant une thèse de médecine (Y Weihert). Il est à noter qu'en Allemagne les doctorants en médecine peuvent réaliser leur thèse sur des sujets fondamentaux dans les laboratoires de recherche. De plus, les ACT n'existant pas en Allemagne il n'y a pas de reconnaissance officielle d'un co-encadrement sans posséder au préalable l'équivalent de l'HDR. Depuis mon retour en France j'ai encadré une étudiante en M2 (J Martin) et je co-encadre deux doctorants (M Bardin) et (V Dufrost). J'ai également co-encadrer un étudiant de M1 au printemps 2021 sur un sujet portant sur la dégradation du glycocalyx dans une cohorte de patients que nous possédons à Nancy. La suite de ce projet sera réalisée par un doctorant qui débutera son doctorat en octobre 2021 et pour lequel je viens d'obtenir un financement *via* l'UL (LUE) et que je co-encadrerai avec N Mercier. Mes encadrements sont résumés dans le tableau page suivante et les résumés des projets sont disponibles annexes page 24.

Tableau 1 : résumé des encadrements

Encadrant et Co-encadrant	Nom	Niveau	Année, durée et lieux	Titre	Valorisation
Regnault Lagrange	Docq	SIR	Juillet-aout 2012 Nancy	Influence de l'activation plaquettaire sur la génération de thrombine évaluée par thrombinographie	Publication dans *Platelet* en 2017
Lagrange Toupance	Thomas	Master 1	Avril-Juin 2021 Nancy	Étude des rôles respectifs des contraintes hémodynamiques et du statut inflammatoire dans la dégradation du glycocalyx endothélial dans une cohorte de patients adultes.	
Lagrange	Martin	Master 2	Janvier-Juin 2020 Nancy	Étude du potentiel thrombotique chez le rat-taupe nu	
Wenzel Lagrange	Weihert	Doctorat	2014-2017, soutenance le 16 novembre 2020 Mayence	Analysis of thrombin generation by calibrated automated thrombography in plasma of hypertensive patients (HT).	Publication dans Science Translational Medicine en 2017
Bäck Lagrange (ACT du 23/10/2019)	Bardin	Doctorat	Début en octobre 2018 Nancy	Résolution de l'inflammation par les médiateurs lipidiques dans le vieillissement vasculaire.	
Wahl Lagrange (ACT en cours)	Dufrost	Doctorat	Début en janvier 2021	Implication de TREM-1 et des NETs dans la thrombogénèse du SAPL.	
Mercier Lagrange	Jahangiri	Doctorat	Début en octobre 2021 Nancy	Le glycocalyx des cellules musculaires lisses endothéliales et vasculaires : base des interactions entre l'insudation sanguine et la mécanotransduction artérielle au cours du vieillissement vasculaire.	
Lagrange Peyrin-Biroulet	A recruter	Postdoctorat	Début en decembre 2021	Exploration de l'implication du facteur von Willebrand (VWF) dans l'immunothrombose des maladies inflammatoires chroniques de l'intestin (MICI)	

VI. Publications et rayonnement scientifique.

A. Travaux originaux.

Orcid : 0000-0002-0811-565X (* indique une position partagée, # auteur correspondant)

1. **Lagrange J***, Regnault V*, Pizard A*, Safar M, Fay R, Pitt B, Challande P, Rossignol P, Zannad F, Lacolley P. Opposite predictive value of pulse pressure and aortic pulse wave velocity on heart failure with reduced left ventricular ejection fraction. ***Hypertension***. 2014; 63(1):105-11. IF: 6.4

2. **Lagrange J**, Bourhim M, Fassot C, Louis H, Nguyen Dinh Cat A, Parlakian A, Wahl D, Lacolley P, Jaisser F, Regnault V. Endothelial mineralocorticoid receptor activation enhances endothelial protein C receptor and decrease vascular thrombosis. ***FASEB J.*** 2014; 28(5):2062-72. IF: 5.0

3. **Lagrange J***, Ait Aissa K*, Mohamadi A*, Louis H, Houppert B, Challande P, Wahl D, Lacolley P, Regnault V. Vascular smooth muscle cells are responsible for a prothrombotic phenotype of spontaneously hypertensive rats arteries. ***Arterioscler Thromb Vasc Biol.*** 2015; 35:930-7. IF: 6.0

4. Wenzel P, Rossmann H*, Müller C*, Kossmann S*, Oelze M, Schulz A, Arnold N, Simsek C, **Lagrange J**, Klemz R, Schönfelder T, Brandt M, Karbach SH, Knorr M, Finger S, Neukirc h C, Häuser F, Beutel ME, Kröller-Schön S, Schulz E, Schnabel RB, Lackner K, Wild PS, Zeller T, Daiber A, Blankenberg S, Münzel T. Heme oxygenase-1 suppresses a pro-inflammatory phenotype in monocytes and determines endothelial function and arterial hypertension in mice and humans. ***Eur Heart J.*** 2015; 36(48):3437-46. IF: 15.0

5. Karbach SH, Schönfelder T, Brandão I, Wilms E, Hörmann N, Jäckel S, Schüler R, Finger S, Knorr M, **Lagrange J**, Brandt M, Waisman A, Kossmann S, Schäfer K, Münzel T, Reinhardt C, Wenzel P. Gut Microbiota Promote Angiotensin II-Induced Arterial Hypertension and Vascular Dysfunction. ***J Am Heart Assoc.*** 2016; 5(9). IF:5.1

6. Kossmann S*, **Lagrange L***, Jäckel S, Jurk K, Ehlken M, Schönfelder T, **Weihert Y**, Knorr M, Brandt M, Xia N, Li H, Daiber A, Oelze M, Reinhardt C, Lackner K, Monia M, Karbach SH, Walter U, Ruggeri Z, Renné T, Ruf W, Münzel T, Wenzel P. Platelet-localized FXI promotes a vascular coagulation-inflammatory circuit in arterial hypertension. ***Sci Trans Med.*** 2017; 9(375). IF: 16.

7. **Lagrange J**, Didelot M, Mohamadi A, A. Walton L. A, Bloemen S, de Laat B, Louis H, Thornton S. N, Derby B, Sherratt M. J, Fève B, Challande P, Akhtar R, Cruickshank J. K, Lacolley P, Regnault V. Implication of free fatty acids in thrombin generation and fibrinolysis in vascular inflammation in aged Zucker rats and evolution with aging. ***Front. Physiol.*** 2017; 8:949. IF: 4.1

8. **Lagrange J,** Kossmann S, Kiouptsi K, Wenzel P. Visualizing Leukocyte Rolling and Adhesion in Angiotensin II-Infused Mice: Techniques and Pitfalls. ***J Vis Exp.*** 2018; (131). IF : 1.2

9. Didelot M, **Docq C**, Wahl D, Lacolley P, Regnault V, # **Lagrange** J. Platelet aggregation impacts thrombin generation assessed by calibrated automated thrombography. ***Platelets.*** 2018; (2):156-161. IF: 2.5

10. Jansen T, Kröller-Schön S, Schönfelder T, Foretz M, Viollet B, Daiber A, Oelze M, Brandt M, Steven S, Kvandová M, Kalinovic S, **Lagrange J**, Keaney JF Jr, Münzel T, Wenzel P, Schulz E. α1AMPK deletion in myelomonocytic cells induces a pro-inflammatory phenotype and enhances angiotensin II-induced vascular dysfunction. ***Cardiovasc Res*.** 2018; 114(14):1883-1893. IF: 6.3

11. Kröller-Schön S, Jansen T, Tran TLP, Kvandová M, Kalinovic S, Oelze M, Keaney JF Jr, Foretz M, Viollet B, Daiber A, Kossmann S, **Lagrange J**, Frenis K, Wenzel P, Münzel T, Schulz E. Endothelial alpha1AMPK modulates angiotensinII-madiated vascular inflammation and dysfunction. ***Basic Res Cardiol***. 2019; 114(2):8 IF: 5.7

12. Schüler R, Efentakis P, Wild J, **Lagrange J**, Garlapati V, Molitor M, Kossmann S, Oelze M, Stamm P, Li H, Schäfer K, Münzel T, Daiber A, Waisman A, Wenzel P, Karbach SH. T-Cell-derived IL-17A induces vascular dysfunction via perivascular fibrosis formation and dysregulation of NO/cGMP signaling. ***Oxid Med Cell Longev*** 2019 IF: 4.8

13. Makhoul S, Panova-Noeva M, Regnault V, Ruf W, Wenzel P, # **Lagrange J**. Rivaroxaban effects illustrate the underestimated importance of activated platelets in thrombosis generation assessed by calibrated automated thrombography. ***J Clin Med*** 2019; 8(11) IF: 5.6

14. **Lagrange J**, Finger S, Kossmann S, Garlapati V, Ruf W, Wenzel P. Angiotensin II Infusion Leads to Aortic Dissection in LRP8 Deficient Mice. ***Int J Mol Sci*.** 2020; 21(14):4916. IF: 4.6

15. **Lagrange J**, Wagner B, Nagler M, Ten Cate V, Pallares Robles A, Koeck T, Rapp S, Prochaska JH, Spronk HM, Wenzel P, Ruf W, Ten Cate H, Wild PS, Panova-Noeva M. Characterization of thrombin generation curve shape in presence of platelets from acute venous thromboembolism patients. ***J Clin Med*** 2020; 9(9):2892 IF: 5.5

16. Molitor M, Rudi WS, Garlapati V, Finger S, Schüler R, Kossmann S, **Lagrange J**, Nguyen TS, Wild J, Knopp T, Karbach SH, Knorr M, Ruf W, Münzel T, Wenzel P. Nox2+ Myeloid cells drive vascular inflammation and endothelial dysfunction in heart failure after myocardial infarction via angiotensin II receptor type 1. ***Cardiovasc Res*.** 2021; 117(1):162-177 IF: 6.3

17. **Lagrange J***, Worou ME, Michel J-B, Raoul A, Didelot M, Muczynski V, Legendre P, Plénat F, Gauchotte G, Lourenco-Rodrigues M-D, Christophe OD, Lenting PJ, Lacolley P, Denis CV, Regnault V. The VWF/LRP4/$\alpha_V\beta_3$-axis represents a novel pathway regulating proliferation of human vascular smooth muscle cells. ***Cardiovasc Res*** 2021. IF: 8.2

18. Efentakis P, Molitor M, Kossmann S, Bochenek ML, Wild J, **Lagrange J**, Finger S, Jung R, Karbach S, Schäfer K, Schulz A, Wild P, Münzel T, Wenzel P. Tubulin-folding cofactor E deficiency promotes vascular dysfunction by increased endoplasmic reticulum stress. ***Eur Heart J***. 2021 epub. IF: 22,6

B. Revues et chapitres de livres.

18. Mao XQ, Ait-Aissa K, **Lagrange J**, Youcef G, Louis L. Hypertension, hypercoagulability and the metabolic syndrome: a cluster of risk factors for cardiovascular disease. ***Bio-medical materials and engineering*.** 2012; 22(1-3):35-48

19. Regnault V, **Lagrange J**, Patrick L. Early Aging of Enothelial Functions and Platelet-Vessel Wall Interactions. Early Vascular Aging (EVA): New Directions in Cardiovascular Protection, 1st Edition. Editors: Nilsson PM, Hecht Olsen M, Laurent S. 2015

20. # **Lagrange J**, Ait-Aissa K, Mohamadi A, Wahl D, Lacolley P, Regnault V. Pro- and anti-coagulants properties of vascular smooth muscles cells. ***Hématologie*** (en Français) 2016, 22(6)

21. **Lagrange J**, Kossmann S, Wenzel P. Assessment of vascular dysfunction and inflammation induced by angiotensin II in mice. Inflammation: Methods and Protocols. Editors: Clausen B, Laman J. ***Methods Mol Biol*****.** 2017; 1559:439-453

22. Kabach SH, **Lagrange J**, Wenzel P. Thromboinflammation and vascular dysfunction. ***Hämostaseologie*** 2019; 39(2):180-187

23. # **Lagrange J**, Wenzel P. The regulatory role of coagulation factors in vascular function. ***Front in Bioscience***. 2019; 24:494-513

24. # **Lagrange J**, Lacolley P, Wahl D, Peyrin-Biroulet L, Regnault V. Shedding new light on the role of hemostasis in inflammatory bowel disease. ***Clin Gastroenterol Hepatol***. 2021 jun; 16(6) 1088-1097 IF: 11,3

25. # **Lagrange J**, Schellenberg C. Implications des proteins de l'hémostase dans la physiopathologie de la paroi vasculaire : exemple du facteur von Willebrand. ***Rev Francoph Hémost Thromb.*** 2021 ; 3(2) 101-107 (En français)

C. Selection de présentations en congrès internationaux (sélection).

1. Lagrange J, Bourhim M, Fassot C, Nguyen Dinh Cat A, Wahl D, Lacolley P, Jaisser F, Regnault V. Aldosterone decreases thrombine generation via enhancement of thrombomodulin-mediated protein C activation. XXIV ISTH congress of the international society on thrombosis and haemostasis, Amsterdam, 29 Juin - 4 Juillet 2013.
2. Lagrange J, Walton L, Bloemen S, Cruickshank K, Benetos A, Lacolley P, Regnault V. Arterial stiffness and haemostasis changes in obese Zucker rats. 7th international meeting of the French society of hypertension. Paris, 19-20 décembre 19-2013.
3. Lagrange J, Ait Aissa K, Mohamadi A, Lacolley P, Regnault V. Vascular smooth muscle cells are responsible for a prothrombotic phenotype of spontaneously hypertensive rat. The Science and practice of venous thromboembolism, Sithonia 4-10 mai 4-10 2015. Prix de la meilleure communication orale.
4. Lagrange J, Kossmann S, Daiber A, Oelze M, Monia B, Ruf W, Münzel T, Wenzel P. Vascular inflammation in two rat models of arterial hypertension is promoted by coagulation FXI. DGK, Mannheim March 30, 2 avril 2016.
5. Lagrange J, Kossmann S, Münzel T, Wenzel P. Conditional knockout of heme oxygenase-1 in lysozyme M positive cells attenuates angiotensin II induced vascular inflammation. DGK, Mannheim 19-22 avril 2017.
6. Lagrange J, Kossmann S, Münzel T, Wenzel P. Knockout of heme oxygenase-1 in lysozyme M positive cells attenuates angiotensin II induced vascular inflammation.

ICCAD, 12th International Congress on Innovations in Coronary Artery Disease. Venice 15-17 octobre 2017.
7. Lagrange J, The regulatory role of coagulation factors on arterial function. ARTERY18 18-20 octobre 2018. Lauréat du« Career development award ».
8. Lagrange J, Platelet activation and thrombin generation: from bench to hypertension and thrombosis in humans, Geneva Platelet Group. Geneva, 6 novembre 2018. **(sur invitation)**
9. Lagrange J, Coagulation factors and arterial stiffness, **North America ARTERY** mai 2019. **(sur invitation)**
10. **Lagrange J**, The regulatory role of coagulation factors on arterial function, **Gordon Research Conference**, 10 février 2020 **(sur invitation)**
11. Lagrange J, Toupance S, Thomas A, Labat C, Regnault V, Benetos A, Lacolley L. Respective roles of hemodynamic conditions and inflammatory status in the degradation of endothelial glycocalyx in adults. ARTERY, 21 octobre 2021

D. Communications affichées (sélection).

1. Lagrange J, Fassot C, Nguyen Dinh Cat A, Lacolley P, Jaisser F, Regnault V. Paxadoxical involvement of the endothelial mineralocorticoid receptor in platelet activation and vascular thrombosis in mousse. ARTERY Paris, 13-15 octobre 2011
2. Lagrange J, Louis H, Max JP, Thornton SN, Wahl D, Fève B, Benetos A, Lacolley P, Regnault V. Increased fibrinogen rises thrombin generation and fibrin clot formation in obese Zucker rats. XXIV ISTH congress of the international society on thrombosis and haemostasis, Amsterdam, 29 juin-4 juillet 2013
3. Lagrange J, Walton L, Bloemen S, Cruickshank K, Benetos A, Lacolley P, Regnault V. Arterial stiffness and haemostasis changes in obese Zucker rats. ARTERY London 17-18 octobre 2013
4. Lagrange J, Kossmann S, Ehlken M, Monia B, Ruf W, Münzel T, Wenzel P. Platelet-localized FXI promotes a glycoprotein Ibα dependent feedback loop in arterial hypertension, and vascular inflammation. ARTERY, Krakow, 15-17 octobre 2015
5. Lagrange J, Weihert Y, Karbach S, Wenzel P. Increased platelet reactivity is responsible of modifications of thrombin generation in hypertensive crisis patients ARTERY, Krakow, 15-17 octobre 2015
6. Lagrange J, Kossmann S, Ehlken M, Monia B, Ruf W, Münzel T, Wenzel P. Platelet-localized FXI promotes a glycoprotein Ibα dependent feedback loop in arterial hypertension, and vascular inflammation. ASH, Orlando, 4-8 decembre 2015
7. Lagrange J, Weihert Y, Münzel T, Karbech S, Wenzel P. In patients with uncontrolled arterial hypertension platelets and coagulation factor FXI are responsible of modifications of thrombin generation. ATVB, Nashville, 4-6 mai 2016
8. Lagrange J, Kossmann S, Münzel T, Ruggeri Z, Ruf W, Wenzel P. Contributions of von Willebrand Factor to the development of angiotensin II-induced vascular inflammation. XXVI ISTH congress of the international society on thrombosis and haemostasis, Berlin, 8-13 juillet 2017
9. Lagrange J, Kossmann K, Münzel T, Ruf W, Wenzel P. Role of Lysozyme M+ cells in the development of angiotensin II-induced vascular inflammation. XXVI ISTH congress of the international society on thrombosis and haemostasis, Berlin, 8-13 juillet 2017
10. Lagrange J, Kossmann K, Ruf W, Wenzel P. Lack of LRP8 on bone marrow derived cells triggers the formation of aortic dissection in angiotensin II infused mice. ESC, Munich, 25-29 août 2018 Prix du meilleur poster.

11. Lagrange J, Michel J-B , Raoul A, Lenting P J, Lacolley P, Denis CV, Regnault V. Von Willebrand Factor Induces Vascular Smooth Muscle Cell Proliferation And Migration Through Low Density Lipoprotein-Related Receptor Protein 4 And $\alpha_v\beta_3$ Integrin. 23-24 Ocotbre 2020 (congrès en ligne).

E. Liste des revues d'articles et de demandes de financements.

Revues d'articles :
04-2018 : 1 article pour ***Journal of Molecular Medicine***
07-2018 : 1 article pour ***Thrombosis and Haemostasis***
10-2018 : 1 article pour ***Thrombosis Research***
07-2019 : 1 article pour ***Atherosclerosis***
12-2019 : 1 article pour ***Journal of Clinical Medicine***
12-2019 : 1 article pour ***Journal of Molecular Medicine***
01-2020 : 1 article pour ***Journal of Clinical Medicine***
02-2020 : 1 article pour ***International Journal of Molecular Sciences***
03-2020 : 1 article pour ***International Journal of Molecular Sciences***
04-2020 : 1 article pour ***British Journal of Haematology***
05-2020 : 1 article pour ***International Journal of Molecular Sciences***
05-2020 : 1 article pour ***British Journal of Pharmacology***
06-2020 : 1 article pour ***International Journal of Molecular Sciences***
07-2020 : 1 article pour ***International Journal of Molecular Sciences***
08-2020 : 1 article pour ***Oxidative Medicine and Cellular Longevity***
09-2020 : 1 article pour ***International Journal of Molecular Sciences***
10-2020 : 1 article pour ***Journal of Clinical Medicine***
11-2020 : 1 article pour ***International Journal of Molecular Sciences***
01-2021 : 1 article pour ***Journal of Clinical Medicine***
01-2021 : 1 article pour ***Scientific Reports***
01-2021 : 1 article pour ***Frontiers in Physiology***
02-2021 : 1 article pour ***International Journal of Molecular Sciences***
04-2021 : 1 article pour ***Journal of Thoracic Disease***
05-2021 : 1 article pour ***Journal of Molecular Medicine***
05-2021: 1 article pour ***Metabolites***
06-2021: 1 article pour **European Heart Journal Open**
07-2021: 1 article pour **Antioxidants and redox signaling**
08-2021: 1 article pour **Hämostaseologie**
09-2021: 1 article pour **Frontiers in Cardiovascular Medicine**

Evaluation de demandes de financements :
10-2017 : évaluation d'une demande de financements pour la **FRM (Fondation pour la Recherche Médicale).**
02-2019 : évaluation d'une demande de financements pour le **BMBF (Federal Ministry of Education and Research of Germany).**
03-2020 : évaluation d'une demande de financements pour le **National Science Center in Poland.**
10-2020 : évaluation d'une demande de financements pour le **National Science Center in Poland.**

F. Contrats de recherche et financements.

Les contrats de recherche et financements que j'ai obtenus ainsi que leurs utilisations et pour quels projets sont résumés dans le tableau suivant.

Tableau 2 : résumé des contrats de recherche et financements

Investigateur principal et Co-investigateur	Organisme	Montant	Année et lieux	Utilisation	Titre
Lagrange	DSHF Fondation allemande pour le cœur	40 k€	2018 Mayence	Fonctionnement	Exploration of the role of Heme oxygenase-1 on polarization and regulation of LysM+ cells in vascular inflammation and hypertension.
Lagrange	BMBF ministère de la recherche allemand	50 k€	2019 Mayence -Nancy	Fonctionnement et salaire d'un technicien	Endothelial glycocalyx as interaction base between coagulation and the endothelium in vascular inflammation and ageing.
Lagrange	FRM Fondation pour la recherche médicale	138 k€	2019 Nancy	Salaire pour 24 mois	Mécanismes des manifestations thrombotiques et vasculaires dans les maladies inflammatoires chroniques de l'intestin (MICI).
Lagrange	FFC Fédération française de cardiologie	30 k€	2019 Nancy	Fonctionnement	Mécanismes immunothrombotiques et vasculaires dans les maladies inflammatoires chroniques de l'intestin (MICI)**.**
Regnault Lagrange	Pfizer	50 k€	2020 Nancy	Fonctionnement	VASCIBD: Role of VASCular changes in the development of complications in Inflammatory Bowel Diseases.
Lagrange	UL-BMS	10 k€	2021 Nancy	Fonctionnement	Etude des cellules endothéliales et des cellules musculaires lisses vasculaires dans l'interface sang-

					vaisseaux : implication du glycocalyx
Mercier Lagrange	UL (LUE)	107 k€	2021 Nancy	Salaire doctorant et 15 k€ de fonctionnement	Le glycocalyx des cellules musculaires lisses endothéliales et vasculaires : base des interactions entre l'insudation sanguine et la mécanotransduction artérielle au cours du vieillissement vasculaire.
Lagrange Peyrin-Biroulet	CHRU Nancy-Région Grand Est	45 k€	2021	Salaire postdoctorant	Exploration de l'implication du facteur von Willebrand (VWF) dans l'immunothrombose des maladies inflammatoires chroniques de l'intestin (MICI)

G. Autres responsabilités.

2019- : Membre du comité d'éthique de Lorraine.
2021- : *topic editor* pour *JCM (Journal of Clinical Medicine)*
2021 : Membre du comité de sélection d'un MCF à l'UMR_S 1116

VII. Projet de recherche : Étude de l'interface sang-vaisseaux : rôles cellulaires des facteurs de la coagulation et implication de l'immunothrombose, du glycocalyx et des globules rouges.

Mon projet de recherche est un projet transversal à la fois thématiquement mais également en termes de cibles. En effet, je vais étudier différents processus transverses dans le vaisseau sanguin : de l'IT intraluminal au glycocalyx de la surface des CEs, pour finir dans la paroi artérielle et les modifications des CMLVs.

A. Introduction Générale.

Les maladies athérothrombotiques sont caractérisées par un épaississement intimal provoqué par une convection de lipides du sang vers la paroi vasculaire. Ces lipides engendrent le développement de plaques athéromateuses composées d'un noyau lipidique entouré d'une matrice fibreuse et de CMLVs provenant de la media. La pathologie peut ensuite évoluer en incluant une néoangiogenèse et la migration de leucocytes depuis le sang dont l'un des évènements finals sont des hémorragies dans la plaque. Enfin, la déstructuration de la paroi provoquée par le développement de plaques se traduit par la rupture de ces plaques et des évènement thrombotiques.

Cette pathologie est un exemple typique de ce que peut provoquer le déséquilibre de l'interface sang-vaisseaux. Mes travaux ont jusqu'à présent porté sur un aspect particulier de ce déséquilibre qui pourrait être résumé en l'étude des rôles cellulaires des facteurs de la coagulation. La première partie de l'état de l'art ciblera ces aspects.

Ces effets cellulaires des facteurs de la coagulation dans la paroi vont de pair avec les effets cellulaires qu'ils peuvent avoir sur les cellules circulantes. Ces cellules sont bien connues pour participer aussi au développement des pathologies athéromateuses et vasculaires de manière générale.

Pour que les facteurs de la coagulation et les cellules circulantes puissent interagir avec les cellules de la paroi vasculaire il est nécessaire qu'ils migrent dans la paroi depuis le sang **(Figure 10)**. Cela nécessite une altération de la barrière endothéliale et en particulier du glycocalyx endothélial qui recouvre ces cellules. De manière intéressante ce glycocalyx a été très peu étudié dans sa participation à la barrière endothéliale. Pourtant cette barrière physique empêche en conditions physiologiques le roulement et l'adhésion des cellules immunitaires aux CEs et permet la présence d'un microenvironnement plasmatique limitant les échanges entre les cellules de la paroi et le plasma (et *vice et versa*). Pour mieux comprendre les altérations de l'interface sang-vaisseaux je souhaite donc étudier plus en détails la biologie du glycocalyx endothélial en conditions physiologiques et pathologiques.

Enfin, les études de ces dernières années montrent des interactions entre cellules et processus jusqu'à présent sous-estimés qui pourraient être directement impliqués dans l'interface sang-vaisseaux. C'est par exemple le cas de l'immunothrombose (IT) qui correspond à un processus de protection contre la dissémination de pathogènes via

l'hémostase et l'immunité innée. Les GRs sont aussi sous le feu des projecteurs car ces cellules qui historiquement étaient considérées comme passives dans l'hémostase ont montré qu'elles pouvaient à la fois contribuer au développement de thrombose et des pathologies vasculaires.

Ainsi je souhaite focaliser mon travail sur l'IT et l'implication des GRs dans l'interface sang-vaisseaux. Les connaissances actuelles concernant ces processus et implications cellulaires seront aussi résumées dans l'état de l'art.

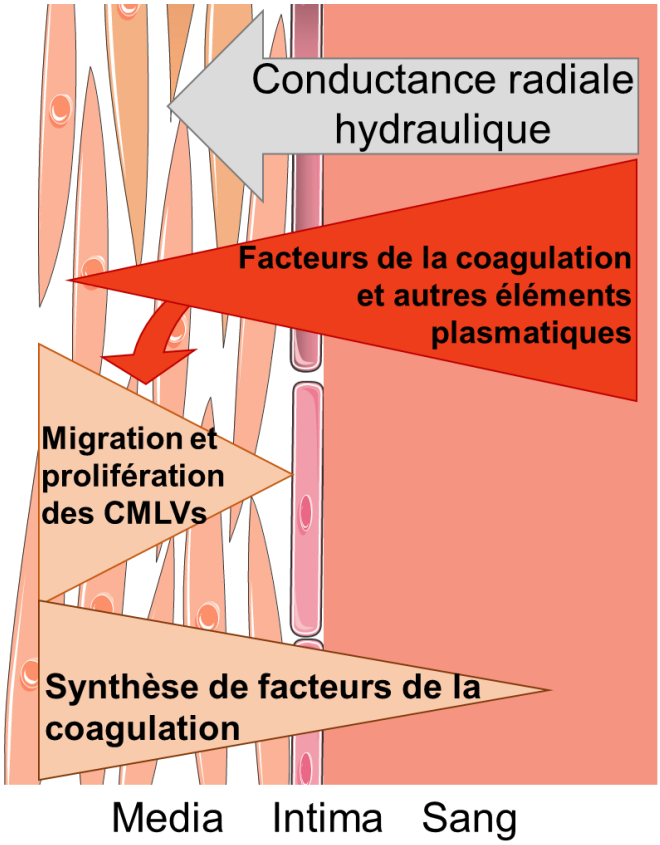

Figure 10. Vue générale des échanges entre les compartiments sanguin et parietal.

B. Etat de l'art.

1. L'interface sang-vaisseaux : exemple des facteurs de la coagulation.

Une brèche vasculaire provoque l'adhésion des plaquettes et la formation d'un caillot destiné à limiter les saignements. La fibrinolyse quant à elle suit la formation du caillot et permet sa dissolution. La coagulation est possible en présence de phospholipides, de calcium et surtout avec les zymogènes et les récepteurs cellulaires engendrant l'activation de ces zymogènes dans une cascade impliquant plusieurs boucles d'amplification et de régulation. L'hémostase est altérée dans de nombreuses maladies et aboutit à des risques de thromboses ou d'hémorragies augmentés. Un résumé général de l'hémostase est présenté en ***Figure 11***.

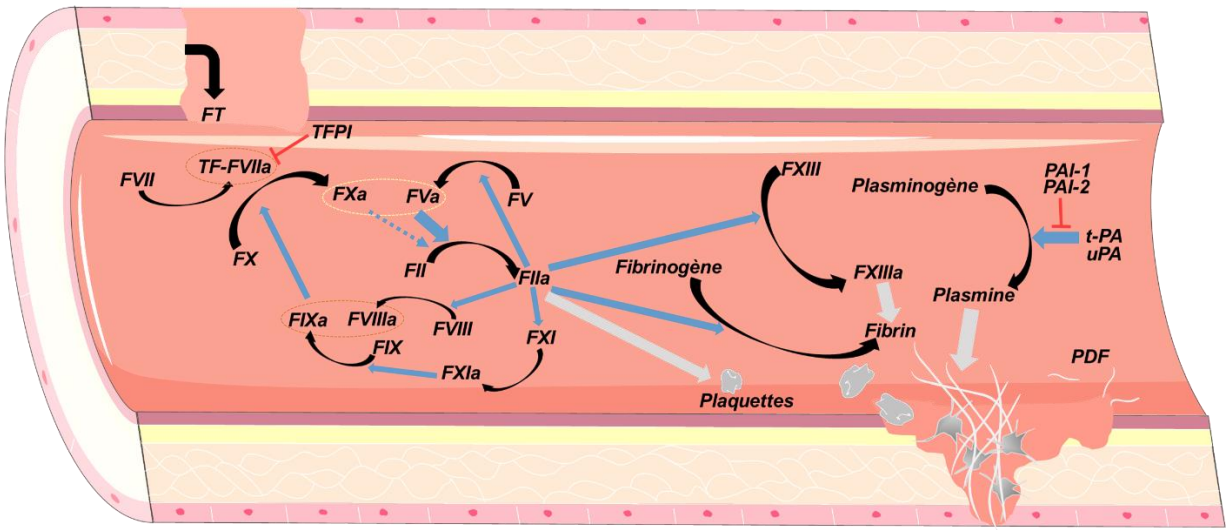

Figure 11. Vue Générale de la cascade de coagulation.

En présence d'une brèche vasculaire les cellules du sous-endothélium exposent du facteur tissulaire (FT) qui permet l'activation du facteur VII (FVIIa) puis l'activation du facteur X (FXa). Les premières molécules de FXa vont convertir la prothrombine (FII) en thrombine (FIIa) et celles-ci vont amplifier leur formation en activant les facteurs V (FVa), VIII (FVIIIa) et XI (FXIa). Le FXIa peut ensuite activer le facteur IX (FIXa) qui avec l'aide du FVIIIa activera plus de FX. En même temps, la thrombine peut cliver le fibrinogène aboutissant à la formation du caillot de fibrine qui sera stabilisé par l'intermédiaire du facteur XIII activé (FXIIIa). La lyse du caillot commence lorsque le plasminogène est converti en plasmine par l'activateur tissulaire du plasminogène (t-PA) ou de l'urokinase (uPA) aboutissant à la formation de produits de dégradation du fibrinogène (PDF). La fibrinolyse peut être inhibée par les inhibiteurs de l'activateur du plasminogène (PAI-1, PAI-2). Les flèches noires courbées indiquent une conversion, les flèches bleues une activation et les flèches grises indiquent des effets pléiotropiques supplémentaires.

Le lien entre les modifications de l'hémostase et les pathologies vasculaires est bien établi. L'hypertension artérielle en est un bon exemple. Cette pathologie touche près de 20% de la population adulte et est le principal facteur de risque cardiovasculaire [7]. Si elle n'est pas traitée, l'hypertension peut aboutir à une insuffisance cardiaque ou rénale ou encore des infarctus du myocarde ou cérébraux. En ce qui concerne l'hémostase, l'hypertension augmente les concentrations circulantes de facteur VII (FVII), de fibrinogène ou encore de D-dimère suggérant la présence d'un état prothrombotique. Les facteurs anticoagulants sont aussi modifiés avec une augmentation de l'antithrombine (AT) ou de la protéine C (PC) chez les patients hypertendus.

L'athérosclérose est liée à une dysfonction vasculaire et une augmentation de la synthèse de facteur tissulaire (FT) ou encore de FVII, tous deux synthétisés par les macrophages et les CMLVs de la plaque et de la paroi vasculaire [8]. Le FX est également présent dans les macrophages de la plaque [9] et les produits de dégradations de la fibrine sont associés à la gravité de l'athérosclérose.

Les CEs permettent au sang de ne pas coaguler au contact du vaisseau, en particulier des surfaces procoagulantes telles que le collagène ou les CMLVs. La fonction endothéliale est dégradée dans les pathologies cardiovasculaires. Le VWF est normalement stocké dans les corps de Weibel-Palade et dans une moindre mesure dans les granules alpha des plaquettes. Cependant, il voit sa concentration circulante augmenter chez les patients hypertendus ou insuffisants cardiaques où la présence d'une

dysfonction endothéliale est bien décrite [10]. D'autres marqueurs de l'activation endothéliale telle que la part soluble de l'EPCR sont augmentés dans l'hypertension [11]. Ces modifications et les altérations de la synthèse d'autres facteurs de la coagulation indiquent de profondes modifications de la régulation de l'hémostase dans le cadre des pathologies vasculaires.

Le risque de thrombose est majoritairement considéré comme une conséquence des pathologies vasculaires. Pourtant il y a une vingtaine d'années, la possibilité que l'hémostase elle-même affecte directement le cours de la maladie a été proposée[12].

L'hypothèse d'une implication directe des facteurs de la coagulation sur les cellules vasculaires a également remis en cause la fonction de barrière « totalement » étanche de l'endothélium. Ce changement de paradigme a permis de développer l'hypothèse de l'existence d'une interface sang-vaisseaux définie comme étant un échange constant cellulaire ou de composants cellulaires et plasmatiques à la fois du sang vers le vaisseau et *vice et versa*. La présence d'une conductance hydraulique provoquée par la pression du sang sur la paroi et la migration vers le sang de produits synthétisés par les cellules vasculaires ainsi que les conséquences phénotypiques pour les CMLVs a très bien été résumé dans la revue « *The vascular smooth muscle cell in arterial pathology: a cell that can take on multiple roles* »[13].

2. Implication des facteurs de la coagulation sur la fonction vasculaire.

Le FT initie la voie extrinsèque de la cascade de la coagulation. Dans la paroi vasculaire les CEs, les CMLVs, les fibroblastes mais aussi les cellules myéloïdes telles que les macrophages et les neutrophiles sont capables de synthétiser du FT [14]. Dans le sang la source principale de FT provient des monocytes [15]. La majorité du FT exprimé par les monocytes est cryptique et l'activation des cellules permet son exposition [16]. Le ionophore calcique, la phosphatidylsérine et l'activation des monocytes par l'activation d'autres cellules ou vésicules extracellulaires sont impliqués dans le décryptage [17,18].

Les cellules immunitaires sont une des principales sources de FT impliquées dans les thromboses veineuses et l'athérothrombose [19,20]. De plus, des vésicules extracellulaires exposant du FT peuvent être générées à partir des monocytes et avoir une activité procoagulante [21,22]. La délétion spécifique du FT dans les monocytes et les neutrophiles empêche la formation des thromboses veineuses chez la souris [23,24]. Chez la souris l'absence de FT est léthal au stade embryonnaire et aucune déficience n'a été observé chez l'homme [25]. Une désorganisation des vaisseaux du sac vitellin a été observé chez les embryons de souris déficientes pour le FT suggérant l'importance du FT dans le développement des vaisseaux [26]. Le complexe formé pour le FT et le FVIIa peut activer le récepteur 2 activé par les protéases (PAR-2) et contribuer à l'angiogenèse, l'inflammation ou encore la cancérogénèse (***Figure 12***)[27,28]. De plus, l'inhibition du complexe FT-FVIIa a une action anti-angiogénique via le récepteur PAR-2 dans un modèle de neoangiogenèse induite par l'hypoxie [29]. La migration et la prolifération des CMLVs peut être induite par le complexe FT-FVIIa via l'activation de PAR-2 et la voie ERK [30,31]. Plus récemment il a été montré que la liaison entre le FVIIa et le site de liaison aux intégrines était nécessaire pour la formation du complexe intégrant l'intégrine β1 déclenchant un signal proangiogénique dépendant de la voie du TF et de PAR-2 [32].

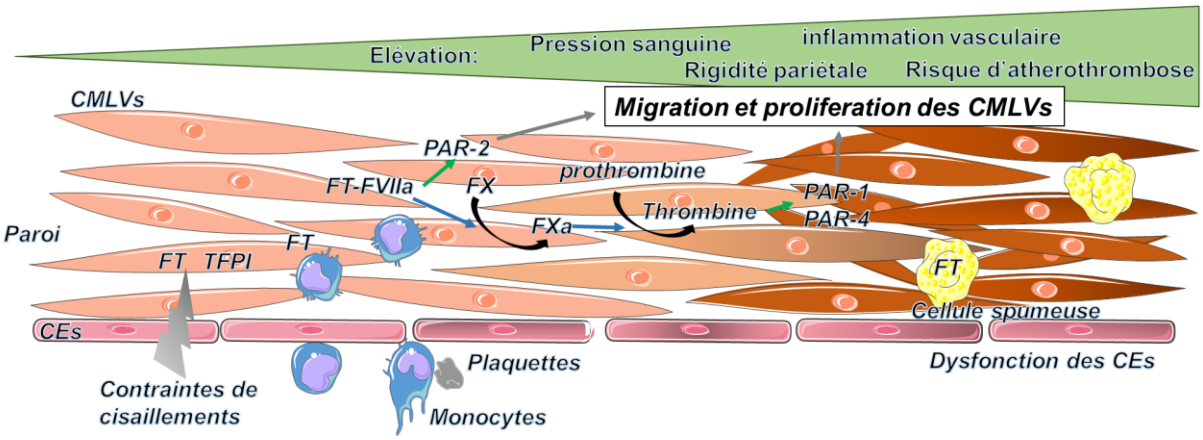

Figure 12. Implication des facteurs de la coagulation dans le développement de la dysfonction vasculaire.

Les contraintes de cisaillement stimulant la synthèse de facteur tissulaire (FT) et l'inhibiteur de la voie du FT (TFPI) par les cellules musculaires lisses vasculaires (CMLVs). Les monocytes activés, en plus de produire du FT, peuvent adhérer aux cellules endothéliales (CEs) et migrer dans la paroi vasculaire. Le complexe FT/FVIIa ainsi que la thrombine peuvent activer les récepteurs activés par les protéases (PAR-1, -2 et -4) et induire la prolifération des CMLVs. Les flèches noires courbées indiquent une conversion, les flèches bleues une activation, les flèches verte une activation des récepteurs et les flèches grises des effets pléiotropiques supplémentaires.

Les CEs et les CMLVs sont stimulées par les contraintes de cisaillement, la pression sanguine ou encore l'onde de pouls. Les battements cardiaques créent des contraintes cycliques de cisaillement sur les CMLVs aboutissant à un amincissement de la paroi vasculaire via des signaux de mécanotransduction par l'intermédiaire d'intégrines, de récepteurs tyrosines kinases ou encore de canaux ioniques [33]. Appliquées aux CEs, les contraintes de cisaillements diminuent la synthèse de TNF-α induite par le FT [34]. L'inhibiteur de la voie du FT (TFPI) est aussi régulé par ces contraintes de cisaillement. Une contrainte de 10% à 1 Hz augmente la synthèse de TFPI par les CMLVs [35]. Cette relation entre le TFPI et les contraintes de cisaillement cycliques a été observée dans une cohorte de femme ménopausées (***Figure 13***).

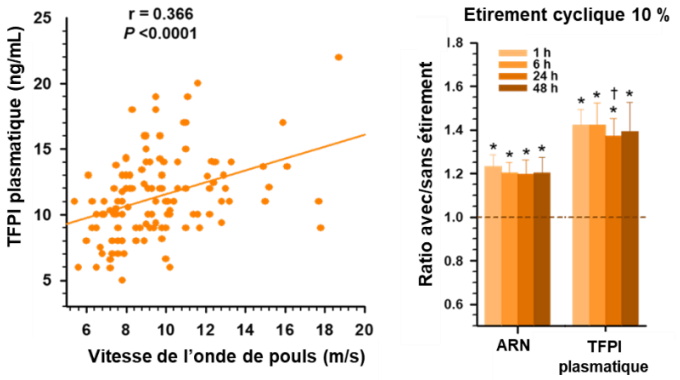

Figure 13. Rôle des contraintes pulsatiles sur la synthèse de l'inhibiteur de la voie du facteur tissulaire (TFPI) par les cellules musculaires lisses vasculaires (CMLVs).

Le TFPI circulant est corrélé à la vitesse d'onde de pouls dans une cohorte de femmes ménopausées (panel de gauche) et un étirement cyclique appliqué à des CMLVs augmente la synthèse de TFPI (panel de droite)[35].

De plus le TFPI induit l'apoptose des CMLVs et ainsi participe à l'athérothrombose [36]. Enfin, le TFPI a la capacité d'inhiber la prolifération des CEs en liant le récepteur des lipoprotéines de très basse densité (VLDLR) [37].

Le fibrinogène est à la fois un marqueur d'inflammation et d'hypercoagulabilité. Son augmentation est décrite dans les maladies à composantes inflammatoires affectant la paroi vasculaire telle que l'hypertension, l'athérosclérose et la maladie coronaire [38,39]. Les cytokines pro-inflammatoires comme l'IL-6 augmentent la synthèse hépatique de fibrinogène qui en retour est capable d'induire la production d'autres cytokines proinflammatoires (TNF-α, IL-1β) [40,41]. Au niveau des CMLVs, le fibrinogène, la fibrine et les produits de dégradation de la fibrine ont tous des effets délétères [40,42]. Les produits de dégradation de la fibrine augmentent la perméabilité de l'endothélium et la migration de CEs [43]. Les concentrations plasmatiques en fibrinogène sont augmentées chez les rats spontanément hypertendus et hyperlipidémiques [44]. Au contraire, les IL-4, IL-10 et IL-13 limitent les altérations vasculaires impliquées dans le développement de l'athérosclérose aboutissant à une diminution de la synthèse de fibrinogène [45]. Tous ces résultats suggèrent que le fibrinogène participe à la progression des pathologies vasculaires.

Le FXIIIa qui a également la capacité d'influencer la migration des CMLVs [46]. Les cellules immunitaires, en particulier les monocytes, participent à la fois au développement de l'hypertension et de l'athérosclérose et le FXIII peut se lier au récepteur 1 de l'angiotensine sur les monocytes permettant une activation complète de ces cellules par l'angII [47,48]. Dans un modèle d'infarctus du myocarde chez la souris, l'absence de FXIII limite le renouvellement de la matrice extracellulaire et diminue la réparation des tissus [49].

Le plasminogène est converti en plasmine par l'activateur tissulaire de la plasmine (t-PA) ce qui déclenche la fibrinolyse. Le récepteurs 2 de la bradykinine (B2R) et le récepteur beta-2-adrénergique (AR) peuvent former des hétérodimères et la bradykinine ainsi que le récepteur AR augmente la synthèse de l'activateur tissulaire de la plasmine (t-PA) ce qui peut être inhibé par des betabloquants [50,51]. L'urokinase (U-PA) peut aussi participer à la migration de CMLVs soumises à des contraintes pulsatiles alors que le PAI-1 inhibe ces effets [52,53].

3. Le rôle central de la thrombine dans le couplage sang-vaisseaux.

La conversion de la prothrombine en thrombine est l'étape essentielle aboutissant à la polymérisation des fibres de fibrine et la formation du caillot. La thrombine à des effets cellulaires importants pour l'hémostase par l'intermédiaire des récepteurs PARs, principalement *via* l'activation des plaquettes.

La famille des récepteurs PARs fait partie des récepteurs à 7 domaines transmembranaires couplés aux protéines G. Il existe 4 récepteurs PARs, tous exprimés par les plaquettes et les cellules vasculaires [54]. La synthèse peut différer en fonction du type cellulaire et de l'espèce. Par exemple, les plaquettes humaines expriment PAR-1 et PAR-4 tandis que les plaquettes de souris expriment PAR-3 et PAR-4 [55,56]. L'activation des PARs par les protéases provoquent un démasquage de la partie N-terminale [57]. Après activation, ce domaine se lie au domaine extracellulaire du récepteur provoquant

un changement conformationnel permettant d'initier la cascade de signalisation [58]. PAR-1, PAR-2 et PAR-4 sont activés de cette manière mais l'activation de PAR-3 est différente puisqu'il agit comme un cofacteur de PAR-4 en présence de thrombine ***(Figure 14)*** [59]. Les récepteurs PARs peuvent former des hétérodimères constitués en différentes isoformes de PARs ce qui rend d'autant plus complexe l'identifications des voies de signalisation dépendantes de ces récepteurs. Des activations non canoniques des PARs ont aussi été décrites. Certaines protéases peuvent directement cliver la partie N-terminale. C'est par exemple le cas de la protéine C activée (PCa) qui peut activer PAR 1 [60].

Ces récepteurs sont présents sur d'autres types cellulaires que les plaquettes ce qui confère à la thrombine des propriétés pléiotropiques indépendantes de l'hémostase. La thrombine a des effets sur la différenciation cellulaire, la migration, la réponse inflammatoire ou encore l'expression de certains gènes [61]. La thrombine peut activer les récepteurs PAR-1 et -4, mais également PAR-2 [62]. Dans la paroi vasculaire, PAR-1 est présent sur les CEs et les CMLVs [63]. Dans les artères pulmonaires, la thrombine peut induire une relaxation dépendante de l'endothélium via une activation non canonique de PAR-1 et une vasoconstriction des vaisseaux où l'endothélium n'est pas présent [64]. De la même manière que pour le FT, la déficience en PAR-1 est léthale dès le stade embryonnaire suggérant la aussi une implication de ce récepteur dans le développement vasculaire [65].

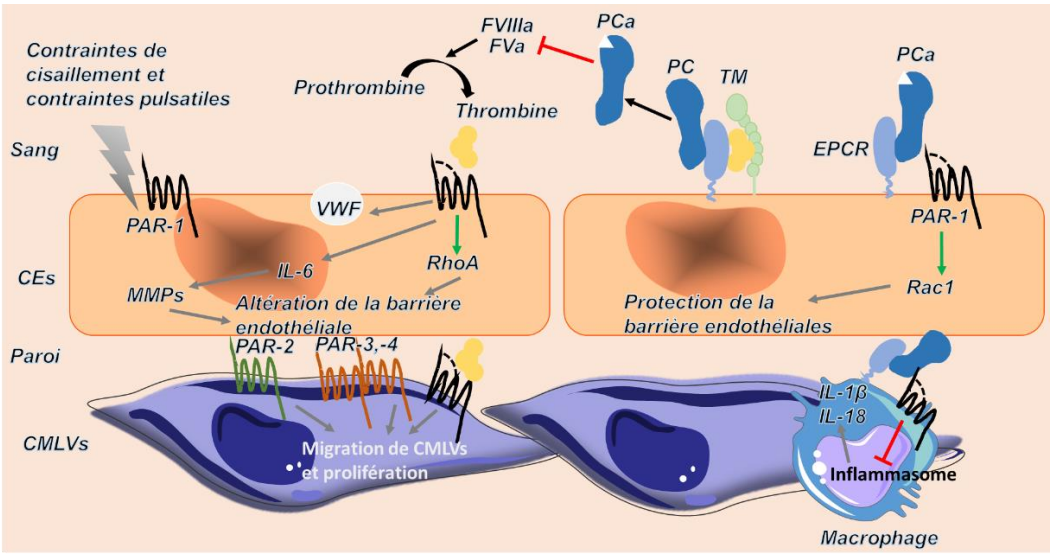

Figure 14. Effets cellulaires des facteurs de la coagulation via les récepteurs activés par les protéases (PARs).

Les contraintes de cisaillement augmentent la synthèse de PAR-1 par les cellules endothéliales (CEs). Les facteurs VIII et V activés (FVIIIa, FVa) augmentent la génération de thrombine (FIIa) et l'activation de PAR-1 active le relargage de facteur von Willebrand (VWF) par les CEs. La synthèse d'interleukine 6 et de metalloprotéinases (MMPs) peut aussi être induite par PAR-1 et la voie de signalisation dépendant de RhoA. Cette cascade de signalisation aboutit à une altération de la barrière endothéliale. De plus, la thrombine peut activer les PAR-2 et PAR-4 avec l'aide de PAR-3 et stimuler la migration et la prolifération des cellules musculaires lisses vasculaires (CMLVs). L'interaction entre la thrombine, la thrombomoduline (TM) et le récepteur endothélial de la protéine C (EPCR) aboutit à l'activation de la protéine C (PCa) qui peut aussi activer PAR-1 et qui, via Rac-1 et l'inflammasome des monocytes, permet une protection de la barrière endothéliale. La flèche noire courbe indique une conversion, les flèches noires droites une activation, les barres en T une inhibition, les flèches vertes l'activation d'un récepteur, et les flèches grises des effets pleiotropiques.

La thrombine agit comme un facteur de croissance en conditions pathologiques et participe au remodelage vasculaire *via* son action sur la prolifération des CMLVs [66]. PAR-1, PAR-2 et PAR-4 provoquent la migration des CMLVs, leur prolifération et leur hypertrophie [67]. Les contraintes pulsatiles augmentent la synthèse de PAR-1 par les CMLVs et en retour la prolifération induite par la thrombine [68]. La thrombine est aussi importante dans la réponse inflammatoire puisqu'elle stimule la synthèse de *monocyte chemoattractant protein 1* (MCP-1 ou CCL2) et d'IL-6 ou encore la production de MMPs qui participent à la dégradation de la matrice extracellulaire et au remodelage vasculaire [69,70]. La thrombine peut aussi augmenter la chimiotaxie des monocytes en stimulant la production de MCP-1, participer à la réponse immune et moduler la réponse inflammatoire aigue et chronique [71].

Concernant le rôle des récepteurs PARs sur le système cardiovasculaire, le PAR-4 dans les cardiomyocytes peut transactiver le facteur de croissance de l'épithélium (EGFR) [72]. Dans les CEs humaines de cordon ombilical de prééclampsie, PAR—2 induit l'expression de VEGF [73]. Le récepteur B2R induit une vasodilatation dépendante de la bradykinine provoquant des œdèmes et peut interagir avec PAR-4 [74]. Le système rénine angiotensine aldostérone, qui intervient aussi dans la régulation de la voie de la bradykinine est aussi lié aux PARs. En effet l'angiotensine augmente la synthèse de PAR-1 dans les CMLVs par l'intermédiaire du récepteur 1 de l'angiotensine [75]. PAR-1 est également important dans le remodelage vasculaire induit par l'AngII tandis que les inhibiteurs du FXa et de la thrombine peuvent tout deux limiter le développement de l'athérosclérose et d'anévrysmes dans des modèles expérimentaux [76].

Chez les patients atteints d'anévrysmes de l'aorte ascendante, les marqueurs de la génération de thrombine *in vivo* sont corrélés à la dilatation de l'aorte [77]. Dans les vaisseaux touchés par l'athérosclérose la concentration en thrombine présente dans la paroi est suffisante pour activer PAR-1 [78]. La thrombine de la media peut ainsi participer à la déstabilisation de la paroi vasculaire qui en retour aura un potentiel thrombogénique augmenté.

Enfin, l'utilisation des inhibiteurs du FXa a récemment été étudiée dans l'IC lors de l'étude COMMANDER [79]. L'inhibition du FXa n'a pas pu diminuer le risque d'infarctus, d'AVC ni de décès cependant l'évolution de la réactivité vasculaire n'a pas été étudiée dans cette étude. La question se pose de l'intérêt de l'inhibition des effets cellulaires de la thrombine sur le long terme chez les patients atteints de pathologies ayant des retentissements cardiovasculaires.

4. Conclusion sur les fonctions cellulaires des facteurs de coagulation.

Les facteurs de la coagulation ont des fonctions allant bien au-delà de l'hémostase. Certains ont des fonctions directes *via* les récepteurs PARs, d'autres indirectes sur les cellules de la paroi vasculaire. De nombreuses questions restent ouvertes notamment sur la provenance de ces facteurs (circulant ou produit par les cellules vasculaires) ou sur les quantités provenant de chaque compartiment. L'interface sang-vaisseaux implique la présence d'une communication entre compartiments. Cette communication dépend de l'endothélium qui n'est pas une barrière complètement étanche même en conditions physiologiques. Le rôle protecteur des CEs a particulièrement été étudié dans les pathologies mais en omettant la présence à leur surface d'une couche de

protéoglycanes protecteurs, le glycocalyx, servant d'interface entre le sang et le compartiment vasculaire. En outre la barrière endothéliale ne commence pas à la surface des CEs mais par cette couche de glycocalyx. Ce glycocalyx pourrait ainsi jouer un rôle majeur dans l'interface sang-vaisseau.

C. Rôle du glycocalyx des cellules endothéliales et des cellules musculaires lisses dans l'interface sang-vaisseaux.

1. Glycocalyx endothélial et interface sang-vaisseaux.

En conditions physiologiques, la couche de CEs n'est pas en contact direct avec le sang. Ces cellules sont recouvertes de protéoglycanes (des syndécanes, des glycasaminoglycanes) qui forment le glycocalyx. Cette couche est une zone d'interface entre le sang et les cellules pariétales (**Figure 15**). Il est ainsi aisé d'envisager l'importance cruciale du glycocalyx endothélial dans l'interface sang-vaisseau.

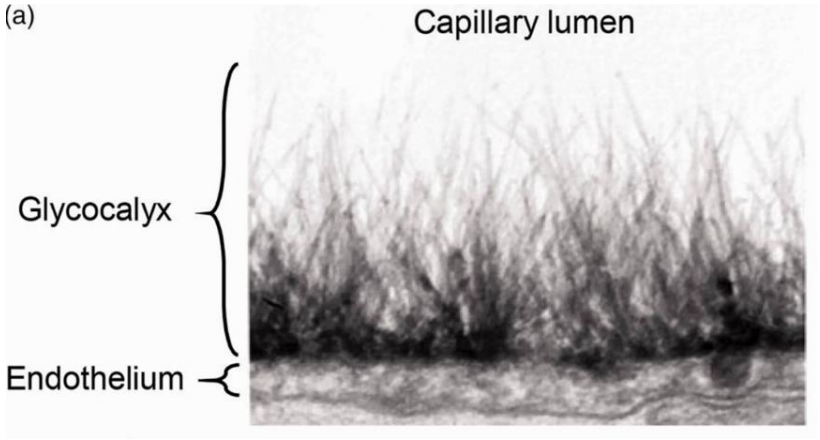

Figure 15. Glycocalyx des cellules endothéliales en microscopie électronique.
Reproduction de Oshima, K et al., Pulm. Circ. (2018).[80]

Le filet de protection formé par le glycocalyx contient entre 1 et 1,5 litres de plasma qui forment un équilibre dynamique avec le sang [81]. Le glycocalyx participe ainsi par exemple à la fonction anticoagulante de l'endothélium en emprisonnant ou en protégeant des protéines anticoagulantes à la surface des CEs. C'est le cas par exemple pour la TM ou l'EPCR. A cela s'ajoute une fonction de barrière physique puisque le glycocalyx endothélial empêche le roulement et l'adhésion des cellules immunitaires.

En conditions pathologiques une dégradation du glycocalyx peut être observée et évaluée par la mesure des produits de dégradations plasmatiques tels que le syndécane-1. Ainsi des patients ayant subi un infarctus du myocarde avec segment ST élevé (STEMI) présentent des concentrations circulantes de syndécane-1 et de TM élévées [82]. Dans le sepsis, les concentrations circulantes de syndécane-1 sont associées au risque de coagulation intravasculaire disséminé [83]. Ces résultats récents mettent en évidence le lien direct entre l'état du glycocalyx endothélial et le risque cardiovasculaire.

Il est intéressant de noter que l'immense majorité des études réalisées sur les liens existants entre les compartiments sanguin et pariétal ne prennent pas en compte la présence (ou l'absence) du glycocalyx. Par exemple, dans l'article où nous avons démontré le rôle du FXI dans le développement de la dysfonction vasculaire par l'intermédiaire de l'infiltration monocytaire, j'ai observé le roulement et l'adhésion des cellules immunitaires sur l'endothélium de carotides d'animaux traités à l'AngII sans envisager que cette étape ne puisse être possible que parce que le glycocalyx était dégradé. J'ai par la suite mesuré le syndécane-1 chez des animaux traités à l'AngII et il apparait que les niveaux étaient bien supérieurs à ceux des souris contrôles (ce résultat est visible **Figure 20** p48 de la partie « résultats soutenant le projet »). Il est également à noter que chez les souris contrôles les évènements de roulement et d'adhésion de cellules immunitaires circulantes à l'endothélium sont très rares.

De manière intéressante le glycocalyx a attiré l'attention dans les années 1980 avant de tomber en désuétude pendant près de 25 ans. Depuis 5 à 6 ans l'intérêt de l'étude du glycocalyx augmente de nouveau. Cette variation inhabituelle s'explique en partie par la difficulté que représente l'étude du glycocalyx. En effet, la principale méthode utilisée a longtemps été la microscopie électronique et les études fonctionnelles sont difficiles à réaliser. Cela ne fait que quelques années que d'autres techniques sont utilisées, notamment par la mesure des produits de dégradation. A cela s'ajoute plusieurs techniques d'imagerie permettant d'évaluer de manière directe ou indirecte l'épaisseur du glycocalyx *in vivo*.

Une autre fonction du glycocalyx a récemment été démontrée dans la biologie du VWF. En effet il apparait que le glycocalyx permet au VWF de s'ancrer à la surface des CEs[84]. Un résultat que j'ai obtenu renforce aussi l'hypothèse d'une implication très sous-estimée du glycocalyx endothélial dans l'interface sang-vaisseau. J'ai en effet étudié les modifications de l'hémostase dans un modèle de rat obèse (le rat Zucker) adulte et âgé pour lequel le phénotype vasculaire a été réalisé en parallèle [85]. Il apparait que les modifications de l'hémostase apparaissent très tôt en comparaison des altérations vasculaires ce qui va dans le sens d'une influence causale de l'hémostase sur la fonction vasculaire. L'élément qui est venu encore renforcer cette hypothèse est la forte activité gélatinolytique (MMP-2 et MMP-9) *in situ* visible au niveau de l'endothélium chez les animaux âgés qu'ils soient sains ou obèses (ces résultats sont visibles **Figure 2)** [86]. Les MMPs jouent un rôle majeur dans la dégradation du glycocalyx et cette différence plus importante en fonction de l'âge que de l'obésité est en lien avec les modifications de la fonction vasculaire dégradée de manière plus importante avec l'âge. Un article récent allant dans le sens de cette hypothèse a ainsi montré une dégradation du glycocalyx augmentée durant le vieillissement [87].

Cependant la manière dont le glycocalyx régule le vieillissement vasculaire en interaction avec les facteurs de la coagulation (du point de vue de leurs fonctions cellulaires) et l'infiltration pariétale d'autres protéines et cellules n'a, jusqu'à présent, pas été étudiée.

2. Rôles du glycocalyx des cellules musculaires lisses vasculaires.

Une couche de glycocalyx n'est pas seulement présente autour des CEs, un glycocalyx entoure également les CMLVs et a une importance fonctionnelle au niveau de ces cellules. En effet le glycocalyx des CMLVs a une fonction de modulateur de la prolifération et de la production de NO en fonction des contraintes pulsatiles [88]. Il joue aussi sur le

phénotype des CMLVs à la fois en modifiant l'expression de certains gènes [89] et la motilité des cellules [90]. L'héparane sulfate et la chondroïtine sulfate sont aussi directement impliqués dans la mécanotransduction induite par les contraintes pulsatiles et la réponse contractile des CMLVs [91]. Cette mécanotransduction est realisée par la voie Rho kinase (ROCK)- phosphatase de la chaine légère de la myosine (MLPC) [92]. Le glycocalyx des CMLVs est aussi impliqué dans le remodelage vasculaire induit par les contraintes hémodynamiques. Cet effet il a été montré suite à une dégradation du glycocalyx *via* l'utilisation de hyaluronidase [93]. De plus, une diminution du glycocalyx des CMLVs a été observée suite à un traitement par une concentration en sel élevée destinée à induire une hypertrophie des CMLVs [94].

Le vieillissement provoque un épaississement intimal principalement par l'intermédiaire des CMLVs et une rigidification artérielle associée aux contraintes hémodynamiques et au développement d'une dysfonction endothéliale augmentant les échanges entre le sang et la paroi [95].

Les résultats récents présentés plus haut remis dans le contexte de l'interface sang-vaisseaux laissent penser que le glycocalyx des CEs et des CMLVs serait impliqué dans de nombreuses pathologies.

D. Altération de l'interface sang-vaisseaux : exemple de l'immunothrombose dans les maladies inflammatoires chronique de l'intestin.

Le concept d'IT a été décrit pour la première fois en 2013 [96]. Il désigne une activation adaptée de la coagulation, des plaquettes et des cellules immunitaires pour limiter la diffusion de pathogènes. Ce concept fait l'objet d'une attention croissante en pathologie humaine et est en train de changer profondément l'approche thérapeutique des maladies thromboemboliques. Une dérégulation de l'IT (locale ou touchant d'autres territoires pathologiques) peut être à l'origine de thromboses veineuses ou artérielles dans la microcirculation voire dans la macrocirculation. Les acteurs identifiés et étudiés jusqu'à présent sont les pièges extracellulaires de neutrophiles (NETs). Les NETs peuvent se fixer au VWF [97]. Actuellement cette vision peut être considérée comme réductrice car l'IT implique bien d'autres cellules et molécules que les NETs. Le rôle de l'IT a été décrit principalement jusqu'ici dans des maladies telles que le sepsis ou la polyarthrite rhumatoïde [96].

L'IT pourrait être impliquée dans d'autres pathologies inflammatoires telles que les maladies inflammatoires chroniques de l'intestin (MICI). Les deux complications principales de ces pathologies sont une augmentation du risque de thrombose qui pourrait provenir d'une IT dérégulée et le développement d'une fibrose intestinale et vasculaire. La fibrose vasculaire, en plus d'être provoquée par les aspects inflammatoires de la pathologie pourrait être exacerbée par l'IT et l'activation continuelle de la coagulation et des cellules immunitaires.

1. Les MICI et le risque de thrombose.

Les MICI incluent la maladie de Crohn (MC) et la rectocolite hémorragique (RCH) et sont aussi des facteurs de risque indépendants pour les premiers évènements thrombotiques

ou les thromboses récurrentes. Les larges études de populations ont montré une augmentation du risque de MTEV dans les MICI comparés à la population générale [98].

Les MICI augmentent aussi le risque de récurrence des thromboses comparativement aux patients ayant eu un évènement thrombotique mais pas atteints de MICI [99]. L'activité de la maladie est également un facteur de risque indépendant pour les MTEV. Le risque de thrombose artérielle est également augmenté dans les MICI (infarctus du myocarde, ischémies mésentériques, accidents vasculaires cérébraux) [100]. De la même manière que pour les MTEV le risque de thrombose artérielle augmente avec l'activité de la maladie.

2. Implication des plaquettes dans les MICI.

L'augmentation du compte plaquettaire dans les MICI a été décrit pour la première fois il y a 50 ans [101] puis rapporté dans de nombreux autres travaux (**Figure 16**). Ce phénomène est appelé thrombocytose réactionnelle. Dans les modèles murins de MICI au dextran sulfate de sodium (DSS), la numération plaquettaire ainsi que le renouvellement des plaquettes sont augmentés [102]. Dans ce même modèle les plaquettes activées et agrégées à des cellules immunitaires (neutrophiles, monocytes, lymphocytes) sont augmentées.

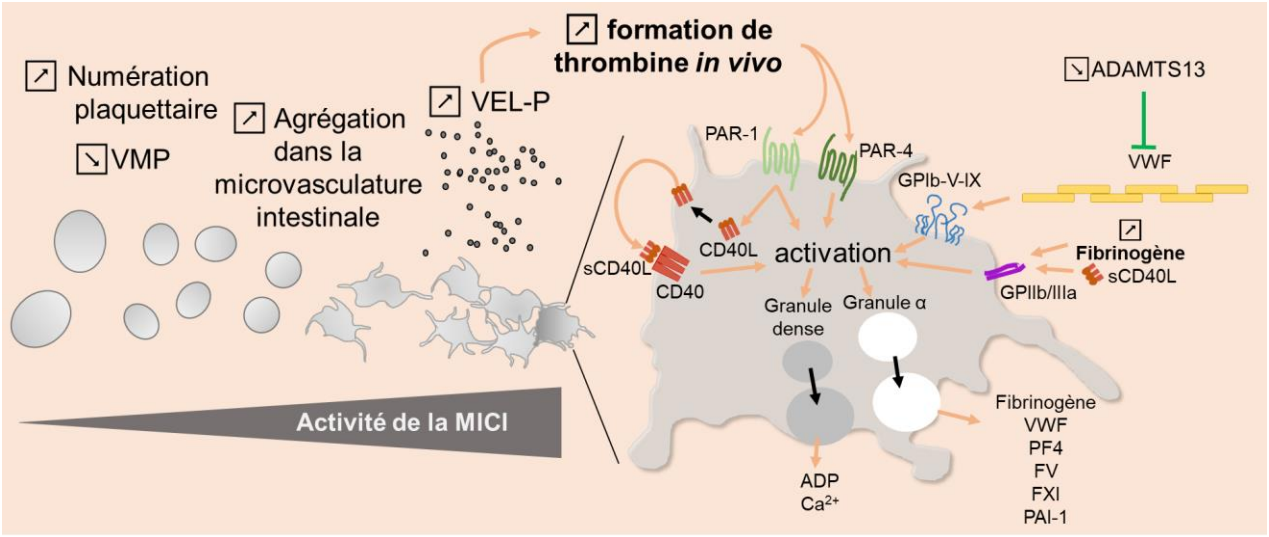

Figure 16. Altération plaquettaire chez les patients atteints de MICI.
Chez les patients atteints de MICI, la numération plaquettaire est augmentée suite à une thrombocytose réactive. De plus, le volume moyen plaquettaire (VMP) est diminué et les larges vésicules extracellulaires dérivées des plaquettes (VEL-P) sont augmentés. Ces vésicules ont un fort pouvoir procoagulant et la génération de thrombine in vivo est augmentée chez les malades en phase active. L'augmentation de la réactivité plaquettaire aboutit à :
- une augmentation des concentrations de facteur von Willebrand (VWF) et de fibrinogène qui activent les plaquettes via les récepteurs GPIIb/IIIa et GPIb-V-IX ;
- une activation des récepteurs activés par les protéases (PAR)-1 et PAR-4.
- une augmentation du relargage des contenus des granules denses et α (fibrinogène, VWF, facteur plaquettaire 4 (PF4), facteur (F) V, XI, ou inhibiteur de l'activateur du plasminogène (PA-1)).

Le volume plaquettaire moyen (VPM) est également modifié par la thrombocytose réactionnelle. Il diminue lors d'un processus inflammatoire et est associé à une augmentation de la production de plaquettes ainsi que leur consommation. Le VPM est lié à l'inflammation et aux maladies thrombotiques [103]. La diminution du VPM dans les MICI est lié à l'activité de la maladie [104]. De manière intéressante le VPM est un bon marqueur dans la MC de la réponse aux anti-TNF-α (Infliximab) [105]. En ce qui concerne la fonction plaquettaire, l'activation et l'agrégation sont augmentées avec l'activité de la maladie [106]. Certains ont montré une augmentation de l'agrégation même pendant les phases inactives de la maladie [107]. Le facteur plaquettaire 4 (PF4) qui est un marqueur de l'activation plaquettaire est augmenté dans les MICI et il est également corrélé à l'activité de la maladie [108]. Il a même été montré une agrégation spontanée des plaquettes dans les MICI traduisant une hypersensibilité de ces cellules [109]. Les récepteurs à la thrombine, les récepteurs activeés par les protéases (PAR)-1 et -4 qui participent à l'activation plaquettaire augmentent l'activation plaquettaire dans la MC [110]. Un autre facteur participant à l'hémostase peut influencer la réactivité plaquettaire dans les MICI : le VWF. Ce facteur est produit en majorité par les CEs et dans une moindre mesure par les cellules précurseurs des plaquettes, les mégacaryocytes. Le VWF est impliqué dans la formation du thrombus *via* sa capacité à transporter le FVIII et à participer à l'activation et l'adhésion plaquettaire par l'intermédiaire du récepteur GPIbα [111]. Les niveaux du VWF circulant sont augmentés dans les MICI et la métalloprotéinase impliquée dans sa dégradation (ADAMTS 13) est diminuée [112]. Les niveaux circulants de VWF sont aussi associés à l'activité de la maladie [113].

Les complexes formés par le VWF et ADAMTS13 sont augmentés quel que soit l'état de la maladie [112]. Il est intéressant de noter que chez les patients souffrant d'hémophilie A et B ou encore de maladie de Willebrand l'incidence des MICI est diminuée [114].

Les plaquettes ont un rôle majeur dans l'hémostase mais de nouvelles fonctions leur ont été attribuées en particulier dans l'inflammation [115]. Elles peuvent participer à l'inflammation en interagissant avec les cellules immunitaires et de la paroi vasculaire. De plus l'activation des plaquettes aboutit à la fois au relargage des molécules inflammatoires et à l'expression membranaire de récepteurs de l'inflammation [116].

Chez les souris traitées au DSS l'expression plaquettaire de l'épitope permettant l'activation du récepteur GPIIb/IIIa est augmentée [102]. Ce récepteur, avec le concours de l'antigène macrophage-1 (Mac-1 ou intégrine $\alpha_M\beta_2$) permet la liaison entre les leucocytes et les plaquettes et leur adhésion à d'autres surfaces cellulaires [117]. Malgré le grand nombre d'études cliniques réalisées sur les inhibiteurs de GPIIb/IIIa aucune n'a été faite dans les MICI [118]. Puisque certains anti-intégrines, notamment $\alpha_4\beta_7$, qui limite le trafic des cellules immunitaires, se sont montrés bénéfiques dans les MICI, le fait de cibler d'autres intégrines notamment impliquées dans le risque thrombotique telles que GPIIb/IIIa pourrait aussi présenter un intérêt thérapeutique.

3. Les altérations de la coagulation dans les MICI.

La conversion de prothrombine en thrombine est l'étape centrale de la coagulation et les marqueurs de l'activation continuelle de cette étape (complexes thrombine-antithrombine (TAT), fragments 1+2 (F1+2 de la prothrombine) sont tous augmentés dans les MICI en phases actives [119–121]. La présence d'une augmentation de ces marqueurs est en revanche bien moins claire dans les phases inactives de la maladie. Un autre marqueur

de l'activation de la coagulation sont les D-dimères, là encore la majorité des études ont montré une augmentation des concentrations circulantes [119,120,122] (mais certaines autres n'ont pas rapporté de différences significatives. [123–125]). Les concentrations en prothrombine ne sont pas différentes [126], et bien que les complexes TAT soient augmentés, il n'y a pas de variation claire de l'AT [119,122]. Concernant la génération de thrombine mesurée *in vitro* par la méthode CAT elle n'est pas différente excepté après ajout de TM pour évaluer l'inhibition de la voie de la PCa et uniquement en présence d'une inflammation importante (évaluée par mesure de la protéine C réactive) [126]. Une autre étude a cependant montré une augmentation de la génération de thrombine uniquement en phase aiguë [127]. Chez des jeunes patients la génération de thrombine était augmentée mais d'autres paramètres telles que le temps de latence étaient augmentés le tout corrélé à l'activité de la maladie [128].

Très récemment un travail portant sur les variations de génération de thrombine chez les patients traités avec un anti-TNFα (infliximab) a été publié [129]. La génération de thrombine était augmentée chez les patients atteints de MICI par rapport à des personnes saines avec et sans TM (1865 (1270-2337) *versus* 2120 (1611-3041) nM x min). De plus un traitement anti-TNFα pendant 22 semaines a permis de diminuer la génération de thrombine (2082 (1678-3041) *versus* 1883 (1339-2929) nM x min). Plus particulièrement le FVIII, le VWF et le fibrinogène étaient diminués de façon significative à la suite de ce traitement.

Le TF a été trouvé comme ayant une fonction délétère dans les modèles expérimentaux de colite [130,131]. L'utilisation d'anticorps dirigés contre le TF dans le modèle au DSS ou chez des souris synthétisant très peu de TF (1% de la concentration normale) a montré une diminution de la migration des cellules immunitaires dans le colon conjointement à une diminution des marqueurs inflammatoires dans les organes.

Pour ce qui est du FVII, les résultats concernant sa variation divergent puisque certains ont observé une augmentation et d'autres une diminution de son activation dans les MICI [122,132]. Les deux études présentent un résultat commun avec une augmentation de l'activité du FVII dans la MC. Le FX a quant à lui été montré comme étant augmenté dans la RCH aigue tandis que le FV a été trouvé augmenté à la fois dans le RCH et dans la MC [119,123,124]. Le FXa n'est pas associé à l'activité de la maladie en dépit du fait que les marqueurs *in vivo* de la coagulation soient augmentés avec l'activité de la maladie [133]. Le FVIII a en revanche été trouvé augmenté dans la plupart des publications [119,122,123]. L'implication du FVIII dans les thromboses veineuses est bien établi et pourrait avoir un rôle également dans les thromboses chez les patients atteints de MICI [134]. Cependant une concentration élevée en FVIII n'est pas associée au risque de récidive de thrombose [99].

Les variations en FXII plasmatique diffèrent en fonction des études [119,120]. Le FXI est l'un des facteurs de la coagulation les plus augmentés dans les MICI quelle que soit l'activité de la maladie [119,120].

L'absence de FIX chez la souris, de la même manière que l'inhibition du FT, est capable de diminuer les symptômes d'une colite induite au DSS en limitant l'infiltration des neutrophiles dans le tissu colique[135]. L'épithélium intestinal est capable de synthétiser le FIX et une activation locale de la coagulation pourrait avoir des effets cellulaires par l'intermédiaire des récepteurs PARs. Il est intéressant de noter en revanche que les souris déficientes en FXII ne sont pas protégées des effets de la colite induite au DSS[136].

Cet effet différentiel entre deux facteurs de la voie intrinsèque pourrait être similaire à celui que nous avions décrit dans le cadre du développement de la dysfonction vasculaire[71]. Les souris déficientes en FXI étaient protégées des effets de l'Ang II en termes de développement de la dysfonction vasculaire tandis que les souris déficientes en FXII n'étaient pas protégées.

4. Formation du caillot et altération de la fibrinolyse au cours des MICI.

De la même manière que pour la majorité des facteurs de la coagulation les concentrations circulantes mesurées en fibrinogène diffèrent en fonction des études. Certains ont montré une augmentation dans la MC et dans la RCH [120,122,128] et d'autres uniquement dans la MC [122,132] ou seulement dans la RCH [121]. Une explication possible provient du fait que le fibrinogène est bien connu comme étant corrélé à l'état inflammatoire, état qui varie énormément au cours de la maladie dans les MICI.

Une diminution du FXIII corrélée à l'activité de la maladie a été montrée chez les patients atteints de MICI[137–139]. Cette diminution pourrait provenir d'une consommation du FXIII dans des microthrombi disséminés dans la microcirculation et les capillaires intestinaux. Ce résultat est en faveur de la présence d'une IT chez ces patients

De la même manière que pour les marqueurs *in vivo* de la fibrine, les tests de temps de coagulation (APTT, temps de céphaline avec activateur, PT : temps de prothrombine) montrent des variations importantes en fonction des études. Si certaines études ne montrent pas de différences de l'APTT ou du PT dans la MC ni la RCH, d'autres ont observé un prolongement des temps de coagulation [119–122]. Il est à noter qu'aucune étude n'a montré de temps de coagulation plus courts dans les MICI.

Tous les résultats ne sont pas clairs concernant la fibrinolyse mais plusieurs études indiquent une altération de la capacité fibrinolytique chez les patients. Les concentrations circulantes en plasminogène sont inchangées chez les patients atteints de MICI [120,123]. Alors que les variations du tPA sont importantes, plusieurs études ont rapporté une augmentation [120,137] tandis que d'autres ont montré une diminution à la fois pour l'antigène et pour l'activité [140,141]. Enfin, certaines études n'ont pas rapporté de différences [142,143]. De manière similaire les concentrations en PAI-1 montrent de larges variations. Cependant la majorité des études a montré une augmentation [120,137,142,144]. Récemment Kaiko *et al*. ont observé que l'expression du PAI-1 était élevée chez les patients atteints de MICI ne répondant pas aux anti-TNF [145]. En bloquant le tPA, le PAI-1 amplifie les altérations de la muqueuse intestinale et son inhibition les réduit. Le PAI-1 peut également interagir avec des composants de la matrice tels que la vitronectine ou le LDL-1, et l'uPA avec son récepteur intervient dans la migration cellulaire [146]. Ainsi, l'inhibition de PAI-1 diminue la migration des CMLVs et la formation de la neointima [147]. Ces effets cellulaires pourraient avoir une importance dans les atteintes vasculaires des MICI. Récemment une étude a montré que le PAI-1 pouvait se lier au FXIa à la surface des CEs aboutissant à sa clairance et dégradation [148]. Ce nouveau mécanisme met en lumière les interactions entre la coagulation, la fibrinolyse et la fonction endothéliale qui pourraient participer à la pathogénèse des MICI. L'augmentation du PAI-1 suggère une diminution de la fibrinolyse tout comme la diminution de l'inhibiteur de la fibrinolyse activable par la thrombine (TAFI) [144].

Concernant les tests intégratifs, le temps de lyse du caillot est prolongé chez les patients atteints de MICI (**Figure 17**) [149]. L'aire sous les courbes de fibrinolyse est aussi plus importante chez les patients ayant déjà présenté un évènement thromboembolique [149].

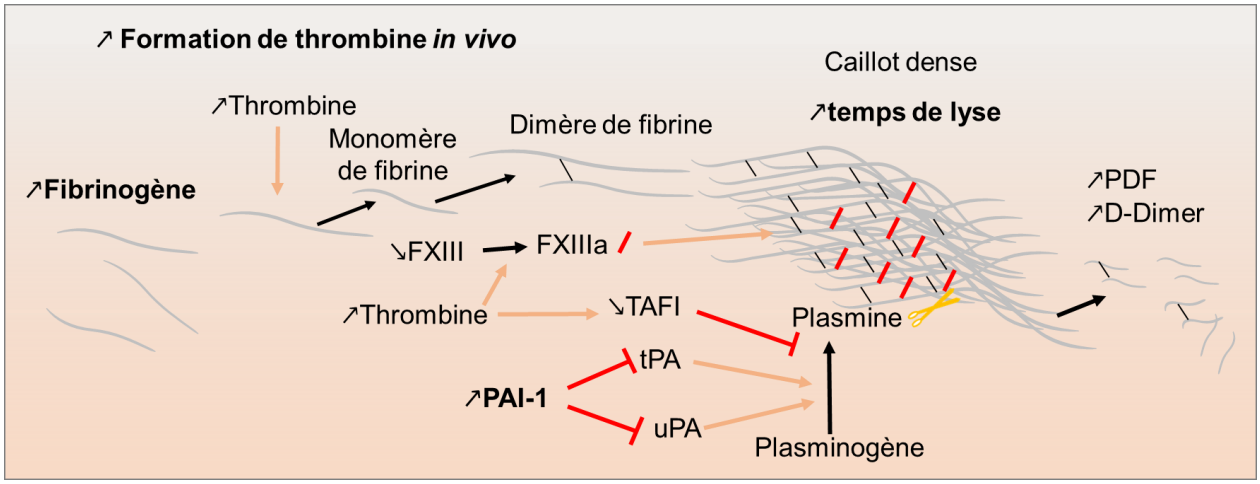

Figure 17. Modification de la fibrinolyse chez les patients atteints de MICI.
Les concentrations de fibrinogène sont augmentées par l'inflammation. La thrombine provoque la polymérisation des fibres de fibrine. De plus la thrombine active le FXIII qui va lier la fibrine et stabiliser le caillot. La fibrinolyse est diminuée du fait de l'augmentation de l'inhibiteur de l'activateur du plasminogène (PAI-1) qui inhibe l'activateur tissulaire du plasminogène (tPA) et l'urokinase, limitant ainsi l'activation de la plasmine. Dans les MICI le caillot est plus dense et le temps de lyse allongé. Les produits de dégradation de la fibrine (PDF) sont augmentés. TAFI : inhibiteur de la fibrinolyse activable par la thrombine.

5. Endothélium vasculaire.

Une dysfonction de l'endothélium peut conduire au relargage de TFPI. C'est le cas des MICI où les patients présentent des concentrations de TFPI circulantes augmentées. De plus ces concentrations sont corrélées aux biomarqueurs du statut inflammatoire et de l'activité de la maladie [150]. Le TFPI et le FT sont tous deux augmentés dans les tissus du colon des patients RCH [151]. De plus chez des patients jeunes atteints de MICI l'activité anticoagulante du TFPI est diminuée [152]. Enfin, l'ajout de TFPI dans du plasma de patients atteints de MICI modifie très peu la génération de thrombine comparé aux contrôles où la diminution est plus importante. Cette résistance au TFPI pourrait expliquer le fait que même avec des augmentations à la fois du TFPI et du FT la balance soit reste en faveur du coté procoagulant.

Il en va de même pour la TM dont les concentrations circulantes sont augmentées alors que dans le même temps l'expression dans les CEs est diminuée [153]. Enfin, l'EPCR présente des variations similaires à celles de la TM et tout comme la TM son expression est diminuée dans la muqueuse colique [153]. La PC ne montre pas de variation dans les MICI [120,122,123] à l'exception d'un seul article ayant observé une augmentation des concentrations de PC dans les RCH en phase active[119]. Les résultats présentés pour le cofacteur de la PCa, la protéine S (PS) sont aussi ambigus avec certaines études montrant des diminutions [120,154] et d'autres pas de variations significatives [119,122,123]. Une concentration en PS basse est généralement associée au risque de thrombose [155]. Il est à noter que la PS est aussi un cofacteur du TFPI et que ce dernier peut aussi inhiber le FXa. Ainsi une altération dans les MICI à la fois de la PS et du TFPI pourrait être d'autant

plus délétère pour moduler et limiter la génération de thrombine. Des déficiences acquises transitoires en PC et PS ont été observées chez un patient atteint de MICI et ayant fait un AVC [156]. Plusieurs autres études ont émis l'hypothèse qu'une altération de la voie de la PC pourrait contribuer au développement de thromboses veineuses [154,157]. De plus la PC, de par son effet protecteur via les PARs, a montré un effet bénéfique au niveau des cellules épithéliales intestinales dans les MICI [158]. A cela s'ajoute le fait que des souris avec des concentrations très faibles en PC présentent un phénotype de colite spontanée pointant une nouvelle fois les interactions très proches entre système de la coagulation et pathologies inflammatoires [153].

Enfin et pour faire le lien avec la partie précédente portant sur les rôles cellulaires des facteurs de la coagulation, un travail récent a permis de montrer que l'épithélium intestinal était capable de synthétiser de la prothrombine. Une fois activée et convertie en thrombine, cette dernière a la capacité de dégrader le biofilm matriciel qui entoure les batteries intestinales et ainsi limite la migration des bactéries à travers l'épithélium[159].

En conclusion, de manière surprenante pour des maladies qui touchent autant de personnes, il n'y a pas de résultats suffisamment forts publiés concernant les modifications de l'hémostase pour conclure sur les facteurs responsables de l'augmentation du risque de thrombose et leurs variations en fonction de la maladie ou de son activité. De plus, d'autres acteurs non considérés jusqu'à présent pourraient intervenir dans la modulation du risque de thrombose dans les MICI. C'est notamment le cas des GRs qui sont des cellules historiquement considérées comme passives vis-à-vis de l'hémostase. En plus de tout cela les GRs sont modifiés dans les MICI et mes résultats de postdoctorat indiquent qu'ils sont aussi importants dans l'IT.

E. Implication des globules rouges dans les MICI.

1. Les globules rouges dans les thromboses.

Historiquement, le risque de thrombose a été associé aux facteurs de la coagulation, aux plaquettes, au flux sanguin et à la paroi vasculaire. Cependant des données récentes suggèrent que l'importance des GRs a été très sous-estimée.

En effet les GRs peuvent, par exemple, s'agglutiner et former des rouleaux. L'agglutination des GRs augmente lorsque le flux sanguin diminue. Dans les microvaisseaux la diminution du flux favorise l'agglutination ce qui peut aboutir à l'occlusion de ces microvaisseaux [160]. L'agglutination des GRs augmente notamment en présence d'une réponse inflammatoire [161].
Les GRs peuvent servir de support cellulaire pour la génération de thrombine [162]. En effet une population de GRs peut exprimer de la phosphatidylsérine à leur surface et permettre la conversion de prothrombine en thrombine [163].
Les caillots artériels sont généralement riches en plaquettes mais les GRs peuvent participer à leur formation en facilitant le transport et l'orientation des plaquettes vers la paroi vasculaire [164].
Les caillots veineux comprennent généralement une forte proportion de GRs [165].

Les globules peuvent exprimer à leur surface des molécules d'adhésion telles que ICAM-4 qui peut par exemple lier le récepteur plaquettaire αIIbβ3 [166]. De manière inverse les GRs pourraient aussi exprimer à leur surface de l'αIIbβ3 [167]. Ainsi les GRs peuvent à la fois faciliter la génération de thrombine, participer au développement du caillot et également à sa stabilisation [163].
Une stase sanguine permet l'adhésion du VWF aux GRs [168]. Ce résultat met en perspective le fait que les GRs peuvent être retenus dans les thrombi veineux en cas de faible flux via leur interaction avec le VWF [169]. Cependant, aucun récepteur n'a été identifié jusqu'à présent à la surface des GRs pour permettre l'adhésion du VWF [168].

Une élévation de l'hématocrite est associée avec une réduction du saignement et une augmentation de la thrombose [170]. Les GRs sont des éléments centraux de l'augmentation de la viscosité du sang et cette viscosité n'augmente pas de manière linéaire avec l'augmentation de l'hématocrite. Le risque de thrombose est augmenté dans un modèle de souris sélectionné pour son hématocrite constitutionnellement élevé [170].

Le modèle de thrombose au chlorure ferrique est le modèle le plus utilisé chez la souris [171]. Dans ce modèle les premières cellules à adhérer à la paroi vasculaire sont les GRs qui, par la suite, permettent de recruter des plaquettes et de former un caillot [172].
Chez des souris anémiques soumises à une thrombose au chlorure ferrique le temps d'occlusion est prolongé [173]. L'effet inverse a été observé chez des souris avec une hématocrite élevée [170]. Ces deux études ont aussi montré l'importance des GRs dans la modulation de la formation du thrombus.

Les marqueurs inflammatoires tels que la CRP sont associés au risque de maladie coronaire [174]. Ces mêmes marqueurs sont aussi associés à l'agglutination des GRs qui peut participer au développement de la maladie en limitant le flux sanguin et les apports en oxygène [175].

Une déficience en fer tout comme des concentrations trop élevées sont associées au risque de thrombose [176]. Chez des souris, l'administration de fer augmente le stress oxydatif et la thrombose artérielle [177].

L'association entre le risque de thrombose et les GRs est bien établie, cependant certaines situations compliquent le tableau. En effet, j'ai observé avec surprise que dans le cadre d'une inflammation chronique élevée associée aux MICI, l'agglutination des GRs limitait l'augmentation du risque de thrombose. Je compte poursuivre ce travail dans mon projet et ai déjà obtenu de nouveaux résultats confirmant mes premières observations.

2. Les globules rouges dans les maladies inflammatoires chroniques de l'intestin.

Une diminution de l'hémoglobine et de l'hématocrite aboutissent à une anémie qui est une complication commune des MICI [178]. Dans les MICI d'autres marqueurs sont utilisés

pour diagnostiquer la présence d'une anémie, c'est le cas de la ferritine ou encore de la transferrine [179].

Il existe deux formes d'anémie associées aux MICI : l'anémie ferriprive et l'anémie inflammatoire chronique. La plus commune est l'anémie ferriprive qui est provoquée par une malabsorption du fer au niveau intestinal à laquelle s'ajoute des saignements du fait de la maladie [180].

L'hépcidine est une hormone qui est secrétée par le foie et régule le métabolisme du fer en particulier au niveau de l'absorption intestinale [181]. Cette hormone permet de réduire la concentration circulante en fer en limitant son relargage par les cellules, en particulier les macrophages et les entérocytes. La diminution en hépcidine augmente l'absorption intestinale en fer et dans les macrophages ce qui conduit à une surconcentration en fer. En revanche, des concentrations en hépcidine trop élevées sont liées à l'anémie inflammatoire. Dans ces conditions la diminution en fer causée par l'hépcidine limite l'érythropoïèse ce qui caractérise l'anémie inflammatoire [182]. De manière inverse une synthèse en hépcidine déficiente pourrait être un facteur favorisant le développement de la maladie dans le cadre des MICI [181].

Les patients atteints de MICI ayant une anémie inflammatoire ont des niveaux circulants en hépcidine plus importants comparativement aux patients souffrant d'anémie ferriprive [183].

Le FXIII peut aussi participer à la rétention des GRs et augmenter la taille du thrombus [184]. Un modèle de souris ayant une mutation pour le fibrinogène a moins de GRs incorporés dans un thrombus. Un résultat similaire a été observé avec l'inhibition du FXIII [184]. De manière intéressante les patients atteints de MICI ont des concentrations circulantes en FXIII diminuées [185]. Cette diminution pourrait être provoquée par une consommation du FXIII au niveau des sites de coagulation ou de formation de microthrombi.

L'augmentation de l'agglutination des GRs est associée à une diminution du flux dans les capillaires et une diminution de l'oxygénation des tissus. La présence d'une forte tendance à l'agglutination des GRs chez les patients atteints de MICI est bien documentée [186]. Cette agglutination des GRs est aussi présente dans les vaisseaux mésentériques de rats traités au DSS [187].

F. Rôles des globules rouges dans la dysfonction vasculaire et implications possibles dans l'immunothrombose.

En plus de leurs rôles dans les thromboses intraluminales les GRs montrent des fonctions dans le développement de l'athérome et ainsi seraient impliqués en amont des thromboses. Delbosc *et al*., ont montré que l'efférocytose des GRs par les cellules de la paroi artérielle, en particulier les CMLVs, déclenchait les processus d'oxydation cellulaires participant au développement précoce de l'athérome [188].

Dans des aortes humaines avec des stries lipidiques, des produits associés aux GRs (hémoglobine, fer ferreux, glycophorin A) sont présents dans la paroi ce qui n'est pas le

cas dans des aortes saines. Ce phénotype a pu être reproduit grâce à une co-culture de GRs senescents et de CMLVs et par l'injection de GRs scénecents à des rats.

L'infiltration des globules rouges dans l'intima ne peut cependant se faire que si l'endothélium ne joue plus son rôle de barrière et que le glycocalyx endothélial est dégradé. Une revue très récente de Jean-Baptiste Michel et José Luis Martin-Ventura a résumé l'état de l'art concernant les rôles des GRs et de l'hémoglobine dans le développement de l'athérosclérose et les pathologies associées[189]. L'implication principale des GRs dans le développement de pathologies vasculaires provient du fer ferreux présent dans l'hème qui en cas d'hémolyse a un très fort pouvoir oxydant. Les CEs et les CMLVs peuvent être affectées par le fer ferreux allant jusqu'à la mort des cellules. Ainsi une hémolyse locale est associée au développement de l'athérosclérose. Ce même processus pourrait aussi avoir son importance dans des pathologies telles que les anévrysmes aortiques abdominaux où la présence d'un thrombus au niveau de la paroi de l'anévrysme provoque une lyse des GRs et un stress oxydant continu sur les cellules pariétales qui dégraderait encore plus la paroi. Le développement de calcifications vasculaires pourrait aussi être associé aux GRs puisque ces calcifications vont provoquer des hémorragies intrapariétales et les GRs lysés vont en retour amplifier le develppement des calcifications.

La toxicité cellulaire directe du fer ferreux de l'hème n'est pas le seul mécanisme par lequel les GRs peuvent altérer la paroi. En effet, l'hème libre a la capacité de chélater le NO ce qui peut provoquer la contraction des CMLVs voire participer au développement de l'hypertension.

Dans les MICI, le rôle des GRs dans le développement des complications vasculaires n'a pas été étudié. En revanche l'augmentation de dégradation du glycocalyx a été observée et est un argument en faveur d'une déstabilisation de la barrière endothéliale permettant aux GRs d'exercer leurs fonctions délétères dans la paroi.

L'implication des GRs dans l'immunothrombose est aussi un concept nouveau qui n'a pas été décrit. Pour reprendre l'exemple des MICI, la présence d'une agglutination des GRs en plus de la dégradation du glycocalyx endothélial va limiter le flux sanguin, en particulier dans les microvaisseaux, et pourrait de ce fait participer à l'IT.

Résumé des points importants et résultats soutenant le projet.

L'importance de l'interface sang-vaisseaux et des fonctions cellulaires des facteurs de la coagulation

Une des particularités des maladies athérothrombotiques est l'épaississement intimal provoqué par une convection de lipides du sang vers la paroi vasculaire. Cette convection comprend aussi des facteurs de la coagulation qui peuvent exercer différentes actions sur les cellules de la paroi vasculaire.

Les thromboses, une complication fréquente et parfois mortelle des MICI.

Les évènements thromboemboliques sont une complication fréquente des MICI [190]. Etant donné la gravité et la fréquence de ces complications une recherche active [191,192] a été menée au cours des dernières décennies sans pouvoir identifier de mécanismes responsables [193]. Point important, il a été montré que ces évènements thromboemboliques différaient de ceux observés dans la population générale [194]. Par exemple, ces patients ne présentent pas de raccourcissement des temps de coagulation et la présence d'un nombre de plaquettes élevé n'est pas associée avec la survenue de thromboses.

L'immunothrombose explique-t-elle le risque thrombotique au cours des MICI ?

Le concept d'IT désigne une activation adaptée de la coagulation, des plaquettes et des effecteurs immunitaires pour limiter la diffusion de pathogènes. Le rôle de l'IT a été décrit dans le sepsis ou la polyarthrite rhumatoïde, mais son rôle au cours des MICI n'est pas connu [96]. L'inflammation peut induire l'agglutination des GRs, mais les répercussions sur la formation des immunothrombi ne sont pas connues. Au cours des MICI l'agglutination des GRs va modifier la rhéologie sanguine et pourrait être l'un des mécanismes de l'IT en limitant la perfusion de l'intestin. Les preuves s'accumulent pour désigner les GRs comme une composante jusque-là peu prise en compte dans l'hémostase [195], mais rien n'est connu concernant leurs rôles dans l'IT. Ainsi l'agglutination des GRs diminue les surfaces phospholipidiques libres disponibles pour les réactions de coagulation et pourrait aussi intervenir dans la modulation du risque thrombotique au cours des MICI. Mes résultats préliminaires sont en faveur de cette hypothèse. J'ai également pu montrer que la voie de signalisation IL-6 et son récepteur (IL-6R)/JAK/Stat3 induisait la synthèse d'alpha-2-macroglobuline (A2M) qui est un inhibiteur de la thrombine. En conditions normales, l'A2M est plasmatique, mais j'ai montré qu'en conditions inflammatoires elle était localisée à la surface des GRs ce qui pourrait limiter le risque de thrombose et participer au rôle protecteur de l'IT (**Figure 18**). L'inhibition de JAK pourrait provoquer une diminution de la synthèse d'A2M chez les patients, levant ainsi l'inhibition basale de la thrombine tout en désagrégeant les GRs, ce qui aboutirait à une augmentation du risque de thrombose. Par ailleurs, il a récemment été montré que le VWF pouvait se lier aux GRs uniquement dans des conditions de faible flux ce qui correspond aux conditions provoquées par l'IT dans la circulation mésentérique [196]. Le VWF apparait de plus en plus comme une molécule centrale de l'IT. Nos résultats préliminaires vont dans ce sens (**Figure 19**).

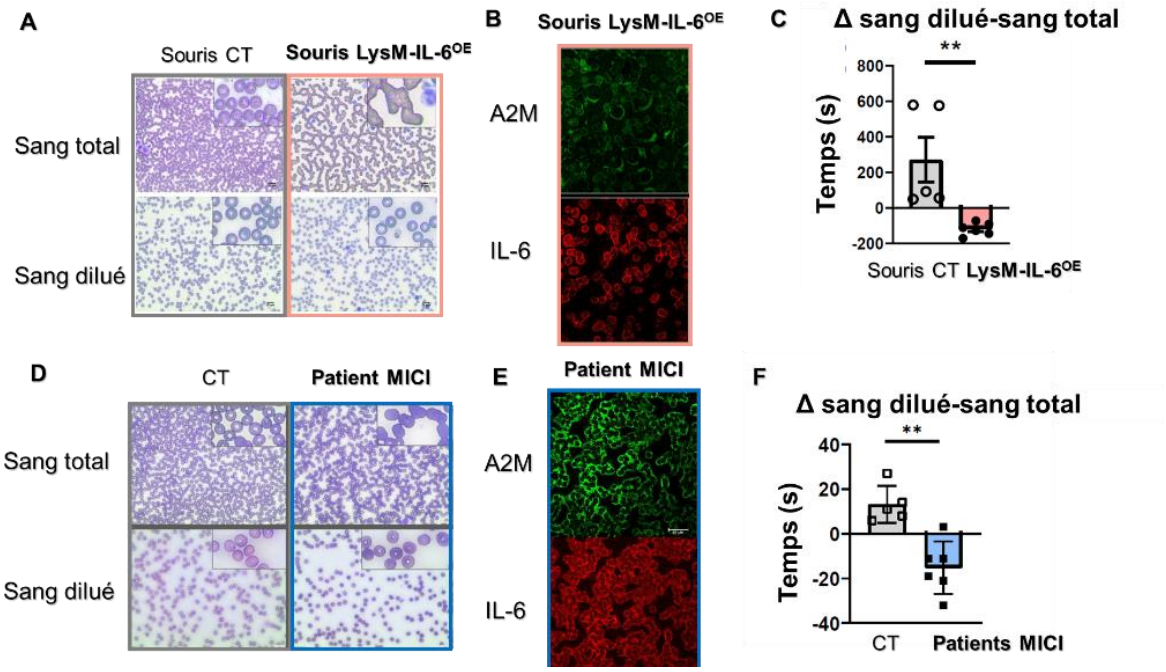

Figure 18. Implication des globules rouges dans la modification du temps de coagulation en sang total.

*La surexpression d'IL-6 chez la souris induit une agglutination des globules rouges (**A**) et la dilution du sang désagrège les globules rouges. Les globules rouges agrégés portent à leur surface de grandes quantités d'IL-6 et d'A2M (**B**). Un temps de coagulation en sang total montre un allongement du temps de formation du caillot chez ces souris tandis que la dilution du sang (désagrégeant les globules rouges) aboutit à une formation accélérée du caillot (**C**). Ce résultat montre l'importance des surfaces des globules rouges combinée à l'anticoagulation par l'A2M dans la formation du caillot. Toutes ces observations ont été trouvées également chez des patients atteints de MICI (**D, E, F**).*

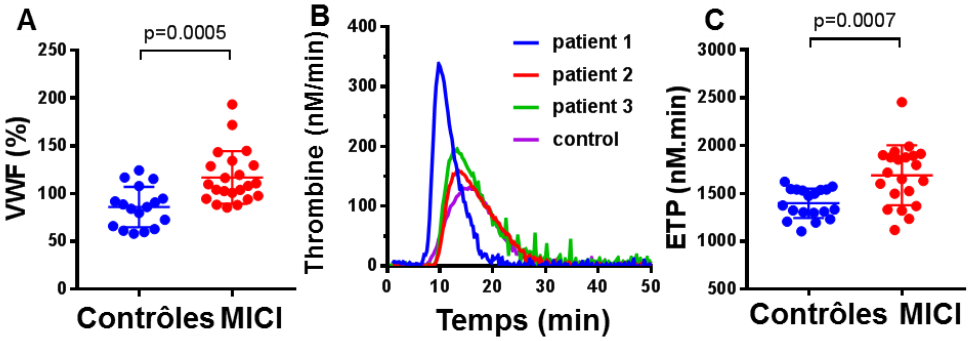

Figure 19. Modification de marqueurs liés à la nétose chez les patients atteints de MICI.

*Concentrations circulantes en VWF au cours des MICI (**A**), courbes de génération de thrombine en plasma riche en plaquettes (**B**) et potentiel thrombinique correspondant (ETP) (**C**).*

<u>La dégradation du glycocalyx endothélial, première étape du déséquilibre de l'interface sang-vaisseaux.</u>

Pour que les facteurs de la coagulation et les cellules circulantes, en particulier les GRs puissent interagir avec les cellules de la paroi il est nécessaire qu'ils migrent dans

la paroi depuis le sang. Cela nécessite une altération de la barrière endothéliale et en particulier du glycocalyx endothélial qui recouvre ces cellules (**Figure 20**).

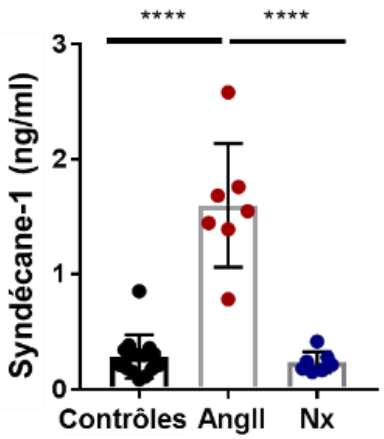

Figure 20. L'augmentation des concentrations circulantes de syndécane-1 indique une dégradation du glycocalyx endothélial.

Des rats hypertendus par traitement à l'angiotensine II présentent une dégradation du glycocalyx plus importante que des rats hypertendus par néphrectomie 5/6ème. Cette différence pourrait résulter de l'inflammation induite par l'angiotensine II tandis que l'hypertension par néphrectomie est une hypertension volume-dépendant

<u>*Le pouvoir oxydatif des GRs altère les CMLVs*</u>**.**

En plus de leur implication dans l'hémostase, les GRs vont exercer un stress oxydant et une chélation du NO en cas d'hémolyse *via* l'hème. L'efférocytose des GRs par les CMLVs va participer à la modification du phénotype de ces cellules et participer au développement de pathologies vasculaires (**Figure 21**).

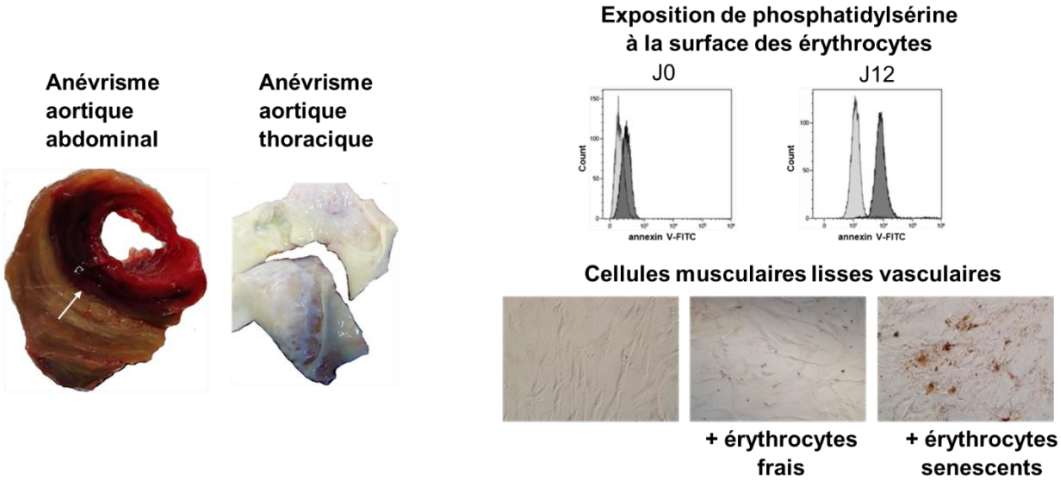

Figure 21. Implication du thrombus intraluminal dans les anevrysmes aortiques abdominaux (AAA).

Les globules rouges piégés dans les thrombi des AAA peuvent être dégradés par les CMLVs de la paroi et induire un stress oxydant pouvant conduire à la mort de ces cellules.

G. Hypothèses générales de travail et objectifs.

Mes hypothèses de travail sont les suivantes (**Figure 22**) *:*

1. Les GRs et leurs interactions avec les autres cellules circulantes (plaquettes, leucocytes) jouent un rôle essentiel dans le processus d'IT au cours des MICI.

2. La voie de signalisation IL-6/JAK/Stat3/A2M ainsi que le VWF sont des acteurs moléculaires majeurs de l'IT et sa dérégulation aboutit à des thromboses pathologiques au cours des MICI.

3. La dégradation du glycocalyx endothélial dépend du stress oxydant plus que des contraintes physiques provoquées par le sang et elle est responsable d'un déséquilibre de l'interface sang-vaisseaux.

4. Les GRs provoquent un stress oxydant pariétal qui modifie les CMLVs et participe au développement de la dysfonction vasculaire.

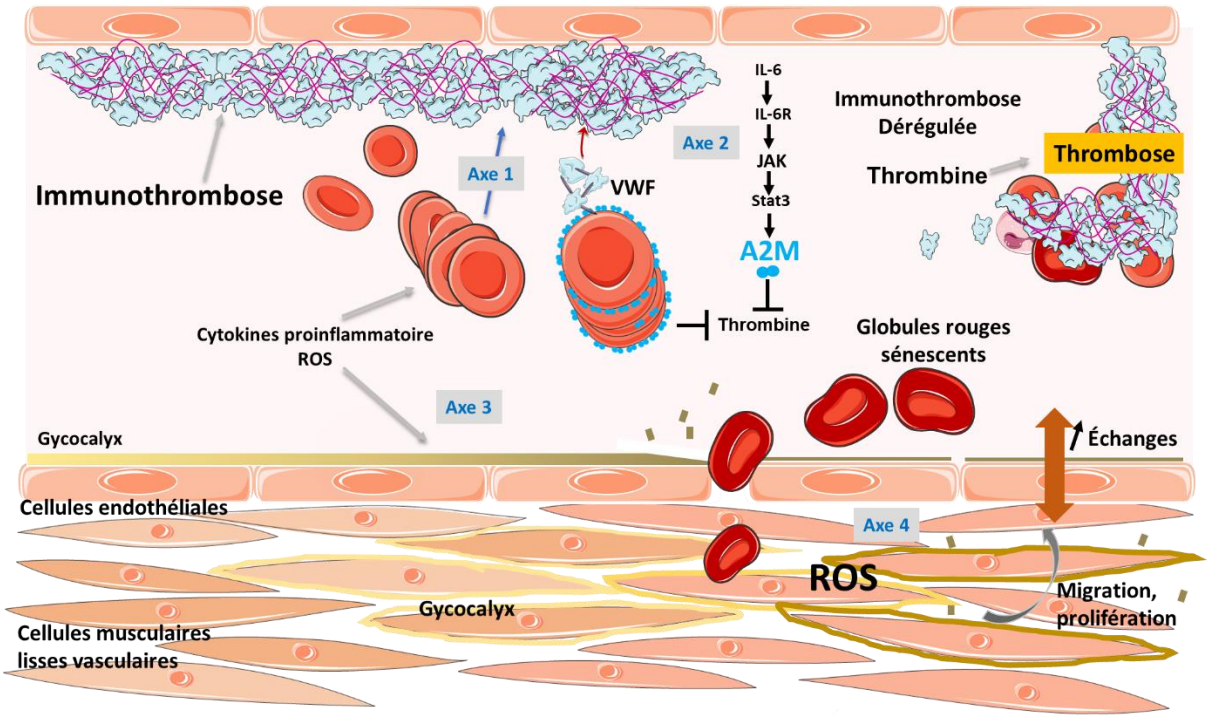

Figure 22. Résumé des hypothèses de travail et axes de recherche.

H. Approches méthodologiques : modèles animaux et cohortes de patients.

Pour répondre aux différentes questions posées, des modèles cellulaires, des modèles transgéniques et de traitements murins et également des cohortes de patients seront utilisés.

Modèles cellulaires

Des cultures primaires de CEs et de CMLVs aortiques humaines commerciales seront utilisées pour les aspects moléculaires des hypothèses de travail. Des GRs sénescents ou non seront préparés pour être mis en contacts avec les CMLVs.

Modèles murins

- LysM cre^{+} IRG^{+} (DsRed-express, Cre-mediated GFP) permettant le suivi de lignées cellulaires.
- Des souris déficientes en VWF.
- Un modèle de souris unique généré à Mayence qui surexpriment l'IL-6 dans les cellules LysM^{+} (neutrophiles, monocytes, macrophages).
- Des souris surexprimant JAK2 dans les cellules LysM^{+}.

Plus particulièrement pour les MICI, j'utiliserai le modèle de colite au sulfate de dextran sodique (DSS) avec une administration dans l'eau de boisson (solution de 3 à 5 %) pendant 5 jours. Ce modèle est maîtrisé depuis plusieurs années dans l'équipe 2 de l'UMR_S 1256. Les modèles « aigu, chronique et en rémission » peuvent être obtenus en modifiant les concentrations de DSS et la fréquence d'administration. Tous les modèles de colite expérimentale seront induits à 2 mois. Il existe une disparité d'induction d'une colite en fonction du fond génétique et du sexe. Ainsi, le modèle DSS sera réalisé sur un fond génétique C57BL/6, chez des mâles. La saisine pour ces travaux a été obtenue (APAFiS #23548).

- Des souris contrôles traitées avec de l'ang II par minipompes osmotiques.

Pour l'étude du glycocalyx et de l'implication des GRs sur les cellules de la paroi vasculaire, des souris seront traitées avec l'ang II par minipompe osmotique (0,5 mg/kg/jour pendant 2 semaines) pour induire une inflammation permettant la dégradation du glycocalyx, et seront ensuite traitées avec des GRs sénescents (injection *iv* de 2.10^{7} cellules).

Cohortes ciblées de patients

Cette étude sera réalisée en collaboration avec le service de gastroentérologie et l'équipe 2 de l'unité UMR_S 1256 (Pr L Peyrin-Biroulet). J'utiliserai la cohorte I-BANK (NCT03809728) qui est issue d'une étude prospective monocentrique de patients atteints de MICI, diagnostiqués sur des critères radiologiques, endoscopiques et histologiques. Les premières inclusions ont débuté fin 2019. La population finale atteindra 1000 patients d'ici 2024. Toutes les caractéristiques de la maladie, les traitements ainsi que les complications thrombotiques seront notamment disponibles

chez ces patients. Cette MICI-thèque est hébergée dans la biobanque du CHRU de Nancy (CRB Lorrain). Elle contiendra du sérum, du plasma citraté ainsi que des cellules mononuclées sanguines périphériques isolées par ficoll auxquels j'aurai accès pour mon projet. J'aurai également accès aux pièces chirurgicales que j'utiliserai pour l'étude histologique des microvaisseaux et des capillaires mésentériques.

Pour explorer les causes de la dégradation du glycocalyx endothélial, j'utiliserai les prélèvements plasmatiques de la cohorte TELARTA (NCT02176941) qui est une cohorte de patients recrutés car devant subir diverses procédures chirurgicales (chirurgie vasculaire, chirurgie orthopédique, chirurgie plastique, greffe de rein, pose de défibrillateur). Cette cohorte initialement créée pour étudier les variations de taille des télomères en fonction du vieillissement vasculaire est très bien phénotypée au niveau cardiovasculaire et au niveau du statut inflammatoire (CRP, IL-6, IL-1β). Ainsi je pourrai faire le lien entre les marqueurs de la dégradation du glycocalyx et le vieillissement cardiovasculaire physiologique ou pathologique.

I. Axes de recherche.

1. Axe de recherche 1 : Rôle des cellules circulantes dans l'immunothrombose au cours des MICI.

Il est nécessaire dans un premier temps de définir la contribution des cellules circulantes à l'IT au cours des MICI. Dans le but de visualiser les immunothrombi et de mesurer la perfusion des microvaisseaux mésentériques, des souris LysM cre^{+} IRG^{+} traitées au DSS seront utilisées. Ce modèle de souris permettra de discriminer en microscopie confocale intravitale les GRs et les plaquettes (par leur taille) et les neutrophiles qui fluoresceront dans le vert (GFP). Ainsi je pourrai évaluer la contribution de chaque type cellulaire à l'IT. *In vitro,* l'agglutination des GRs sera mesurée par la vitesse de sédimentation (VS), la réalisation de frottis sanguins et une étude protéomique des protéines membraniaires pouvant participer à la modulation de l'agglutination sera faite en utilisant la plateforme dédiée de l'unité mixte de service (UMS) 2008 de la faculté de médecine de l'UL. Des marquages pour l'IL-6, l'A2M et le VWF seront réalisés sur les frottis sanguin. De plus, un temps de coagulation en sang total non dilué sera réalisé pour intégrer l'effet des agrégats de GRs à l'hémostase (j'ai développé ce test lors de mon postdoctorat). Les interactions entre cellules circulantes seront étudiées chez les souris LysM cre^{+} IRG^{+} traitées au DSS directement en microscopie confocale intravitale mais également en cytométrie en flux. Le VWF pouvant se fixer en faible flux aux globules, la même expérience sera réalisée avec des GRs (fluorescents) de souris LysM cre^{+} IRG^{+}.

Dans la cohorte I-BANK la VS des GRs sera corrélée aux différents paramètres de l'IT (activation *in vivo* des plaquettes de la coagulation et génération de NETs) dans le but d'évaluer ceux impliqués dans leur agglutination. De la même manière le VWF et l'A2M circulants seront mesurés par ELISA pour permettre une stratification des patients. Cette stratification prendra aussi en compte l'état de la maladie (phase active ou rémission) et le traitement. Les interactions entre GRs, plaquettes et cellules immunitaires seront évaluées par cytométrie en flux.

Chez les souris traitées au DSS et chez les patients de la cohorte, les marqueurs de l'activation *in vivo* de l'hémostase et les marqueurs de la formation et de la dégradation des NETs (ADN, myéloperoxidase, complexes ADN-histones, FT, polyphosphates, protéine disulfure isomérase, …) seront mesurés. *In vitro,* l'évaluation de l'activation des cellules circulantes impliquées dans la génération et l'inhibition de la thrombine et/ou impliquées dans la formation des NETs (GRs, plaquettes, monocytes, neutrophiles) permettront de mieux cibler l'implication de chaque type cellulaire dans l'IT.

Enfin, une étude plus fondamentale des GRs sera nécessaire. En effet, j'ai montré lors de mon postdoctorat que l'agglutination de GRs ne dépendait pas d'interactions récepteur/ligand et que l'inhibition du récepteur de l'A2M ne changeait pas cette capacité d'agglutination. Ainsi, une étude physico-chimique des GRs sera réalisée en collaboration avec le LIBio (Jordane Jasniewski, MCF, LIBio, Nancy). Cette caractérisation consistera dans un premier temps en l'étude du potentiel Zêta des GRs, c'est-à-dire la mesure de la charge de surface des cellules. De plus, des mesures de microrhéologie par diffusion dynamique de la lumière seront mises en œuvre pour évaluer l'impact de la viscosité du sang sur l'agglutination des GRs. La composition de la membrane des GRs sera étudiée en dosant notamment chaque type de phospholipides par chromatographie sur couche mince couplée à un détecteur à ionisation de flamme (Iatroscan) et les caractéristiques macroscopiques des GRs, à savoir hydrophobie/hydrophilie et caractère acide/base de Lewis par une approche de mesure d'affinité aux solvants. Une mesure de la fluidité membranaire par anisotropie de fluorescence est envisagée si des différences de composition en phospholipides sont relevées. Enfin, des mesures de pH cytoplasmique et de potentiel de membrane pourront être réalisées par des approches de fluorescence spécifique.

2. Axe de recherche 2 : Implication du VWF et de l'A2M dans l'immunothrombose et sa dérégulation au cours des MICI.

Pour disséquer les acteurs moléculaires dérégulant l'IT, des souris déficientes pour le VWF et traitées au DSS seront utilisées. L'activité des cellules immunitaires circulantes sera évaluée par microscopie intravitale du tissu mésentérique. Les leucocytes seront marqués avec de l'acridine orange et le nombre de cellules roulant et adhérant à l'endothélium sera évalué à l'aide d'enregistrements vidéo [197]. De plus, l'ischémie mésentérique étant l'événement thrombotique le plus courant au cours des MICI un modèle de thrombose au $FeCl_3$ sera réalisé chez ces souris traitées au DSS pour évaluer la participation du VWF à ces thromboses.

Un modèle de souris surexprimant l'IL-6 dans les cellules $LysM^+$ (disponible dans le cadre de ma collaboration avec le CTH de Mayence) sera utilisé pour étudier le rôle de cette cytokine dans l'IT. Concernant l'étude des thrombi des microvaisseaux de l'intestin et les interactions entre les cellules circulantes, elle se fera par microscopie confocale intravitale. Ces souris ne seront pas traitées au DSS car elles développent spontanément un phénotype proche d'une MICI. Ce phénotype est à lier au fait que l'IL-6 est l'une des cytokines principales augmentées dans les MICI.

J'utiliserai également des souris surexprimant JAK2 (Jackson labs) qui permettront d'induire la production d'A2M sans IL-6. Une dérégulation de l'IT chez ces souris permettrait de mettre en évidence l'importance de l'interaction entre IL-6 et A2M et ainsi de mieux cibler les candidats potentiels pour limiter l'IT dépendante de l'agglutination des GRs. Il sera nécessaire de différencier les effets indirects de l'IL-6 (*via* la liaison à l'A2M) par rapport aux effets directs via la voie de signalisation JAK1/2 puisque des inhibiteurs de l'IL-6 et de son récepteur ont été testés au cours des MICI.

Chez les patients de la cohorte I-BANK, les niveaux circulants de VWF libre ou sous forme multimérique ainsi que l'ADAMTS13 qui permet le clivage des multimètres seront mesurés. Les pièces chirurgicales permettront de réaliser des histologies des microvaisseaux et capillaires intestinaux dans le but d'observer les microthrombi et caractériser leur composition cellulaire ainsi que la distribution de VWF et d'A2M.

3. Axe de recherche 3 : Altération du glycocalyx endothelial et répercutions sur l'interface sang-vaisseaux.

Des travaux récents ont montré un rôle inattendu des GRs dans le développement de la plaque d'athérome [188]. La transmigration des GRs dans la paroi peut arriver lorsque les CEs ne remplissent plus leur rôle de barrière. Cette barrière repose en particulier sur la présence du glycocalyx endothélial que j'ai trouvé endommagé dans un contexte inflammatoire. L'objectif sera d'explorer les interactions entre les cellules circulantes et les CEs (altération du glycocalyx endothélial, insudation des molécules plasmatiques dans la paroi vasculaire) provoquées par l'inflammation systémique et leurs conséquences dans la modulation de l'IT.

Pour évaluer l'importance de la dégradation du glycocalyx j'utiliserai un modèle de souris traité à l'AngII et mesurerai la dégradation du glycocalyx par dosage des produits de dégradation (syndécane-1) mais également des protéines anticoagulantes normalement présentes à la surface de l'endothélium (TM, EPCR). *In vivo*, l'épaisseur du glycocalyx peut être estimée grâce au changement de perfusion avant et après le passage d'un leucocyte dans un capillaire [87]. Toujours *in vivo*, le glycocalyx pourra être directement visualisé à l'aide d'anticorps dirigés contre l'héparane sulfate et la connexine 43 [198]. L'estimation de l'insudation de cellules et de protéines du sang dans la paroi sera réalisée par histologie des facteurs de la coagulation (prothrombine, fibrinogène) et des cellules circulantes (macrophages, lymphocytes, neutrophiles, plaquettes, GRs). Les modifications structurales seront quant à elles étudiées par colorations histologiques (trichrome de Masson, Safranin O et Alcian pour les glycosaminoglycanes (GAG)) [199]. Les MMP-2 et -9 seront marquées *in situ* comme marqueurs de dégradation du glycocalyx (observation faite chez les rats Zucker). La différenciation des CMLVs sera évaluée avec différents marqueurs : α-SMA, SM22α SM-MHC, smootheline, caldesmone, calponine and vimentine. La capacité proliférative des CMLVs sera mesurée à l'aide de BrDU et la senescence avec des marquages de la β-galactosidase, de p16 et de p21. Enfin la production de ROS sera quantifiée avec la sonde fluorescente CM-H2DCFDA.

Au niveau cellulaire des CEs des GRs seront utilisés. Les CEs seront traitées avec des GRs, sénescents ou non, pour évaluer la dégradation du glycocalyx. Les techniques utilisées seront les mêmes que celles présentées précédemment.

Pour évaluer l'importance des relations entre dégradation du glycocalyx et état cardiovasculaire, les marqueurs de dégradation du glycocalyx seront mesurés dans la cohorte TELARTA dont les patients ont été phénotypés pour les paramètres cardiovasculaires et de l'inflammation. Ceci pourra confirmer les résultats trouvés chez les souris.

De plus, l'état du glycocalyx endothélial pourra aussi être mesuré chez les patients de la cohorte IBANK et corrélé au type et à l'état de la maladie. Une technique *in vivo* pourra aussi être utilisée : le Glycocheck, un microscope sublingual qui mesure l'épaisseur du glycocalyx à l'aide de la distance entre les GRs circulants et la surface de l'endothélium. Ce microscope permet également de voir la présence d'agrégats de GRs chez l'homme.

4. Axe de recherche 4 : Implication des globules rouges dans la dysfonction vasculaire.

Les réactions d'immunothrombose pourraient participer au développement des anomalies vasculaires et j'ai récemment montré que le VWF était présent dans l'intima avec remodelage des plaques d'athéromes et induisait la prolifération des CMLVs. A cela s'ajoute les fonctions pro-oxydantes des GRs sur les CMLVs qui pourraient, directement ou dans un contexte d'immunothrombose, exacerber le développement de la dysfonction vasculaire. L'objectif sera d'étudier l'implication des GRs dans le remodelage vasculaire.

Chez des souris déficientes en VWF et traitées au DSS le phénotype artériel sera évalué : mesures de pression artérielle par télémétrie, rigidité artérielle (VOP), structure et composition de la paroi et réactivité vasculaire (carotide et artère mésentérique). Concernant l'hémostase, la modification des propriétés anticoagulantes de l'endothélium sera étudiée au même titre que les propriétés procoagulantes des CMLVs (mesure de la thrombomoduline soluble et de l'expression de FT et de TFPI). De la même manière que pour l'axe 3 l'insudation sanguine dans la paroi sera mesurée.

In vitro, des cultures de CMLVs en présence de GRs sénescents ou non seront réalisées. Les altérations fonctionnelles provoquées par les GRs seront évaluées au même titre que les marqueurs de différenciation et les répercussions sur l'activation de la coagulation. L'implication du VWF dans l'exacerbation de ces phénomènes sera également évaluée.

La présence d'altérations dépendantes des GRs chez des patients sera visualisée via l'histologie de tissus vasculaires (aortes, carotides) de personnes saines ou présentant des pathologies vasculaires (athérosclérose, anévrysme) provenant de la biobanque constituée par Jean-Baptiste Michel.

L'une des poursuites de ce travail se fera via l'étude du glycocalyx des CMLVs. Des CMLVs aortiques humaines en culture seront traitées avec un mélange d'héparanase et de hyaluronidase. Les interactions cellule-matrice au niveau des adhésions focales seront visualisées à l'aide de la kinase FA (FAK), de l'activation de l'intégrine α_v et de leur activation. La dynamique des adhésions focales en présence ou absence de

glycocalyx pourra être visualisée avec un microscope TIRF (total internal reflaxtion fluoresence microscopy) en collaboration avec l'UMR CNRS 7213 (Strasbourg, P. Rondé).

5. Résultats attendus.

Ce projet permettra d'identifier les causes de l'augmentation du risque de thromboses liée à l'IT dérégulée ainsi que les implications des GRs et du glycocalyx dans le développement de la dysfonction vasculaire.

Les données obtenues devraient permettre :

1) La découverte d'un profil biologique prothrombotique chez les patients MICI et donc l'identification de sous-groupes présentant un risque plus élevé de thrombose et pour lesquels un traitement antithrombotique pourrait être envisagé. Cette approche préventive s'inscrirait ainsi dans le cadre d'une médecine de précision.

2) Le développement de nouvelles approches thérapeutiques ayant une fonction anti-thrombotique ciblée et également anti-inflammatoire, par exemple en ciblant les mécanismes d'action de l'A2M, du VWF et l'agglutination des GRs pour prévenir la dérégulation de l'IT.

3) Une meilleure compréhension des implications respectives du glycocalyx endothélial et des GRs dans le développement de pathologies vasculaires. La restauration d'un glycocalyx endothélial fonctionnel et l'inhibition du VWF à l'aide d'anticorps à domaine variable unique (nanobody) pourront être testées à moyen terme.

Les avancées de ce projet pourront être applicables à d'autres maladies inflammatoires chroniques qui touchent au total un Français sur 10.

J. Activités de direction et collaborations.

J'ai commencé à coordonner mon groupe dans l'équipe d'accueil en participant à la supervision à la fois de doctorants et d'étudiants en master travaillant sur mon projet (**Figure 23**). J'ai également déjà déposé une demande de financement à la Région (Financement CHU-Région) pour faire venir à Nancy une postdoctorante de Mayence qui est compétente sur les aspects de l'hémostase et immunitaire de mon projet. Je consoliderai les financements déjà obtenus en postulant cette année à une ANR jeunes chercheurs et dans les prochaines années à des demandes bi-nationales (France-Allemagne, ANR-DFG) et européennes. Concernant les ressources techniques, je peux compter sur l'UMS2008 (IBSLOR) où l'UMR_S 1116 accueille la plateforme de cytométrie.

Je souhaite poursuivre la formation d'étudiants en master pour les préparer au concours de l'école doctorale BioSE. J'encourage également mes étudiants à s'investir à différents niveaux à l'université, que ce soit dans les conseils scientifiques (Pôle Biologie/Médecine/Santé, conseil scientifique de l'université), dans l'association des doctorants, ou encore à l'école doctorale puisque toutes ces activités m'ont beaucoup apporté lors de mon doctorat.

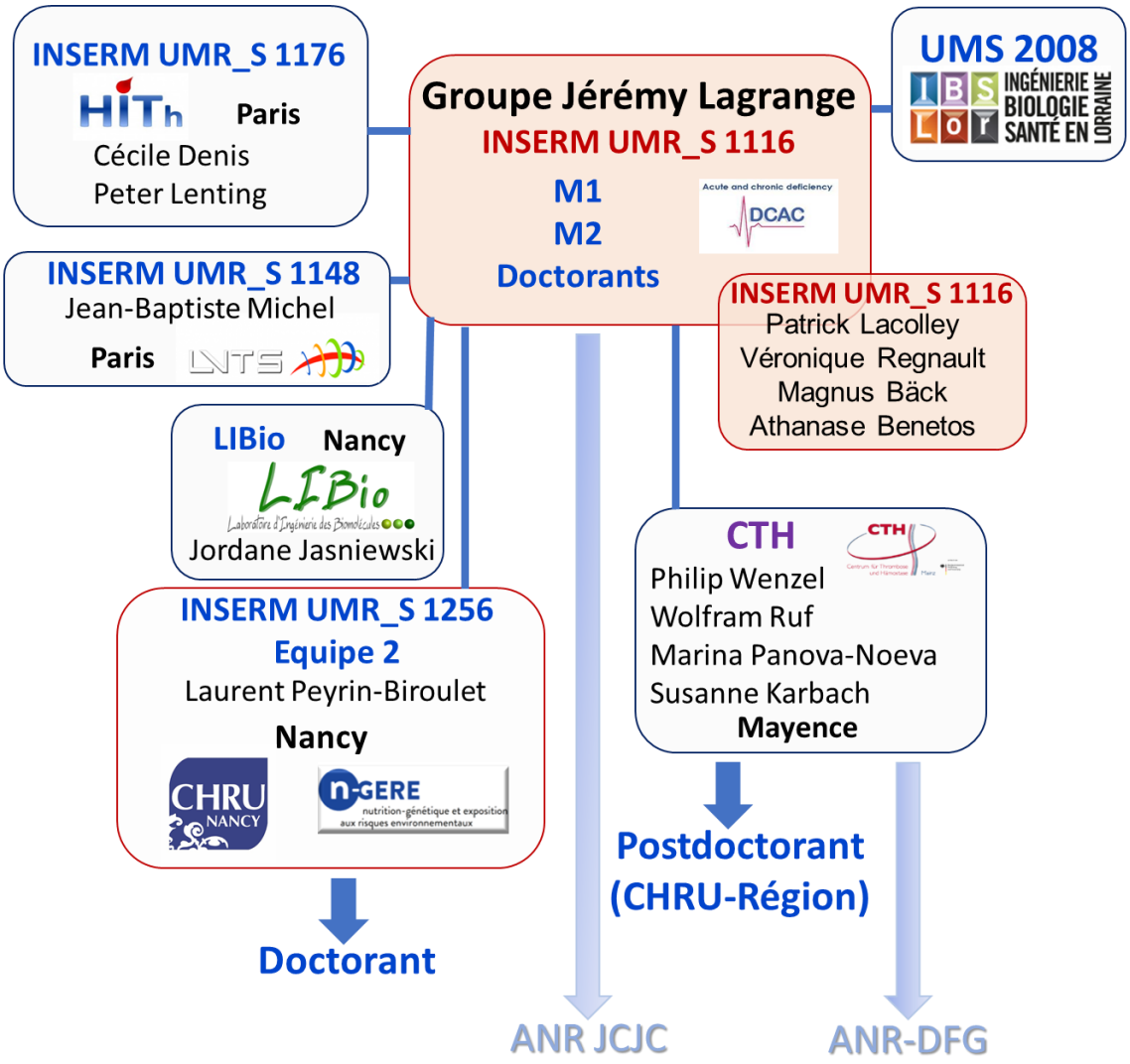

Figure 23 Résumé de l'environnement de recherche et des collaborations

J'ai établi des collaborations locales, nationales et internationales qui me permettront de mener à bien mon projet. A la faculté de médecine de Nancy je peux compter sur l'UMR_S 1256 « Nutrition – génétique et exposition aux risques environnementaux (Dir. Pr Jean-Louis Guéant) et en particulier l'équipe 2 « Interactions métaboliques-génomiques en médecine personnalisée et thérapeutique innovante de la maladie inflammatoire chronique de l'intestin » (Pr Laurent Peyrin-Biroulet) ayant l'expertise de la physiopathologie des MICI et des modèles de colite expérimentale ainsi que des approches translationnelles *via* la Plateforme de Recherche sur les Maladies Inflammatoires Chroniques de l'Intestin du CHRU de Nancy. J'aurai également accès aux prélèvements de la cohorte TELARTA constituée par Athanase Benetos (UMR _S 1116). Toujours au niveau local, j'ai établi une collaboration avec Jordane Jasnieswki, MCF au laboratoire LIBio à l'ENSAIA pour ce qui concerne les mesures physico-chimiques des GRs.

Au niveau national je bénéficierai de l'aide de Cécile Denis (directrice de l'UMR_S 1176) et Peter Lenting, spécialistes du VWF et qui ont produit les souris déficientes en VWF. Je bénéficierai également de toute l'expérience de Jean-Baptiste Michel (DR

INSERM émérite) au niveau de la physiopathologie cardiovasculaire et également *via* la large biobanque de tissus qu'il a constitué.

Au niveau international je poursuivrai des collaborations avec mon laboratoire de postdoctorat (Pr Wolfram Ruf, directeur du CTH, Pr Philip Wenzel, Dr Marina Panova-Noeva, directeurs d'équipes au CTH). J'utiliserai notamment la plateforme intravitale pour les parties du projet relatives au glycocalyx sur les souris LysM cre^{+} IRG^{+}. Je poursuis aussi d'autres projets sur l'implication du FXI, de l'HO-1 et l'implication des inhibiteurs du FXa et de la thrombine sur la génération de thrombine. A cela s'ajoute ma collaboration avec le Dr Susanne Karbach (également directrice d'équipe au CTH) qui a mis au point les souris surexprimant l'IL-6 et m'a permis d'étudier les modifications de l'hémostase chez ces souris. Je continue également une collaboration établie lors que mon doctorat pour le travail portant sur le rat Zucker avec Kennedy Cruickshank et Chris Faulkes à Londres (Kings College et Queen Mary University) concernant un projet portant sur le rat taupe nu. Ces animaux peuvent vivre près de 30 ans sans présenter de vieillissement vasculaire. Leur étude fera également partie de la thèse qui commencera en fin d'année. Enfin, je travaille avec Magnus Bäck (Pr au Karolinska Institutet) qui a constitué plusieurs cohortes qui pourront être utilisées pour pousser l'exploration des implications physiopathologiques de l'altération du glycocalyx des CEs.

VIII. References.

1. Zannad, F. *et al.* Rivaroxaban in Patients with Heart Failure, Sinus Rhythm, and Coronary Disease. *N. Engl. J. Med.* **379**, 1332–1342 (2018).
2. Lagrange, J. *et al.* Endothelial mineralocorticoid receptor activation enhances endothelial protein C receptor and decreases vascular thrombosis in mice. *FASEB J. Off. Publ. Fed. Am. Soc. Exp. Biol.* **28**, 2062–2072 (2014).
3. Didelot, M. *et al.* Platelet aggregation impacts thrombin generation assessed by calibrated automated thrombography. *Platelets* 1–6 (2017) doi:10.1080/09537104.2017.1356452.
4. Makhoul, S. *et al.* Rivaroxaban Effects Illustrate the Underestimated Importance of Activated Platelets in Thrombin Generation Assessed by Calibrated Automated Thrombography. *J. Clin. Med.* **8**, (2019).
5. Lagrange, J. *et al.* Characterization of Thrombin Generation Curve Shape in Presence of Platelets from Acute Venous Thromboembolism Patients. *J. Clin. Med.* **9**, (2020).
6. Lagrange, J. *et al.* The VWF/LRP4/αVβ3-axis represents a novel pathway regulating proliferation of human vascular smooth muscle cells. *Cardiovasc. Res.* (2021) doi:10.1093/cvr/cvab042.
7. Oparil, S. *et al.* Hypertension. *Nat. Rev. Dis. Primer* **4**, 18014 (2018).
8. Wilcox, J. N., Noguchi, S. & Casanova, J. Extrahepatic synthesis of factor VII in human atherosclerotic vessels. *Arterioscler. Thromb. Vasc. Biol.* **23**, 136–141 (2003).
9. Borissoff, J. I. *et al.* Early atherosclerosis exhibits an enhanced procoagulant state. *Circulation* **122**, 821–830 (2010).
10. Marti, C. N. *et al.* Endothelial dysfunction, arterial stiffness, and heart failure. *J. Am. Coll. Cardiol.* **60**, 1455–1469 (2012).
11. Yilmaz, H. *et al.* Association of ambulatory arterial stiffness index with sEPCR in newly diagnosed hypertensive patients. *Ren. Fail.* **37**, 1409–1413 (2015).
12. Lip, G. Y. & Gibbs, C. R. Does heart failure confer a hypercoagulable state? Virchow's triad revisited. *J. Am. Coll. Cardiol.* **33**, 1424–1426 (1999).
13. Lacolley, P., Regnault, V., Nicoletti, A., Li, Z. & Michel, J.-B. The vascular smooth muscle cell in arterial pathology: a cell that can take on multiple roles. *Cardiovasc. Res.* **95**, 194–204 (2012).
14. Ruf, W. & Riewald, M. *Regulation of Tissue Factor Expression*. (Landes Bioscience, 2013).
15. Østerud, B. Tissue factor expression in blood cells. *Thromb. Res.* **125 Suppl 1**, S31-34 (2010).
16. Østerud, B. & Bjørklid, E. *Blood-Borne Tissue Factor (Including Microparticles)*. (Landes Bioscience, 2013).
17. Rao, L. V. M., Kothari, H. & Pendurthi, U. R. Tissue Factor: Mechanisms of Decryption. *Front. Biosci. Elite Ed.* **4**, 1513–1527 (2012).
18. Wolberg, A. S., Monroe, D. M., Roberts, H. R. & Hoffman, M. R. Tissue factor de-encryption: ionophore treatment induces changes in tissue factor activity by phosphatidylserine-dependent and -independent mechanisms. *Blood Coagul. Fibrinolysis Int. J. Haemost. Thromb.* **10**, 201–210 (1999).
19. Owens, A. P. & Mackman, N. Role of tissue factor in atherothrombosis. *Curr. Atheroscler. Rep.* **14**, 394–401 (2012).
20. Schulz, C., Engelmann, B. & Massberg, S. Crossroads of coagulation and innate immunity: the case of deep vein thrombosis. *J. Thromb. Haemost. JTH* **11 Suppl 1**, 233–241 (2013).
21. Osterud, B. & Bjorklid, E. Tissue factor in blood cells and endothelial cells. *Front. Biosci. Elite Ed.* **4**, 289–299 (2012).
22. Rothmeier, A. S. *et al.* Caspase-1-mediated pathway promotes generation of thromboinflammatory microparticles. *J. Clin. Invest.* **125**, 1471–1484 (2015).
23. Subramaniam, S. *et al.* Distinct contributions of complement factors to platelet activation and fibrin formation in venous thrombus development. *Blood* **129**, 2291–2302 (2017).
24. von Brühl, M.-L. *et al.* Monocytes, neutrophils, and platelets cooperate to initiate and propagate venous thrombosis in mice in vivo. *J. Exp. Med.* **209**, 819–835 (2012).
25. Toomey, J. R., Kratzer, K. E., Lasky, N. M., Stanton, J. J. & Broze, G. J. Targeted disruption of the murine tissue factor gene results in embryonic lethality. *Blood* **88**, 1583–1587 (1996).
26. Carmeliet, P. *et al.* Role of tissue factor in embryonic blood vessel development. *Nature* **383**, 73–75 (1996).
27. Reinhardt, C. *et al.* Protein disulfide isomerase acts as an injury response signal that enhances fibrin generation via tissue factor activation. *J. Clin. Invest.* **118**, 1110–1122 (2008).
28. Schaffner, F. & Ruf, W. Tissue factor and PAR2 signaling in the tumor microenvironment. *Arterioscler. Thromb. Vasc. Biol.* **29**, 1999–2004 (2009).

29. Uusitalo-Jarvinen, H. *et al.* Role of protease activated receptor 1 and 2 signaling in hypoxia-induced angiogenesis. *Arterioscler. Thromb. Vasc. Biol.* **27**, 1456–1462 (2007).
30. Cirillo, P. *et al.* Tissue factor binding of activated factor VII triggers smooth muscle cell proliferation via extracellular signal-regulated kinase activation. *Circulation* **109**, 2911–2916 (2004).
31. Marutsuka, K. *et al.* Protease-activated receptor 2 (PAR2) mediates vascular smooth muscle cell migration induced by tissue factor/factor VIIa complex. *Thromb. Res.* **107**, 271–276 (2002).
32. Rothmeier, A. S. *et al.* Identification of the integrin-binding site on coagulation factor VIIa required for proangiogenic PAR2 signaling. *Blood* **131**, 674–685 (2018).
33. Haga, J. H., Li, Y.-S. J. & Chien, S. Molecular basis of the effects of mechanical stretch on vascular smooth muscle cells. *J. Biomech.* **40**, 947–960 (2007).
34. Matsumoto, Y. *et al.* Fluid shear stress attenuates tumor necrosis factor-alpha-induced tissue factor expression in cultured human endothelial cells. *Blood* **91**, 4164–4172 (1998).
35. Regnault, V. *et al.* Tissue factor pathway inhibitor: a new link among arterial stiffness, pulse pressure, and coagulation in postmenopausal women. *Arterioscler. Thromb. Vasc. Biol.* **31**, 1226–1232 (2011).
36. Fu, Y. *et al.* Adenovirus-mediated tissue factor pathway inhibitor gene transfer induces apoptosis by blocking the phosphorylation of JAK-2/STAT-3 pathway in vascular smooth muscle cells. *Cell. Signal.* **24**, 1909–1917 (2012).
37. Hembrough, T. A., Ruiz, J. F., Papathanassiu, A. E., Green, S. J. & Strickland, D. K. Tissue factor pathway inhibitor inhibits endothelial cell proliferation via association with the very low density lipoprotein receptor. *J. Biol. Chem.* **276**, 12241–12248 (2001).
38. Folsom, A. R., Wu, K. K., Rosamond, W. D., Sharrett, A. R. & Chambless, L. E. Prospective study of hemostatic factors and incidence of coronary heart disease: the Atherosclerosis Risk in Communities (ARIC) Study. *Circulation* **96**, 1102–1108 (1997).
39. Eidelman, R. S. & Hennekens, C. H. Fibrinogen: a predictor of stroke and marker of atherosclerosis. *Eur. Heart J.* **24**, 499–500 (2003).
40. Lu, P. *et al.* Pro-inflammatory effect of fibrinogen and FDP on vascular smooth muscle cells by IL-6, TNF-α and iNOS. *Life Sci.* **88**, 839–845 (2011).
41. Yamaguchi, T. *et al.* Involvement of interleukin-6 in the elevation of plasma fibrinogen levels in lung cancer patients. *Jpn. J. Clin. Oncol.* **28**, 740–744 (1998).
42. Lominadze, D., Dean, W. L., Tyagi, S. C. & Roberts, A. M. Mechanisms of fibrinogen-induced microvascular dysfunction during cardiovascular disease. *Acta Physiol. Oxf. Engl.* **198**, 1–13 (2010).
43. Ge, M., Ryan, T. J., Lum, H. & Malik, A. B. Fibrinogen degradation product fragment D increases endothelial monolayer permeability. *Am. J. Physiol.* **261**, L283-289 (1991).
44. Gomibuchi, H. *et al.* Development of hyperfibrinogenemia in spontaneously hypertensive and hyperlipidemic rats: a potentially useful animal model as a complication of hypertension and hyperlipidemia. *Exp. Anim. Jpn. Assoc. Lab. Anim. Sci.* **56**, 1–10 (2007).
45. Vasse, M. *et al.* Regulation of fibrinogen biosynthesis by cytokines, consequences on the vascular risk. *Haemostasis* **26 Suppl 4**, 331–339 (1996).
46. Naito, M., Nomura, H., Iguchi, A., Thompson, W. D. & Smith, E. B. Effect of crosslinking by factor XIIIa on the migration of vascular smooth muscle cells into fibrin gels. *Thromb. Res.* **90**, 111–116 (1998).
47. AbdAlla, S., Lother, H., Langer, A., el Faramawy, Y. & Quitterer, U. Factor XIIIA transglutaminase crosslinks AT1 receptor dimers of monocytes at the onset of atherosclerosis. *Cell* **119**, 343–354 (2004).
48. Wenzel, P. *et al.* Lysozyme M-positive monocytes mediate angiotensin II-induced arterial hypertension and vascular dysfunction. *Circulation* **124**, 1370–1381 (2011).
49. Nahrendorf, M. *et al.* Factor XIII deficiency causes cardiac rupture, impairs wound healing, and aggravates cardiac remodeling in mice with myocardial infarction. *Circulation* **113**, 1196–1202 (2006).
50. Haack, K. K. V. *et al.* A novel bioassay for detecting GPCR heterodimerization: transactivation of beta 2 adrenergic receptor by bradykinin receptor. *J. Biomol. Screen.* **15**, 251–260 (2010).
51. Aspelin, T. *et al.* β-blockade abolishes the augmented cardiac tPA release induced by transactivation of heterodimerised bradykinin receptor-2 and β2-adrenergic receptor in vivo. *Thromb. Haemost.* **112**, 951–959 (2014).
52. Redmond, E. M. *et al.* Effect of pulse pressure on vascular smooth muscle cell migration: the role of urokinase and matrix metalloproteinase. *Thromb. Haemost.* **81**, 293–300 (1999).

53. Cullen, J. P. *et al.* Ethanol inhibits pulse pressure-induced vascular smooth muscle cell migration by differentially modulating plasminogen activator inhibitor type 1, matrix metalloproteinase-2 and -9. *Thromb. Haemost.* **94**, 639–645 (2005).
54. Nieman, M. T. Protease-activated receptors in hemostasis. *Blood* **128**, 169–177 (2016).
55. Kahn, M. L., Nakanishi-Matsui, M., Shapiro, M. J., Ishihara, H. & Coughlin, S. R. Protease-activated receptors 1 and 4 mediate activation of human platelets by thrombin. *J. Clin. Invest.* **103**, 879–887 (1999).
56. Kahn, M. L. *et al.* A dual thrombin receptor system for platelet activation. *Nature* **394**, 690–694 (1998).
57. Gieseler, F., Ungefroren, H., Settmacher, U., Hollenberg, M. D. & Kaufmann, R. Proteinase-activated receptors (PARs) - focus on receptor-receptor-interactions and their physiological and pathophysiological impact. *Cell Commun. Signal. CCS* **11**, 86 (2013).
58. Vu, T. K., Hung, D. T., Wheaton, V. I. & Coughlin, S. R. Molecular cloning of a functional thrombin receptor reveals a novel proteolytic mechanism of receptor activation. *Cell* **64**, 1057–1068 (1991).
59. Nakanishi-Matsui, M. *et al.* PAR3 is a cofactor for PAR4 activation by thrombin. *Nature* **404**, 609–613 (2000).
60. Riewald, M., Petrovan, R. J., Donner, A. & Ruf, W. Activated protein C signals through the thrombin receptor PAR1 in endothelial cells. *J. Endotoxin Res.* **9**, 317–321 (2003).
61. Chung, S.-W., Park, J.-W., Lee, S.-A., Eo, S.-K. & Kim, K. Thrombin promotes proinflammatory phenotype in human vascular smooth muscle cell. *Biochem. Biophys. Res. Commun.* **396**, 748–754 (2010).
62. Mihara, K. *et al.* Thrombin-Mediated Direct Activation of Proteinase-Activated Receptor-2: Another Target for Thrombin Signaling. *Mol. Pharmacol.* **89**, 606–614 (2016).
63. Kataoka, H. *et al.* Protease-activated receptors 1 and 4 mediate thrombin signaling in endothelial cells. *Blood* **102**, 3224–3231 (2003).
64. Hamilton, J. R., Moffatt, J. D., Frauman, A. G. & Cocks, T. M. Protease-activated receptor (PAR) 1 but not PAR2 or PAR4 mediates endothelium-dependent relaxation to thrombin and trypsin in human pulmonary arteries. *J. Cardiovasc. Pharmacol.* **38**, 108–119 (2001).
65. Griffin, C. T., Srinivasan, Y., Zheng, Y. W., Huang, W. & Coughlin, S. R. A role for thrombin receptor signaling in endothelial cells during embryonic development. *Science* **293**, 1666–1670 (2001).
66. McNamara, C. A. *et al.* Thrombin stimulates proliferation of cultured rat aortic smooth muscle cells by a proteolytically activated receptor. *J. Clin. Invest.* **91**, 94–98 (1993).
67. Borissoff, J. I., Spronk, H. M. H., Heeneman, S. & ten Cate, H. Is thrombin a key player in the 'coagulation-atherogenesis' maze? *Cardiovasc. Res.* **82**, 392–403 (2009).
68. Nguyen, K. T. *et al.* Cyclic strain increases protease-activated receptor-1 expression in vascular smooth muscle cells. *Hypertens. Dallas Tex 1979* **38**, 1038–1043 (2001).
69. Lehoux, S., Lemarié, C. A., Esposito, B., Lijnen, H. R. & Tedgui, A. Pressure-induced matrix metalloproteinase-9 contributes to early hypertensive remodeling. *Circulation* **109**, 1041–1047 (2004).
70. Tokunou, T. *et al.* Thrombin induces interleukin-6 expression through the cAMP response element in vascular smooth muscle cells. *Arterioscler. Thromb. Vasc. Biol.* **21**, 1759–1763 (2001).
71. Kossmann, S. *et al.* Platelet-localized FXI promotes a vascular coagulation-inflammatory circuit in arterial hypertension. *Sci. Transl. Med.* **9**, (2017).
72. Sabri, A. *et al.* Mechanisms of protease-activated receptor-4 actions in cardiomyocytes. Role of Src tyrosine kinase. *J. Biol. Chem.* **278**, 11714–11720 (2003).
73. Al-Ani, B. *et al.* Activation of proteinase-activated receptor 2 stimulates soluble vascular endothelial growth factor receptor 1 release via epidermal growth factor receptor transactivation in endothelial cells. *Hypertens. Dallas Tex 1979* **55**, 689–697 (2010).
74. Houle, S., Papez, M. D., Ferazzini, M., Hollenberg, M. D. & Vergnolle, N. Neutrophils and the kallikrein-kinin system in proteinase-activated receptor 4-mediated inflammation in rodents. *Br. J. Pharmacol.* **146**, 670–678 (2005).
75. Fisslthaler, B., Schini-Kerth, V. B., Fleming, I. & Busse, R. Thrombin receptor expression is increased by angiotensin II in cultured and native vascular smooth muscle cells. *Cardiovasc. Res.* **38**, 263–271 (1998).
76. Antoniak, S. *et al.* Protease-Activated Receptor 1 Contributes to Angiotensin II-Induced Cardiovascular Remodeling and Inflammation. *Cardiology* **136**, 258–268 (2017).

77. Touat, Z. *et al.* Dilation-dependent activation of platelets and prothrombin in human thoracic ascending aortic aneurysm. *Arterioscler. Thromb. Vasc. Biol.* **28**, 940–946 (2008).
78. Stoop, A. A., Lupu, F. & Pannekoek, H. Colocalization of thrombin, PAI-1, and vitronectin in the atherosclerotic vessel wall: A potential regulatory mechanism of thrombin activity by PAI-1/vitronectin complexes. *Arterioscler. Thromb. Vasc. Biol.* **20**, 1143–1149 (2000).
79. Zannad, F. *et al.* Rivaroxaban in Patients with Heart Failure, Sinus Rhythm, and Coronary Disease. *N. Engl. J. Med.* (2018) doi:10.1056/NEJMoa1808848.
80. Oshima, K., Haeger, S. M., Hippensteel, J. A., Herson, P. S. & Schmidt, E. P. More than a biomarker: the systemic consequences of heparan sulfate fragments released during endothelial surface layer degradation (2017 Grover Conference Series). *Pulm. Circ.* **8**, 2045893217745786 (2018).
81. Reitsma, S., Slaaf, D. W., Vink, H., van Zandvoort, M. A. M. J. & oude Egbrink, M. G. A. The endothelial glycocalyx: composition, functions, and visualization. *Pflugers Arch.* **454**, 345–359 (2007).
82. Frydland, M. *et al.* Plasma Concentration of Biomarkers Reflecting Endothelial Cell- and Glycocalyx Damage are Increased in Patients With Suspected ST-Elevation Myocardial Infarction Complicated by Cardiogenic Shock. *Shock Augusta Ga* **50**, 538–544 (2018).
83. Ikeda, M. *et al.* Circulating syndecan-1 predicts the development of disseminated intravascular coagulation in patients with sepsis. *J. Crit. Care* **43**, 48–53 (2018).
84. Kalagara, T. *et al.* The endothelial glycocalyx anchors von Willebrand factor fibers to the vascular endothelium. *Blood Adv.* **2**, 2347–2357 (2018).
85. Sloboda, N. *et al.* Fatty acids impair endothelium-dependent vasorelaxation: a link between obesity and arterial stiffness in very old Zucker rats. *J. Gerontol. A. Biol. Sci. Med. Sci.* **67**, 927–938 (2012).
86. Lagrange, J. *et al.* Implication of Free Fatty Acids in Thrombin Generation and Fibrinolysis in Vascular Inflammation in Zucker Rats and Evolution with Aging. *Front. Physiol.* **8**, 949 (2017).
87. Machin, D. R. *et al.* Advanced age results in a diminished endothelial glycocalyx. *Am. J. Physiol. Heart Circ. Physiol.* **315**, H531–H539 (2018).
88. Kang, H., Fan, Y. & Deng, X. Vascular smooth muscle cell glycocalyx modulates shear-induced proliferation, migration, and NO production responses. *Am. J. Physiol. Heart Circ. Physiol.* **300**, H76-83 (2011).
89. Shi, Z.-D., Abraham, G. & Tarbell, J. M. Shear stress modulation of smooth muscle cell marker genes in 2-D and 3-D depends on mechanotransduction by heparan sulfate proteoglycans and ERK1/2. *PloS One* **5**, e12196 (2010).
90. Shi, Z.-D., Wang, H. & Tarbell, J. M. Heparan sulfate proteoglycans mediate interstitial flow mechanotransduction regulating MMP-13 expression and cell motility via FAK-ERK in 3D collagen. *PloS One* **6**, e15956 (2011).
91. Ainslie, K. M., Garanich, J. S., Dull, R. O. & Tarbell, J. M. Vascular smooth muscle cell glycocalyx influences shear stress-mediated contractile response. *J. Appl. Physiol. Bethesda Md 1985* **98**, 242–249 (2005).
92. Kang, H. *et al.* Vascular smooth muscle cell glycocalyx mediates shear stress-induced contractile responses via a Rho kinase (ROCK)-myosin light chain phosphatase (MLCP) pathway. *Sci. Rep.* **7**, 42092 (2017).
93. Liu, J. *et al.* Vascular Cell Glycocalyx-Mediated Vascular Remodeling Induced by Hemodynamic Environmental Alteration. *Hypertens. Dallas Tex 1979* **71**, 1201–1209 (2018).
94. Bkaily, G., Simon, Y., Menkovic, I., Bkaily, C. & Jacques, D. High salt-induced hypertrophy of human vascular smooth muscle cells associated with a decrease in glycocalyx. *J. Mol. Cell. Cardiol.* **125**, 1–5 (2018).
95. Lacolley, P., Regnault, V. & Avolio, A. P. Smooth muscle cell and arterial aging: basic and clinical aspects. *Cardiovasc. Res.* **114**, 513–528 (2018).
96. Engelmann, B. & Massberg, S. Thrombosis as an intravascular effector of innate immunity. *Nat. Rev. Immunol.* **13**, 34–45 (2013).
97. Lenting, P. J., Casari, C., Christophe, O. D. & Denis, C. V. von Willebrand factor: the old, the new and the unknown. *J. Thromb. Haemost. JTH* **10**, 2428–2437 (2012).
98. Murthy, S. K. & Nguyen, G. C. Venous thromboembolism in inflammatory bowel disease: an epidemiological review. *Am. J. Gastroenterol.* **106**, 713–718 (2011).
99. Novacek, G. *et al.* Inflammatory bowel disease is a risk factor for recurrent venous thromboembolism. *Gastroenterology* **139**, 779–787, 787.e1 (2010).
100. Kirchgesner, J. *et al.* Increased risk of acute arterial events in young patients and severely active IBD: a nationwide French cohort study. *Gut* **67**, 1261–1268 (2018).

101. Morowitz, D. A., Allen, L. W. & Kirsner, J. B. Thrombocytosis in chronic inflammatory bowel disease. *Ann. Intern. Med.* **68**, 1013–1021 (1968).
102. Yan, S. LS. *et al.* Platelet abnormalities during colonic inflammation. *Inflamm. Bowel Dis.* **19**, 1245–1253 (2013).
103. Aliosmanoglu, I. *et al.* Can mean platelet volume be a new risk factor in portal venous thrombosis? *Clin. Appl. Thromb. Off. J. Int. Acad. Clin. Appl. Thromb.* **19**, 433–436 (2013).
104. Liu, Z. *et al.* Prevention of experimental colitis in SCID mice reconstituted with CD45RBhigh CD4+ T cells by blocking the CD40-CD154 interactions. *J. Immunol. Baltim. Md 1950* **164**, 6005–6014 (2000).
105. Sobolewska, A., Włodarczyk, M., Stec-Michalska, K., Fichna, J. & Wiśniewska-Jarosińska, M. Mean Platelet Volume in Crohn's Disease Patients Predicts Sustained Response to a 52-Week Infliximab Therapy: A Pilot Study. *Dig. Dis. Sci.* **61**, 542–549 (2016).
106. Collins, C. E., Cahill, M. R., Newland, A. C. & Rampton, D. S. Platelets circulate in an activated state in inflammatory bowel disease. *Gastroenterology* **106**, 840–845 (1994).
107. Andoh, A. *et al.* Increased aggregation response of platelets in patients with inflammatory bowel disease. *J. Gastroenterol.* **41**, 47–54 (2006).
108. Ye, L. *et al.* Serum platelet factor 4 is a reliable activity parameter in adult patients with inflammatory bowel disease. *Medicine (Baltimore)* **96**, (2017).
109. Webberley, M. J., Hart, M. T. & Melikian, V. Thromboembolism in inflammatory bowel disease: role of platelets. *Gut* **34**, 247–251 (1993).
110. Schmid, W. *et al.* Increased responsiveness to thrombin through protease-activated receptors (PAR)-1 and -4 in active Crohn's disease. *J. Crohns Colitis* **8**, 495–503 (2014).
111. Broos, K., Feys, H. B., De Meyer, S. F., Vanhoorelbeke, K. & Deckmyn, H. Platelets at work in primary hemostasis. *Blood Rev.* **25**, 155–167 (2011).
112. Cibor, D. *et al.* Levels and activities of von Willebrand factor and metalloproteinase with thrombospondin type-1 motif, number 13 in inflammatory bowel diseases. *World J. Gastroenterol.* **23**, 4796–4805 (2017).
113. Stevens, T. R. *et al.* Circulating von Willebrand factor in inflammatory bowel disease. *Gut* **33**, 502–506 (1992).
114. Thompson, N. P., Wakefield, A. J. & Pounder, R. E. Inherited disorders of coagulation appear to protect against inflammatory bowel disease. *Gastroenterology* **108**, 1011–1015 (1995).
115. Stokes, K. Y. & Granger, D. N. Platelets: a critical link between inflammation and microvascular dysfunction. *J. Physiol.* **590**, 1023–1034 (2012).
116. Voudoukis, E., Karmiris, K. & Koutroubakis, I. E. Multipotent role of platelets in inflammatory bowel diseases: A clinical approach. *World J. Gastroenterol. WJG* **20**, 3180–3190 (2014).
117. Zarbock, A., Polanowska-Grabowska, R. K. & Ley, K. Platelet-neutrophil-interactions: linking hemostasis and inflammation. *Blood Rev.* **21**, 99–111 (2007).
118. Ley, K., Rivera-Nieves, J., Sandborn, W. J. & Shattil, S. Integrin-based Therapeutics: Biological Basis, Clinical Use and New Drugs. *Nat. Rev. Drug Discov.* **15**, 173–183 (2016).
119. Kume, K., Yamasaki, M., Tashiro, M., Yoshikawa, I. & Otsuki, M. Activations of coagulation and fibrinolysis secondary to bowel inflammation in patients with ulcerative colitis. *Intern. Med. Tokyo Jpn.* **46**, 1323–1329 (2007).
120. Alkim, H., Ayaz, S., Alkim, C., Ulker, A. & Sahin, B. Continuous active state of coagulation system in patients with nonthrombotic inflammatory bowel disease. *Clin. Appl. Thromb. Off. J. Int. Acad. Clin. Appl. Thromb.* **17**, 600–604 (2011).
121. Shen, J. *et al.* Biomarkers of altered coagulation and fibrinolysis as measures of disease activity in active inflammatory bowel disease: A gender-stratified, cohort analysis. *Thromb. Res.* **123**, 604–611 (2009).
122. Yazici, A. *et al.* Thrombophilic Risk Factors in Patients With Inflammatory Bowel Disease. *Gastroenterol. Res.* **3**, 112–119 (2010).
123. Dolapcioglu, C. *et al.* Coagulation parameters in inflammatory bowel disease. *Int. J. Clin. Exp. Med.* **7**, 1442–1448 (2014).
124. Lam, A., Borda, I. T., Inwood, M. J. & Thomson, S. Coagulation studies in ulcerative colitis and Crohn's disease. *Gastroenterology* **68**, 245–251 (1975).
125. Zezos, P. *et al.* Elevated plasma von Willebrand factor levels in patients with active ulcerative colitis reflect endothelial perturbation due to systemic inflammation. *World J. Gastroenterol.* **11**, 7639–7645 (2005).
126. Saibeni, S. *et al.* Increased thrombin generation in inflammatory bowel diseases. *Thromb. Res.* **125**, 278–282 (2010).

127. Saladino, V. *et al.* Increased Thrombin Generation in Inflammatory Bowel Diseases. *Gastrointest. Endosc.* **67**, AB319 (2008).
128. Bernhard, H. *et al.* Calibrated automated thrombin generation in paediatric patients with inflammatory bowel disease. *Hamostaseologie* **29 Suppl 1**, S90-93 (2009).
129. Tripodi, A. *et al.* Anti-TNF-α Treatment Reduces the Baseline Procoagulant Imbalance of Patients With Inflammatory Bowel Diseases. *Inflamm. Bowel Dis.* (2021) doi:10.1093/ibd/izaa351.
130. Anthoni, C. *et al.* Tissue factor: a mediator of inflammatory cell recruitment, tissue injury, and thrombus formation in experimental colitis. *J. Exp. Med.* **204**, 1595–1601 (2007).
131. Queiroz, K. C. S. *et al.* Tissue factor-dependent chemokine production aggravates experimental colitis. *Mol. Med. Camb. Mass* **17**, 1119–1126 (2011).
132. Hudson, M. *et al.* Thrombotic vascular risk factors in inflammatory bowel disease. *Gut* **38**, 733–737 (1996).
133. Undas, A. *et al.* Activated factor XI and tissue factor in inflammatory bowel disease. *Inflamm. Bowel Dis.* **16**, 1447–1448 (2010).
134. Koster, T., Blann, A. D., Briët, E., Vandenbroucke, J. P. & Rosendaal, F. R. Role of clotting factor VIII in effect of von Willebrand factor on occurrence of deep-vein thrombosis. *Lancet* **345**, 152–155 (1995).
135. Khandagale, A. *et al.* Coagulation factor 9-deficient mice are protected against dextran sulfate sodium-induced colitis. *Biol. Open* **7**, bio034140 (2018).
136. Wang, B. *et al.* The Plasma Kallikrein–Kininogen Pathway Is Critical in the Pathogenesis of Colitis in Mice. *Front. Immunol.* **9**, (2018).
137. Hayat, M., Ariëns, R. A. S., Moayyedi, P., Grant, P. J. & O'Mahony, S. Coagulation factor XIII and markers of thrombin generation and fibrinolysis in patients with inflammatory bowel disease. *Eur. J. Gastroenterol. Hepatol.* **14**, 249–256 (2002).
138. Chamouard, P. *et al.* Significance of diminished factor XIII in Crohn's disease. *Am. J. Gastroenterol.* **93**, 610–614 (1998).
139. Seitz, R. *et al.* Ulcerative colitis and Crohn's disease: factor XIII, inflammation and haemostasis. *Digestion* **55**, 361–367 (1994).
140. de Jong, E., Porte, R. J., Knot, E. A., Verheijen, J. H. & Dees, J. Disturbed fibrinolysis in patients with inflammatory bowel disease. A study in blood plasma, colon mucosa, and faeces. *Gut* **30**, 188–194 (1989).
141. Gris, J. C. *et al.* Impaired fibrinolytic capacity in patients with inflammatory bowel disease. *Thromb. Haemost.* **63**, 472–475 (1990).
142. Weber, P., Husemann, S., Vielhaber, H., Zimmer, K. P. & Nowak-Göttl, U. Coagulation and fibrinolysis in children, adolescents, and young adults with inflammatory bowel disease. *J. Pediatr. Gastroenterol. Nutr.* **28**, 418–422 (1999).
143. Souto, J. C. *et al.* Prothrombotic state and signs of endothelial lesion in plasma of patients with inflammatory bowel disease. *Dig. Dis. Sci.* **40**, 1883–1889 (1995).
144. Koutroubakis, I. E. *et al.* Plasma thrombin-activatable fibrinolysis inhibitor and plasminogen activator inhibitor-1 levels in inflammatory bowel disease. *Eur. J. Gastroenterol. Hepatol.* **20**, 912–916 (2008).
145. Kaiko, G. E. *et al.* PAI-1 augments mucosal damage in colitis. *Sci. Transl. Med.* **11**, (2019).
146. Czekay, R.-P. *et al.* PAI-1: An Integrator of Cell Signaling and Migration. *Int. J. Cell Biol.* **2011**, (2011).
147. Ji, Y. *et al.* Pharmacological Targeting of Plasminogen Activator Inhibitor-1 Decreases Vascular Smooth Muscle Cell Migration and Neointima Formation. *Arterioscler. Thromb. Vasc. Biol.* **36**, 2167–2175 (2016).
148. Puy, C. *et al.* Endothelial PAI-1 (Plasminogen Activator Inhibitor-1) Blocks the Intrinsic Pathway of Coagulation, Inducing the Clearance and Degradation of FXIa (Activated Factor XI). *Arterioscler. Thromb. Vasc. Biol.* **39**, 1390–1401 (2019).
149. Bollen, L. *et al.* The Occurrence of Thrombosis in Inflammatory Bowel Disease Is Reflected in the Clot Lysis Profile. *Inflamm. Bowel Dis.* **21**, 2540–2548 (2015).
150. Cibor, D., Szczeklik, K., Mach, T. & Owczarek, D. Levels of tissue factor pathway inhibitor in patients with inflammatory bowel disease. *Pol. Arch. Intern. Med.* **129**, 253–258 (2019).
151. He, H.-L., Zhang, J.-B. & Li, Q. Clinical significance of expression of tissue factor and tissue factor pathway inhibitor in ulcerative colitis. *World J. Gastroenterol.* **20**, 7461 (2014).
152. Schlagenhauf, A. *et al.* Children with Inflammatory Bowel Disease Exhibit Insensitivity to Tissue Factor Pathway Inhibitor. *Blood* **132**, 2504–2504 (2018).

153. Faioni, E. M. *et al.* Expression of endothelial protein C receptor and thrombomodulin in the intestinal tissue of patients with inflammatory bowel disease. *Crit. Care Med.* **32**, S266-270 (2004).
154. Aadland, E., Odegaard, O. R., Røseth, A. & Try, K. Free protein S deficiency in patients with chronic inflammatory bowel disease. *Scand. J. Gastroenterol.* **27**, 957–960 (1992).
155. Pintao, M. C. *et al.* Protein S levels and the risk of venous thrombosis: results from the MEGA case-control study. *Blood* **122**, 3210–3219 (2013).
156. Jorens, P. G. *et al.* Acquired protein C and S deficiency, inflammatory bowel disease and cerebral arterial thrombosis. *Blut* **61**, 307–310 (1990).
157. Aadland, E., Odegaard, O. R., Røseth, A. & Try, K. Free protein S deficiency in patients with Crohn's disease. *Scand. J. Gastroenterol.* **29**, 333–335 (1994).
158. Vetrano, S. *et al.* Unexpected role of anticoagulant protein C in controlling epithelial barrier integrity and intestinal inflammation. *Proc. Natl. Acad. Sci. U. S. A.* **108**, 19830–19835 (2011).
159. Motta, J.-P. *et al.* Active thrombin produced by the intestinal epithelium controls mucosal biofilms. *Nat. Commun.* **10**, 3224 (2019).
160. Chien, S. Rheology in the microcirculation in normal and low flow states. *Adv. Shock Res.* **8**, 71–80 (1982).
161. Késmárky, G., Fehér, G., Koltai, K., Horváth, B. & Tóth, K. Viscosity, hemostasis and inflammation in atherosclerotic heart diseases. *Clin. Hemorheol. Microcirc.* **35**, 67–73 (2006).
162. Horne, M. K., Cullinane, A. M., Merryman, P. K. & Hoddeson, E. K. The effect of red blood cells on thrombin generation. *Br. J. Haematol.* **133**, 403–408 (2006).
163. Whelihan, M. F. & Mann, K. G. The role of the red cell membrane in thrombin generation. *Thromb. Res.* **131**, 377–382 (2013).
164. Pivkin, I., Richardson, P. & Karniadakis, G. Effect of red blood cells on platelet aggregation. *IEEE Eng. Med. Biol. Mag. Q. Mag. Eng. Med. Biol. Soc.* **28**, 32–37 (2009).
165. Owens, A. P. & Mackman, N. Tissue factor and thrombosis: The clot starts here. *Thromb. Haemost.* **104**, 432–439 (2010).
166. Hermand, P. *et al.* Red Cell ICAM-4 Is a Novel Ligand for Platelet-activated αIIbβ3 Integrin. *J. Biol. Chem.* **278**, 4892–4898 (2003).
167. Carvalho, F. A. *et al.* Atomic Force Microscopy-Based Molecular Recognition of a Fibrinogen Receptor on Human Erythrocytes. *ACS Nano* **4**, 4609–4620 (2010).
168. Diamond, S. L. When flow goes slow, von Willebrand Factor can bind red blood cells. *Arterioscler. Thromb. Vasc. Biol.* **37**, 1595 (2017).
169. Smeets Michel W.J., Mourik Marjon J., Niessen Hans W.M., & Hordijk Peter L. Stasis Promotes Erythrocyte Adhesion to von Willebrand Factor. *Arterioscler. Thromb. Vasc. Biol.* **37**, 1618–1627 (2017).
170. Walton, B. L. *et al.* Elevated hematocrit enhances platelet accumulation following vascular injury. *Blood* **129**, 2537–2546 (2017).
171. Iii, A. P. O. *et al.* Towards a standardization of the murine ferric chloride-induced carotid arterial thrombosis model. *J. Thromb. Haemost.* **9**, 1862–1863 (2011).
172. Barr, J. D., Chauhan, A. K., Schaeffer, G. V., Hansen, J. K. & Motto, D. G. Red blood cells mediate the onset of thrombosis in the ferric chloride murine model. *Blood* **121**, 3733–3741 (2013).
173. Klatt, C. *et al.* Platelet-RBC interaction mediated by FasL/FasR induces procoagulant activity important for thrombosis. *J. Clin. Invest.* **128**, 3906–3925.
174. Pai, J. K. *et al.* Inflammatory markers and the risk of coronary heart disease in men and women. *N. Engl. J. Med.* **351**, 2599–2610 (2004).
175. Madjid, M. & Fatemi, O. Components of the Complete Blood Count as Risk Predictors for Coronary Heart Disease. *Tex. Heart Inst. J.* **40**, 17–29 (2013).
176. Franchini, M., Targher, G., Montagnana, M. & Lippi, G. Iron and thrombosis. *Ann. Hematol.* **87**, 167–173 (2008).
177. Day Sharlene M. *et al.* Chronic Iron Administration Increases Vascular Oxidative Stress and Accelerates Arterial Thrombosis. *Circulation* **107**, 2601–2606 (2003).
178. Wilson, A., Reyes, E. & Ofman, J. Prevalence and outcomes of anemia in inflammatory bowel disease: a systematic review of the literature. *Am. J. Med.* **116**, 44–49 (2004).
179. Gasche, C., Lomer, M. C. E., Cavill, I. & Weiss, G. Iron, anaemia, and inflammatory bowel diseases. *Gut* **53**, 1190–1197 (2004).
180. Oustamanolakis, P., Koutroubakis, I. E. & Kouroumalis, E. A. Diagnosing anemia in inflammatory bowel disease: Beyond the established markers. *J. Crohns Colitis* **5**, 381–391 (2011).

181. Arnold, J., Sangwaiya, A., Bhatkal, B., Geoghegan, F. & Busbridge, M. Hepcidin and inflammatory bowel disease: dual role in host defence and iron homoeostasis. *Eur. J. Gastroenterol. Hepatol.* **21**, 335–339 (2009).
182. Ganz, T. Hepcidin and Its Role in Regulating Systemic Iron Metabolism. *Hematology* **2006**, 29–35 (2006).
183. Bergamaschi, G. *et al.* Serum hepcidin in inflammatory bowel diseases: biological and clinical significance. *Inflamm. Bowel Dis.* **19**, 2166–2172 (2013).
184. Aleman, M. M. *et al.* Factor XIII activity mediates red blood cell retention in venous thrombi. *J. Clin. Invest.* **124**, 3590–3600 (2014).
185. Hudson, M. *et al.* Factor XIIIA subunit and Crohn's disease. *Gut* **34**, 75–79 (1993).
186. Zilberman, L. *et al.* Inflammation-related erythrocyte aggregation in patients with inflammatory bowel disease. *Dig. Dis. Sci.* **50**, 677–683 (2005).
187. Mchedlishvili, G., Gobejishvili, L., Mamaladze, A., Momtselidze, N. & Varazashvili, M. Microcirculatory Stasis Induced by Hemorheological Disorders: Further Evidence. *Microcirculation* **6**, 97–106 (1999).
188. Delbosc, S. *et al.* Erythrocyte Efferocytosis by the Arterial Wall Promotes Oxidation in Early-Stage Atheroma in Humans. *Front. Cardiovasc. Med.* **4**, 43 (2017).
189. Michel, J.-B. & Martin-Ventura, J. L. Red Blood Cells and Hemoglobin in Human Atherosclerosis and Related Arterial Diseases. *Int. J. Mol. Sci.* **21**, (2020).
190. Lentz, S. R. Thrombosis in the setting of obesity or inflammatory bowel disease. *Blood* **128**, 2388–2394 (2016).
191. Danese, S. *et al.* Identification of Endpoints for Development of Antifibrosis Drugs for Treatment of Crohn's Disease. *Gastroenterology* **155**, 76–87 (2018).
192. Melhem, H. *et al.* Methyl-deficient diet promotes colitis and SIRT1-mediated endoplasmic reticulum stress. *Gut* **65**, 595–606 (2016).
193. He, Z. *et al.* Phosphotidylserine exposure and neutrophil extracellular traps enhance procoagulant activity in patients with inflammatory bowel disease. *Thromb. Haemost.* **115**, 738–751 (2016).
194. Lagrange, J., Lacolley, P., Wahl, D., Peyrin-Biroulet, L. & Regnault, V. Shedding Light on Hemostasis in Patients With Inflammatory Bowel Diseases. *Clin. Gastroenterol. Hepatol. Off. Clin. Pract. J. Am. Gastroenterol. Assoc.* (2020) doi:10.1016/j.cgh.2019.12.043.
195. Klatt, C. *et al.* Platelet-RBC interaction mediated by FasL/FasR induces procoagulant activity important for thrombosis. *J. Clin. Invest.* **128**, 3906–3925 (2018).
196. Smeets, M. W. J., Mourik, M. J., Niessen, H. W. M. & Hordijk, P. L. Stasis Promotes Erythrocyte Adhesion to von Willebrand Factor. *Arterioscler. Thromb. Vasc. Biol.* **37**, 1618–1627 (2017).
197. Lagrange, J., Kossmann, S., Kiouptsi, K. & Wenzel, P. Visualizing Leukocyte Rolling and Adhesion in Angiotensin II-Infused Mice: Techniques and Pitfalls. *J. Vis. Exp. JoVE* (2018) doi:10.3791/56948.
198. Mensah, S. A. *et al.* Regeneration of glycocalyx by heparan sulfate and sphingosine 1-phosphate restores inter-endothelial communication. *PloS One* **12**, e0186116 (2017).
199. Dahan, N. *et al.* Dynamic Autologous Reendothelialization of Small-Caliber Arterial Extracellular Matrix: A Preclinical Large Animal Study. *Tissue Eng. Part A* **23**, 69–79 (2017).

Annexe I

Encadrements : Résumé des projets.

Clémence Docq, co-encadrée lors d'un stage de SIR (2012).
Ce travail a été publié dans la journal ***Platelet*** **en 2017**[3]
Titre : Influence de l'activation plaquettaire sur la génération de thrombine évaluée par thrombinographie
Résumé : La mesure de génération de thrombine par thrombinographie est réalisée principalement avec du PPP (Plasma pauvre en plaquettes) mais également avec du PRP (Plasma Riche en Plaquettes). Dans le cas du PRP on peut penser que les conditions présentes in vivo ne sont pas parfaitement reproduites puisque les plaquettes ne sont pas stimulées de la même manière. En effet, le milieu de réaction est statique, ce qui ne favorise pas l'agrégation des plaquettes en PRP, bien qu'elles puissent être activées du fait de la présence de thrombine. De plus, les surfaces phospholipidiques issues des plaquettes, qui supportent la coagulation, peuvent s'en trouver modifiées. Notre but est donc de déterminer le rôle des éléments relargués par les plaquettes, et le rôle de l'agrégation de ces dernières, sur la génération de thrombine. Pour cela nous avons réalisé une agrégation plaquettaire avant de faire une thrombinographie. Nos résultats révèlent une diminution significative du temps de latence et du temps pour atteindre le pic dans le PRP après agrégation, que l'agoniste utilisé soit l'ADP ou le collagène. Le pic et la vélocité ne varient pas dans le PRP après agrégation en collagène alors qu'ils augmentent avec l'ADP. Ces variations sont partiellement reversées dans le cas où la thrombinographie est réalisée avec les agrégats isolés et resuspendus en PDP. En conclusion, les variations dans le PRP après agrégation sont dues à la fois aux plaquettes agrégées mais de manière plus importante aux substances et microparticules libérées. Ainsi l'agrégation plaquettaire influence la cinétique de génération de thrombine. La réaliser avant une thrombinographie pourrait être un outil permettant de mettre en relation le phénotypage de l'hémostase primaire et de la coagulation.

Arthur Thomas co-encadrée pour son Master 1 Biologie Santé (Avril-Mai 2021).
Titre : Etude des rôles respectifs des contraintes hémodynamiques et du statut inflammatoire dans la dégradation du glycocalyx endothélial dans une cohorte de patients adultes.
Résumé : Les résultats préliminaires obtenu dans des modèles animaux et chez l'homme de l'étude portant sur les altérations du glycocalyx ont montré de manière étonnante que les contraintes de cisaillements n'étaient pas responsables de la dégradation du glycocalyx. Il semble en revanche que la composante inflammatoire ait un rôle central. Le travail de ce M1 portera sur la mesure des produits de dégradation du glycocalyx dans la cohorte TELARTA. Cette cohorte de patients recrutés suite à des chirurgies est très bien phénotypée au niveau cardiovasculaire et permettra d'identifier les facteurs responsables de la dégradation du glycocalyx.

Julie Martin encadrée pour son Master 2 Biologie Santé (Janvier-Mai 2020).
Titre : Étude du potentiel thrombotique chez le rat-taupe nu
Résumé : La rigidité artérielle et l'état prothrombotique augmentent avec l'âge. Les cellules musculaires lisses vasculaires (CMLVs) ont un rôle majeur dans le développement de la rigidité artérielle et supportent la génération de thrombine. Le rat-taupe nu (NMR, de l'anglais « naked mole rat ») est l'espèce de rongeurs qui vit le plus

longtemps avec une durée de vie maximale supérieure à 30 ans. Des études antérieures ont mis en évidence que ces mammifères ont un vieillissement similaire à celui de l'Homme, sans cependant présenter d'augmentation de la pression artérielle ou de la vitesse d'onde de pouls, témoin d'une élasticité artérielle conservée avec l'âge. Aucune étude n'a été réalisée dans ce modèle de vieillissement concernant les changements de l'hémostase. Notre hypothèse est que le rat-taupe nu possède une hémostase intacte tout au long de sa vie. L'objectif a ainsi été d'analyser les variations de l'hémostase et ainsi que la composition artérielle chez les NMRs âgés de 2, 10 et 20 ans et de comparer les résultats à ceux de souris jeunes (4 mois) et âgées (16 mois). La mesure de l'activité des facteurs de coagulation a été réalisée à partir de plasma et leur expression à partir du foie. Nos résultats indiquent qu'il n'y a eu aucune augmentation de la génération de thrombine plasmatique ni aucune augmentation significative du fibrinogène, tous deux connus pour augmenter normalement avec l'âge chez l'Homme. Cependant, une augmentation du FVIII semble apparaitre avec l'âge chez les NMRs.
Nos résultats confirment que comme pour la réactivité vasculaire, les NMRs sont capables de maintenir une hémostase fonctionnellement intacte de 2 ans jusqu'à 20 ans. L'ensemble de ces résultats suggère d'utiliser une stratégie comparative afin de trouver des facteurs influencés par l'âge et augmentant le risque de thrombose chez l'Homme au cours du vieillissement mais pas chez les NMRs. Des résultats préliminaires sur l'étude de la paroi artérielle ont été réalisés sur des aortes thoraciques. Les analyses histologiques d'aortes ont montré des modifications au cours du vieillissement chez les NMRs. La densité des CMLVs est identique chez les NMRs de 2 et 10 ans, tandis qu'une hyperplasie cellulaire est observée chez les animaux plus âgés. Il sera intéressant par la suite d'étudier le couplage sang/vaisseaux pour comprendre comment le NMR peut conserver ses fonctions vasculaires et de l'hémostase au cours du vieillissement tout en présentant des modifications cellulaires et d'expressions.

Yvonne Weihert, encadrée pour sa thèse de médecine (2014-2017, soutenance le 16 novembre 2019).
Ce travail a été publié dans le journal ***Science Translationnal medicine*** **en 2017**[7]
Titre: Analysis of thrombin generation by calibrated automated thrombography in plasma of hypertensive patients (HT).
Résumé : We found a significant relation in the platelets examination and the thrombin generation of HT patients. This applies in particular to kinetic parameters like velocity, peak of TG and time to peak. They are correlated with BP. TG is literally accelerated in HT circumstances. The management of HT did not lower ETP or kinetic parameters in our patients. Hence, we consider TG to be increased chronically. Inhibition of GP1bα showed no effect on TG. This result however might be falsified by aspirin. Outstanding results of FXI inhibition were found which showed a significant decrease of ETP and of the kinetic parameters in HT. FXI presumably has a stronger impact on TG than GP1bα via a positive feedback loop.
The results confirmed the pivotal interaction between inflammation and coagulation system as a potential cause for vascular dysfunction and HT. Pharmaceutically, this will be of great interest for the development of new treatment principles. Thrombin inhibitors are already available and FXI inhibitor will be on the market in the coming years but their clinical benefit-risk balance is discussed controversially due to severe bleeding occasions (Eikelboom et al., 2017; Jansa et al., 2010). Further studies must

reveal if a non-full-anticoagulant therapy improves HT and inflammation (Makhoul et al., 2019). FXI inhibitors promise an effective future strategy for the treatment of HT and vascular dysfunction.
Next to therapeutic consequences, TG measurements by CAT might operate as a precursor to identify cardiovascular endangered patients as we found an increased TG to be a chronic state. It might not be a potent running parameter, but may be a future criterium for an evaluation of the overall cardiovascular risk`s.

Matthieu Bardin, actuellement en doctorat (UMR_S 1116), co-encadrement.
Titre : Résolution de l'inflammation par les médiateurs lipidiques dans le vieillissement vasculaire. ACT du 23-10-2019.
Résumé : L'inflammation chronique est un déterminant majeur du vieillissement cardiovasculaire. Les médiateurs lipidiques dérivés des acides gras polyinsaturés peuvent être pro-inflammatoires ; c'est le cas des leucotriènes. Ils peuvent au contraire exercer des effets de résolution de l'inflammation comme les résolvines qui sont des médiateurs lipidiques dérivées des acides gras oméga-3. Parmi ces médiateurs lipidiques pro-résolutifs spécifiques (SPMs), la résolvine D2 (RvD2) possède un fort potentiel anti-inflammatoire via son récepteur spécifique : le récepteur GPR18, un récepteur couplé aux protéine G exprimés par différents types cellulaires dont les cellules musculaires lisses vasculaires (CMLVs).
L'hypothèse est que l'inflammation chronique au cours du vieillissement vasculaire résulte d'un dysfonctionnement des mécanismes de résolution liés aux SPMs. Notre objectif est de déterminer si les SPMs peuvent retarder le vieillissement vasculaire et métabolique en agissant principalement sur les propriétés des CMLVs qui régulent la rigidité artérielle, les calcifications et le stress oxydatif, et de préciser les mécanismes impliqués.

Virginie Dufrost, actuellement en doctorat (UMR_S 1116), co-encadrement.
Titre : Implication de TREM-1 et des NETs dans la thrombogénèse du SAPL. (ACT en cours)
Résumé : Le syndrome des anticorps antiphospholipides (SAPL) est une thrombophilie acquise définie par la présence d'anticorps antiphospholipides (aPL) et la présence de manifestations clinique (thrombose veineuse, artérielle et/ou microcirculatoire, et/ou manifestation obstétricale). Le risque thrombotique est variable d'un patient à l'autre. L'enjeu principale au cours du SAPL est ainsi de déterminer les patients à risque d'évènement thrombotique afin de personnaliser les stratégies thérapeutiques. Des travaux ont permis de montrer que les neutrophils extracellular traps (NETs) pourraient jouer un rôle favorisant dans le processus thrombotique au cours du SAPL. D'autre part, un récepteur exprimé sur les cellules myéloïdes, triggering receptor on myeloïd cells 1 (TREM-1) semble impliqué dans de nombreux phénomènes inflammatoire, auto-immun et thrombotique. Au cours du SAPL, une seule étude est disponible rapportant une élévation de la forme soluble de ce récepteur (sTREM-1) chez des patients avec un SAPL thrombotique.
Notre objectif principal est de démontrer que les aPL sont pathogènes par l'intermédiaire de l'activation de TREM-1 et la production de NETs. Pour cela, nous souhaitons vérifier sur un modèle animal si l'inactivation de TREM-1 permet de diminuer la formation de thrombi au cours du SAPL et évaluer si l'inactivation de TREM-1 diminue la production de NETs. Nos objectifs secondaires sont premièrement de vérifier si le taux de NETs circulants est prédictifs de la survenue d'évènement au

sein d'une cohorte de patients SAPL. Deuxièmement, nous souhaitons explorer si les aPL au cours du COVID-19 sont pathogènes autant que les aPL du SAPL par leur caractérisation et l'étude de ces même voies de l'immunité (TREM-1 et NETs).

Les hypothèses auxquelles ce travail de thèse répondra sont les suivantes :
- L'inactivation de TREM-1 diminue la formation de thrombus au cours du SAPL par la diminution de l'activation des neutrophiles, monocytes et cellules endothéliales par les aPL
- Les taux de NETs circulants sont augmentés chez les patients SAPL par rapport aux sujets porteurs d'aPL asymptomatiques et aux sujets contrôles et prédictifs de la survenue d'évènement au cours de leur suivi
- Les aPL présents au cours de la COVID-19 ont la même pathogénicité que les aPL des patients SAPL avec le même profil immunologique, profil hypercoagulable et leurs impacts sur les voies NETs et TREM-1

Mohammad Jahangiri et qui débutera son doctorat le 1 er octobre 2021
Titre : Le glycocalyx des cellules musculaires lisses endothéliales et vasculaires : base des interactions entre l'insudation sanguine et la mécanothransduction artérielle au cours du vieillissement vasculaire chez le rat-taupe nu et les souris traitées à l'angiotensine II.
Résumé : L'importance du glycocalyx des cellules vasculaires (cellules endothéliales, EC et cellules musculaires lisses vasculaires, CMLV) a commencée à être étudiée au cours de la dernière décennie et a largement bénéficié de l'avancée méthodologique pour étudier ses effets. Dans des conditions physiologiques, la couche endothéliale n'est pas directement en contact avec le sang. Elle est recouverte d'abondants protéoglycanes (syndécanes, glycosaminoglycanes) appelés glycocalyx qui forment l'interface entre le sang et les cellules ainsi que les composés pariétaux. De plus, les composants sanguins (plaquettes, cellules immunitaires et molécules) peuvent pénétrer dans la paroi en fonction du gradient de pression entre la pression artérielle (100 mmHg) et la pression interstitielle (12 mmHg) et la perméabilité endothéliale (appelée insudation). Il reste à étudier comment les modifications du glycocalyx endothélial affectent la fonction artérielle et le phénotype des cellules vasculaires au cours du vieillissement normal et accéléré. Le vieillissement vasculaire provoque un épaississement intimal progressif dû à la prolifération des VSMC, une matrice plus rigide en plus d'altérations hémodynamiques telles que l'hypertension et des flux sanguins perturbés. Des études récentes ont montré des associations entre les altérations du glycocalyx et (i) le remodelage vasculaire (ii) la réponse de vasoconstriction induite par la contrainte de cisaillement et (iii) l'hypertrophie des CML induite par le sel élevé. Ces données récentes suggèrent que le glycocalyx pourrait retarder le vieillissement artériel.
Nous visons à étudier comment le glycocalyx des CE et des CMLV participent au développement du vieillissement vasculaire avec un accent particulier sur les propriétés anticoagulantes endothéliales et la mécanotransduction des CMLV. Deux modèles animaux et un modèle cellulaire seront utilisés : - Les rats-taupes nus comme modèle exceptionnel de résistance au vieillissement - Le Modèle de souris traitée à l'angiotensine II comme modèle de vieillissement accéléré dans lequel l'inflammation et l'hypertension sont induites.69 - Les cellules en culture primaire de CMLV d'aorte humaine in vitro (AoSMC de chez LONZA) dans un glycocalyx normal ou altéré.
Ces modèles *in vivo* et *in vitro* nous permettront de nous concentrer sur les objectifs suivants : (i) Évaluer la composition / l'intégrité de l'aorte et de la carotide en utilisant

une analyse histologique avancée pour quantifier les marqueurs de différenciation et de sénescence, l'insudation des produits sanguins et le statut glycocalyx de rats-taupes nus (RMN) à 2, 10 et 20 ans comme ainsi que des souris adultes et âgées (20 semaines d'âge). (ii) Réaliser des études mécanistes sur les AoSMC (de la membrane matrice-cellule à la mécanotransduction nucléaire associée à la plasticité des VSMC (marqueurs de migration, de sénescence et de différenciation).

Annexe II : 5 publications significatives

Endothelial mineralocorticoid receptor activation enhances endothelial protein C receptor and decreases vascular thrombosis in mice

Jérémy Lagrange,[*,†] Zhenlin Li,[‡,1] Céline Fassot,[‡,§,1] Mustapha Bourhim,[*,†] Huguette Louis,[*,†] Aurélie Nguyen Dinh Cat,[‡,§] Ara Parlakian,[‡] Denis Wahl,[*,†,‖] Patrick Lacolley,[*,†,‖] Fréderic Jaisser,[‡,§,‖] and Véronique Regnault[*,†,‖,1,2]

*Institut National de la Santé et de la Recherche Médicale (INSERM), U1116, Faculté de Médecine, Vandoeuvre-les-Nancy, France; [†]Université de Lorraine, Nancy, France; [‡]Pierre et Marie Curie University, Paris, France; [§]INSERM, U872, Centre de Recherche des Cordeliers, Paris, France; and [‖]Centre Hospitalier Universitaire (CHU) Nancy, Nancy, France

ABSTRACT **Previous studies have shown that aldosterone, which activates the mineralocorticoid receptor (MR), promotes thrombosis in animal models. Our objective was to determine whether MR activation/expression in the vascular endothelium could modify thrombotic risk *in vivo* and to examine thrombin generation at the surface of aortic endothelial cells (HAECs). MR was conditionally overexpressed *in vivo* in vascular endothelial cells in mice (MR-EC mice) or stimulated with aldosterone in HAECs. Thrombosis after ferric chloride injury was delayed in MR-EC mice compared with controls as well as in wild-type FVB/NRj mice treated with aldosterone (60 μg/kg/d for 21 d). Thrombin generation in platelet-poor plasma did not differ between MR-EC mice and controls. In MR-EC mice, aortic endothelial cell protein C receptor (EPCR) expression was increased. Aldosterone (10^{-8} M) attenuated thrombin generation at the surface of cultured HAECs, and this effect was associated with up-regulation of expression of EPCR, which promotes formation of activated protein C. Aldosterone increases EPCR expression *via* a transcriptional mechanism involving interaction of MR with the specificity protein 1 site. These findings demonstrate that MR activation acts on endothelial cells to protect against thrombosis in physiological conditions and that MR-mediated EPCR overexpression drives this antithrombotic property through enhancing protein C activation.—Lagrange, J., Li, Z., Fassot, C., Bourhim, M., Louis, H., Nguyen Dinh Cat, A., Parlakian, A., Wahl, D., Lacolley, P., Jaisser, F., Regnault, V. Endothelial mineralocorticoid receptor activation enhances endothelial protein C receptor and decreases vascular thrombosis in mice. *FASEB J.* 28, 2062–2072 (2014). www.fasebj.org**

Key Words: aldosterone · thrombin · SP1 · smooth muscle cell · transcriptional regulation

Since the discovery of aldosterone by Simpson *et al.* (1) in 1953, the role of this mineralocorticoid hormone was thought to be limited to salt and water homeostasis in the kidney. The pioneering work of Brilla *et al.* (2) in the mid-1990s showed a profibrotic effect of aldosterone in the myocardium and gave new dimensions to this hormone and its receptor, the mineralocorticoid receptor (MR). Significant progress has been made in understanding the pathological situations in which MR antagonism is beneficial, but the underlying mechanisms remain unclear. Clinical trials have demonstrated the therapeutic benefit of MR blockade in heart failure (3–5), and aldosterone is often considered as a deleterious hormone in the cardiovascular system (6). In certain situations, however, aldosterone has a paradoxical effect: in diabetic cardiomyopathy, cardiac aldosterone synthesis is beneficial (7); in the vasculature, aldosterone increases either vasodilation (8, 9) or vasoconstriction (10). Therefore, the effect of aldosterone may be site-specific and may also depend on the pathological context.

Abbreviations: ActD, actinomycin D; APC, activated protein C; CAT, calibrated automated thrombography; CHX, cycloheximide; CT, control; EGM-2, endothelial cell growth medium 2; EPCR, endothelial protein C receptor; ETP, endogenous thrombin potential; GR, glucocorticoid receptor; HAEC, human aortic endothelial cell; HASMC, human aortic smooth muscle cell; ICAM-1, intercellular adhesion molecule 1; MR, mineralocorticoid receptor; MR-EC, mineralocorticoid receptor overexpression in vascular endothelial cells; PCR, polymerase chain reaction; PPP, platelet-poor plasma; RT-PCR, reverse transcription polymerase chain reaction; SP1, specificity protein 1; TF, tissue factor; TFPI, tissue factor pathway inhibitor; TM, thrombomodulin; VCAM-1, vascular cell adhesion molecule 1; VSMC, vascular smooth muscle cell; vWF, von Willebrand factor; WT, wild type

[1] These authors contributed equally to this work.

[2] Correspondence: INSERM U1116, Faculté de Médecine, 9 Avenue de la Forêt de Haye, 54500 Vandoeuvre-les-Nancy, France. E-mail: veronique.regnault@inserm.fr

doi: 10.1096/fj.13-238188

This article includes supplemental data. Please visit *http://www.fasebj.org* to obtain this information.

0892-6638/14/0028-2062 © FASEB

Aldosterone has been proposed to be a prothrombotic factor in animal models (11, 12), through enhancement of platelet activation and impairment of fibrinolysis (13). These effects are partially or totally prevented by MR antagonism (14, 15). In human bone marrow endothelial cells, aldosterone up-regulates the endothelial protein C receptor (EPCR; ref. 16). However, no direct measurements of thrombin generation have been reported in this context. Thus, our objective was to determine the role of MR activation/expression restricted to endothelial cells on thrombin generation.

We have therefore developed a strategy combining transgenic mice and cell-based assays to investigate the role of endothelial MR in the putative prothrombotic and antithrombotic properties of aldosterone. We first explored EPCR expression and arterial thrombus formation in response to vascular injury in a transgenic mouse strain with conditional overexpression of hMR restricted to the vascular endothelium. To get insights into the underlying mechanisms, we then examined the *in vitro* procoagulant and anticoagulant properties of human aortic endothelial cells (HAECs) in response to aldosterone. The *in vivo* functional consequence of endothelial MR activation is to reduce arterial thrombus formation in mice. Aldosterone decreased thrombin generation at the surface of HAECs *via* EPCR overexpression and activated protein C (APC) generation.

MATERIALS AND METHODS

Cell culture

Clonetics HAECs or human aortic smooth muscle cells (HASMCs) from Lonza (Basel, Switzerland) were used at passages 5–7. Cells were grown to subconfluence in Clonetics endothelial cell growth medium 2 (EGM-2) or smooth muscle growth medium 2 (SmGM-2), respectively, and incubated for 18 h in desteroidized serum. Cells were then incubated for 24 h with 10^{-8} M aldosterone (Sigma-Aldrich, St. Louis, MO, USA), in the presence or absence of 10^{-6} M MR antagonist RU28318 (Tocris Bioscience, Bristol, UK) or glucocorticoid receptor (GR) antagonist RU486 (Mifepristone, Sigma-Aldrich), or drospirenone, a progesterone receptor/MR antagonist (Sigma-Aldrich) or actinomycin D (ActD; Sigma-Aldrich, 5×10^{-6} M, pretreatment 1 h), or cycloheximide (CHX; Sigma-Aldrich, 10 μg/ml, pretreatment 1 h).

Plasmid constructions and reporter gene assay

pGL4.10 vectors (Promega, Madison, WI, USA) containing the firefly luciferase reporter gene were used for *in vitro* reporter gene analysis. pGL4.10 does not contain any eukaryotic promoter. Different lengths of human EPCR 5′ regulatory regions were amplified by high-fidelity polymerase chain reaction (PCR) using the specific oligonucleotides (see Supplemental Table S1) and inserted into the *Xho*I-*Bgl*II sites of the pGL4.10 vector by using the In-Fusion PCR Cloning System kit (Clontech, Mountain View, CA, USA). Mutation of the transcription factor specificity protein 1 (SP1) binding site (from TCCTCCC to cCtTCaa) was performed using the mutated oligonucleotides. The constructions were verified by sequencing and used to transfect HAECs. Cells were plated in 24-well plates at 50,000 cells/well and cotransfected the next day with 500 ng of the reporter plasmid and 50 ng of transfecting efficiency control (CT) plasmid hRLuc containing the renia luciferase gene by using lipofectamine 2000 (Life Technologies, Carlsbad, CA, USA). After 24 h, transfected cells were starved in the EGM-2 medium containing 0.5% desteroidized serum for 18 h and stimulated with 10^{-8} M aldosterone for 24 h. Luciferase activity was determined with the dual-luciferase kit (Promega).

Mouse strains

Mice with conditional hMR overexpression in vascular endothelial cells (MR-EC) were generated as described previously (10). Monotransgenic tetO-hMR mice and monotransgenic transactivator VE-cadherin-tetOFF mice were mated to obtain double-transgenic MR-EC mice. Monotransgenic VE-Cadh-tetOFF, tetO-hMR, and wild-type (WT) FVB/NRj mice were used as CT mice. WT FVB/NRj mice were also treated with aldosterone (60 μg/kg/d for 21 d) *via* osmotic minipumps. Male mice aged 3–7 mo were used for experiments. All procedures were conducted in accordance with and approved by the Animal Ethics Committee of the Institut National de la Santé et de la Recherche Médicale and conformed to the U.S. National Institutes of Health Guide for the Care and Use of Laboratory Animals.

Endothelial cell activation markers

Circulating and cell-associated von Willebrand factor (vWF) antigen was measured by ELISA vWF (Asserachrom; Diagnostica Stago, Asnière-sur-Seine, France). Each sample was assayed at 2 dilutions chosen to interpolate results using the calibration curve obtained with the human calibrator supplied within the kit (17).

Soluble CD146 was measured using a homemade ELISA. Costar high-binding 96-well plates (Corning, Corning, NY, USA) were coated overnight at 4°C with 100 μl of the anti-CD146 P1H12 clone at 1 μg/ml in carbonate-bicarbonate buffer (0.05 M, pH 9.6). Plates were blocked overnight with 125 μl of PBS containing 0.5% gelatin. Samples (100 μl) were assayed at 2 dilutions (1:5 and 1:10) in PBS containing 0.05% Tween and incubated for 2 h at room temperature. After subsequent revelation with the anti-CD146 2Q401 monoclonal antibody at 1 μg/ml for 1 h and horseradish-conjugated streptavidin at 1:1000 for 15 min at room temperature, color was developed with tetramethylbenzidine/H_2O_2 substrate. Absorbance was measured in a microplate reader at 450 nm.

Cell-associated and secreted EPCR from HAECs was measured by Asserachrom sEPCR (Diagnostica Stago). EPCR in mouse plasma and aorta was measured using a mouse sEPCR ELISA kit (Elabscience, Wuhan, China). Aortic extracts were prepared by 3 freeze-thaw cycles in PBS. A total amount of 2 μg proteins/well was analyzed in ELISA.

Intercellular adhesion molecule 1 (ICAM-1) and vascular cell adhesion molecule 1 (VCAM-1) were measured by Quantikine ELISA (R&D Systems, Abingdon, UK). Tissue factor pathway inhibitor (TFPI) activity was measured by a chromogenic assay (Actichrome TFPI; American Diagnostica, Stamford, CT, USA). Thrombomodulin (TM) was measured by ELISA (USCN Life Science, Wuhan, China) and ADAM metallopeptidase domain 17 (ADAM17) by ELISA (Cusabio Biotech, Wuhan, China). A total amount of 10 μg aortic proteins/well was analyzed for TM and ADAM17.

Thrombin generation assay

Mice were anesthetized with isoflurane. Whole blood was collected by cardiac puncture and mixed with 10% citrate (109 mM) for calibrated automated thrombography (CAT) experiments. Platelet-poor plasma (PPP) was prepared within 2 h following sampling by 2 successive centrifugations (190 *g* for 10 min and 1750*g* for 10 min at room temperature), and then supernatants were centrifuged at 13,000 *g* for 30 min to remove all platelets and cell fragments. PPP was frozen and stored at −80°C until use.

CAT was performed for mouse PPP (18) without or with rabbit TM (American Diagnostica) at 60 nM, and for human PPP with washed HAECs in a microtiter plate fluorometer (Fluoroskan Ascent; ThermoLabsystems, Helsinki, Finland) using dedicated software (Thrombinoscope BV, Maastricht, The Netherlands) as previously reported (19, 20). Round-bottom 96-well Greiner blue plates (Greiner Bio One, Frickenhausen, Germany) were used for mouse PPP and 96-well tissue culture plates for cultured cells (Microtest96; BD Biosciences, Heidelberg, Germany) for human PPP with washed HAEC monolayers. Coagulation was triggered by recalcification in the presence of 6 pM recombinant human tissue factor (TF; Dade Behring, Marburg, Germany) for mouse PPP. Where indicated, a goat anti-human TM directed against the EGF1-EGF2 domains (American Diagnostica; 30 μg/ml) was added. Some experiments were performed with protein C-deficient PPP in the absence or in the presence of homemade purified protein C (17) at a final concentration of 1 U/ml. Thrombin generation curves were recorded in triplicate. The parameters calculated by the software were the lag time, thrombin peak, time-to-peak, velocity, and endogenous thrombin potential (ETP).

Protein C activation assay

APC generation on HAECs was measured as described elsewhere (21). Cell monolayers were washed with 20 mM HEPES, 150 mM NaCl, and 2 mM $CaCl_2$ (pH 7.4), and 50 μl of protein C (65 nM) was incubated together with 50 μl of bovine thrombin (DiaThrombin; DiaMed SA, Cressier s/Morat, Switzerland; from 0 to 30 nM) on the surface of HAECs at 37°C. After 1 h, thrombin was inhibited with 10 μl of 500 nM hirudin, and 100 μl of each sample was transferred to wells of 96-well Polysorp plates (Nunc, Roskilde, Denmark) containing 50 μl of S2366 substrate (0.4 mM). APC activity was determined by measuring the rate of hydrolysis of S2366 at 405 nm. Dilutions of known concentrations of purified APC (0–5 nM; ref. 22) were used for preparation of the calibration curve.

$FeCl_3$-induced arterial thrombosis

Mice were anesthetized with pentobarbital (50 mg/kg i.p.), and the carotid arteries were exposed using blunt dissection. An ultrasound transit-time flow probe (0.5 PSB Nanoprobe; Transonic, Ithaca, NY, USA) was placed on the left carotid artery to monitor blood flow. Data were recorded, stored, and analyzed using a Data Translation analog-to-digital converter and IOX software (EMKA Technologies, Paris, France). Thrombus formation was induced by applying 2 pieces of filter paper, soaked in a 3% aqueous $FeCl_3$ solution, to the outside of the carotid artery. After 3 min of exposure, the filter papers were removed, and the vessel was washed with physiological saline. Carotid blood flow was monitored for 5 min before ferric chloride application to measure the basal level and continuously after $FeCl_3$ application; flow rates were illustrated before (time 0) and at the end of $FeCl_3$ application. Total carotid occlusion was checked visually after each experiment.

Isolation of RNA and gene expression

Total RNA was isolated from HAECs using the RNeasy Mini kit (Qiagen, Venlo, The Netherlands). First-strand cDNA was synthesized according to the manufacturer's instructions (Fermentas; Thermo Fisher Scientific, Waltham, MA, USA). Quantitative real-time PCR analysis was then performed with SYBR green PCR technology (Bio-Rad, Hercules, CA, USA) using the following conditions: 10 s at 95°C; 45 s at the annealing temperature (T_a); 60 s at 72°C, repeated for 40 cycles. PCR primers and T_a for genes of interest are listed in Supplemental Table S1. Results from ≥3 independent reverse transcription PCR (RT-PCR) analyses were expressed relative to glyceraldehyde-3 phosphate dehydrogenase (GAPDH) or ribosomal protein S29 (RPS29) expression.

Western blot analysis

Protein lysates were analyzed by standard SDS-PAGE techniques, as described previously (23). Membranes were incubated with primary antibodies at 4°C overnight according to the following conditions: EPCR (1:1000 dilution; Santa Cruz Biotechnology, Santa Cruz, CA, USA), TM (1:1000; Santa Cruz Biotechnology), and TFPI (1:1000; Santa Cruz Biotechnology). Equal protein loading was ensured by probing with 1:2000 α-tubulin antibody (Sigma-Aldrich). Horseradish peroxidase (HRP)-conjugated secondary antibodies specific for the host species of the primary antibodies were applied to the membranes for 1 h at 20°C. Reactions were visualized using the ECL Western blot Detection Kit (Bio-Rad). Densitometry was measured in pixel intensity by Multi Gauge 3.0 (Fujifilm, Tokyo, Japan).

Immunostaining

Immunostaining was performed as described previously (24). HAECs and cryosections of mouse aortas were fixed with paraformaldehyde [4% w/v in Tris buffered saline (TBS)] for 10 min, blocked with 5% BSA in TBS for 30 min. HAECs were incubated for 1 h at room temperature with an anti-EPCR antibody (1:50, mouse monoclonal, R&D Systems) and a rabbit polyclonal antibody against TM (1:50, Santa Cruz Biotechnology). The DyLight488-conjugated anti-mouse antibody (1:100; Abcam, Cambridge, MA, USA) and DyLight549-conjugated anti-rabbit antibody (1:100; Abcam) were then incubated with the cells for 1 h at room temperature. Mouse aortas were stained with a rat monoclonal antibody against EPCR (1:100; EBioscience, San Diego, CA, USA) and a mouse monoclonal antibody against smooth muscle actin (1:400; Sigma) for 1 h at room temperature and then biotinylated-conjugated anti-rat from goat (1:100; Santa Cruz Biotechnology) or Alexa488-conjugated anti-mouse (1:100, Molecular Probes, Eugene, OR, USA) secondary antibody was applied for 60 min followed by Cy3-conjugated streptavidin (Jackson Immunoresearch, West Grove, PA, USA) for 30 min. Nuclei were counterstained with DAPI (Sigma). Cells and cryosections were then observed by fluorescence confocal microscopy (Leica TCS SP5; Leica Microsystems, Wetzlar, Germany).

Statistical analysis

Results are expressed as means ± SD. Statistical analyses were performed using the Student's *t* test for unpaired or paired data as appropriate.

RESULTS

Aldosterone infusion and endothelial MR overexpression increases the time to vessel occlusion after $FeCl_3$ injury

We first explored whether aldosterone produces a net prothrombotic or antithrombotic effect by challenging the WT FVB/NRj mice with aldosterone for 3 wk before assessing thrombus formation in a thrombosis model based on external application of $FeCl_3$ to the carotid artery. As normal vascular endothelium is known to act as an anticoagulant blood container, an antithrombotic effect of aldosterone signaling on endothelial cells could be hypothetized. To assess the specific role of MR in the endothelium in absence of secondary effects related to global aldosterone challenge, we also examined whether targeted increase in MR expression in endothelial cells only affects thrombosis in MR-EC mice. Before $FeCl_3$ application, blood flow was similar between MR-EC or aldosterone-treated WT mice and their respective CTs. After $FeCl_3$ application, blood flow decreased more slowly in aldosterone-treated WT and MR-EC mice compared with respective CTs (**Fig. 1*A*, *B***). Aldosterone-treated WT and MR-EC mice exhibited successive increases and decreases in blood flow, suggesting the presence of unstable clots before the establishment of a stable one. Occlusion time was longer in aldosterone-treated WT and MR-EC mice (by a factor of 1.5 and 1.7, respectively) than in CT mice (Fig. 1*C*), supporting an antithrombotic effect of MR on endothelium. In the absence of the APC pathway and endothelial cell surfaces, thrombin generation in PPP did not differ between MR-EC and CT groups (Fig. 1*D*) and between aldosterone-treated and untreated mice (not shown). The addition of soluble TM to plasma improves the physiological relevance of coagulation assays by allowing the protein C system to exert its crucial role in the down-regulation of thrombin formation. Added TM diminished ETP, thrombin peak, and velocity of thrombin conversion similarly in the 2 groups of mice (Fig. 1*D*, *E* and **Table 1**), thus suggesting that the effect of MR required endothelial cellular surfaces.

In vivo endothelial MR overexpression increases EPCR expression in mouse aorta

To test an involvement of soluble endothelial proteins, we evaluated the effect of endothelial MR activation on soluble markers of endothelial function. Plasma vWF was increased in MR-EC compared with CT mice (**Table 2**). No difference between MR-EC and CT mice was found either for the other soluble markers of endothelial function, sCD146 (a marker of endothelial junction), sICAM and sVCAM (inflammatory markers), sTM and TFPI (anticoagulant molecules), or for the soluble form of EPCR. Unlike the soluble form, membrane-bound EPCR favors protein C activation mainly in the macrovasculature. We therefore investigated EPCR expression in mouse aorta. The EPCR protein level was increased in the aorta of MR-EC compared with CT mice without changes in ADAM17 (Table 2), a metalloproteinase responsible for EPCR ectodomain shedding. Expression of TM, the other component of the APC pathway on the endothelial cell surface, was unchanged. Confocal microscopy revealed higher levels of EPCR expression in endothelial cells but not in smooth muscle cells in MR-EC compared to CT mice (Fig. 1*F*). These results suggest that increase EPCR expression may be involved in the antithrombotic effect of MR activation.

Aldosterone decreases thrombin generation on HAECs

To explore the effects of MR activation on thrombin generation at the surface of endothelial cells, HAECs were stimulated for 24 h with 10^{-8} M aldosterone. Aldosterone increased vWF mRNA expression 1.4 fold (n=6; P=0.04) as well as cell-associated vWF (641 ± 62 *vs.* 556 ± 43 ng/mg; n=16; P=0.04) and vWF released into the cell supernatant (132 ± 14 *vs.* 116 ± 18 ng/ml; n=16; P=0.04). Thrombin generation was significantly reduced at the surface of aldosterone-treated HAECs (**Fig. 2**), with changes in all kinetic parameters: a small but statistically significant delay of the lag time and the time to peak, an obvious decrease in the peak size, and a more modest reduction in the velocity of thrombin formation (**Table 3**). To assess the relative involvement of the MR and the GR in these effects, HAECs were incubated with aldosterone along with the MR antagonist RU28318 or the GR antagonist RU486. All aldosterone effects were prevented by RU28318 but not by RU486, whereas the antagonists added to CT cells failed to modify the thrombin generation pattern (Fig. 2). These results support an MR-dependent limitation of thrombin generation and suggest that activation of the MR on the endothelium may enhance its thromboresistance. In contrast to the limitation of thrombin generation at the surface of aldosterone-stimulated HAECs, we observed a significant increase in thrombin generated at the surface of aldosterone-stimulated HASMCs (Supplemental Fig. S1). These effects of aldosterone were prevented by the MR antagonist RU28318 and by drospirenone.

Impaired thrombin generation in response to MR activation is driven by EPCR overexpression

At the protein level, both cell-associated and secreted EPCR were significantly elevated (**Fig. 3*A***). These changes were reversed by the RU28318 MR antagonist, confirming the role of MR. By contrast, TM and TFPI protein expressions were unchanged in response to aldosterone (Supplemental Fig. S2). Confocal analysis revealed that the MR-dependent increase in EPCR was not associated with any increase in colocalization of EPCR and TM (Fig. 3*B*). To evaluate a possible effect of cell-bound EPCR overexpression on TM-mediated protein C activation and subsequent inhibition of throm-

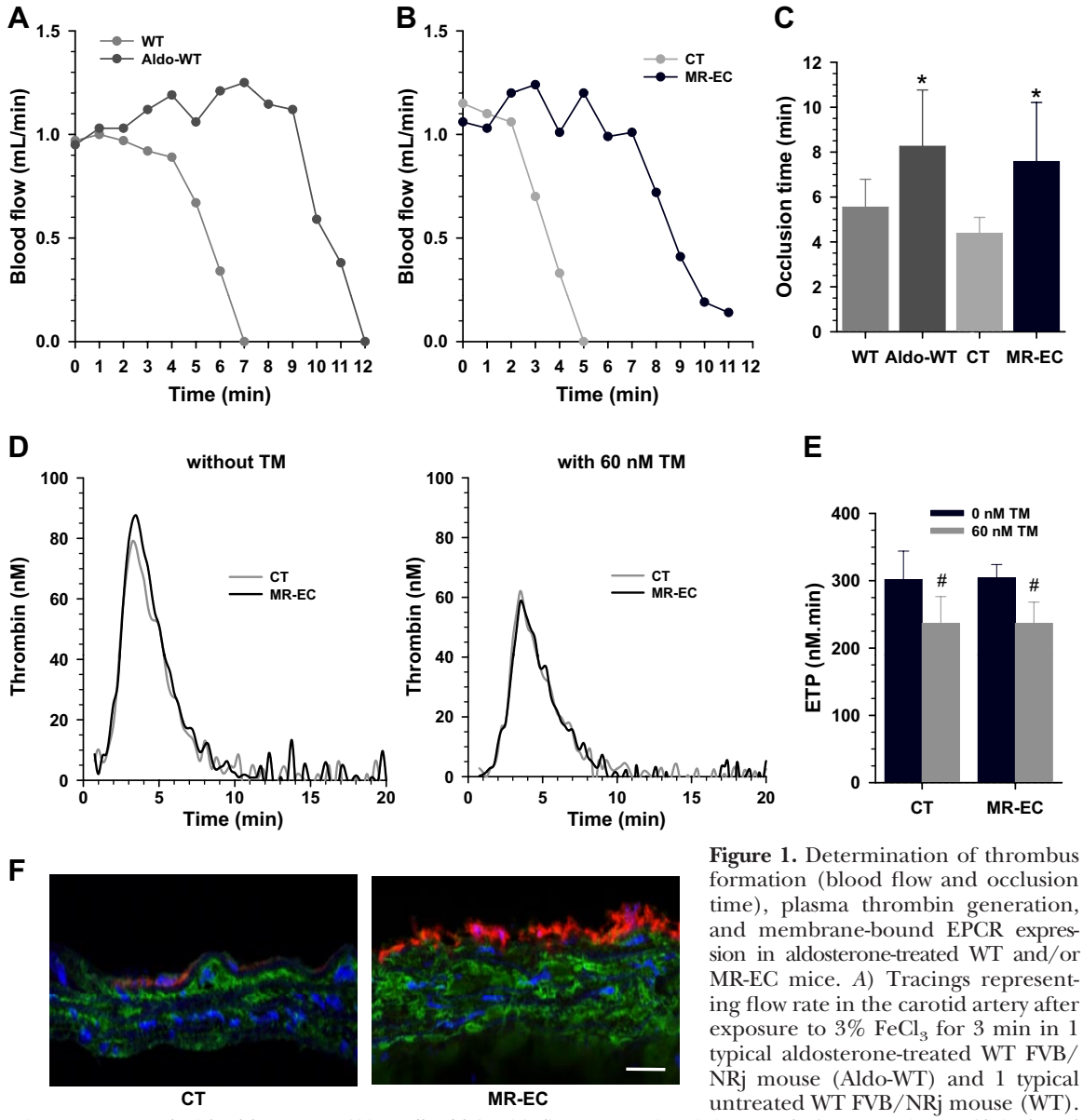

Figure 1. Determination of thrombus formation (blood flow and occlusion time), plasma thrombin generation, and membrane-bound EPCR expression in aldosterone-treated WT and/or MR-EC mice. *A*) Tracings representing flow rate in the carotid artery after exposure to 3% $FeCl_3$ for 3 min in 1 typical aldosterone-treated WT FVB/NRj mouse (Aldo-WT) and 1 typical untreated WT FVB/NRj mouse (WT). Mice were treated with aldosterone (60 μg/kg/d for 21 d) *via* osmotic minipumps before assessing $FeCl_3$-induced thrombosis. *B*) Tracings representing flow rate in the carotid artery after exposure to 3% $FeCl_3$ for 3 min in 1 typical MR-EC mouse and 1 typical CT mouse. *C*) Vascular occlusion times in Aldo-WT, WT, MR-EC, and CT mice. Results are means ± SD (n=4–10). *$P < 0.05$ *vs.* respective CT mice. *D*) Representative thrombin generation curves in PPP triggered with 6 pM of tissue factor in MR-EC (solid black trace) or CT mice (gray trace) in absence (left panel) or in presence (right panel) of 60 nM TM. *E*) ETP values were significantly lower in CT and MR-EC mice in presence of TM. Results are means ± SD of 9 experiments. #$P < 0.05$ *vs.* 0 nM TM group. *F*) Confocal micrographs of representative cross sections of thoracic aortas. Nuclei were visualized by DAPI staining; EPCR is identified by red immunostaining, and smooth muscle actin by green immunostaining. Scale bar = 20 μm.

bin generation, experiments were performed in presence of an anti-TM antibody. Inhibition of protein C activation by the anti-TM antibody resulted in an enhancement of both the thrombin peak and ETP, which was not impaired by aldosterone (Fig. 3*C*). Similar results were obtained with protein C-deficient PPP (Fig. 3*D*), and aldosterone did not modify the pattern of thrombin generation; the addition of purified protein C to this PPP totally restored the effect of aldosterone, indicating that the ability of aldosterone to reduce thrombin formation is mainly attributable to enhanced protein C activation. This hypothesis was confirmed in a purified system where washed HAECs were incubated with purified protein C and increasing concentrations of thrombin. Aldosterone enhanced APC generation on these cells in a thrombin dose-dependent manner (Fig. 3*E*). This effect was prevented by RU28318, indicating the causal role of MR.

SP1 is a cofactor for MR interaction with the EPCR promoter gene

To provide a mechanistic insight into the inhibitory effects of MR activation on thrombin generation, we

TABLE 1. *Thrombin generation parameters in mouse PPP*

Parameter	No TM		TM		No TM		TM	
	CT	MR-EC	CT	MR-EC	WT	Aldo-WT	WT	Aldo-WT
n	15	10	9	9	7	8	5	5
ETP (nM·min)	302 ± 42	304 ± 20	236 ± 40	235 ± 32	253 ± 21	255 ± 48	153 ± 30	177 ± 71
Lag time (min)	1.5 ± 0.4	1.6 ± 0.3	2.2 ± 0.4	2.1 ± 0.3	1.6 ± 0.3	1.5 ± 0.3	1.9 ± 0.6	1.8 ± 0.4
Peak (nM)	86 ± 11	87 ± 10	63 ± 11	60 ± 7	86 ± 14	85 ± 18	33 ± 12	38 ± 18
Time to peak (min)	3.4 ± 0.3	3.5 ± 0.4	4.4 ± 0.7	4.2 ± 0.4	3.3 ± 0.3	3.2 ± 0.5	5.3 ± 1.2	5.2 ± 1.8
Velocity (nM/min)	48 ± 10	44 ± 5	31 ± 7	30 ± 4	50 ± 11	50 ± 13	12 ± 7	15 ± 9
SR_{TM}			0.75 ± 0.05	0.77 ± 0.10			0.60 ± 0.17	0.74 ± 0.23

Results are means ± SD. Thrombin generation was determined in PPP in the absence or presence of 60 nM rabbit TM. SR_{TM}, TM sensitivity ratio ($ETP_{TM}/ETP_{No\ TM}$).

examined the effects of aldosterone on gene expression of EPCR, TM, and TFPI in HAECs. EPCR but not TM and TFPI gene expression was increased in response to aldosterone (**Fig. 4*A***). This increase was specifically dependent on MR activation, because it was abrogated only by RU28318 and not by RU486.

We determined EPCR mRNA expression over an aldosterone stimulation time course (1, 3, 9, and 24 h). A significant increase in EPCR mRNA was observed at 1 h and sustained over 24 h (Supplemental Fig. S3).

To explore the mechanism for the mRNA increase in response to aldosterone, we measured aldosterone-stimulated EPCR mRNA levels after pretreatment with the transcriptional inhibitor ActD or the translation inhibitor CHX. The aldosterone-induced up-regulation of EPCR mRNA was completely inhibited by pretreatment with ActD or CHX (Fig. 4*B*).

To determine the binding region necessary for the interaction between the EPCR promoter and activated MR, we cloned different lengths of EPCR promoter regions (−5837 to −145 bp) into the reporter gene pGL4.10. We found that the fold induction achieved by aldosterone was similar for plasmids containing the fragments −5837 and −153 bp (Fig. 4*C*). By contrast, the deletion (−145) or mutation (−153mut) of the SP1 site blunted the response to aldosterone treatment.

TABLE 2. *Endothelial markers in MR-EC and CT mice*

Marker	CT	MR-EC
Plasma		
n	12	14
vWF (ng/ml)	658 ± 349	1006 ± 332*
sCD146 (OD_{450nm})	0.66 ± 0.12	0.69 ± 0.16
sICAM-1 (ng/ml)	4.2 ± 0.5	4.4 ± 1.0
sVCAM-1 (ng/ml)	7.9 ± 1.0	8.5 ± 2.0
TFPI (U/ml)	3.4 ± 0.6	3.3 ± 0.5
sTM (ng/ml)	1.2 ± 0.3	1.06 ± 0.19
sEPCR (ng/ml)	22 ± 11	17 ± 6
Aorta		
n	6	7
TM (ng/ml)	2.1 ± 0.5	2.3 ± 0.8
EPCR (ng/ml)	13.5 ± 1.0	15.7 ± 1.7*
ADAM17 (ng/ml)	1.2 ± 0.4	1.1 ± 0.4

Data are means ± SD. *$P < 0.05$ *vs.* CT.

DISCUSSION

We show here that MR activation attenuates thrombus formation in the mouse carotid artery and thrombin generation at the surface of HAECs. The mechanism involves up-regulation of EPCR gene and protein expression and thereby enhancement of protein C activation.

Endothelial activation by aldosterone has been previously reported in HAECs: aldosterone incubation for 1 h stimulated endothelial exocytosis of Weibel-Palade bodies, externalizing P-selectin and releasing vWF into the culture medium (25). We confirmed this result in HAECs after 24 h aldosterone stimulation. Our results showed that MR, as an aldosterone-activated transcription factor, up-regulates EPCR gene expression with subsequent attenuation of thrombin generation. EPCR has long been known to play a central role in orchestrating the functions of the protein C pathway (26, 27). EPCR down-regulates blood coagulation on the surface of large vessels by concentrating protein C on the endothelium and accelerating its activation by the thrombin/TM complex. APC combined with cell-expressed TFPI synergistically inhibits thrombin generation on vascular cells (28). The absence of changes in TM and TFPI expression excludes the possibility that these 2 other endothelial anticoagulant molecules are involved in downregulating thrombin generation on HAECs.

To test the effect of MR-dependent EPCR stimulation on thrombin generation *in vivo*, we took advantage of the fact that MR overexpression in mouse vascular endothelium is not accompanied by stimulation of the renin-angiotensin system. These mice exhibited a mild increase in blood pressure (113±4 *vs.* 125±5 mmHg) mainly due to increased sensitivity to vasoactive agents. We cannot therefore exclude the possibility that endothelial activation in our study may result in part from

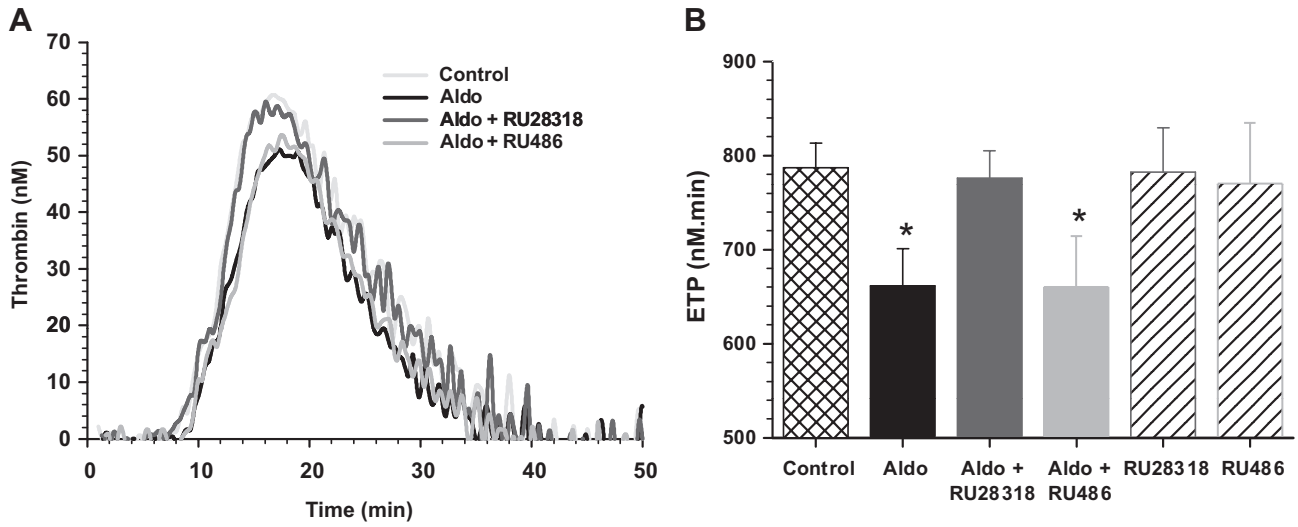

Figure 2. MR mediates the aldosterone-induced decrease in thrombin formation in cultured HAECs. Pooled normal human PPP was added to confluent cell monolayers incubated for 24 h with 10^{-8} M aldosterone, 10^{-8} M aldosterone plus 10^{-6} M RU28318, 10^{-8} M aldosterone plus 10^{-6} M RU486, 10^{-6} M RU28318, or 10^{-6} M RU486 alone. Thrombin generation was triggered by recalcification with 16.7 mM $CaCl_2$ and monitored with the CAT assay. *A*) Representative thrombin generation curves. *B*) ETP values were significantly lower in aldosterone and aldosterone plus RU486-treated cells than in untreated cells. Results are means ± SD of 10 independent experiments. *$P < 0.05$ *vs.* CT cells.

this blood pressure elevation (10). Among endothelial markers, only plasma levels of vWF are elevated in MR-EC mice relative to CT animals, and we previously reported no decrease in flow-mediated dilation. Moreover, several genes involved in oxidative stress were not increased in this model, suggesting that endothelial activation is a direct aldosterone/MR-mediated effect, as previously demonstrated in HAECs (25). Together, these findings might be taken as evidence that modest endothelial activation, rather than endothelial damage, occurs in MR-EC mice. Such endothelial activation may be driven by MR activation with subsequent modulation of vascular gene expression (29).

The temporal pattern of mRNA EPCR expression indicates that the EPCR gene is an early target for MR action. The aldosterone-induced up-regulation of EPCR mRNA was completely inhibited by pretreatment with ActD or CHX, suggesting that aldosterone-induced EPCR expression is mediated by a genomic action with requirement of *de novo* protein synthesis. The finding that 5.8 kb upstream of the EPCR translation start site is necessary for maximal EPCR expression in HAECs is in agreement with previous work in HUVECs identifying an enhancer region near −5.5 kb (30). The presence of a MR-response element in the −153-bp construction is demonstrated by the similar fold induction achieved by aldosterone for plasmids containing the −5837- and −153-bp fragments.

Recently, Meinel *et al.* (31) identified a 65-bp fragment (MRE1) of the EGFR promoter as a specific MR-response element and confirmed that SP1 is a compulsory cofactor for the interaction. The results obtained with the deleted or mutated SP1 site indicate that the SP1 site is essential for the MR response since these two constructions do not respond to aldosterone treatment. Thus our results support the hypothesis that MR-SP1 interaction might be a new mechanism of MR-mediated gene expression applicable to several genes.

MR overexpression in the vascular endothelium *in vivo* attenuated thrombus formation in a mouse $FeCl_3$ carotid injury model. This argues for a stimulation of the antithrombotic rather than the prothrombotic role of the activated endothelium. The demonstration that

TABLE 3. *Thrombin generation parameters at the surface of HAECs*

Parameter	CT	Aldosterone	Aldosterone + RU28318	Aldosterone + RU486	CT + RU28318	CT + RU486
ETP (nM·min)	785 ± 17	661 ± 17*	770 ± 19	688 ± 35*	778 ± 32	763 ± 33
Lag time (min)	10.8 ± 1.0	11.5 ± 1.4*	11.0 ± 1.3	11.5 ± 0.7*	11.0 ± 1.3	10.7 ± 1.4
Peak (nM)	60 ± 7	51 ± 7*	61 ± 7	55 ± 3*	63 ± 7	59 ± 7
Time to peak (min)	17.1 ± 1.6	18.1 ± 1.4*	17.4 ± 1.3	18.4 ± 1.3*	17.3 ± 1.5	16.8 ± 1.7
Velocity (nM/min)	9.7 ± 1.9	8.6 ± 1.2*	9.6 ± 1.7	9.0 ± 0.8*	10.1 ± 2.0	9.4 ± 0.5

Results are means ± SD of 10 to 20 experiments. *$P < 0.05$ *vs.* CT.

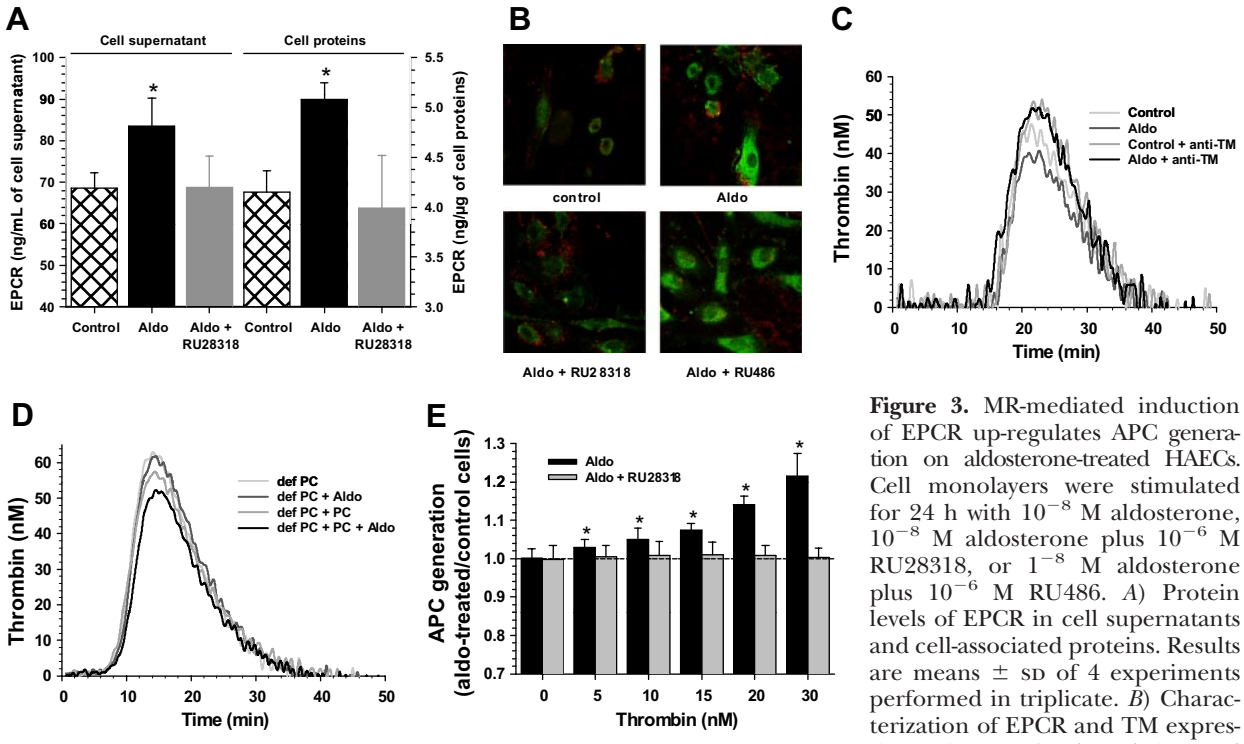

Figure 3. MR-mediated induction of EPCR up-regulates APC generation on aldosterone-treated HAECs. Cell monolayers were stimulated for 24 h with 10^{-8} M aldosterone, 10^{-8} M aldosterone plus 10^{-6} M RU28318, or 1^{-8} M aldosterone plus 10^{-6} M RU486. *A*) Protein levels of EPCR in cell supernatants and cell-associated proteins. Results are means ± SD of 4 experiments performed in triplicate. *B*) Characterization of EPCR and TM expression using confocal analysis. Dual immunofluorescence was performed using antibodies specific for EPCR (green) and TM (red). Scale bar = 20 µm. *C*) Typical thrombin generation curves obtained in the presence of an anti-TM antibody (30 µg/ml) in PPP added to washed untreated (CT) and aldosterone-treated (aldo) HAECs. Thrombin generation was triggered by recalcification with 16.7 mM $CaCl_2$ and monitored with the calibrated automated thrombogram assay. One representative experiment of 3 is shown. *D*) Representative tracings of 3 experiments performed with protein C-deficient PPP (def PC) added to CT and aldosterone-treated HAECs in the presence or absence of purified protein C (PC) at a final concentration of 1 U/ml. *E*) PC activation at the surface of CT, aldosterone-treated or aldosterone plus RU28318-treated HAECs was evaluated with purified PC and thrombin. APC is expressed as the ratio of values with aldosterone-treated cells to those with CT cells (means±SD of 9–12 experiments). $^*P < 0.05$ *vs.* CT cells.

aldosterone reduced thrombin generation on HAECs *via* EPCR up-regulation points to an *in vivo* mechanism involving an MR-mediated increase in endothelial EPCR expression. The finding that plasma levels of EPCR were not elevated in MR-EC mice rules out any involvement of this soluble form in the regulation of thrombin generation and is consistent with the absence of change in ADAM17, which is responsible for EPCR shedding (32). The increase in membrane EPCR in MR-EC aorta supports this hypothesis. This assumption is also corroborated by the observation that decreased thrombin generation does not occur in MR-EC PPP, even in the presence of TM but where membrane EPCR is not operating. Although previous findings suggested that $FeCl_3$ application leads to endothelial denudation, it has been recently demonstrated that this model does not include endothelial damage within the frame of thrombosis (33), supporting the idea that MR activation and up-regulation of EPCR contribute to the observed phenotype in our study. This beneficial anticoagulant role of EPCR is consistent with previous observations: MR-mediated EPCR induction increased the prolongation of coagulation time by APC (16); mice overexpressing EPCR on endothelial cells displayed increased circulating APC levels in response to thrombin infusion and decreased thrombin/antithrombin complex formation on challenge with FXa and phospholipids (34); and membrane EPCR ligand binding site occupancy by antibodies promoted thrombus formation in a mouse $FeCl_3$ carotid injury model (35).

Our finding that aldosterone delayed $FeCl_3$-induced thrombosis, as in MR-EC mice, is in favor of an overall antithrombotic effect of aldosterone in the presence of an intact endothelium. Published data demonstrating that aldosterone increases thrombosis in mice or rats have used carotid photochemical injury (11) or ligation of the vena cava (12, 13).

In the work by Bodary et al (11), Rose Bengal was used for carotid photochemical-induced vascular injury. Rose Bengal also targets endothelial cells, and results in complete endothelial denudation (36). In contrast, in our experimental model, we used a low concentration of ferric chloride (3%). This low concentration is indeed less violent for the endothelial layer as recently demonstrated (33), allowing the endothelial layer to be present, at least during the early stages of thrombus formation. As such, the endothelial MR is still able to contribute to the endothelial response in this thrombotic process.

Our mechanistic hypothesis is that aldosterone-activated endothelial MR possesses antithrombotic proper-

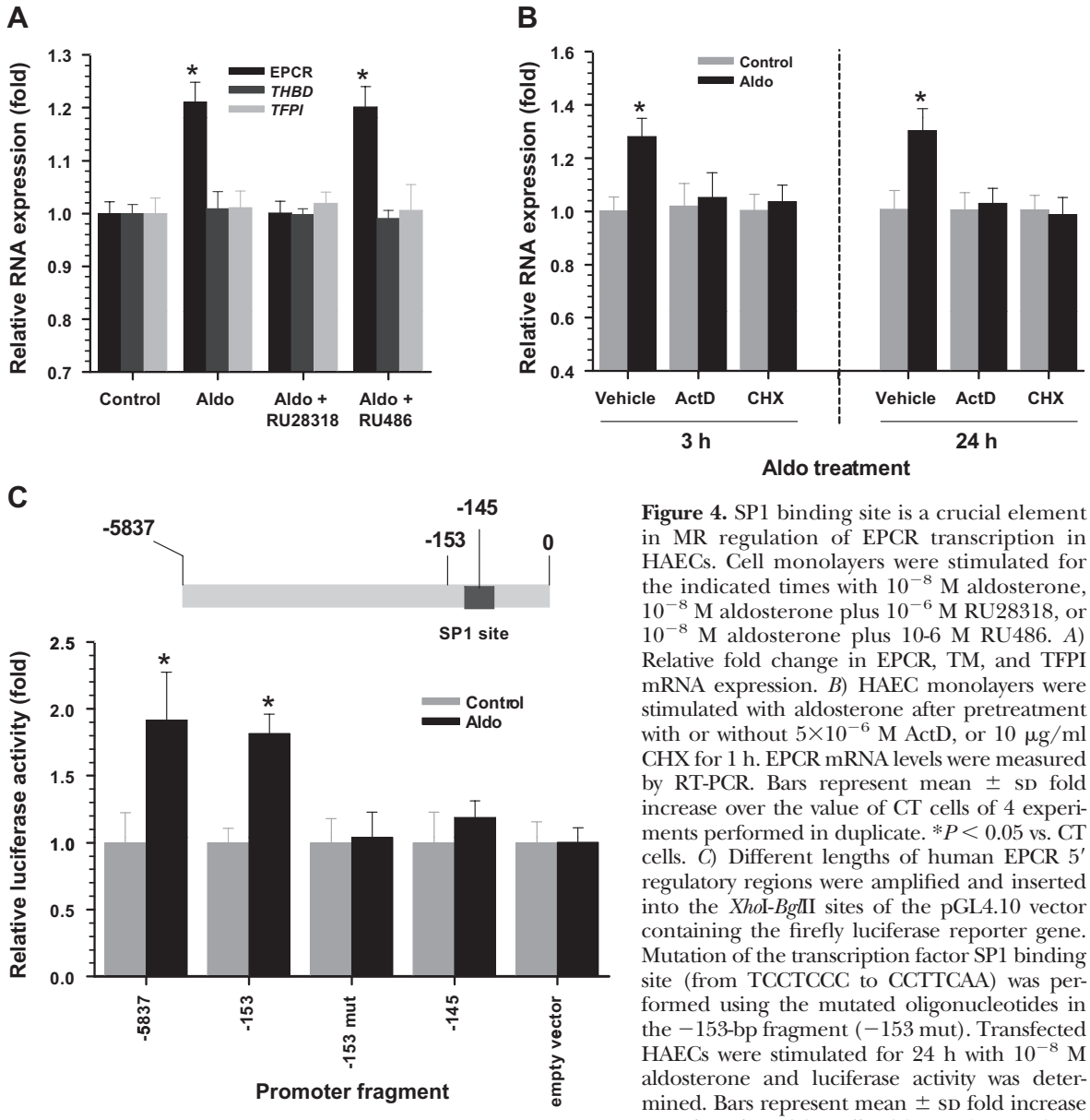

Figure 4. SP1 binding site is a crucial element in MR regulation of EPCR transcription in HAECs. Cell monolayers were stimulated for the indicated times with 10^{-8} M aldosterone, 10^{-8} M aldosterone plus 10^{-6} M RU28318, or 10^{-8} M aldosterone plus 10-6 M RU486. *A*) Relative fold change in EPCR, TM, and TFPI mRNA expression. *B*) HAEC monolayers were stimulated with aldosterone after pretreatment with or without 5×10^{-6} M ActD, or 10 μg/ml CHX for 1 h. EPCR mRNA levels were measured by RT-PCR. Bars represent mean ± SD fold increase over the value of CT cells of 4 experiments performed in duplicate. $^*P < 0.05$ vs. CT cells. *C*) Different lengths of human EPCR 5′ regulatory regions were amplified and inserted into the *Xho*I-*Bgl*II sites of the pGL4.10 vector containing the firefly luciferase reporter gene. Mutation of the transcription factor SP1 binding site (from TCCTCCC to CCTTCAA) was performed using the mutated oligonucleotides in the −153-bp fragment (−153 mut). Transfected HAECs were stimulated for 24 h with 10^{-8} M aldosterone and luciferase activity was determined. Bars represent mean ± SD fold increase over the value of CT cells of 4 experiments. $^*P < 0.05$ *vs.* CT cells.

ties in healthy vessels while aldosterone is known to act synergistically with endothelial injury to exert prothrombotic effects (37). Because vascular smooth muscle cells (VSMCs) express high levels of TF and MR, prothrombotic effects may occur at the surface of VSMCs when endothelial cells are absent. Our finding that aldosterone increased thrombin generation at the surface of human VSMCs supports this hypothesis. These effects of aldosterone were prevented by the MR antagonist RU28318, indicating that vascular MR mediates opposite thrombotic effects on endothelial cells and VSMCs that may contribute to the beneficial and detrimental effects of aldosterone on vascular physiology and diseases in humans, especially when the endothelium is injured.

The net effects of aldosterone/MR in thrombosis may therefore be dependent on the cellular context and the pathological setting. A balance between beneficial and deleterious effects of aldosterone has been reported in other situations. While aldosterone/MR is clearly deleterious for arrhythmia, myocardial infarction and heart failure, cardiac aldosterone prevents harmful effects of diabetes in the mouse heart by preserving capillary density (7). In the vasculature, aldosterone may promote vasodilation in situations with low levels of oxidative stress, while at higher levels (high salt intake, vascular injury, high oxygen tension, and inflammation) aldosterone is associated with vasoconstriction (8, 29). Discrepant results from clinical studies show that inhibition of MR improves endothelial vasodilator dysfunction and NO bioavailability in patients with heart failure but worsens endothelial function patients with type 2 diabetes (8). All these data suggest that vascular health status, extent, duration, and the combination of endothelial dysfunction/damage and vascular oxidative stress are critical contribu-

tors to the net effect of MR activation on vascular function. A detrimental prothrombotic role of MR activation in disease is attractive, based on the concept that a stressed/damaged endothelium shifts from a quiescent healthy antithrombotic state to a provasoconstrictive, proinflammatory, and prothrombotic phenotype in response to specific challenges (38, 39).

Our finding showing the inhibitory effect of drospirenone on the antithrombotic property of MR activation in endothelial cells may have clinical implications in oral contraceptive administration. Recently, drospirenone-containing oral contraceptives were reported to be unexpectedly associated with an increased risk of deep vein thrombosis and pulmonary embolism relative to other combined oral contraceptives (40–42). Unlike the other contraceptives, drospirenone is also a potent MR antagonist (43). Further studies are thus required to test the effect of drospirenone on hemostatic properties in comparison to other third-generation oral contraceptives and to evaluate the implication of its MR antagonist property.

In summary, our results demonstrate that MR activation in the endothelium protects against thrombosis through interactions with the APC pathway supported by MR-mediated EPCR overexpression *via* a transcriptional mechanism. This protective effect could be lost in the presence of endothelial damage, which is consistent with the beneficial effect of MR antagonists in cardiovascular diseases. FJ

The authors thank Christos Chatzantoniou and Sandrine Placier for assistance in setting up the arterial thrombosis model. The authors are grateful to Sebastien Hupont (FR 3209) for his participation. The authors thank Mary Osborne-Pellegrin and Peter Lenting for helpful discussion and comments on the manuscript, and Simon N. Thornton for manuscript editing. This study was supported by the Agence Nationale de la Recherche (ANR) Blanc program NT09_450866. J.L. is supported by the Region Lorraine and the Communauté Urbaine du Grand Nancy (Nancy, France).

REFERENCES

1. Simpson, S. A., Tait, J. F., Wettstein, A., Neher, R., Von Euw, J., and Reichstein, T. (1953) [Isolation from the adrenals of a new crystalline hormone with especially high effectiveness on mineral metabolism]. *Experientia* **9,** 333–335
2. Brilla, C. G., Pick, R., Tan, L. B., Janicki, J. S., and Weber, K. T. (1990) Remodeling of the rat right and left ventricles in experimental hypertension. *Circ. Res.* **67,** 1355–1364
3. Messaoudi, S., Azibani, F., Delcayre, C., and Jaisser, F. (2012) Aldosterone, mineralocorticoid receptor, and heart failure. *Mol. Cell. Endocrinol.* **350,** 266–272
4. Pitt, B., Remme, W., Zannad, F., Neaton, J., Martinez, F., Roniker, B., Bittman, R., Hurley, S., Kleiman, J., and Gatlin, M. (2003) Eplerenone, a selective aldosterone blocker, in patients with left ventricular dysfunction after myocardial infarction. *N. Engl. J. Med.* **348,** 1309–1321
5. Zannad, F., McMurray, J. J., Krum, H., van Veldhuisen, D. J., Swedberg, K., Shi, H., Vincent, J., Pocock, S. J., and Pitt, B. (2011) Eplerenone in patients with systolic heart failure and mild symptoms. *N. Engl. J. Med.* **364,** 11–21
6. Funder, J. W. (2004) Is aldosterone bad for the heart? *Trends Endocrinol. Metab.* **15,** 139–142
7. Messaoudi, S., Milliez, P., Samuel, J. L., and Delcayre, C. (2009) Cardiac aldosterone overexpression prevents harmful effects of diabetes in the mouse heart by preserving capillary density. *FASEB J.* **23,** 2176–2185
8. Skott, O., Uhrenholt, T. R., Schjerning, J., Hansen, P. B., Rasmussen, L. E., and Jensen, B. L. (2006) Rapid actions of aldosterone in vascular health and disease–friend or foe? *Pharmacol. Ther.* **111,** 495–507
9. Zhao, M., Celerier, I., Bousquet, E., Jeanny, J. C., Jonet, L., Savoldelli, M., Offret, O., Curan, A., Farman, N., Jaisser, F., and Behar-Cohen, F. (2012) Mineralocorticoid receptor is involved in rat and human ocular chorioretinopathy. *J. Clin. Invest.* **122,** 2672–2679
10. Nguyen Dinh Cat, A., Griol-Charhbili, V., Loufrani, L., Labat, C., Benjamin, L., Farman, N., Lacolley, P., Henrion, D., and Jaisser, F. (2010) The endothelial mineralocorticoid receptor regulates vasoconstrictor tone and blood pressure. *FASEB J.* **24,** 2454–2463
11. Bodary, P. F., Sambaziotis, C., Wickenheiser, K. J., Rajagopalan, S., Pitt, B., and Eitzman, D. T. (2006) Aldosterone promotes thrombosis formation after arterial injury in mice. *Arterioscler. Thromb. Vasc. Biol.* **26,** 233
12. Stankiewicz, A., Gromotowicz, A., Szemraj, J., Wojewodzka-Zelezniakowicz, M., Skrzypkowski, P., and Chabielska, E. (2007) Acute aldosterone infusion enhances thrombosis development in normotensive rats. *Thromb. Haemost.* **98,** 697–699
13. Gromotowicz, A., Szemraj, J., Stankiewicz, A., Zakrzeska, A., Mantur, M., Jaroszewicz, E., Rogowski, F., and Chabielska, E. (2011) Study of the mechanisms of aldosterone prothrombotic effect in rats. *J. Renin Angiotensin Aldosterone Syst.* **12,** 430–439
14. Schafer, A., Fraccarollo, D., Hildemann, S., Christ, M., Eigenthaler, M., Kobsar, A., Walter, U., and Bauersachs, J. (2003) Inhibition of platelet activation in congestive heart failure by aldosterone receptor antagonism and ACE inhibition. *Thromb. Haemost.* **89,** 1024–1030
15. Schafer, A., Vogt, C., Fraccarollo, D., Widder, J., Flierl, U., Hildemann, S. K., Ertl, G., and Bauersachs, J. (2010) Eplerenone improves vascular function and reduces platelet activation in diabetic rats. *J. Physiol. Pharmacol.* **61,** 45–52
16. Ducros, E., Berthaut, A., Mirshahi, S. S., Faussat, A. M., Soria, J., Agarwal, M. K., and Mirshahi, M. (2008) Aldosterone modifies hemostasis via upregulation of the protein-C receptor in human vascular endothelium. *Biochem. Biophys. Res. Commun.* **373,** 192–196
17. Regnault, V., Rivat, C., Pfister, M., and Stoltz, J. F. (1991) Monoclonal antibodies against human plasma protein C and their uses for immunoaffinity chromatography. *Thromb. Res.* **63,** 629–640
18. Tchaikovski, S. N., van Vlijmen, B. J., Rosing, J., and Tans, G. (2007) Development of a calibrated automated thrombography based thrombin generation test in mouse plasma. *J. Thromb. Haemost.* **5,** 2079–2086
19. Hemker, H. C., Giesen, P., Al Dieri, R., Regnault, V., de Smedt, E., Wagenvoord, R., Lecompte, T., and Beguin, S. (2003) Calibrated automated thrombin generation measurement in clotting plasma. *Pathophysiol. Haemost. Thromb.* **33,** 4–15
20. Regnault, V., Hemker, H. C., Wahl, D., and Lecompte, T. (2004) Phenotyping the haemostatic system by thrombography–potential for the estimation of thrombotic risk. *Thromb. Res.* **114,** 539–545
21. Hackeng, T. M., Tans, G., Koppelman, S. J., de Groot, P. G., Rosing, J., and Bouma, B. N. (1996) Protein C activation on endothelial cells by prothrombin activation products generated in situ: meizothrombin is a better protein C activator than alpha-thrombin. *Biochem. J.* **319**(Pt. 2), 399–405
22. Regnault, V., de Maistre, E., Geschier, C., Briquel, M. E., André, E., Stoltz, J. F., and Lecompte, T. (1995) A new fast one-step immunopreparation for activated protein C. *Thromb. Haemost.* **73,** 1365
23. Mao, X., Said, R., Louis, H., Max, J. P., Bourhim, M., Challande, P., Wahl, D., Li, Z., Regnault, V., and Lacolley, P. (2012) Cyclic stretch-induced thrombin generation by rat vascular smooth muscle cells is mediated by the integrin alphavbeta3 pathway. *Cardiovasc. Res.* **96,** 513–523
24. Parlakian, A., Gomaa, I., Solly, S., Arandel, L., Mahale, A., Born, G., Marazzi, G., and Sassoon, D. (2010) Skeletal muscle phenotypically converts and selectively inhibits metastatic cells in mice. *PLoS One* **5,** e9299

25. Jeong, Y., Chaupin, D. F., Matsushita, K., Yamakuchi, M., Cameron, S. J., Morrell, C. N., and Lowenstein, C. J. (2009) Aldosterone activates endothelial exocytosis. *Proc. Natl. Acad. Sci. U. S. A.* **106,** 3782–3787
26. Esmon, C. T. (2004) Structure and functions of the endothelial cell protein C receptor. *Crit. Care Med.* **32,** S298–301
27. Weiler, H. (2011) Multiple receptor-mediated functions of activated protein C. *Hamostaseologie* **31,** 185–195
28. Van 't Veer, C., Golden, N. J., Kalafatis, M., and Mann, K. G. (1997) Inhibitory mechanism of the protein C pathway on tissue factor-induced thrombin generation. Synergistic effect in combination with tissue factor pathway inhibitor. *J. Biol. Chem.* **272,** 7983–7994
29. McCurley, A., and Jaffe, I. Z. (2012) Mineralocorticoid receptors in vascular function and disease. *Mol. Cell. Endocrinol.* **350,** 256–265
30. Mollica, L. R., Crawley, J. T., Liu, K., Rance, J. B., Cockerill, P. N., Follows, G. A., Landry, J. R., Wells, D. J., and Lane, D. A. (2006) Role of a 5′-enhancer in the transcriptional regulation of the human endothelial cell protein C receptor gene. *Blood* **108,** 1251–1259
31. Meinel, S., Ruhs, S., Schumann, K., Stratz, N., Trenkmann, K., Schreier, B., Grosse, I., Keilwagen, J., Gekle, M., and Grossmann, C. (2013) Mineralocorticoid receptor interaction with SP1 generates a new response element for pathophysiologically relevant gene expression. *Nucleic Acids Res.* **41,** 8045–8060
32. Qu, D., Wang, Y., Esmon, N. L., and Esmon, C. T. (2007) Regulated endothelial protein C receptor shedding is mediated by tumor necrosis factor-alpha converting enzyme/ADAM17. *J. Thromb. Haemost.* **5,** 395–402
33. Barr, J. D., Chauhan, A. K., Schaeffer, G. V., Hansen, J. K., and Motto, D. G. (2013) Red blood cells mediate the onset of thrombosis in the ferric chloride murine model. *Blood* **121,** 3733–3741
34. Li, W., Zheng, X., Gu, J., Hunter, J., Ferrell, G. L., Lupu, F., Esmon, N. L., and Esmon, C. T. (2005) Overexpressing endothelial cell protein C receptor alters the hemostatic balance and protects mice from endotoxin. *J. Thromb. Haemost.* **3,** 1351–1359
35. Centelles, M. N., Puy, C., Lopez-Sagaseta, J., Fukudome, K., Montes, R., and Hermida, J. (2010) Blocking endothelial protein C receptor (EPCR) accelerates thrombus development in vivo. *Thromb. Haemost.* **103,** 1239–1244
36. Itoh, Y., Toriumi, H., Yamada, S., Hoshino, H., and Suzuki, N. (2010) Resident endothelial cells surrounding damaged arterial endothelium reendothelialize the lesion. *Arterioscler. Thromb. Vasc. Biol.* **30,** 1725–1732
37. Newfell, B. G., Iyer, L. K., Mohammad, N. N., McGraw, A. P., Ehsan, A., Rosano, G., Huang, P. L., Mendelsohn, M. E., and Jaffe, I. Z. (2011) Aldosterone regulates vascular gene transcription via oxidative stress-dependent and -independent pathways. *Arterioscler. Thromb. Vasc. Biol.* **31,** 1871–1880
38. Burger, D., and Touyz, R. M. (2012) Cellular biomarkers of endothelial health: microparticles, endothelial progenitor cells, and circulating endothelial cells. *J. Am. Soc. Hypertens.* **6,** 85–99
39. Deanfield, J. E., Halcox, J. P., and Rabelink, T. J. (2007) Endothelial function and dysfunction: testing and clinical relevance. *Circulation.* **115,** 1285–1295
40. Lidegaard, O., Lokkegaard, E., Jensen, A., Skovlund, C. W., and Keiding, N. (2012) Thrombotic stroke and myocardial infarction with hormonal contraception. *N. Engl. J. Med.* **366,** 2257–2266
41. Lidegaard, O., Nielsen, L. H., Skovlund, C. W., Skjeldestad, F. E., and Lokkegaard, E. (2011) Risk of venous thromboembolism from use of oral contraceptives containing different progestogens and oestrogen doses: Danish cohort study, 2001–2009. *BMJ* **343,** d6423
42. Wu, C., Grandi, S., Filion, K., Abenhaim, H., Joseph, L., and Eisenberg, M. (2013) Drospirenone-containing oral contraceptive pills and the risk of venous and arterial thrombosis: a systematic review. *BJOG* **120,** 801–810
43. Kolkhof, P., and Borden, S. A. (2012) Molecular pharmacology of the mineralocorticoid receptor: prospects for novel therapeutics. *Mol. Cell. Endocrinol.* **350,** 310–317

Received for publication August 20, 2013.
Accepted for publication January 13, 2014.

Endothelial mineralocorticoid receptor activation enhances endothelial protein C receptor and decreases vascular thrombosis in mice

Jérémy Lagrange, Zhenlin Li, Céline Fassot, et al.

FASEB J 2014 28: 2062-2072 originally published online January 22, 2014
Access the most recent version at doi:10.1096/fj.13-238188

HYPERTENSION

Platelet-localized FXI promotes a vascular coagulation-inflammatory circuit in arterial hypertension

Sabine Kossmann,[1,2]* Jeremy Lagrange,[1]* Sven Jäckel,[1†] Kerstin Jurk,[1†] Moritz Ehlken,[1,2†] Tanja Schönfelder,[1] Yvonne Weihert,[2] Maike Knorr,[2] Moritz Brandt,[2] Ning Xia,[3] Huige Li,[3] Andreas Daiber,[2] Matthias Oelze,[2] Christoph Reinhardt,[1] Karl Lackner,[4] Andras Gruber,[5,6] Brett Monia,[7] Susanne H. Karbach,[2] Ulrich Walter,[1] Zaverio M. Ruggeri,[8] Thomas Renné,[9,10] Wolfram Ruf,[1,11,12] Thomas Münzel,[2,12] Philip Wenzel[1,2,12‡]

Multicellular interactions of platelets, leukocytes, and the blood vessel wall support coagulation and precipitate arterial and venous thrombosis. High levels of angiotensin II cause arterial hypertension by a complex vascular inflammatory pathway that requires leukocyte recruitment and reactive oxygen species production and is followed by vascular dysfunction. We delineate a previously undescribed, proinflammatory coagulation-vascular circuit that is a major regulator of vascular tone, blood pressure, and endothelial function. In mice with angiotensin II–induced hypertension, tissue factor was up-regulated, as was thrombin-dependent endothelial cell vascular cellular adhesion molecule 1 expression and integrin $\alpha_M\beta_2$– and platelet-dependent leukocyte adhesion to arterial vessels. The resulting vascular inflammation and dysfunction was mediated by activation of thrombin-driven factor XI (FXI) feedback, independent of factor XII. The FXI receptor glycoprotein Ibα on platelets was required for this thrombin feedback activation in angiotensin II–infused mice. Inhibition of FXI synthesis with an antisense oligonucleotide was sufficient to prevent thrombin propagation on platelets, vascular leukocyte infiltration, angiotensin II–induced endothelial dysfunction, and arterial hypertension in mice and rats. Antisense oligonucleotide against FXI also reduced the increased blood pressure and attenuated vascular and kidney dysfunction in rats with established arterial hypertension. Further, platelet-localized thrombin generation was amplified in an FXI-dependent manner in patients with uncontrolled arterial hypertension, suggesting that platelet-localized thrombin generation may serve as an inflammatory marker of high blood pressure. Our results outline a coagulation-inflammation circuit that promotes vascular dysfunction, and highlight the possible utility of FXI-targeted anticoagulants in treating hypertension, beyond their application as antithrombotic agents in cardiovascular disease.

INTRODUCTION

Arterial hypertension is a risk factor for cardiovascular disease and death (*1*). Vascular inflammation is a hallmark of atherosclerosis (*2*) and arterial and venous thromboembolic disease (*3*). In this setting, vascular injury occurs with infiltration of lymphocyte antigen 6 complex locus C1^{high} (Ly6C^{hi}) monocytes into the vessel wall (*4*). Vascular inflammation and hypertension (*5*) induced by angiotensin II (ATII) similarly depends on the recruitment of ATII receptor type 1 (Agtr1)–expressing Ly6C^{hi} monocytes to the vasculature (*6*), which cause NADPH (reduced form of nicotinamide adenine dinucleotide phosphate) oxidase–dependent reactive oxygen species (ROS) production in arteries (*7*). The combined effects of the inflammation and oxidative stress triggered by infiltrating immune cells result in NADPH oxidase–dependent vascular dysfunction and high blood pressure (*8*, *9*). ATII induces infiltration of immune cells into the vessel walls by promoting their adhesion to endothelial cells and transmigration (*10*). Vascular cellular adhesion molecule 1 (VCAM-1) is induced by ATII (*11*) and thrombin (*12*), which can be generated by coagulation activation through tissue factor (TF), another ATII-induced gene product (*13*). Platelets provide a pro-coagulant surface for amplified thrombin generation (TG) in hemostasis and thrombosis (*14*). They also promote leukocyte recruitment in arterial injury and angiogenesis models (*15*, *16*) through the interaction of platelet glycoprotein Ibα (GPIbα) with the integrin $\alpha_M\beta_2$ (CD11b/CD18 or Mac-1) on leukocytes (*17*) and also regulate monocyte and neutrophil activation (*18*).

How platelets, coagulation factors, leukocytes, and the vessel wall interact to promote vascular inflammation in arterial hypertension remains unclear. We have therefore investigated the roles of factor XII (FXII), FXI, thrombin, and TF on inflammatory monocyte-driven vascular dysfunction and arterial hypertension in ATII-infused mice and rats, as well as in partially nephrectomized rats.

RESULTS

The hemostatic system contributes to ATII-induced leukocyte adhesion

We investigated mechanisms underlying leukocyte adhesion to the vascular endothelium of arteries by epifluorescence intravital video microscopy (IVM) imaging in normocholesterolemic C57BL/6 mice

[1]Center for Thrombosis and Hemostasis Mainz, University Medical Center Mainz, Langenbeckstrasse 1, 55131 Mainz, Germany. [2]Center for Cardiology, Cardiology I, University Medical Center Mainz, 55131 Mainz, Germany. [3]Department of Pharmacology, University Medical Center Mainz, 55131 Mainz, Germany. [4]Institute of Clinical Chemistry and Laboratory Medicine, University Medical Center Mainz, 55131 Mainz, Germany. [5]Department of Biomedical Engineering, Oregon Health and Science University, 3303 Southwest Bond Avenue, CH13B, Portland, OR 97239, USA. [6]Aronora Inc., 4640 Southwest Macadam Avenue, Suite 200A, Portland, OR 97239, USA. [7]Ionis Pharmaceuticals Inc., 2855 Gazelle Court, Carlsbad, CA 92010, USA. [8]Department of Molecular and Experimental Medicine, The Scripps Research Institute, 10550 North Torrey Pines Road, La Jolla, CA 92037, USA. [9]Department of Molecular Medicine and Surgery, L1:00, Karolinska Institutet, SE-171 71 Stockholm, Sweden. [10]Institute of Clinical Chemistry and Laboratory Medicine, University Medical Center Hamburg-Eppendorf, Martinistrasse 52, 20246 Hamburg, Germany. [11]Department of Immunology and Microbial Science, The Scripps Research Institute, La Jolla, CA 92037, USA. [12]DZHK (German Center for Cardiovascular Research), Partner Site Rhine Main, University Medical Center Mainz, 55131 Mainz, Germany.
*These authors contributed equally as first authors.
†These authors contributed equally as second authors.
‡Corresponding author. Email: wenzelp@uni-mainz.de

chronically infused with ATII (1 mg kg^{-1} day^{-1} for 7 days via osmotic minipumps). This model is characterized by robust arterial hypertension and accumulation of $CD11b^+$ leukocytes in arterial vessels (*8*). ATII treatment induced extensive rolling and adhesion of leukocytes to the endothelium in the carotid artery (Fig. 1A and videos S1 and S2). Leukocyte integrin α_4 [very late antigen 4 (VLA-4)] recognizes endothelial VCAM-1 to mediate leukocyte adhesion to inflamed endothelium (*19*). Short-term blockade of this interaction with anti–VLA-4 (10 mg kg^{-1}) or anti–VCAM-1 (1 mg kg^{-1}) antibody prevented both leukocyte rolling and adhesion in ATII-infused mice (Fig. 1, B and C, and videos S3 and S4). Short-term inhibition of TF with an anti-TF antibody (25 mg kg^{-1}) or thrombin with lepirudin (1.7 mg kg^{-1}) (*20*) immediately before IVM imaging also markedly reduced leukocyte rolling and adhesion (Fig. 1, D and E). Depletion of platelets with an anti-GPIbα antibody (3.4 mg kg^{-1}) and antibody inhibition of the leukocyte integrin CD11b/CD18 (6.5 mg kg^{-1}) similarly prevented leukocyte rolling and adhesion (Fig. 1, F and G), indicating that both coagulation and platelets contributed to ATII-induced leukocyte adhesion in high flow arterial vascular beds.

Platelet GPIbα is required for thrombin-dependent vascular inflammation

To further investigate this interaction of coagulation factors, platelets, and arterial vessels, we evaluated the contribution of coagulation to ATII-induced vascular inflammation and endothelial dysfunction by intervention with the anticoagulant and specific thrombin inhibitor lepirudin. In ATII-infused mice, simultaneous thrombin inhibition substantially improved endothelial dysfunction, as quantified by acetylcholine (ACh)–induced vascular relaxation (Fig. 2A). Consistent with previously established roles for thrombin in the induction of endothelial cell VCAM-1 (*12*) and monocyte chemoattractant protein 1 (MCP-1; encoded by *Ccl2*) (*21*), which is required for ATII-induced monocyte recruitment (*22*), lepirudin prevented expression of these genes in the vessel wall and attenuated *Ly6c* mRNA levels (Fig. 2D), indicating reduced vascular recruitment of inflammatory monocytes. This was paralleled by diminished vascular ROS production assessed by the superoxide-sensitive dye dihydroethidium (DHE) (Fig. 2G).

Because platelets promote localized thrombin formation by providing a pro-coagulant surface, we evaluated their role in vascular dysfunction in ATII-infused mice. Platelet depletion with anti-GPIbα antibody (3.4 mg kg^{-1}) during chronic ATII administration significantly reduced or prevented endothelial dysfunction (Fig. 2B); *Vcam-1*, *Ccl2*, and *Ly6C* mRNA expression in the vessel wall (Fig. 2E); and vascular ROS production (Fig. 2G). Thus, depletion of platelets largely recapitulated the effects of thrombin inhibition, suggesting a crucial role for platelets in promoting TG or mediating its proinflammatory effects.

To better understand thrombin interactions with platelets, we analyzed human interleukin-4 receptor (hIL-4R)/Ibα mice with a defective

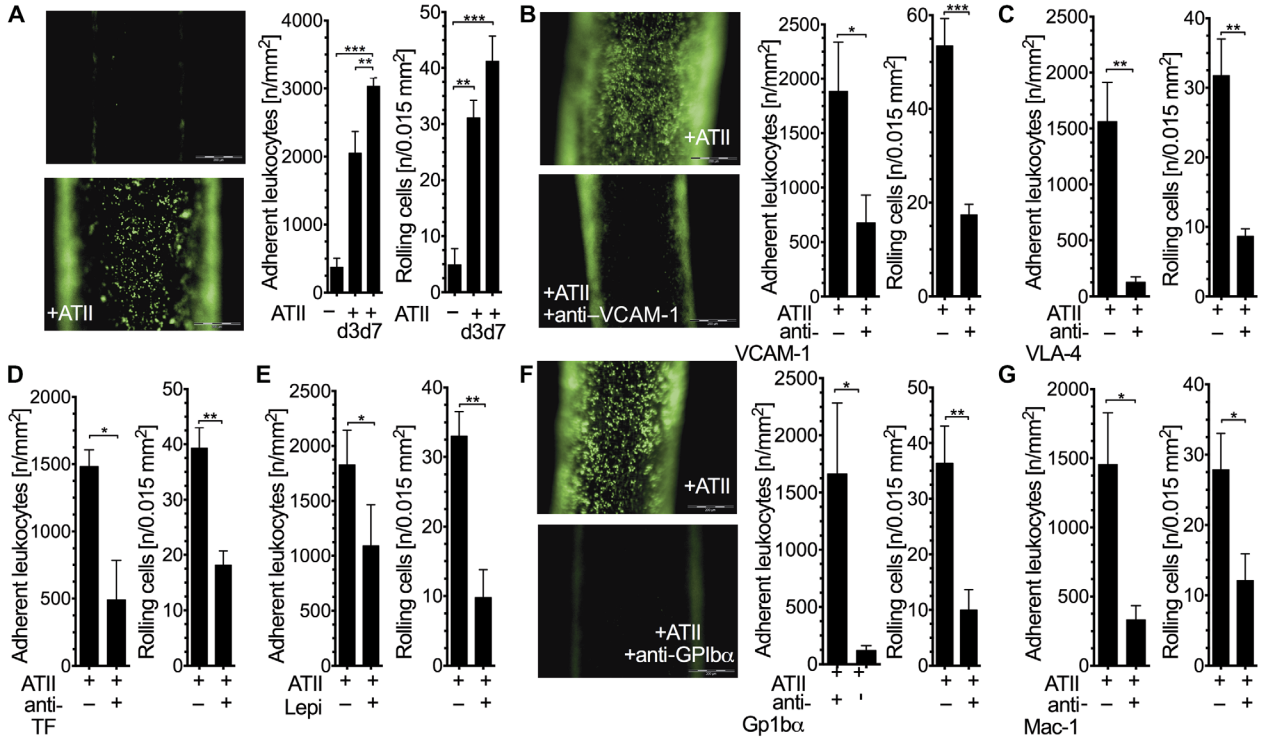

Fig. 1. A proinflammatory circuit of TF, thrombin, and platelets promotes ATII-induced endothelial leukocyte adhesion. (**A** to **G**) Epifluorescence IVM of endothelial adherent and rolling leukocytes in the common carotid artery of ATII-infused mice. Nucleated cells were visualized with acridine orange (green fluorescence). (A) IVM of carotids at day 3 (d3) and day 7 (d7) of continuous ATII infusion compared to sham. Left: Representative image at day 3. Right: Quantification of adherent and rolling leukocytes. $^{**}P < 0.01$; $^{***}P < 0.001$, one-way analysis of variance (ANOVA); $n = 4$ to 7 animals per group. (B to G) IVM of carotids at day 3 of ATII infusion, the time point of deflection of the blood pressure curve in response to ATII 60 hours after initial increase of blood pressure (*8*), before and 30 min after single intravenous injections of anti–VCAM-1 (B), anti–VLA-4 (C), anti-TF (D), the thrombin inhibitor lepirudin (Lepi) (E) of anti-GPIbα to acutely deplete platelets (F), and anti–Mac-1 (G). Injection of isotype control immunoglobulin G (IgG) antibodies had no significant effect on rolling (ATII versus ATII + control IgG: 39 ± 3.7 versus 44 ± 4.8 rolling cells/0.015 mm^2) or adhesion (ATII versus ATII + control IgG: 1683 ± 377 versus 1486 ± 270 adherent cells per mm^2). Left: Representative image at day 3. Right: Quantification of adherent and rolling leukocytes. $^{*}P < 0.05$; $^{**}P < 0.01$; $^{***}P < 0.001$, unpaired *t* test; $n = 5$ to 6 animals per group. Data are means ± SEM.

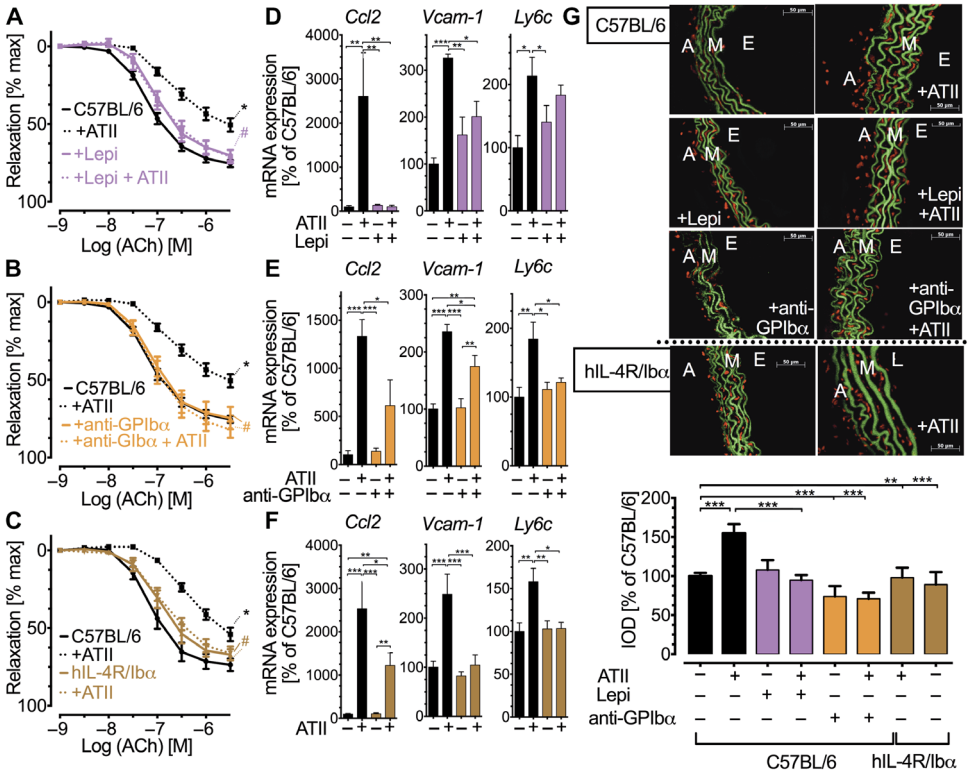

Fig. 2. Blockade of thrombin and GPIbα protects against endothelial dysfunction and preserves regulation of vascular tone. (**A** to **C**) Concentration-relaxation curves in response to ACh of isolated aortic segments from C57BL/6 mice treated for 7 days with either lepirudin (Lepi) (A) or anti-GPIbα (B) or hIL-4R/1bα chimeric mice and C57BL/6 controls (C) treated with or without ATII for 7 days. $^{*}P < 0.05$ versus C57BL/6; $^{\#}P < 0.05$ versus C57BL/6 + ATII, one-way ANOVA and Bonferroni's multiple comparison test of maximal relaxation; $n = 5$ to 8 animals per group. (**D** to **F**) Aortic mRNA expression of *Ccl2*, *Vcam-1*, and *Ly6c*. (**G**) Oxidative fluorescence microtopography. Top: Representative photomicrographs of isolated aortic segments incubated with DHE (1 μM, 30 min at 37°C). Green, laminae (autofluorescence); red fluorescence, superoxide formation; E, endothelium; M, media; A, adventitia. Bottom: Densitometric analysis, integrated optical density (IOD). $^{*}P < 0.05$; $^{**}P < 0.01$; $^{***}P < 0.001$, one-way ANOVA and Bonferroni's multiple comparison test; $n = 4$ to 6 animals per group. Data are means ± SEM.

platelet GPIbα, a well-characterized thrombin receptor (*23*). These mice lack the extracellular ligand-binding domains of GPIbα but retain GPIbα cytosolic receptor interactions, surface expression of additional subunits of the GPIb-IX complex, GPIbβ and GPIX, and normal platelet size (*24*). ATII-infused hIL-4R/Ibα mice were completely or largely protected from ATII-induced vascular endothelial dysfunction (Fig. 2C), oxidative stress (Fig. 2G), and increased expression of *Ccl2*, *Vcam-1*, and *Ly6c* mRNA (Fig. 2F), as also seen in platelet-depleted mice. These findings identified platelet GPIbα as a relevant platelet receptor for ATII-induced endothelial dysfunction and vascular inflammation.

FXI promotes vascular dysfunction by amplifying thrombin formation involving platelet GPIbα

We next determined how coagulation is initiated in ATII-dependent vascular dysfunction. As expected from diminished leukocyte adhesion seen in ATII-infused mice after acute anti-TF treatment (Fig. 1D), long-term blockade of TF during ATII administration attenuated endothelial dysfunction (Fig. 3A) and reduced oxidative stress within the vessel wall [DHE staining: C57BL/6 + ATII versus C57BL/6 + ATII + anti-TF: 163 ± 16% versus 87 ± 5% IOD (% of C57BL/6 ± SEM)]. We analyzed ATII-induced endothelial dysfunction in FXII$^{-/-}$ mice or wild-type mice treated with an antibody (14E11) that interferes with FXII-dependent activation of FXI and found that contact-phase FXII-mediated FXI activation played no major role in mediating ATII-induced endothelial dysfunction (Fig. 3B). This result indicated that initiation of TG by the TF pathway was necessary and sufficient to cause endothelial dysfunction in response to chronically elevated levels of ATII in mice.

Thrombin can amplify coagulation by feedback activation of FXI (*25*, *26*). In addition to binding thrombin, GPIbα can recruit FXI via binding to its apple 3 domain (*27*–*29*). We found that endothelial dysfunction in ATII-infused mice was significantly improved in FXI$^{-/-}$ mice (Fig. 3C) and in wild-type mice after pharmacologic inhibition of FXI synthesis by FXI-specific antisense oligonucleotides (FXI ASOs; Fig. 3D). FXI ASO interferes with *F11* mRNA and leads to *F11* mRNA degradation (*30*). FXI ASO treatment dose-dependently reduced FXI plasma pro-coagulant activity, hepatic *F11* mRNA levels, and FXI protein expression in plasma (Fig. 3, E to H). Specificity of the effects of FXI depletion was confirmed by continuous in vivo supplementation with human FXI (hFXI) (Hemoleven). This treatment restored the reduction plasma FXI activity caused by FXI ASO application (Fig. 4A) and reestablished vascular endothelial dysfunction in FXI ASO–treated mice infused with ATII (Fig. 3I).

IVM showed that ATII-induced leukocyte rolling, as well as adhesion in the carotid artery, was also reduced by FXI ASO treatment. Supplementation of FXI-depleted mice with hFXI restored ATII-induced leukocyte adhesion (Fig. 4B and videos S5 to S8). These results demonstrate that FXI activity is required for the ATII-induced and coagulation-dependent vascular pathology and indicate a role for thrombin-FXI feedback activation in the vasculature in vivo.

ATII also increased association of CD11b^{+} monocytes with CD41^{+} platelets; this process may involve interaction of GPIbα on platelets with leukocyte-expressed Mac-1 (*15*). Treatment of ATII-infused mice with the Mac-1–inhibiting antibody M1/70 significantly attenuated endothelial dysfunction (Fig. 4F) as well as vascular *Ccl2* and *Vcam-1* mRNA expression (Fig. 4G) and circulating platelet-monocyte conjugates (Fig. 4H). The number of platelet-monocyte conjugates was also normalized in FXI ASO–treated mice (Fig. 4C), indicating that coagulation activation was crucial for the inflammation-promoting interaction of Mac-1 with platelets. Circulating levels of thrombin-antithrombin (TAT) complexes, a marker for intravascular thrombin formation, were neither increased by ATII infusion nor altered by FXI ASO (Fig. 4D), excluding the possibility that the platelet-monocyte interaction was promoted by overt intravascular coagulation in the circulation.

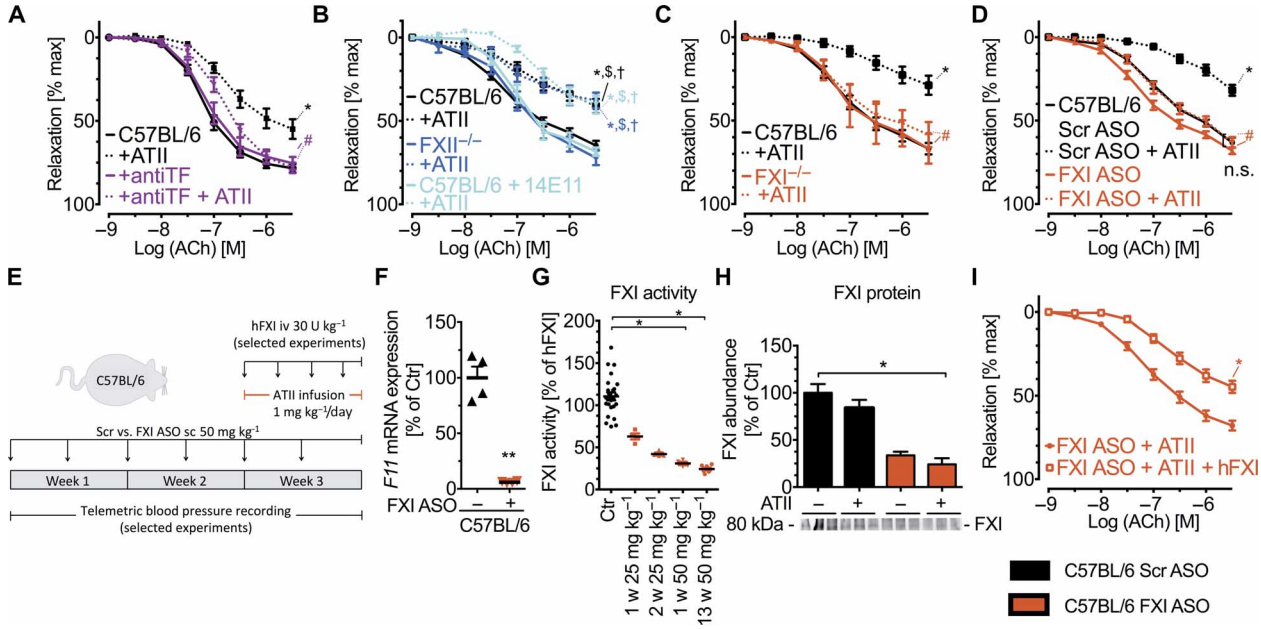

Fig. 3. FXI promotes ATII-induced vascular dysfunction initiated by TF. (**A** to **D**) Concentration-relaxation curves in response to ACh (endothelium-dependent) of isolated aortic segments of mice treated with or without ATII (1 mg kg^{-1} day^{-1} for 7 days). (A) C57BL/6 mice treated for 7 days with anti-TF or control IgG (n = 8 to 9 animals per group). (B) C57BL/6 ± 14E11 (antibody blocking FXII-dependent activation of FXI) and $FXII^{-/-}$ mice (n = 4 to 12 animals per group). (C) $FXI^{-/-}$ and C57BL/6 mice (n = 4 to 7 animals per group). (D) C57BL/6 mice with continuous in vivo inhibition of FXI synthesis by FXI ASO or scrambled control ASO (FXI ASO and Scr ASO, respectively; n = 4 to 10 animals per group). *P < 0.05 versus C57BL/6 or C57BL/6 + Scr ASO; #P < 0.05 versus C57BL/6 + ATII or C57BL/6 + Scr ASO + ATII; $$P$ < 0.05 versus $FXII^{-/-}$; †P < 0.05 versus C57BL/6 + 14E11, one-way ANOVA and Bonferroni's multiple comparison test of maximal relaxation. n.s., not significant. (**E**) Experimental protocol of FXI ASO studies. To control for nonspecific effects of ASO injections, mice that were not injected with FXI ASO were control-injected with Scr ASO in all respective experiments. iv, intravenously; sc, subcutaneously. (**F**) Hepatic mRNA expression of *F11* measured by real-time reverse transcription polymerase chain reaction (RT-PCR). Unpaired t test; n = 4 to 10 animals per group. Ctr, control. (**G**) FXI activity in platelet-poor plasma (PPP) of mice assessed after 1, 2, or 3 weeks of treatment with FXI ASO (25 or 50 mg kg^{-1}) in vivo. Kruskal-Wallis and Dunn's multiple comparison test; n = 4 to 25 animals per group. (**H**) FXI protein in plasma. Top: Densitometry. Bottom: One representative Western blot of four independent experiments. Kruskal-Wallis and Dunn's multiple comparison test; n = 4 animals per group. (**I**) Concentration-relaxation curves in response to ACh of isolated aortic segments of FXI-depleted, ATII-infused C57BL/6 mice with or without continuous in vivo reconstitution with hFXI (hemoleven; unpaired t test of maximal relaxation; n = 8 animals per group). Data are means ± SEM. *P < 0.05; **P < 0.01.

We therefore hypothesized that thrombin-FXI feedback activation was localized to platelets in the inflammatory cross-talk of ATII-induced vascular dysfunction. In platelet-rich plasma (PRP), ex vivo addition of thrombin promotes additional TG [thrombin-evoked endogenous thrombin potential (ETP)] (*31*). PRP from ATII-treated mice showed increased TG compared to control mice, but Mac-1 inhibition did not affect platelet-localized TG (Fig. 4I). In contrast, PRP from mice with pharmacological inhibition of FXI production in the liver failed to amplify TG after chronic ATII exposure (Fig. 4E). Addition of hFXI to PRP from these mice was sufficient to restore the platelet-dependent TG. Consistent with the proposed role of GPIbα as a binding site for both thrombin and FXI (*27*, *28*), endogenous TG was not increased in ATII-treated hIL-4R/Ibα mice and remained unchanged after addition of hFXI to PRP in vitro (Fig. 4E). Thus, the FXI-dependent TG feedback loop amplifies TF-initiated coagulation and requires platelet GPIbα, but not Mac-1, to cause vascular inflammation.

Targeting FXI attenuates ATII-induced vascular inflammation

We further evaluated the therapeutic potential of interrupting FXI synthesis and function (*30*, *32*) to attenuate vascular dysfunction in arterial hypertension. Aortas of ATII-infused mice showed an expansion of $CD45^+$ leukocytes, $CD11b^+GR\text{-}1^+$ myelomonocytic cells (C57BL/6 versus C57BL/6 + ATII versus C57BL/6 + FXI ASO versus C57BL/6 + FXI ASO + ATII: 24.3 ± 5.5 versus 329.7 ± 248.2 versus 15.9 ± 4.0 versus 140.3 ± 42.9 cells per aorta), and $CD11b^+Ly6G^-Ly6C^{hi}$ monocytes (Fig. 5A). Vascular injury was also macroscopically visible as inflamed patches at predilection sites of aortic aneurysm formation, a late sequel of ATII challenge (fig. S1). Aortas of ATII-exposed animals showed increased *Ccl2*, *Vcam-1*, and *Nos2* [encoding for inducible nitric oxide synthase (iNOS)] mRNA expression (Fig. 5B). Aortic protein expression of nox2, reflecting the presence of phagocyte-type NADPH oxidase and heme oxygenase-1 (HO-1), a classical anti-inflammatory and antioxidant response gene, was increased by ATII (fig. S2). Lowering FXI levels with FXI ASO treatment normalized all these parameters of vascular inflammation and leukocyte infiltration. In addition, vascular ROS formation and fibrotic remodeling were blocked by FXI ASO administration in ATII-infused mice (Fig. 5, C and D).

Targeting FXI prevents blood pressure increase in arterial hypertension

On the basis of our observation that FXI was critical for ATII-induced vascular dysfunction, we continuously recorded arterial blood pressure by telemetry. Reducing FXI levels by FXI ASO significantly attenuated the ATII-induced blood pressure increase in mice (Fig. 5E).

To exclude species limitations, we confirmed the efficacy of this therapeutic intervention with FXI inhibitors in Wistar rats. Compared

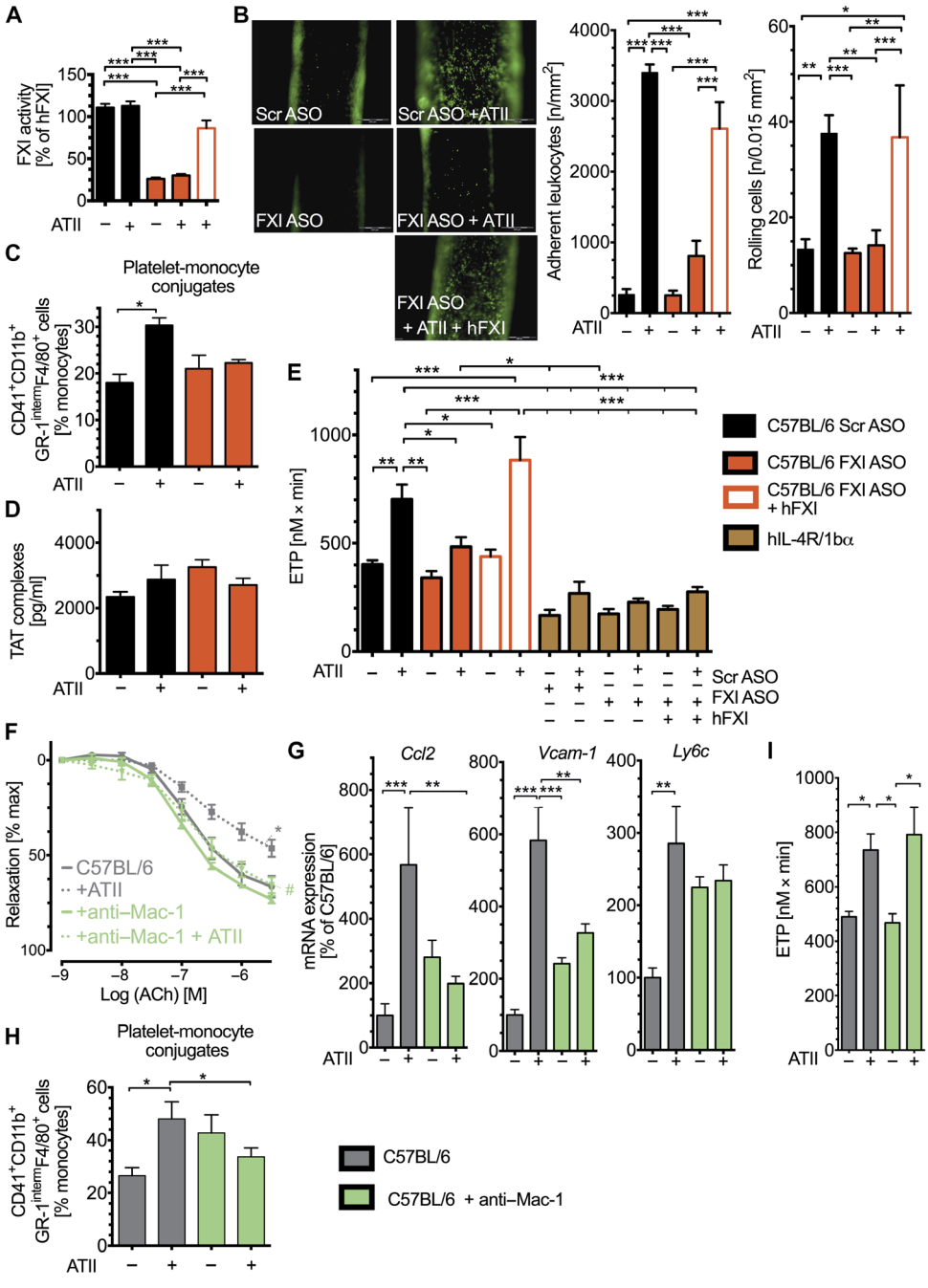

Fig. 4. A platelet localized thrombin-FXI loop promotes ATII-induced vascular inflammation. (**A** to **D**) ATII- and sham-infused C57BL/6 mice were treated with Scr ASO or FXI ASO ± hFXI in vivo, as described in Fig. 3E. (A) FXI activity in PPP. Left: One-way ANOVA and Bonferroni's multiple comparison test; $n = 4$ to 12 animals per group. Right: Mann-Whitney test, $n = 4$ animals per group. (B) IVM showing endothelial adherent leukocytes in the common carotid artery. One-way ANOVA and Bonferroni's multiple comparison test; $n = 3$ to 5 animals per group. (C) Flow cytometry of circulating $CD41^+CD11b^+GR\text{-}1^{interm}F4/80^+$ platelet-monocyte conjugates in blood. Kruskal-Wallis and Dunn's multiple comparison test; $n = 3$ to 5 animals per group. (D) Enzyme-linked immunosorbent assay (ELISA) of circulating TAT complexes. One-way ANOVA and Bonferroni's multiple comparison test; $n = 6$ to 8 animals per group. (**E**) Thrombin-evoked ETP in PRP of ATII- and sham-infused C57BL/6 and hIL-4R/Ibα chimeric mice treated with Scr ASO or FXI ASO in vivo; hFXI was administered ex vivo into PRP, as indicated. In pilot studies, addition of excess hFXI to the PRP of C57BL/6 mice ex vivo increased ETP (C57BL/6 versus C57BL/6 + hFXI versus C57BL/6 + ATII versus C57BL/6 + ATII + hFXI: 100.0 ± 11.6% versus 127.8 ± 12.2% versus 134.9 ± 18.4% versus 152.5 ± 20.2% of C57BL/6, respectively). One-way ANOVA and Bonferroni's multiple comparison test; $n = 5$ to 11 animals per group. (**F**) Endothelium-dependent relaxation of isolated aortic segments of C57BL/6 mice treated with or without M1/70 (anti–Mac-1 antibody) ± ATII for 7 days. $^*P < 0.05$ versus C57BL/6; $^{\#}P < 0.05$ versus C57BL/6 + ATII, one-way ANOVA and Bonferroni's multiple comparison test of maximal relaxation; $n = 5$ to 8 animals per group. (**G**) Aortic mRNA expression of *Ccl2*, *Vcam-1*, and *Ly6c*. One-way ANOVA and Bonferroni's multiple comparison test; $n = 6$ animals per group. (**H**) Flow cytometry of circulating $CD41^+CD11b^+GR\text{-}1^{interm}F4/80^+$ platelet-monocyte conjugates in blood. Kruskal-Wallis and Dunn's multiple comparison test; $n = 3$ to 5 animals per group. (**I**) Thrombin-evoked ETP in PRP. One-way ANOVA and Bonferroni's multiple comparison test; $n = 6$ animals per group. Data are means ± SEM. $^*P < 0.05$; $^{**}P < 0.01$; $^{***}P < 0.001$.

to Scr ASO, rat-specific FXI ASO very effectively reduced *F11* mRNA levels in the liver (control versus FXI ASO: 100 ± 4% versus 7 ± 1% of control). ATII infusion induced endothelial dysfunction (Fig. 6A), which was significantly attenuated by FXI ASO treatment. ATII infusion increased aortic mRNA expression of *Ccl2* and *Vcam-1* as well as of *Ccr2*, which encodes the MCP-1 receptor, and of *Spn*, which encodes sialophorin (CD43) and is involved in leukocyte adhesion (*33*) and a marker for monocytes in rats (Fig. 6B) (*34*). Accordingly, ATII infusion induced vascular accumulation of $CD45^+$ leukocytes (Fig. 6C) and increased vascular oxidative stress in the aorta (Fig. 6D) and systolic blood pressure (Fig. 6E). FXI ASO application attenuated these alterations: neither endothelial function, vascular mRNA expression of inflammatory genes, accumulation of $CD45^+$ cells, vascular oxidative stress, nor blood pressure was significantly different in ATII-infused FXI ASO–treated rats compared to sham-infused Scr ASO– or FXI ASO–treated rats. This recapitulated the findings obtained in the ATII-infused C57BL/6 mice.

To investigate an alternative model of arterial hypertension that reflects human pathology, we next studied 5/6 nephrectomized (5/6Nx) compared to sham-operated Wistar rats. This rat model is an established model of chronic kidney disease characterized by endogenous up-regulation of the renin-angiotensin-aldosterone system (RAAS) with increased systemic ATII levels and progressive and sustained arterial hypertension and vascular dysfunction (*35*). Hepatic

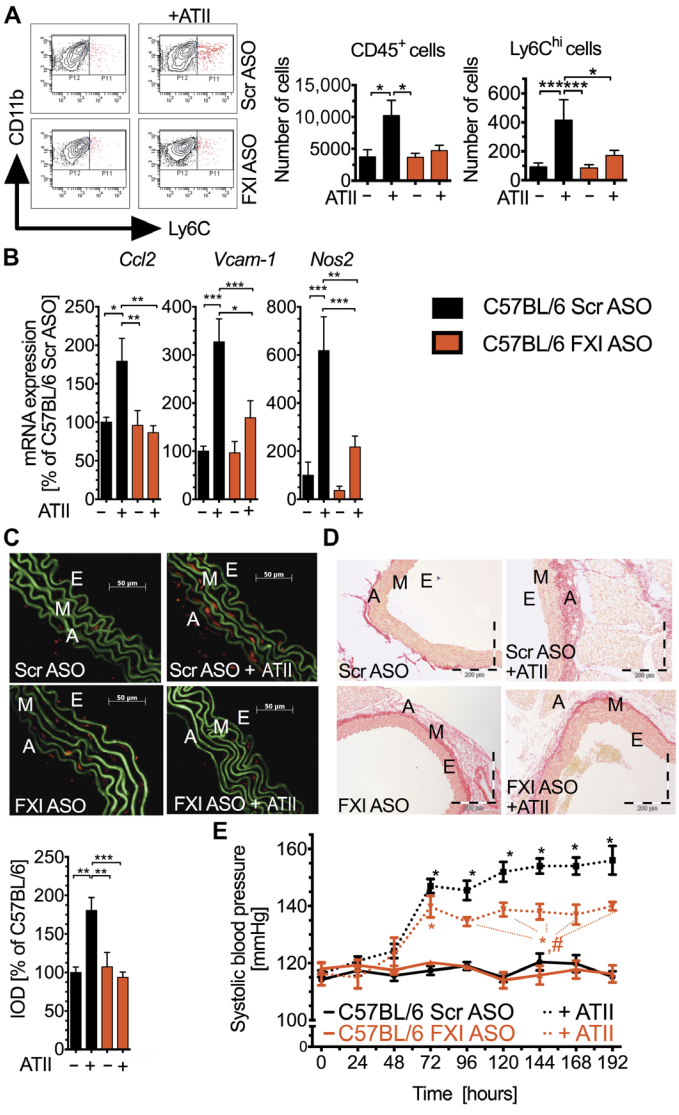

Fig. 5. Inhibition of FXI protects against vascular inflammation. C57BL/6 mice were treated with FXI ASO or Scr ASO and infused with ATII or sham for 7 days (see Fig. 3E for experimental protocol). (**A**) Flow cytometry of $CD45^+$ leukocytes and $CD11b^+Ly6C^{hi}$ cells in aortic lysates and absolute numbers of viable $CD45^+$ and $CD45^+CD11b^+Ly6C^{hi}Ly6G^-NK1.1^-$ cells. Left: Representative original plots of $CD11b^+Ly6C^{hi}Ly6G^-NK1.1^-$ myelomonocytes. Right: Quantification. One-way ANOVA and Bonferroni's multiple comparison test; $n = 5$ animals per group. (**B**) Aortic mRNA expression of *Ccl2*, *Vcam-1*, and *Nos2*. One-way ANOVA and Bonferroni's multiple comparison test; $n = 4$ to 13 animals per group. (**C**) Oxidative fluorescence microtopography. Left: Representative photomicrographs of aortic cryosections; superoxide formation appears in red. Right: Densitometry, IOD. One-way ANOVA and Bonferroni's multiple comparison test; $n = 5$ animals per group. (**D**) Sirius red staining of aortic sections. (**E**) Summary of 192 hours of telemetrically recorded systolic blood pressure (in millimeters of mercury). Two-way ANOVA and Bonferroni post test; $n = 4$ to 5 animals per group. Data are means ± SEM. $^*P < 0.05$; $^{**}P < 0.01$; $^{***}P < 0.001$. In (E), $^*P < 0.05$ versus C57BL/6 + Scr ASO and C57BL/6 + FXI ASO; $^{\#}P < 0.05$ versus C57BL/6 + Scr ASO + ATII.

F11 mRNA levels were not increased by the surgery and were effectively reduced by FXI ASO in both sham-operated and 5/6Nx rats (sham versus 5/6Nx versus sham + FXI ASO versus 5/6Nx + FXI ASO: 100 ± 6% versus 92 ± 8% versus 2 ± 1% versus 1 ± 0% of sham). Four weeks after surgery, 5/6Nx rats had endothelial dysfunction, as compared to sham-operated animals, which was prevented by concomitant FXI ASO administration (Fig. 6F). FXI ASO decreased the vascular oxidative stress in the aorta elicited by the increased RAAS activation in the 5/6Nx rats (Fig. 6F). TG was increased in PRP of 5/6Nx rats and was markedly diminished by FXI ASO application, mimicking the results from hypertensive mice (Fig. 6H). Together, these results indicate that attenuation of the inflammatory pro-coagulant milieu in this rat model prevented blood pressure increase (Fig. 6I), as seen in ATII-infused mice and rats.

Treatment of arterial hypertension with FXI ASO reduces blood pressure, vascular dysfunction, and kidney injury

To extend our finding that FXI ASO could attenuate arterial hypertension when given preventively, we next aimed to treat established hypertension. Eight weeks after 5/6 nephrectomy, 5/6Nx rats were characterized by vascular endothelial dysfunction (Fig. 7A) as well as increased vascular mRNA expression of *Ccr2* and *Spn* (Fig. 7B), vascular accumulation of $CD45^+$ leukocytes (Fig. 7C), and ROS formation (Fig. 7D). In rats that had been nephrectomized for 8 weeks, *Pai-1* mRNA (encoding for plasminogen activator inhibitor-1) expression in the renal cortex was drastically increased (Fig. 7E) and associated with kidney fibrosis, structural kidney damage (Fig. 7, F and G), and impaired kidney function, as indicated by retention of urea nitrogen (urea-N) and creatinine in plasma (Fig. 7H) and proteinuria (Fig. 7I). Blood pressure significantly increased 2 weeks after 5/6 nephrectomy and plateaued between weeks 4 and 8 (Fig. 7J). Continuous treatment of 5/6Nx rats with FXI ASO starting 3 weeks after surgery significantly improved vascular injury, renal damage, and expression of *Pai-1* mRNA and significantly and persistently reduced arterial hypertension. Thus, the coagulation-inflammation circuit involving the thrombin-FXI loop is a major regulator of arterial hypertension, and interruption of this pathway reduces established vascular dysfunction and arterial hypertension and can treat long-term complications of kidney injury associated with hypertension.

FXI-dependent TG is increased in humans with uncontrolled hypertension

To assess the applicability of our findings to human disease, we explored platelet-localized TG in an all-comer population of patients with arterial hypertension who came to the emergency room and outpatient clinic of the University Medical Center Mainz. We observed a positive correlation between mean arterial blood pressure and ETP, which corresponds to the overall thrombin generated over time, as well as peak (maximum amount of thrombin generated) and velocity of TG in PRP (Fig. 8A). According to current guidelines (*36*), we divided our study population into three groups. Except for systolic, diastolic, and mean arterial blood pressure, there were very few demographic differences between the groups (Table 1). Individuals with hypertension grade II or higher showed significantly higher TG than controls, recapitulating our findings from mouse and rat models (Fig. 8B). Addition of an FXI anti–apple 3 domain antibody to block FXI activation by thrombin markedly reduced ETP, peak TG, and velocity of TG in PRP from control subjects and completely abrogated the increase of these markers in PRP from patients with uncontrolled hypertension (Fig. 8C). To exclude the possibility that these results were due to alterations in plasma components and make sure that they were related to platelets, we resuspended washed platelets in PPP from healthy donors. When the resuspended platelets were derived from individuals with uncontrolled hypertension, but not when they were from healthy controls, we measured significantly increased

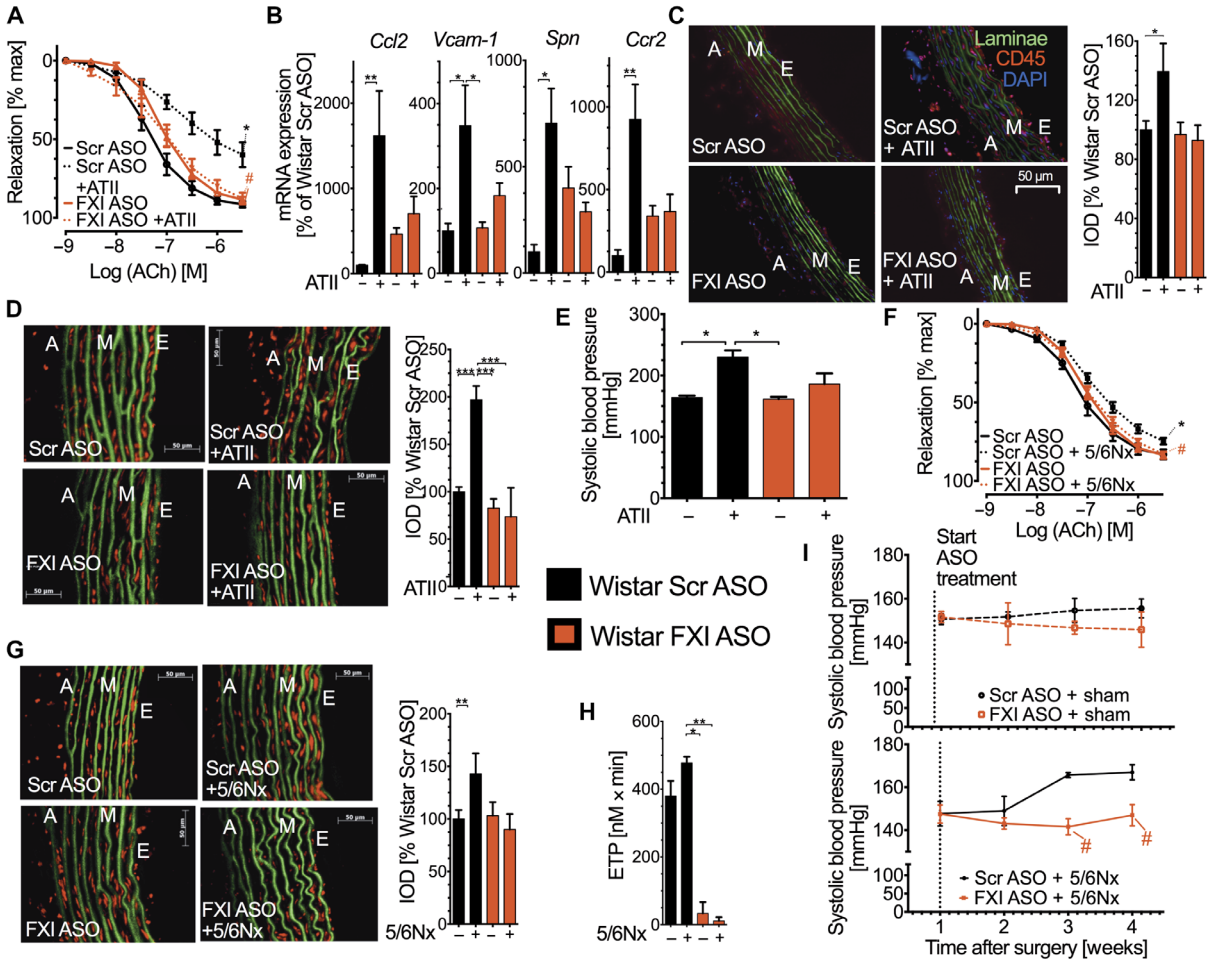

Fig. 6. FXI ASO administration prevents vascular dysfunction and arterial hypertension in ATII-infused and 5/6Nx rats. (**A** to **E**) Wistar rats were treated for 1 week with ATII or sham and with FXI ASO (Wistar + FXI ASO ± ATII) or Scr ASO (Wistar + Scr ASO ± ATII) starting 2 weeks before ATII infusion to be analogous to the mouse treatment scheme (see Fig. 3E). (A) Endothelium-dependent relaxation of isolated aortic segments. $^{*}P < 0.05$ versus Wistar + Scr ASO; $^{\#}P < 0.05$ versus Wistar + Scr ASO + ATII, one-way ANOVA and Bonferroni's multiple comparison test of maximal relaxation; $n = 5$ to 9 animals per group. (B) Aortic mRNA expression of *Ccl2*, *Vcam-1*, sialophorin (*Spn*), and chemokine receptor 2 (*Ccr2*). Kruskal-Wallis and Dunn's multiple comparison test; $n = 3$ to 6 animals per group. (C) Immunostaining of aortic cryosections. Green, autofluorescence; red, CD45; blue, 4′,6-diamidino-2-phenylindole (DAPI). Red fluorescence was quantified in whole aortic rings. One-way ANOVA and Bonferroni's multiple comparison test; $n = 4$ to 5 animals per group. (D) Superoxide formation in aortic cryosections. Left: Representative DHE photomicrotopographs of aortic cryosections; superoxide formation appears in red. Right: Quantification. One-way ANOVA and Bonferroni's multiple comparison test, $n = 6$ animals per group. (E) Systolic blood pressure after 1 week of ATII infusion or sham treatment. Kruskal-Wallis and Dunn's multiple comparison test; $n = 3$ to 14 animals per group. (**F** to **I**) Wistar rats underwent 5/6 nephrectomy (5/6Nx) or sham operation (sham) and were administered for 3 weeks with FXI or Scr ASO, starting 1 week after surgery. (F) Endothelium-dependent relaxation of isolated aortic segments. One-way ANOVA and Bonferroni's multiple comparison test of maximal relaxation; $n = 5$ to 12 animals per group; $^{*}P < 0.05$ versus Wistar + Scr ASO; $^{\#}P < 0.05$ versus Wistar + Scr ASO + 5/6Nx. (G) Oxidative fluorescence microtopography. Left: Representative photomicrographs. Right: Densitometry. One-way ANOVA and Bonferroni's multiple comparison test; $n = 6$ animals per group. (H) ETP in PRP. Kruskal-Wallis and Dunn's multiple comparison test; $n = 4$ to 6 animals per group. (I) Systolic blood pressure after nephrectomy. $^{\#}P < 0.05$ versus Wistar + Scr ASO + 5/6Nx, two-way ANOVA and Bonferroni's post tests; $n = 4$ (sham) and 8 to 10 (5/6Nx) animals per group. Data are means ± SEM. $^{*}P < 0.05$; $^{**}P < 0.01$; $^{***}P < 0.001$ (B to D, F, and G).

peak TG and velocity of TG, confirming that platelets from patients with hypertension are sufficient and essential to support TG in plasma (Fig. 8D).

DISCUSSION

Our findings provide insight into the pathogenic role of the thrombin-FXI loop in inflammation and show that this pathway makes a crucial contribution to arterial hypertension in the absence of overt vascular thrombotic occlusion. We delineate an unexpected sequence of events that specifically fosters vascular inflammation in RAAS-driven arterial hypertension. ATII triggers TF up-regulation in the vasculature, providing initial TG that is amplified by an FXI feedback loop mediated through GPIbα. Additional thrombin generated on platelets leads to leukocyte adhesion and vascular inflammation, which depends on VCAM-1, VLA-4, and Mac-1. We demonstrated that FXI inhibition blocks ATII-driven vascular immune cell infiltration and attenuates arterial hypertension (see scheme in Fig. 8E). FXI inhibition introduces a disruption at the crossroads of an orchestrated inflammatory response that involves platelets, leukocytes, and the vessel wall. Localized platelet-amplified thrombin formation mediates the recruitment of proinflammatory monocytes to the vasculature in a process that leads to arterial

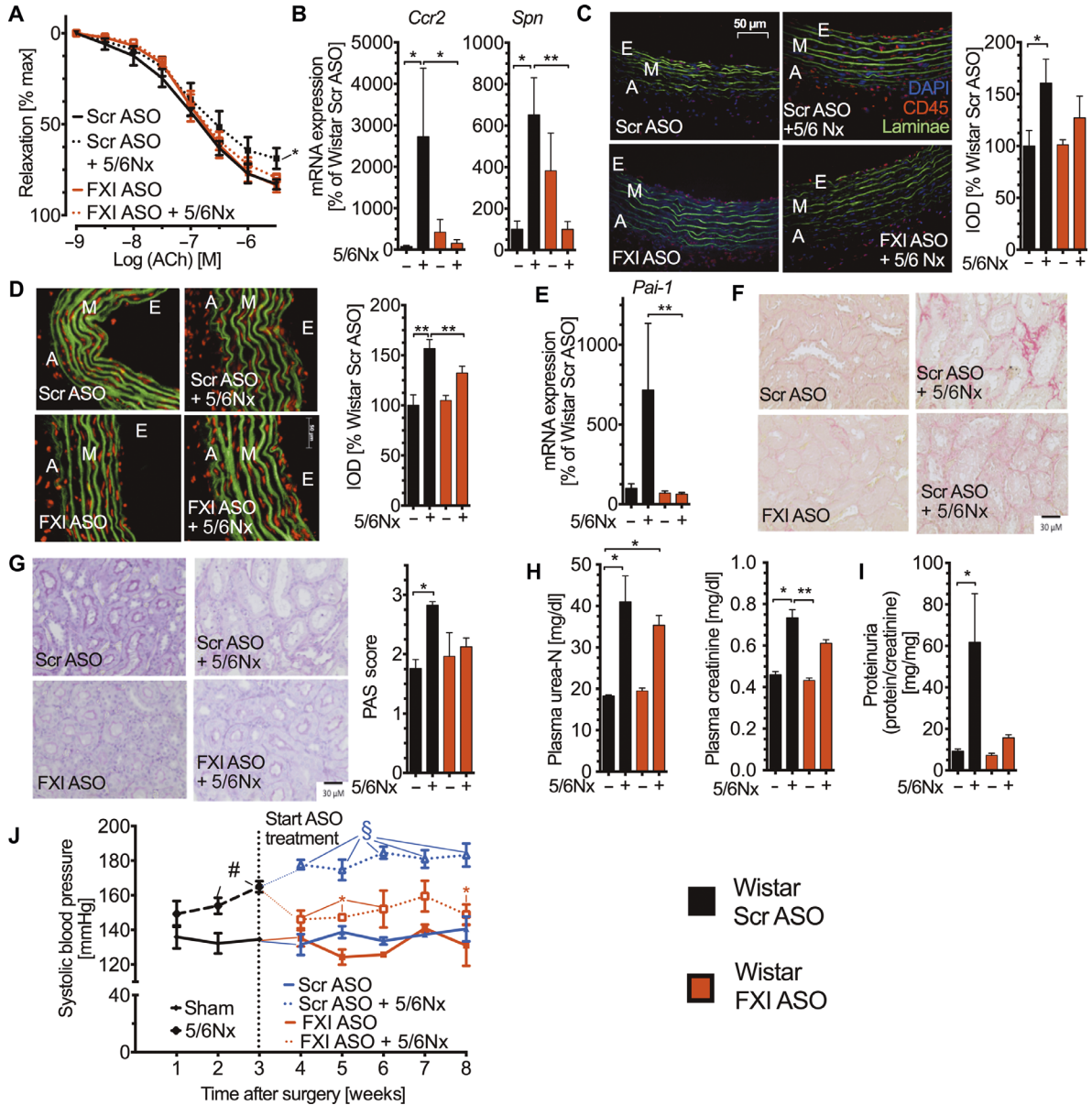

Fig. 7. FXI ASO treatment of established arterial hypertension attenuates vascular and kidney injury and reduces blood pressure in 5/6Nx rats. Wistar rats underwent 5/6 nephrectomy (5/6Nx) or sham operation (sham) and were treated for 5 weeks with FXI ASO or Scr ASO, starting 3 weeks after surgery. (**A**) Endothelium-dependent relaxation of isolated aortic segments. *P < 0.05 versus Wistar sham, one-way ANOVA and Bonferroni's multiple comparison test of maximal relaxation; n = 4 to 6 animals per group. (**B**) mRNA expression levels of *Spn* and *Ccr2* in aortic lysates. Kruskal-Wallis and Dunn's multiple comparison test; n = 4 to 6 animals per group. (**C**) Immunostaining of aortic cryosections. Green, autofluorescence; red, CD45; blue, DAPI. Red fluorescence was quantified in whole aortic rings. One-way ANOVA and Bonferroni's multiple comparison test; n = 4 animals per group. (**D**) Oxidative fluorescence microtopography. Left: Representative photomicrographs. Right: Densitometry. One-way ANOVA and Bonferroni's multiple comparison test; n = 4 to 6 animals per group. (**E**) mRNA expression levels of *Pai-1* in renal cortex. Kruskal-Wallis and Dunn's multiple comparison test; n = 4 to 6 animals per group. (**F**) Sirius red staining and (**G**) periodic acid–Schiff (PAS) staining of kidney sections (left) and score for PAS staining (right). One-way ANOVA and Bonferroni's multiple comparison test; n = 4 to 6 animals per group. Quantification of (**H**) plasma urea-N and creatinine and (**I**) proteinuria. Kruskal-Wallis and Dunn's multiple comparison test; n = 4 to 6 animals per group. (**J**) Systolic blood pressure. $^{\#}P$ < 0.05 versus Wistar + 5/6Nx; $^{\S}P$ < 0.05 versus Wistar + Scr ASO and Wistar + FXI ASO; *P < 0.05 versus Wistar + Scr ASO + 5/6Nx, two-way ANOVA and Bonferroni's post tests; n = 8 (sham) and 12 (5/6Nx) animals per group. Data are means ± SEM. *P < 0.05; **P < 0.01 (B to I).

hypertension. Given that arterial hypertension is a multifactorial disease, which requires combined medical treatment targeting multiple pathways [salt/water retention, increased sympathetic tone, and activated RAAS (*36*)], it is interesting that targeting FXI alone was effective in reducing not only vascular inflammation but also blood pressure.

Platelet inhibitors, such as aspirin (acetylsalicylic acid), which are among the most prescribed drugs worldwide, are very effective in reducing mortality in people who have experienced adverse cardiovascular events such as myocardial infarction and are also being considered for primary prevention in the general population (*37*, *38*). Aspirin has an anti-inflammatory

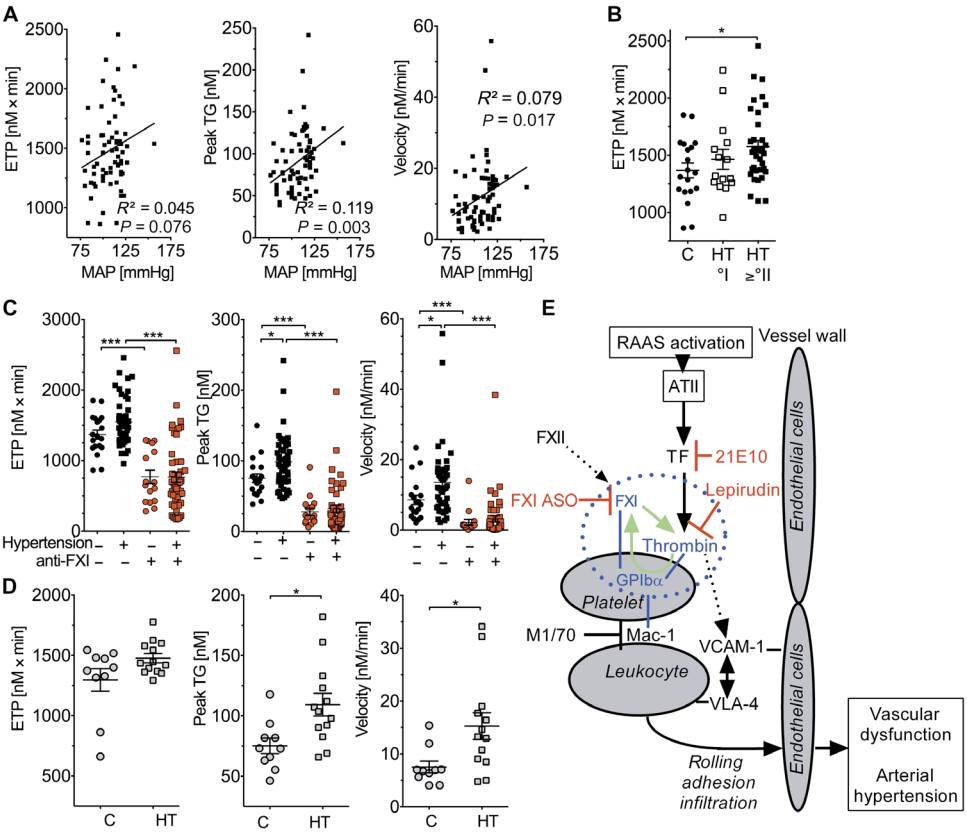

Fig. 8. Blood pressure correlates with platelet-localized, FXI-dependent TG in humans. (**A**) In all participants of the FACTO-RR study, linear regression analysis was performed between mean arterial pressure (MAP) and ETP and between peak TG and velocity of TG; $n = 71$, Pearson correlation coefficient; exact two-tailed P values are given. (**B**) On the basis of current guidelines (*36*), the population was stratified into three groups, for example, controlled hypertension (control, $n = 19$), arterial hypertension grade I (HT°I; $n = 16$), and arterial hypertension grade II or higher (HT≥°II; $n = 36$). ETP in PRP was analyzed for each individual group. Kruskal-Wallis test with Dunn's multiple comparison test was used. (**C**) Participants of the FACTO-RR study were split into two groups: controlled hypertension (C; $n = 19$) and uncontrolled (HT°I and HT≥°II) hypertension (HT; $n = 52$). ETP, peak TG, and velocity of TG were measured before and after addition of 1A6, an anti–apple 3 domain antibody blocking the feedback activation of FXI by thrombin. Data are means ± SEM. Kruskal-Wallis test with Dunn's multiple comparison test was used. (**D**) In selected patients, washed platelets of controlled ($n = 10$) and uncontrolled ($n = 13$) hypertensives were resuspended in PPP of healthy donors and triggered with exogenous TF to evoke ETP. Mann-Whitney test. Data are means ± SEM. *$P < 0.05$; **$P < 0.01$; ***$P < 0.001$. Each measurement was performed in triplicate, yielding one data point. (**E**) Scheme illustrating the main findings. Blue color marks the most relevant interaction partners of the newly identified mechanism. Green, positive feedback loop; red, inhibitory action.

preventive potential in individuals with increased high-sensitivity C-reactive protein, who are at risk for future cardiovascular events (*39*). The pathway we have described here is driven by ATII and critically depends on platelet-expressed GPIbα, a known receptor for both thrombin and FXI. Anti-platelet drugs such as abciximab, a GPIIb/IIIa antagonist, and aspirin only partially influence TF-triggered TG in PRP (*40*). Furthermore, there is no evidence that aspirin or GPIIb/IIIa inhibitors reduce blood pressure. Therefore, our findings suggest that inhibiting the GPIbα-dependent, thrombin-FXI–amplifying loop may provide added cardiovascular benefits that are synergistic with those of established platelet inhibitors.

Anticoagulants blocking vitamin K–dependent synthesis of coagulation factors (vitamin K antagonists) and newer, protease-specific direct oral anticoagulants such as thrombin inhibitors could both be of clinical utility to interrupt the proinflammatory TF-thrombin pathway uncovered in our study. Our data unexpectedly show that pharmacological targeting of FXI can achieve beneficial effects comparable to thrombin inhibition in preventing vascular inflammation in our model. FXI has previously been implicated in the development of thrombosis (*26*, *41*), and more recent evidence suggests that FXI may also be involved in atherogenesis through its ability to promote inflammation. Although reduced numbers of lesional macrophages were described in FXI-deficient ApoE$^{-/-}$ mice, the mechanism remains unclear (*42*); it may involve a pathogenic mechanism similar to that described in our study.

In humans, FXI deficiency is associated with a decreased risk of deep vein thrombosis (*43*) and stroke; however, because hereditary FXI deficiency is rare, there is no conclusive evidence that low FXI levels are linked to decreased prevalence of arterial hypertension in humans (*44*). The pathway that we have described here for FXI-dependent TG is associated with clinically manifest arterial hypertension in humans, and furthermore, platelet-dependent amplified TG may be a candidate surrogate marker to stratify patients for therapeutic intervention with FXI inhibitors. A wide range of antihypertensive drugs are available to control blood pressure; however, we unexpectedly discovered that established arterial hypertension can be attenuated by FXI ASO in rats. Inhibition of FXI was sufficient to prevent PAI-1 expression in the kidney. PAI-1 is induced by thrombin in both the vasculature (*45*) and the kidneys (*46*) and is a surrogate marker for kidney injury (*47*), and PAI-1 activity leads to kidney fibrosis induced by ATII (*48*). Thus, targeting of FXI does not simply modulate a redundant pathway in blood pressure regulation but may substantially improve hypertension-associated renal dysfunction, kidney fibrosis, and injury.

Preclinical (*30*) and clinical (*49*) evidence further indicate that inhibition of FXI is associated with a lower risk of bleeding complications than is warfarin or enoxaparin. The described surrogate marker evaluation of this pathway (Fig. 8), together with the reported safety in avoiding bleeding complications (*30*, *49*), suggests that the pleiotropic effects of FXI inhibitors to prevent vascular inflammation, dysregulation of vascular tone, and ensuing kidney damage should be exploited in medical care. Because our mechanistic results are largely limited to animal models, randomized clinical trials are needed to test whether these effects hold true in humans. At first, the anti-inflammatory and blood pressure–lowering effects of FXI inhibitors should be monitored once this type of drug enters clinical use as antithrombotic medication. FXI inhibitors may prove more therapeutically useful than anticipated in individuals with cardiovascular disease and activated RAAS.

Table 1. Patient characteristics of all participants of the FACTO-RR study. On the basis of the current guidelines on arterial hypertension, the population was stratified into three groups (*36*), for example, controlled hypertension (control), arterial hypertension grade I, and arterial hypertension grade II or higher (summarized as uncontrolled hypertension in some analyses). *$P < 0.05$ versus control; #$P < 0.05$ versus hypertension grade I, Kruskal-Wallis test with Dunn's multiple comparison test or Fisher's exact test. bpm, beats per minute; ACE, angiotensin-converting enzyme; NSAIDs, nonsteroidal anti-inflammatory drugs; BMI, body mass index; MI, myocardial infarction; CAD, coronary artery disease; PAD, peripheral artery disease; COPD, chronic obstructive pulmonary disease; CVD, cardiovascular disease.

	Controlled hypertension	Uncontrolled hypertension	
		Hypertension grade I	Hypertension grade II or >II
n	19	16	36
Male, *n* (%)	7 (36.8)	10 (62.5)	16 (44.4)
Age (years)	65.4 ± 3.5	62.8 ± 3.1	65.3 ± 1.9
Blood pressure (mmHg)			
Systolic	122.6 ± 2.5	138.8 ± 1.2	179.0 ± 1.9*,#
Diastolic	70.8 ± 1.7	85.6 ± 1.6*	88.8 ± 1.7*
Mean	88.1 ± 1.5	103.3 ± 1.2*	118.8 ± 1.5*,#
Heart rate (bpm)	72.5 ± 2.1	75.7 ± 3.6 *	83.3 ± 2.0
BMI (kg m^{-2})	26.5 ± 1.0	28.3 ± 1.3	29.7 ± 1.0
Medication, *n* (%)			
ACE inhibitors	6 (31.6)	2 (12.5)	11 (30.6)
AT_1 receptor blockers	5 (26.3)	10 (62.5)*	12 (33.3)
Ca^{2+} channel blockers	2 (10.5)	4 (25.0)	8 (22.2)
ß Blockers	13 (68.4)	9 (56.3)	13 (36.1)*
Thiazide diuretics	2 (10.5)	8 (50.0)*	8 (22.2)
Loop diuretics	3 (15.8)	4 (25)	5 (13.9)
Aldosterone antagonists	5 (26.3)	1 (6.3)	0*
Renin inhibitors	1 (5.3)	0	1 (2.8)
α Blockers	1 (5.3)	1 (6.3)	3 (8.3)
Statins	6 (31.6)	7 (43.8)	5 (13.9)#
Acetylsalicylic acid	8 (42.1)	10 (62.5)	14 (38.9)
Antidiabetic drugs	4 (21.1)	4 (25)	5 (13.9)
NSAIDs	1 (5.3)	2 (12.5)	1 (2.8)
Thyroid hormone	2 (10.5)	4 (25)	11 (30.6)
Platelet count (10^3 per µl)	183.7 ± 19.1	228.4 ± 14.8	191.2 ± 12.0
Comorbidities, *n* (%)			
Diabetes	8 (42.1)	3 (18.8)	9 (25)
Cigarette smoking	1 (5.3)	2 (12.5)	2 (5.6)
History of smoking	5 (26.3)	5 (31.3)	9 (25)
Dyslipidemia	8 (42.1)	7 (43.8)	11 (30.6)
Obesity, BMI > 30 kg m^{-2}	5 (26.3)	5 (31.3)	11 (30.6)

continued on next page

	Controlled hypertension	Uncontrolled hypertension	
		Hypertension grade I	Hypertension grade II or >II
History of MI or CAD	12 (63.2)	6 (37.5)	5 (13.9)*
History of stroke	1 (5.3)	1 (6.3)	2 (5.6)
PAD	2 (10.5)	3 (18.8)	1 (2.8)
COPD	1 (5.3)	0	0
Family history of CVD	6 (31.6)	8 (50)	17 (47.2)
Alcohol abuse	8 (42.1)	8 (50)	13 (36.1)
Cancer	3 (15.8)	2 (12.5)	1 (2.8)
Chronic kidney disease	5 (26.3)	0*	4 (11.1)

MATERIALS AND METHODS

Study design

The overall objective of the study was to test the hypothesis that leukocytes, platelets, and coagulation factors interact to promote vascular injury in arterial hypertension. We designed a translational study, involving experimentation with laboratory animals (mice, in part genetically modified, and rats) and blood plasma as well as an observational analysis of a monocentric nonrandomized unblinded all-comer clinical cohort. In the experimental studies, samples were measured at least in duplicate and replicated at least three times ($n \geq 3$ animals per group, specified in each figure legend). Experimentators were blinded to the treatment arm by pseudonymization of the samples, whenever feasible.

Chemicals

All chemicals were of highest analytical grade and obtained from either Sigma-Aldrich or Merck. FXI ASOs [mouse: lot nos. 404071 (FXI ASO) and 421208 (control); rat: lot nos. 404088 (FXI ASO) and 141923 (control)] were produced by Ionis Pharmaceuticals. They were designed to suppress hepatic mRNA levels of FXI in mice and rats. The ASOs had a length of 20 nucleotides, and phosphorothioate and 2′-*O*-methoxyethyl were added (*30*).

Animals and in vivo treatment

$FXII^{-/-}$ (*50*), $FXI^{-/-}$ (*51*), and hIL-4R/Ibα mice (*24*) were generated and backcrossed more than 10 times to the C57BL/6J background, as described previously. C57BL/6J mice were purchased from the Jackson Laboratory and used as control mice in all experiments. Male mice (10 to 12 weeks old) were used as experimental animals. Mice were infused subcutaneously with ATII (1 mg kg^{-1} day^{-1} for 7 days) via miniosmotic pumps (model 1007D, ALZET) versus sham. In selected experiments, mice were injected subcutaneously with FXI ASO (50 mg kg^{-1}) or Scr ASO solved in 0.9% NaCl twice per week for a period of 3 weeks, starting 2 weeks ahead of the ATII regimen (see Fig. 3E). After 3 weeks, mice were euthanized by exsanguination under isoflurane anesthesia, and aorta, liver, and blood were collected. In selected experiments, C57BL/6 mice were intraperitoneally or intravenously injected with platelet-depleting anti-GPIbα antibody [5A7 Ab (*52*); 3.4 mg kg^{-1} intraperitoneally three times per week or acutely 3.4 mg kg^{-1} intravenously], TF-inactivating antibody (21E10; 20 mg kg^{-1} intraperitoneally three times per week or acutely 25 mg kg^{-1} intravenously), anti–VCAM-1 antibody (clone 429 MVAM.A, eBioscience; 1 mg kg^{-1}, intravenously), anti–VLA-4 antibody (clone PS2α; 10 mg kg^{-1}, intravenously), anti–Mac-1 antibody (clone M1/70, BioXCell; acutely 6.5 mg kg^{-1}), and an antibody blocking the FXII-dependent activation of FXI (14E11, provided by A. Gruber; 5 mg kg^{-1} intraperitoneally three times per week) or respective control IgGs resolved in phosphate-buffered saline (PBS). In some experiments, mice were reconstituted intravenously with highly purified plasma-derived hFXI (30 U kg^{-1}) (Hemoleven, Swedish Orphan Biovitrum) every second day for 1 week or sham (0.9% NaCl). Thrombin inhibition was achieved by continuous infusion of lepirudin via miniosmotic pumps (model 1007D, ALZET) implanted intraperitoneally (0.3 mg kg^{-1} $hour^{-1}$) or by acute intravenous injections (1.7 mg kg^{-1}). In addition, male Wistar rats (8 to 10 weeks old; 450 to 500 g; Charles River Laboratories) were used. In analogy to the mouse experiments, rats were treated subcutaneously with ATII (1 mg kg^{-1} day^{-1} for 7 days) via miniosmotic pumps (model 2001, ALZET) versus sham. Rats were injected subcutaneously with FXI ASO (50 mg kg^{-1}) or Scr ASO solved in 0.9% NaCl twice per week for a period of 3 weeks, starting 2 weeks ahead of the ATII regimen.

As an additional hypertension model, 5/6Nx rats were used. Studies were carried out on male Wistar rats from Janvier Labs, aged 8 weeks old. Rats underwent one-step 5/6 subtotal nephrectomy, as described previously (*53*), or sham operation performed by Janvier Labs as the commercial provider. Briefly, surgery consists of right nephrectomy and surgical ablation of the lower and upper poles of the left kidney. Depending on the study protocol, 1 week (preventive protocol) or 3 weeks (treatment protocol) after operation, subcutaneous injection of FXI ASO (50 mg kg^{-1}) or Scr ASO twice per week for a period of 3 weeks (or 5 weeks, respectively) was started. Animal treatment was approved by the board of examinations of the state of Rhineland-Palatinate (authorization number 23 177-07/G12-1-002).

Blood pressure recordings

For blood pressure recordings of mice, carotid catheters were implanted into C57BL/6 animals [TA-PA11C10, Data Science International (DSI)]. For anesthesia and analgesia, mice received intraperitoneal injections of midazolam (5 mg kg^{-1}; Ratiopharm GmbH), medetomidine (0.5 mg kg^{-1} body weight), and fentanyl (0.05 mg kg^{-1} body weight; Janssen-Cilag GmbH). After the surgical procedure, the animals were administered atipamezole (0.05 mg kg^{-1}), flumazenil (0.01 mg kg^{-1}), and naloxone (0.024 mg kg^{-1}) subcutaneously to antagonize anesthesia. Postoperative analgesia was carried out with buprenorphine (0.075 mg kg^{-1}). The implantation of the catheters

was performed under sterile conditions. After surgery, mice recovered for 1 to 2 weeks until the recording was started. Blood pressure was continuously recorded to receiver platforms (DSI), and the data were saved using DataQuest system (DSI). Rat blood pressure measurements were performed by tail cuff with the Coda Monitor System (Kent Scientific). Blood pressure in ATII versus sham-infused rats was measured 1 week after pump implantation and in 5/6Nx versus sham-operated rats once a week for a period of 4 or 8 weeks starting 1 week after surgery.

Preparation of PPP and PRP from mice and rats

Blood samples were collected from experimental animals under isoflurane anesthesia by puncture of the inferior caval vein. Complete blood counts and hematocrit were determined with an automatic cell counter KX-21N (Sysmex Corporation). The obtained blood (700 μl; 10:1 with 3.2% sodium citrate) was gently mixed for proper anticoagulation. After centrifugation for 15 min at 2500*g* at 20°C, PPP was transferred into new tubes, snap-frozen, and stored at −80°C until further use. PRP from experimental animals was prepared by differentiated centrifugation of citrate-anticoagulated whole blood, taken by retro-orbital vein puncture using silanized glass capillaries.

FXI activity assay and activated partial thromboplastin time

PPP was defrosted at 37°C, every sample was gently stirred, and assays were performed using the Siemens BCS II according to the manufacturer's protocol. Results are compared to human pooled values.

Preparation of PPP and PRP from human subjects

Blood was obtained by venipuncture via a 21-gauge needle and collected into 0.129 M sodium citrate (9:1, v/v). Complete blood counts and hematocrit were determined with an automatic cell counter KX-21N (Sysmex Corporation). PRP was prepared within 1 hour of blood sampling with a first centrifugation of 190*g* for 10 min at 20°C. The supernatant was removed, and the platelet count was adjusted to 150×10^9 per liter with PPP prepared with a 10-min centrifugation at 1750*g* at 20°C. In platelet resuspension experiments, PRP was centrifuged for 4 min at 1750*g* at 20°C, supernatant was removed, platelets were resuspended in a pool of PPP from healthy volunteers, and platelet count was adjusted at 150×10^9 per liter.

TG assay in PRP

Platelet-dependent TG was assessed in PRP upon stimulation with α-thrombin (0.1 U/ml) by fluorogenic calibrated automated thrombography in vitro in a microtiter plate fluorometer (Fluoroskan Ascent) using the thrombinoscope and Synapse BV software program (*31*, *54*–*56*). Where indicated, an anti–apple 3 domain of FXI (1A6; generated by A. Gruber) was added at a concentration of 5 μg/ml. The parameters calculated by the software were the lag time, thrombin peak, time to peak, velocity, and ETP, which corresponds to the area under the curve.

Vascular reactivity studies

To assess vasodilator properties of isolated aortic segments (~4 mm), they were mounted to force transducers in organ chambers to test their response to ACh. The aortic rings were preconstricted with phenylephrine (0.15 μM) or prostaglandin $F_2\alpha$ (3 nM) to reach 50 to 80% of the tone induced by KCl. Concentration-relaxation curves were recorded in response to the endothelium-dependent vasodilator ACh (1 nM to 3 μM) (*8*).

Fluorescence oxidative microtopography

To quantify vascular ROS production, the aortas were cut into rings of 4 mm in length and then incubated in Krebs-Hepes buffer plus protease inhibitors [NaCl (5.78 g liter^{-1}), KCl (0.35 g liter^{-1}), $CaCl_2$ (0.37 g liter^{-1}), $MgSO_4$ (0.30 g liter^{-1}), $NaHCO_3$ (2.1 g liter^{-1}), K_2HPO_4 (0.14 g liter^{-1}), Hepes (5.21 g liter^{-1}), and D-glucose (2.0 g liter^{-1})] for 10 min at 37°C. The aortic rings were placed in aluminum cups filled with OCT (optimal cutting temperature) resin (Sakura Finetek) and slowly frozen with liquid nitrogen. ROS production was quantified with DHE (1 μM)–derived fluorescence after incubation for 30 min at 37°C. A Zeiss Axiovert 40 CFL microscope and an AxioCam MRm camera (Zeiss) were used for detection, and images were analyzed using the AxioVision data acquisition software (Zeiss) and quantified as IOD.

Reverse transcription polymerase chain reaction

FXI-mRNA expression of hepatic tissue was analyzed by quantitative RT-PCR using 7900HT Fast Real-Time PCR System (Applied Biosystems). Hepatic mouse mRNA was isolated following the manufacturer's instructions of the RNeasy Fibrous Tissue Mini Kit (Qiagen).

For isolation of aortic RNA from snap-frozen mouse or rat aortas, rat kidneys or rat liver tissues were homogenized with the TissueLyser II (Qiagen), and for RNA isolation, the modified guanidine isothiocyanate method of Chomczynski and Sacchi (*57*) was used. RT-PCR was performed with the CFX96 Real-Time PCR Detection System (Bio-Rad). For RT-PCR analysis, total RNA (0.125 μg) was used with the QuantiTect Probe RT-PCR kit (Qiagen). TaqMan Gene Expression assays were used as probe and primer sets (Applied Biosystems) for TATA-box binding protein (mouse: *Tbp*, Mm00446973_m-1; rat: *Tbp*, Rn01455646_m1) and FXI (mouse: *F11*, Mm01194987_m1; rat: *F11*, Rn01767420_m1), *Vcam-1* (mouse: Mm00449197_m1; rat: Rn00563627_m1), MCP-1 (*Ccl2*; mouse: Mm00441242_m1; rat: Rn00580555_m1), *Ly6c* (mouse: Mm03009946_m1), iNOS (*Nos2*; mouse: Mm00440485_m1), *Spn* (rat: Rn02061804_s), *Ccr2* (rat: Rn01637698_s1), and *Pai-1* (mouse: *Serpine1*, Mm00435858_m1; rat: *Serpine1*, Rn01481341_m1). Results were quantified with the relative C_t method and normalized to TATA-box binding protein as the endogenous control. mRNA levels were expressed relative to levels of control.

Western blot analysis

PPP and isolated aortic tissue were used for Western blot analysis. Under nonreducing conditions, proteins of PPP were separated by 7.5% SDS–polyacrylamide gel electrophoresis (PAGE). Sample volume of 1 μl was diluted in sample buffer. Immunoblotting was performed with an antibody against FXI (1:250; Nordic Immunology). Protein suspension of homogenized aortic tissue was separated by 12% SDS-PAGE under reducing conditions. After blotting on a nitrocellulose membrane, immunoblotting was accomplished with antibodies against α-actinin as a loading control (1:1000; Sigma-Aldrich), nox2 ($gp91^{phox}$, 1:500; BD Biosciences), and HO-1 (1:2000; Epitomics). Detection of specific bands was performed with peroxidase-conjugated secondary antibodies (1:10,000; Vector Laboratories) and enhanced chemiluminescence according to the manufacturer's instruction. These bands were analyzed by densitometry.

Enzyme-linked immunosorbent assay

TAT complexes in PPP were quantified by ELISA. Plasma samples were diluted 1:10 with sample diluent. The ELISA Kit for TAT complexes (USCN Life Science, E90831Mu) was performed according to the manufacturer's instructions. The assay was performed with a Millenia

Kinetic Analyzer (Diagnostic Products Corporation), and results were analyzed with SoftMax Pro (Molecular Devices).

Picro-sirius red staining

Isolated aortic rings and decapsulated left kidneys were fixed in paraformaldehyde (4%) directly after removal and embedded afterward in paraffin. After deparaffinization, nuclei were prestained with hemealaun. Samples were stained in picro-sirius red solution (0.1% with 1.2% picric acid). Finally, specimens were dehydrated with ethanol and coverslipped with Entellan. To determine the presence of early fibrosis and collagen accumulation, 10 images per animal were taken using an Olympus IX73 microscope and an Olympus SC30 camera and were examined.

Immunofluorescence staining of rat aorta

Aortic cryosections (5 μm) were blocked with 1% bovine serum albumin in PBS with 0.05% Tween 20. Tissue sections were stained with the primary anti-CD45 antibody (1:150, ab10558; Abcam) at 4°C overnight. Slides were washed three times with PBS and incubated with the secondary antibody Alexa 594 donkey anti-rabbit (1:2000, A21207; Life Technologies) for 1 hour at room temperature in the dark. After three washes in PBS for 5 min each, slides were counterstained with DAPI and mounted using ProLong Diamond Antifade Mounting medium with DAPI (Life Technologies). Sections were imaged with an Olympus IX73 microscope. Negative controls were performed for every set of experiments by omitting the primary antibodies from the procedure. For quantification, red fluorescence of whole aortic rings was quantified by digital image analysis using ImageJ. For publication images with DAPI staining, green autofluorescence and red fluorescence were taken using a 10× objective.

Kidney histological evaluation

The left kidneys were decapsulated, fixed in phosphate-buffered 4% paraformaldehyde (pH 7.4), embedded in paraffin wax, and cut longitudinally to a thickness of 5 μm. Renal tissue sections were stained with PAS and hematoxylin and eosin. All histology stainings were performed by the Histology Core Facility of the Institute of Molecular Biology (University of Mainz, Germany). To determine kidney injury, 10 consecutive cortical and juxtamedullary images per animal were taken using an Olympus IX73 microscope and an Olympus SC30 camera and were examined. Quantitative analysis of kidney injury was determined by semiquantitative injury scoring (PAS score: 0, ≤5%; 1, 5 to 15%; 2, 15 to 25%; 3, 25 to 50%; 4, ≥50%). These examinations were performed blinded by two investigators, and the mean values were calculated.

Protein excretion

Creatinine (milligram per deciliter; Jaffe reaction) in spontaneous urine samples was measured by an Abbott ARCHITECT c8000 Clinical Chemistry Analyzer (Abbott) using Abbott reagents. The total protein content was determined by Bradford assay using Roti-Quant (Bio-Rad) following the manufacturer's instructions. Proteinuria was calculated as milligram of protein per milligram of creatinine.

Plasma analysis of kidney function

Heparinized blood was collected by right ventricular heart puncture. Creatinine (milligram per deciliter; Jaffe reaction) and urea-N (milligram per deciliter; urease method) were measured in mouse heparinized plasma by an Abbott ARCHITECT c8000 Clinical Chemistry Analyzer using Abbott reagents.

Flow cytometric analysis of aortic lysates and of platelet-leukocyte conjugates in peripheral blood

Aortic vessels were cleaned of perivascular fatty tissue and adventitia, minced, and digested by liberase (1 mg/ml; Roche Diagnostics), as described previously (*8*, *58*). Single-cell suspensions were stained with CD45–allophycocyanin (APC)–eFluor 780, CD11b–phycoerythrin (PE), Ly6G– or GR-1–fluorescein isothiocyanate (FITC), Ly6C–peridinin chlorophyll protein (PerCP)–Cy5.5, NK1.1-PE-Cy7, F4/80-APC, and Viability Dye eFluor 506 monoclonal antibodies. At least 2.5×10^5 to 4.0×10^5 cells were treated with Fc-block, washed, and surface-stained. On the basis of a live gate, events were acquired and analyzed using a BF FACSCANTO II flow cytometer (Becton Dickinson) and FACSDiva software (Becton Dickinson), respectively. Monocyte-platelet conjugates were analyzed in citrate-anticoagulated whole blood (*59*), taken by retro-orbital vein puncture using heparinized glass capillaries. Platelets were stained with anti-CD41–FITC antibody; monocytes were stained with anti-CD11b–PE, anti–GR-1–V450, and F4/80-APC antibodies and gated from $CD45^+$ viable cells.

Intravital fluorescence microscopy

Mice were anesthetized with midazolame, medetomidine, and fentanyl injected intraperitoneally as described previously. Animals were fixed on a custom-built stage to maintain a physiological temperature. The right and left common carotid arteries were dissected free. For the quantification of leukocyte adhesion, 100 μl of acridine orange (0.5 mg ml^{-1}; Sigma-Aldrich) was injected via jugular vein catheter (inside diameter, 0.28 mm; outer diameter, 0.61 mm; Smiths Medical Deutschland GmbH) to stain circulating leukocytes in vivo. Measurements were performed with a high-speed wide-field Olympus BX51WI fluorescence microscope using a long-distance condenser and a 10× (numerical aperture, 0.3) water immersion objective with a monochromator (MT 20E; Olympus Deutschland GmbH) and a charge-coupled device camera (ORCA-R^2, Hamamatsu Photonics). For image acquisition and analysis, a Realtime Imaging System eXcellence RT (Olympus Deutschland GmbH) software was used. Cell recruitment was quantified in four fields of view (100 × 150 μm) per carotid artery. Adherent cells were defined in each vessel segment as cells that did not move or detach from the endothelial lining within an observation period of 10 s and presented per square millimeter.

The FACTO-RR study

We enrolled 71 all-comer patients with arterial hypertension admitted to either the outpatient clinic or the emergency room of the Center for Cardiology, University Medical Center Mainz into the "Interaction of coagulation FACtors, Thrombocytes and leukOcytes in patients with aRterial hypeRtension study" (FACTO-RR study, DRKS00011232). Inclusion criteria were age (≥18 years old) and history of essential arterial hypertension of at least 6 months. Exclusion criteria were age (≥90 years old), anticoagulant therapy (unfractionated or low–molecular weight heparin, vitamin K antagonist, FXa inhibitors, and thrombin inhibitors), acute coronary syndromes, exacerbated disease requiring critical care medicine (for example, hypertensive crisis with pulmonary edema and respiratory failure), or immediate surgery (for example, aortic dissection or rupture). The study protocol was approved by the local ethics committee of the state of Rhineland-Palatinate, Germany, reference number 837.354.12 (8455-F). Written informed consent was obtained from every participant. Medical history was taken, and body weight, height, and heart rate were obtained. Office blood pressure was measured in each study participant in an upright sitting

position (room temperature, 22°C) using the Omron 705CP-II device, and upper arm cuffs were adapted to upper arm circumference (17 to 22 cm, 22 to 32 cm, and 32 to 42 cm, respectively). The upper part of the body was undressed, and measurements were taken beginning 5 min after application of the blood pressure cuff. The first measurement was taken on both the left and right arm, and both second and third measurements were taken 3 min after another. If in the first measurement differences between systolic and diastolic blood pressure between the two arms were below 20 or 15 mmHg, the second and third measurements were taken only on the left upper arm. For each individual, the mean of the second and third measurements was calculated and included in the study. According to current guidelines (*36*), grade I hypertension was defined as systolic blood pressure (SP) of 140 to 159 mmHg and/or diastolic blood pressure (DP) of 90 to 99 mmHg; grade II hypertension or higher was defined as SP ≥160 mmHg and/or DP ≥100 mmHg. MAP was calculated as follows: MAP = ((2 × SP) + DP)/3. Here, the groups hypertension grade I and hypertension grade II or higher were called "uncontrolled hypertension"; all others were termed "controlled hypertension." A maximum of 10 ml of venouscitrated blood was drawn from the cubital vein of the right arm to prepare PPP and PRP and to assess blood count using the Sysmex XP300 analyzer (Sysmex Corporation). In a subset of the study participants, in which preparation of PRP exceeded a minimum volume of greater than 3 ml after the TG assays were performed, as described previously (*31*, *54*–*56*), we prepared washed platelets by centrifuging the PRP at 2500*g* for 4 min at room temperature. We resuspended the platelets in aliquots of control PPP that we had obtained from six healthy volunteers (mean age, 28.5 ± 1; 50% female; no cardiovascular risk factors), pooled, aliquoted, frozen at −80°C, and thawed. In those samples, we performed the TG assays as described previously for PRP.

Statistics

Data are expressed as means ± SEM. Statistical calculations were performed with GraphPad Prism 5 (GraphPad Software Inc.). D'Agostino-Pearson normality test was first performed, and Pearson's correlation, Fisher's exact test, Mann-Whitney test, paired or unpaired *t* test, Kruskal-Wallis test, and one- or two-way ANOVA with post hoc Bonferroni's or Dunn's multiple comparison test were used as appropriate. *P* values of <0.05 were considered significant and marked by asterisks (*$P < 0.05$; **$P < 0.01$; ***$P < 0.001$).

SUPPLEMENTARY MATERIALS

www.sciencetranslationalmedicine.org/cgi/content/full/9/375/eaah4923/DC1
Fig. S1. Therapeutic targeting of FXI protects from vascular inflammation.
Fig. S2. Protein expression of gp91phox and HO-1.
Video S1. C57BL/6.
Video S2. C57BL/6 + ATII.
Video S3. C57BL/6 + ATII + control IgG.
Video S4. C57BL/6 + ATII + anti–VCAM-1 antibody.
Video S5. C57BL/6 + Scr ASO.
Video S6. C57BL/6 + ATII + Scr ASO.
Video S7. C57BL/6 + FXI ASO.
Video S8. C57BL/6 + ATII + FXI ASO.

REFERENCES AND NOTES

1. S. S. Lim, T. Vos, A. D. Flaxman, G. Danaei, K. Shibuya, H. Adair-Rohani, M. Amann, H. R. Anderson, K. G. Andrews, M. Aryee, C. Atkinson, L. J. Bacchus, A. N. Bahalim, K. Balakrishnan, J. Balmes, S. Barker-Collo, A. Baxter, M. L. Bell, J. D. Blore, F. Blyth, C. Bonner, G. Borges, R. Bourne, M. Boussinesq, M. Brauer, P. Brooks, N. G. Bruce, B. Brunekreef, C. Bryan-Hancock, C. Bucello, R. Buchbinder, F. Bull, R. T. Burnett, T. E. Byers, B. Calabria, J. Carapetis, E. Carnahan, Z. Chafe, F. Charlson, H. Chen, J. S. Chen, A. T. Cheng, J. C. Child, A. Cohen, K. E. Colson, B. C. Cowie, S. Darby, S. Darling, A. Davis, L. Degenhardt, F. Dentener, D. C. Des Jarlais, K. Devries, M. Dherani, E. L. Ding, E. R. Dorsey, T. Driscoll, K. Edmond, S. E. Ali, R. E. Engell, P. J. Erwin, S. Fahimi, G. Falder, F. Farzadfar, A. Ferrari, M. M. Finucane, S. Flaxman, F. G. Fowkes, G. Freedman, M. K. Freeman, E. Gakidou, S. Ghosh, E. Giovannucci, G. Gmel, K. Graham, R. Grainger, B. Grant, D. Gunnell, H. R. Gutierrez, W. Hall, H. W. Hoek, A. Hogan, H. D. Hosgood III, D. Hoy, H. Hu, B. J. Hubbell, S. J. Hutchings, S. E. Ibeanusi, G. L. Jacklyn, R. Jasrasaria, J. B. Jonas, H. Kan, J. A. Kanis, N. Kassebaum, N. Kawakami, Y.-H. Khang, S. Khatibzadeh, J.-P. Khoo, C. Kok, F. Laden, R. Lalloo, Q. Lan, T. Lathlean, J. L. Leasher, J. Leigh, Y. Li, J. K. Lin, S. E. Lipshultz, S. London, R. Lozano, Y. Lu, J. Mak, R. Malekzadeh, L. Mallinger, W. Marcenes, L. March, R. Marks, R. Martin, P. McGale, J. McGrath, S. Mehta, G. A. Mensah, T. R. Merriman, R. Micha, C. Michaud, V. Mishra, K. M. Hanafiah, A. A. Mokdad, L. Morawska, D. Mozaffarian, T. Murphy, M. Naghavi, B. Neal, P. K. Nelson, J. M. Nolla, R. Norman, C. Olives, S. B. Omer, J. Orchard, R. Osborne, B. Ostro, A. Page, K. D. Pandey, C. D. Parry, E. Passmore, J. Patra, N. Pearce, P. M. Pelizzari, M. Petzold, M. R. Phillips, D. Pope, C. A. Pope III, J. Powles, M. Rao, H. Razavi, E. A. Rehfuess, J. T. Rehm, B. Ritz, F. P. Rivara, T. Roberts, C. Robinson, J. A. Rodriguez-Portales, I. Romieu, R. Room, L. C. Rosenfeld, A. Roy, L. Rushton, J. A. Salomon, U. Sampson, L. Sanchez-Riera, E. Sanman, A. Sapkota, S. Seedat, P. Shi, K. Shield, R. Shivakoti, G. M. Singh, D. A. Sleet, E. Smith, K. R. Smith, N. J. Stapelberg, K. Steenland, H. Stockl, L. J. Stovner, K. Straif, L. Straney, G. D. Thurston, J. H. Tran, R. Van Dingenen, A. van Donkelaar, J. L. Veerman, L. Vijayakumar, R. Weintraub, M. M. Weissman, R. A. White, H. Whiteford, S. T. Wiersma, J. D. Wilkinson, H. C. Williams, W. Williams, N. Wilson, A. D. Woolf, P. Yip, J. M. Zielinski, A. D. Lopez, C. J. Murray, M. Ezzati, M. A. AlMazroa, Z. A. Memish, A comparative risk assessment of burden of disease and injury attributable to 67 risk factors and risk factor clusters in 21 regions, 1990–2010: A systematic analysis for the Global Burden of Disease Study 2010. *Lancet* **380**, 2224–2260 (2012).
2. P. Libby, Inflammation in atherosclerosis. *Nature* **420**, 868–874 (2002).
3. B. Engelmann, S. Massberg, Thrombosis as an intravascular effector of innate immunity. *Nat. Rev. Immunol.* **13**, 34–45 (2013).
4. F. K. Swirski, P. Libby, E. Aikawa, P. Alcaide, F. W. Luscinskas, R. Weissleder, M. J. Pittet, Ly-6C^{hi} monocytes dominate hypercholesterolemia-associated monocytosis and give rise to macrophages in atheromata. *J. Clin. Invest.* **117**, 195–205 (2007).
5. F. C. Luft, R. Dechend, D. N. Müller, Immune mechanisms in angiotensin II-induced target-organ damage. *Ann. Med.* **44** (Suppl. 1), S49–S54 (2012).
6. F. K. Swirski, M. Nahrendorf, M. Etzrodt, M. Wildgruber, V. Cortez-Retamozo, P. Panizzi, J. L. Figueiredo, R. H. Kohler, A. Chudnovskiy, P. Waterman, E. Aikawa, T. R. Mempel, P. Libby, R. Weissleder, M. J. Pittet, Identification of splenic reservoir monocytes and their deployment to inflammatory sites. *Science* **325**, 612–616 (2009).
7. S. Rajagopalan, S. Kurz, T. Munzel, M. Tarpey, B. A. Freeman, K. K. Griendling, D. G. Harrison, Angiotensin II-mediated hypertension in the rat increases vascular superoxide production via membrane NADH/NADPH oxidase activation. Contribution to alterations of vasomotor tone. *J. Clin. Invest.* **97**, 1916–1923 (1996).
8. P. Wenzel, M. Knorr, S. Kossmann, J. Stratmann, M. Hausding, S. Schuhmacher, S. H. Karbach, M. Schwenk, N. Yogev, E. Schulz, M. Oelze, S. Grabbe, H. Jonuleit, C. Becker, A. Daiber, A. Waisman, T. Münzel, Lysozyme M–positive monocytes mediate angiotensin II–induced arterial hypertension and vascular dysfunction. *Circulation* **124**, 1370–1381 (2011).
9. T. J. Guzik, N. E. Hoch, K. A. Brown, L. A. McCann, A. Rahman, S. Dikalov, J. Goronzy, C. Weyand, D. G. Harrison, Role of the T cell in the genesis of angiotensin II–induced hypertension and vascular dysfunction. *J. Exp. Med.* **204**, 2449–2460 (2007).
10. L. Piqueras, P. Kubes, A. Alvarez, E. O'Connor, A. C. Issekutz, J. V. Esplugues, M. J. Sanz, Angiotensin II induces leukocyte-endothelial cell interactions in vivo via AT_1 and AT_2 receptor–mediated P-selectin upregulation. *Circulation* **102**, 2118–2123 (2000).
11. C. Vecchione, E. Patrucco, G. Marino, L. Barberis, R. Poulet, A. Aretini, A. Maffei, M. T. Gentile, M. Storto, O. Azzolino, M. Brancaccio, G. L. Colussi, U. Bettarini, F. Altruda, L. Silengo, G. Tarone, M. P. Wymann, E. Hirsch, G. Lembo, Protection from angiotensin II–mediated vasculotoxic and hypertensive response in mice lacking PI3Kγ. *J. Exp. Med.* **201**, 1217–1228 (2005).
12. G. Kaplanski, V. Marin, M. Fabrigoule, V. Boulay, A.-M. Benoliel, P. Bongrand, S. Kaplanski, C. Farnarier, Thrombin-activated human endothelial cells support monocyte adhesion in vitro following expression of intercellular adhesion molecule-1 (ICAM-1; CD54) and vascular cell adhesion molecule-1 (VCAM-1; CD106). *Blood* **92**, 1259–1267 (1998).
13. M. B. Taubman, J. D. Marmur, C. L. Rosenfield, A. Guha, S. Nichtberger, Y. Nemerson, Agonist-mediated tissue factor expression in cultured vascular smooth muscle cells. Role of Ca^{2+} mobilization and protein kinase C activation. *J. Clin. Invest.* **91**, 547–552 (1993).
14. D. M. Monroe, M. Hoffman, H. R. Roberts, Platelets and thrombin generation. *Arterioscler. Thromb. Vasc. Biol.* **22**, 1381–1389 (2002).
15. Y. Wang, M. Sakuma, Z. Chen, V. Ustinov, C. Shi, K. Croce, A. C. Zago, J. Lopez, P. Andre, E. Plow, D. I. Simon, Leukocyte engagement of platelet glycoprotein Ibα via the integrin Mac-1 is critical for the biological response to vascular injury. *Circulation* **112**, 2993–3000 (2005).

16. S. Chandraratne, M. L. von Bruehl, J. I. Pagel, K. Stark, E. Kleinert, I. Konrad, S. Farschtschi, R. Coletti, F. Gartner, O. Chillo, K. R. Legate, M. Lorenz, S. Rutkowski, A. Caballero-Martinez, R. Starke, A. Tirniceriu, L. Pauleikhoff, S. Fischer, G. Assmann, J. Mueller-Hoecker, J. Ware, B. Nieswandt, W. Schaper, C. Schulz, E. Deindl, S. Massberg, Critical role of platelet glycoprotein ibα in arterial remodeling. *Arterioscler. Thromb. Vasc. Biol.* **35**, 589–597 (2015).
17. D. I. Simon, Z. Chen, H. Xu, C. Q. Li, J.-f. Dong, L. V. McIntire, C. M. Ballantyne, L. Zhang, M. I. Furman, M. C. Berndt, J. A. López, Platelet glycoprotein Ibα is a counterreceptor for the leukocyte integrin Mac-1 (CD11b/CD18). *J. Exp. Med.* **192**, 193–204 (2000).
18. A. Corken, S. Russell, J. Dent, S. R. Post, J. Ware, Platelet glycoprotein Ib-IX as a regulator of systemic inflammation. *Arterioscler. Thromb. Vasc. Biol.* **34**, 996–1001 (2014).
19. M. J. Elices, L. Osborn, Y. Takada, C. Crouse, S. Luhowskyj, M. E. Hemler, R. R. Lobb, VCAM-1 on activated endothelium interacts with the leukocyte integrin VLA-4 at a site distinct from the VLA-4/fibronectin binding site. *Cell* **60**, 577–584 (1990).
20. C. Furlan-Freguia, P. Marchese, A. Gruber, Z. M. Ruggeri, W. Ruf, P2X7 receptor signaling contributes to tissue factor-dependent thrombosis in mice. *J. Clin. Invest.* **121**, 2932–2944 (2011).
21. U. O. Wenzel, B. Fouqueray, G. Grandaliano, Y. S. Kim, C. Karamitsos, A. J. Valente, H. E. Abboud, Thrombin regulates expression of monocyte chemoattractant protein-1 in vascular smooth muscle cells. *Circ. Res.* **77**, 503–509 (1995).
22. M. Ishibashi, K.-i. Hiasa, Q. Zhao, S. Inoue, K. Ohtani, S. Kitamoto, M. Tsuchihashi, T. Sugaya, I. F. Charo, S. Kura, T. Tsuzuki, T. Ishibashi, A. Takeshita, K. Egashira, Critical role of monocyte chemoattractant protein-1 receptor CCR2 on monocytes in hypertension-induced vascular inflammation and remodeling. *Circ. Res.* **94**, 1203–1210 (2004).
23. R. Celikel, R. A. McClintock, J. R. Roberts, G. L. Mendolicchio, J. Ware, K. I. Varughese, Z. M. Ruggeri, Modulation of α-thrombin function by distinct interactions with platelet glycoprotein Ibα. *Science* **301**, 218–221 (2003).
24. T. Kanaji, S. Russell, J. Ware, Amelioration of the macrothrombocytopenia associated with the murine Bernard-Soulier syndrome. *Blood* **100**, 2102–2107 (2002).
25. D. Gailani, G. J. Broze Jr., Factor XI activation in a revised model of blood coagulation. *Science* **253**, 909–912 (1991).
26. E. I. Tucker, U. M. Marzec, T. C. White, S. Hurst, S. Rugonyi, O. J. T. McCarty, D. Gailani, A. Gruber, S. R. Hanson, Prevention of vascular graft occlusion and thrombus-associated thrombin generation by inhibition of factor XI. *Blood* **113**, 936–944 (2009).
27. F. A. Baglia, C. N. Shrimpton, J. Emsley, K. Kitagawa, Z. M. Ruggeri, J. A. López, P. N. Walsh, Factor XI interacts with the leucine-rich repeats of glycoprotein Ibα on the activated platelet. *J. Biol. Chem.* **279**, 49323–49329 (2004).
28. F. A. Baglia, D. Gailani, J. A. López, P. N. Walsh, Identification of a binding site for glycoprotein Ibα in the Apple 3 domain of factor XI. *J. Biol. Chem.* **279**, 45470–45476 (2004).
29. E. I. Tucker, N. G. Verbout, P. Y. Leung, S. Hurst, O. J. T. McCarty, D. Gailani, A. Gruber, Inhibition of factor XI activation attenuates inflammation and coagulopathy while improving the survival of mouse polymicrobial sepsis. *Blood* **119**, 4762–4768 (2012).
30. H. Zhang, E. C. Lowenberg, J. R. Crosby, A. R. MacLeod, C. Zhao, D. Gao, C. Black, A. S. Revenko, J. C. Meijers, E. S. Stroes, M. Levi, B. P. Monia, Inhibition of the intrinsic coagulation pathway factor XI by antisense oligonucleotides: A novel antithrombotic strategy with lowered bleeding risk. *Blood* **116**, 4684–4692 (2010).
31. K. Jurk, J. Lahav, H Van Aken, M. F. Brodde, J.-R. Nofer, B. E. Kehrel, Extracellular protein disulfide isomerase regulates feedback activation of platelet thrombin generation via modulation of coagulation factor binding. *J. Thromb. Haemost.* **9**, 2278–2290 (2011).
32. J. W. Yau, P. Liao, J. C. Fredenburgh, A. R. Stafford, A. S. Revenko, B. P. Monia, J. I. Weitz, Selective depletion of factor XI or factor XII with antisense oligonucleotides attenuates catheter thrombosis in rabbits. *Blood* **123**, 2102–2107 (2014).
33. S. Meiler, Y. Baumer, S. McCurdy, B. H. Lee, S. Kitamoto, W. A. Boisvert, Cluster of differentiation 43 deficiency in leukocytes leads to reduced atherosclerosis—Brief report. *Arterioscler. Thromb. Vasc. Biol.* **35**, 309–311 (2015).
34. A. Scriba, M. Schneider, V. Grau, P. H. van der Meide, B. Steiniger, Rat monocytes up-regulate NKR-P1A and down-modulate CD4 and CD43 during activation in vivo: Monocyte subpopulations in normal and IFN-γ-treated rats. *J. Leukoc. Biol.* **62**, 741–752 (1997).
35. F. T. Spradley, J. J. White, W. D. Paulson, D. M. Pollock, J. S. Pollock, Differential regulation of nitric oxide synthase function in aorta and tail artery from 5/6 nephrectomized rats. *Physiol. Rep.* **1**, e00145 (2013).
36. G. Mancia, R. Fagard, K. Narkiewicz, J. Redon, A. Zanchetti, M. Böhm, T. Christiaens, R. Cifkova, G. De Backer, A. Dominiczak, M. Galderisi, D. E. Grobbee, T. Jaarsma, P. Kirchhof, S. E. Kjeldsen, S. Laurent, A. J. Manolis, P. M. Nilsson, L. M. Ruilope, R. E. Schmieder, P. A. Sirnes, P. Sleight, M. Viigimaa, B. Waeber, F. Zannad, M. Burnier, E. Ambrosioni, M. Caufield, A. Coca, M. H. Olsen, C. Tsioufis, P. van de Borne, J. L. Zamorano, S. Achenbach, H. Baumgartner, J. J. Bax, H. Bueno, V. Dean, C. Deaton, C. Erol, R. Ferrari, D. Hasdai, A. W. Hoes, J. Knuuti, P. Kolh, P. Lancellotti, A. Linhart, P. Nihoyannopoulos, M. F. Piepoli, P. Ponikowski, J. L. Tamargo, M. Tendera, A. Torbicki, W. Wijns, S. Windecker, D. L. Clement, T. C. Gillebert, E. A. Rosei, S. D. Anker, J. Bauersachs, J. B. Hitij, M. Caulfield, M. De Buyzere, S. De Geest, G. A. Derumeaux, S. Erdine, C. Farsang, C. Funck-Brentano, V. Gerc, G. Germano, S. Gielen, H. Haller, J. Jordan, T. Kahan, M. Komajda, D. Lovic, H. Mahrholdt, J. Ostergren, G. Parati, J. Perk, J. Polonia, B. A. Popescu, Z. Reiner, L. Rydén, Y. Sirenko, A. Stanton, H. Struijker-Boudier, C. Vlachopoulos, M. Volpe, D. A. Wood, 2013 ESH/ESC guidelines for the management of arterial hypertension: The Task Force for the management of arterial hypertension of the European Society of Hypertension (ESH) and of the European Society of Cardiology (ESC). *Eur. Heart J.* **34**, 2159–2219 (2013).
37. Antithrombotic Trialists' (ATT) Collaboration, Aspirin in the primary and secondary prevention of vascular disease: Collaborative meta-analysis of individual participant data from randomised trials. *Lancet* **373**, 1849–1860 (2009).
38. J. S. Berger, M. C. Roncaglioni, F. Avanzini, I. Pangrazzi, G. Tognoni, D. L. Brown, Aspirin for the primary prevention of cardiovascular events in women and men: A sex-specific meta-analysis of randomized controlled trials. *JAMA* **295**, 306–313 (2006).
39. P. M. Ridker, M. Cushman, M. J. Stampfer, R. P. Tracy, C. H. Hennekens, Inflammation, aspirin, and the risk of cardiovascular disease in apparently healthy men. *N. Engl. J. Med.* **336**, 973–979 (1997).
40. K. Vanschoonbeek, M. A. Feijge, R. J. Van Kampen, H. Kenis, H. C. Hemker, P. L. Giesen, J. W. M. Heemskerk, Initiating and potentiating role of platelets in tissue factor-induced thrombin generation in the presence of plasma: Subject-dependent variation in thrombogram characteristics. *J. Thromb. Haemost.* **2**, 476–484 (2004).
41. E. D. Rosen, D. Gailani, F. J. Castellino, FXI is essential for thrombus formation following FeCl3-induced injury of the carotid artery in the mouse. *Thromb. Haemost.* **87**, 774–776 (2002).
42. R. Shnerb Ganor, D. Harats, G. Schiby, D. Gailani, H. Levkovitz, C. Avivi, I. Tamarin, A. Shaish, O. Salomon, Factor XI deficiency protects against atherogenesis in apolipoprotein E/Factor XI double knockout mice. *Arterioscler. Thromb. Vasc. Biol.* **36**, 475–481 (2016).
43. O. Salomon, D. M. Steinberg, M. Zucker, D. Varon, A. Zivelin, U. Seligsohn, Patients with severe factor XI deficiency have a reduced incidence of deep-vein thrombosis. *Thromb. Haemost.* **105**, 269–273 (2011).
44. O. Salomon, D. M. Steinberg, N. Koren-Morag, D. Tanne, U. Seligsohn, Reduced incidence of ischemic stroke in patients with severe factor XI deficiency. *Blood* **111**, 4113–4117 (2008).
45. A. Görlach, I. Diebold, V. B. Schini-Kerth, U. Berchner-Pfannschmidt, U. Roth, R. P. Brandes, T. Kietzmann, R. Busse, Thrombin activates the hypoxia-inducible factor-1 signaling pathway in vascular smooth muscle cells: Role of the $p22^{phox}$-containing NADPH oxidase. *Circ. Res.* **89**, 47–54 (2001).
46. P. Pontrelli, E. Ranieri, M. Ursi, G. Ghosh-Choudhury, L. Gesualdo, F. Paolo Schena, G. Grandaliano, jun-N-terminal kinase regulates thrombin-induced PAI-1 gene expression in proximal tubular epithelial cells. *Kidney Int.* **65**, 2249–2261 (2004).
47. A. Lehners, S. Lange, G. Niemann, A. Rosendahl, C. Meyer-Schwesinger, J. Oh, R. Stahl, H. Ehmke, R. Benndorf, A. Klinke, S. Baldus, U. O. Wenzel, Myeloperoxidase deficiency ameliorates progression of chronic kidney disease in mice. *Am. J. Physiol. Renal Physiol.* **307**, F407–F417 (2014).
48. L.-J. Ma, H. Yang, A. Gaspert, G. Carlesso, M. M. Barty, J. M. Davidson, D. Sheppard, A. B. Fogo, Transforming growth factor-β-dependent and -independent pathways of induction of tubulointerstitial fibrosis in $\beta6^{-/-}$ mice. *Am. J. Pathol.* **163**, 1261–1273 (2003).
49. H. R. Büller, C. Bethune, S. Bhanot, D. Gailani, B. P. Monia, G. E. Raskob, A. Segers, P. Verhamme, J. I. Weitz; FXI-ASO TKA Investigators, Factor XI antisense oligonucleotide for prevention of venous thrombosis. *N. Engl. J. Med.* **372**, 232–240 (2015).
50. H.-U. Pauer, T. Renné, B. Hemmerlein, T. Legler, S. Fritzlar, I. Adham, W. Müller-Esterl, G. Emons, U. Sancken, W. Engel, P. Burfeind, Targeted deletion of murine coagulation factor XII gene-a model for contact phase activation in vivo. *Thromb. Haemost.* **92**, 503–508 (2004).
51. D. Gailani, N. M. Lasky, G. J. Broze Jr., A murine model of factor XI deficiency. *Blood Coagul. Fibrinolysis* **8**, 134–144 (1997).
52. N. Yokota, A. Zarpellon, S. Chakrabarty, V. Y. Bogdanov, A. Gruber, F. J. Castellino, N. Mackman, L. G. Ellies, H. Weiler, Z. M. Ruggeri, W. Ruf, Contributions of thrombin targets to tissue factor-dependent metastasis in hyperthrombotic mice. *J. Thromb. Haemost.* **12**, 71–81 (2014).
53. N. Fretellier, J. Idée, P. Bruneval, S. Guerret, F. Daubiné, G. Jestin, C. Factor, N. Poveda, A. Dencausse, F. Massicot, O. Laprévote, C. Mandet, N. Bouzian, M. Port, C. Corot, Hyperphosphataemia sensitizes renally impaired rats to the profibrotic effects of gadodiamide. *Br. J. Pharmacol.* **165**, 1151–1162 (2012).
54. S. N. Tchaikovski, B. J. M. Van Vlijmen, J. Rosing, G. Tans, Development of a calibrated automated thrombography based thrombin generation test in mouse plasma. *J. Thromb. Haemost.* **5**, 2079–2086 (2007).
55. H. C. Hemker, R. Al Dieri, E. De Smedt, S. Béguin, Thrombin generation, a function test of the haemostatic-thrombotic system. *Thromb. Haemost.* **96**, 553–561 (2006).
56. S. J. Wielders, S. Beguin, H. C. Hemker, T. Lindhout, Factor XI–dependent reciprocal thrombin generation consolidates blood coagulation when tissue factor is not available. *Arterioscler. Thromb. Vasc. Biol.* **24**, 1138–1142 (2004).

57. P. Chomczynski, N. Sacchi, Single-step method of RNA isolation by acid guanidinium thiocyanate-phenol-chloroform extraction. *Anal. Biochem.* **162**, 156–159 (1987).
58. S. Kossmann, M. Schwenk, M. Hausding, S. H. Karbach, M. I. Schmidgen, M. Brandt, M. Knorr, H. Hu, S. Kroller-Schon, T. Schonfelder, S. Grabbe, M. Oelze, A. Daiber, T. Munzel, C. Becker, P. Wenzel, Angiotensin II–induced vascular dysfunction depends on interferon-γ–driven immune cell recruitment and mutual activation of monocytes and NK-cells. *Arterioscler. Thromb. Vasc. Biol.* **33**, 1313–1319 (2013).
59. K. Jurk, M. A. Ritter, C. Schriek, H. Van Aken, D. W. Droste, E. B. Ringelstein, B. E. Kehrel, Activated monocytes capture platelets for heterotypic association in patients with severe carotid artery stenosis. *Thromb. Haemost.* **103**, 1193–1202 (2010).

Acknowledgments: We acknowledge the expert technical assistance of A. Conrad, K. Perius, K. Schwierczek, and J. Schreiner. This work contains results that are part of the doctoral theses of M. Ehlken and Y. Weihert. We acknowledge D. Gailani (Vanderbilt University, Nashville) for providing the $FXI^{-/-}$ mice. We thank D. Sollinger and J. Lutz (1st Medical Clinic, Department of Nephrology, University Medical Center Mainz) for expert assistance in analyzing the kidney histology. **Funding:** This work was supported by a grant from the Stiftung Pathobiochemie und Molekulare Diagnostik to P.W. and K.L. and grants from the Federal Ministry of Education and Research (BMBF 01EO1003 and 01EO1503) to P.W., S.K., M.K., M.B., T.M., C.R., K.J., S.J., U.W., and W.R. T.R. acknowledges funding by the German Research Society (SFB841, TP B8) and a European Research Council grant (ERC-StG-2012-311575_F-12). A.G. was supported by NIH grants HL 128016, 106919, and 101972. Z.M.R. is supported by NIH grant HL-42846. Z.M.R. and W.R. are funded by NIH grant HL 31950. W.R. is funded by the Alexander von Humboldt Foundation. In conducting the study, P.W. was supported by further funds of the German Research Foundation (DFG WE 4361/3-1 and WE 4361/4-1), the Stiftung Mainzer Herz, and the Center for Translational Vascular Biology, University Medical Center Mainz. **Author contributions:** S.K. and J.L. performed experiments; collected, analyzed, and discussed data; performed statistical analysis; and contributed to writing the manuscript. S.J., K.J., M.E., T.S., M.K., M.B., N.X., H.L., S.H.K., Y.W., and M.O. performed experiments and collected, analyzed, and discussed data. A.D., C.R., U.W., and T.R. conceived experiments and discussed results and strategy. K.L. discussed results and strategy. A.G. and B.M. made essential methodological contributions. Z.M.R. contributed essential mouse lines and discussed results and strategy. W.R. and T.M. conceived experiments, analyzed data, discussed results and strategy, and contributed to writing the manuscript. P.W. managed and designed the study, conceived and performed experiments, analyzed data, performed statistical analysis, discussed results and strategy, and wrote the manuscript, which was revised and approved by all authors. **Competing interests:** B.M. is an employee and shareholder of Ionis Pharmaceuticals Inc. A.G. and Oregon Health and Science University (OHSU) are equity holders in Aronora Inc. and may have financial interest in the findings of this research. W.R. reports paid consulting relationships with Iconic Therapeutics Inc. A.G. is the inventor on U.S. patents 8236316, 8388959, 8399648, 8940883, and 9125895, which are owned by OHSU and cover the FXI inhibitor 14E11 used in this work. **Data and materials availability:** The data for this study have been deposited at smb://c5-s4/cth$. The FACTO-RR study has been registered at the Deutsches Register für Klinische Studien (DRKS00011232). FXI ASOs and respective controls ASOs are available from Ionis Pharmaceuticals Inc.

Submitted 26 October 2015
Resubmitted 5 July 2016
Accepted 12 December 2016
Published 1 February 2017
10.1126/scitranslmed.aah4923

Citation: S. Kossmann, J. Lagrange, S. Jäckel, K. Jurk, M. Ehlken, T. Schönfelder, Y. Weihert, M. Knorr, M. Brandt, N. Xia, H. Li, A. Daiber, M. Oelze, C. Reinhardt, K. Lackner, A. Gruber, B. Monia, S. H. Karbach, U. Walter, Z. M. Ruggeri, T. Renné, W. Ruf, T. Münzel, P. Wenzel, Platelet-localized FXI promotes a vascular coagulation-inflammatory circuit in arterial hypertension. *Sci. Transl. Med.* **9**, eaah4923 (2017).

Editor's Summary

Spotlight on factor XI

Hypertension, cardiovascular disease, and vascular inflammation are inextricably linked, often co-occurring. Kossmann *et al*. have now discovered a regulatory pathway linking these pathologies that could be inhibited to allow the control of treatment-resistant high blood pressure. In rats and mice with hypertension, the authors found that vascular disease is driven by an overactive thrombin-driven factor XI feedback loop on platelets. Inhibition of this feedback loop with an antisense molecule against factor XI reduced both the vascular pathology and hypertension. The authors show that this factor XI–dependent feedback loop also operates in patients with uncontrolled hypertension, raising the possibility that factor XI inhibition may prove a useful addition to our armamentarium for treating high blood pressure.

frontiers in Physiology

ORIGINAL RESEARCH
published: 22 November 2017
doi: 10.3389/fphys.2017.00949

Implication of Free Fatty Acids in Thrombin Generation and Fibrinolysis in Vascular Inflammation in Zucker Rats and Evolution with Aging

Jérémy Lagrange[1, 2, 3], Mélusine Didelot[1, 2], Amel Mohamadi[1, 2], Lucy A. Walton[4, 5], Saartje Bloemen[6], Bas de Laat[6], Huguette Louis[1, 2], Simon N. Thornton[1, 2], Brian Derby[7], Michael J. Sherratt[8], Bruno Fève[9, 10, 11], Pascal Challande[12, 13], Riaz Akhtar[14], J. Kennedy Cruickshank[15], Patrick Lacolley[1, 2, 16†] and Véronique Regnault[1, 2, 16†]*

[1] Institut National de la Santé et de la Recherche Médicale, UMR_S 1116, Vandœuvre-lès-Nancy, France, [2] Faculté de Médecine, Université de Lorraine, Nancy, France, [3] Center for Thrombosis and Hemostasis, University Medical Center Mainz, Mainz, Germany, [4] Faculty of Medical and Human Sciences, Institute of Cardiovascular Sciences, University of Manchester, Manchester, United Kingdom, [5] Directorate of Radiography, School of Health Sciences, University of Salford, Salford, United Kingdom, [6] Synapse Research Institute, Cardiovascular Research Institute Maastricht, Maastricht University Medical Center, Maastricht, Netherlands, [7] School of Materials, University of Manchester, Manchester, United Kingdom, [8] Faculty of Medical and Human Sciences, Institute of Inflammation and Repair, University of Manchester, Manchester, United Kingdom, [9] Centre de Recherche Saint-Antoine Institut National de la Santé et de la Recherche Médicale-Université Pierre et Marie Curie, UMR_S 938, Paris, France, [10] Institut Hospitalo-Universitaire ICAN, Paris, France, [11] Assistance-Publique des Hôpitaux de Paris, Service d'Endocrinologie, Hôpital Saint-Antoine, Paris, France, [12] UPMC, University of Paris, Paris, France, [13] Centre National de la Recherche Scientifique, UMR 7190, Paris, France, [14] Centre for Materials and Structures, School of Engineering, University of Liverpool, Liverpool, United Kingdom, [15] Diabetes & Cardiovascular Medicine, Nutritional Sciences Division, King's College London, London, United Kingdom, [16] CHRU Nancy, Vandœuvre-lès-Nancy, France

OPEN ACCESS

Edited by:
Gerald A. Meininger,
University of Missouri, United States

Reviewed by:
Carlo Palombo,
University of Pisa, Italy
Aaron J. Trask,
The Research Institute at Nationwide Children's Hospital, United States

***Correspondence:**
Véronique Regnault
veronique.regnault@inserm.fr

[†]These authors have contributed equally to this work.

Specialty section:
This article was submitted to Vascular Physiology, a section of the journal Frontiers in Physiology

Received: 03 May 2017
Accepted: 08 November 2017
Published: 22 November 2017

Citation:
Lagrange J, Didelot M, Mohamadi A, Walton LA, Bloemen S, de Laat B, Louis H, Thornton SN, Derby B, Sherratt MJ, Fève B, Challande P, Akhtar R, Cruickshank JK, Lacolley P and Regnault V (2017) Implication of Free Fatty Acids in Thrombin Generation and Fibrinolysis in Vascular Inflammation in Zucker Rats and Evolution with Aging. Front. Physiol. 8:949. doi: 10.3389/fphys.2017.00949

Background: The metabolic syndrome (MetS) and aging are associated with modifications in blood coagulation factors, vascular inflammation, and increased risk of thrombosis.

Objectives: Our aim was to determine concomitant changes in thrombin generation in the blood compartment and at the surface of vascular smooth muscle cells (VSMCs) and its interplay with adipokines, free fatty acids (FFA), and metalloproteinases (MMPs) in obese Zucker rats that share features of the human MetS.

Methods: Obese and age-matched lean Zucker rats were compared at 25 and 80 weeks of age. Thrombin generation was assessed by calibrated automated thrombography (CAT).

Results: Endogenous thrombin potential (ETP) was increased in obese rats independent of platelets and age. Clot half-lysis time was delayed with obesity and age. Interleukin (IL)-1β and IL-13 were increased with obesity and age respectively. Addition of exogenous fibrinogen, leptin, linoleic, or palmitic acid increased thrombin generation in plasma whereas adiponectin had an opposite effect. ETP was increased at the surface of VSMCs from obese rats and addition of exogenous palmitic acid further enhanced ETP values. Gelatinase activity was increased in aorta at both ages in obese rats and MMP-2 activity was increased in VSMCs from obese rats.

Conclusions: Our study demonstrated in MetS an early prothrombotic phenotype of the blood compartment reinforced by procoagulant properties of dedifferentiated and inflammatory VSMCs. Mechanisms involved (1) increased fibrinogen and impaired fibrinolysis and (2) increased saturated fatty acids responsible for additive procoagulant effects. Whether specifically targeting this hypercoagulability using direct thrombin inhibitors would improve outcome in MetS is worth investigating.

Keywords: vascular aging, blood coagulation test, obesity, fatty acids, thrombin generation

INTRODUCTION

Atherothrombotic events and venous thromboembolism are associated with the metabolic syndrome (MetS), a cluster of risk factors for cardiovascular disease including insulin resistance (IR), abdominal adiposity, dyslipidemia, and hypertension (Dandona et al., 2005). Likewise, obesity is causally related to the high prevalence of MetS. Inflammation in MetS results in endothelial dysfunction and increased arterial stiffness (Weiss et al., 2013), probably through the action of matrix metalloproteinases (MMPs; Halcox et al., 2009). Aging is also associated with intimal thickening, breaks in the internal elastic lamina and impaired endothelial function leading to increased arterial stiffness (Wang et al., 1996).

A further cascade of obesity-induced chronic inflammation leads to increased tissue factor (TF; Samad et al., 2001) through the NF-κB pathway (Sonnenberg et al., 2004). Von Willebrand factor (VWF) participates in the prothrombotic state found in MetS (Lim et al., 2004). Total thrombin generation and platelet reactivity are increased in type 2 diabetes and older obese women (Beijers et al., 2010). Furthermore, as far as fibrinolysis is concerned, chronic inflammation, abdominal obesity, and IR all increase plasminogen activator inhibitor-1 (PAI-1) production, so reducing plasminogen conversion and leading to a hypofibrinolytic state (Alessi and Juhan-Vague, 2008; Suehiro et al., 2012).

Adipokine levels (adiponectin, leptin) as well as free fatty acid (FFA) metabolism are changed significantly in MetS (Matsuzawa et al., 2004; Wakil and Abu-Elheiga, 2009). Both are known also to be directly or indirectly implicated in haemostasis and increased thrombosis (Konstantinides et al., 2001; Restituto et al., 2010). Since haemostasis is modified in the MetS and during aging our hypothesis is that MetS, the related adipokines, and FFAs have a major impact on haemostasis changes, increased thrombotic risk and worsen the vascular phenotype. A major challenge is to elucidate the mechanisms leading to increased thrombosis during MetS and in the natural course of aging, and how they are related to the interaction between blood haemostasis and the vascular wall. Rodent models that mimic human MetS are major tools for understanding this pathophysiology (Sloboda et al., 2012).

Obese Zucker rats have a missense point mutation (fa/fa) in the leptin receptor gene that leads to hyperphagia and marked obesity (Phillips et al., 1996). These rats display also many other aspects of the human condition, such as IR, hypertension, and increased plasma lipid levels. We have shown previously that obese Zucker rats exhibited an increased age-dependent arterial stiffening which was greater in obese than lean, as well as endothelial dysfunction with increased systemic oxidative stress (Sloboda et al., 2012).

We have developed therefore a strategy combining "adult" (25-week-old) and "old" (80-week-old) Zucker rats with MetS characteristics and their lean controls and a vascular smooth muscle cell (VSMC) approach to investigate the role of FFAs and vascular inflammation in the prothrombotic properties of MetS. We first explored thrombin generation and its functional consequences on the fibrin network and on fibrinolysis in the blood compartment. To get insights into the underlying mechanisms we then examined thrombin generation at the surface of Zucker rat VSMCs and their MMP activity. We demonstrated that obesity from at least 25 weeks triggers increased thrombin generation in the blood compartment and at the surface of VSMCs via increased FFAs and associated vascular inflammation.

MATERIALS AND METHODS

Animals

Male Zucker rats with the MetS (MSZR, fa/fa; $n = 18$) and their age-matched male lean Zucker rat controls (LZR, FA/-; $n = 18$) were obtained from the breeding colony (animal facility, Faculty of Medicine, University of Lorraine, France). The animals were maintained at a constant temperature of 22–24°C, with a 12 h light-dark cycle (light beginning at 8 a.m.) and given free access to water and standard chow (A04, Scientific Animal Food and Engineering advance, Augy, France). The metabolic status of MSZR and LZR has been published previously (Sloboda et al., 2012).

Eighty weeks of age corresponds to 5 weeks before the mean maximum life span of rats from our local breeding colony.

This study was carried out in accordance with recommendations of the Animal Ethics Committee of the Institut National de la Santé et de la Recherche Médicale and conformed to the Guide for the Care and Use of Laboratory Animals, published by the National Institutes of Health. The protocols were approved by the Animal Ethics Committee of the Institut National de la Santé et de la Recherche Médicale.

Blood Sampling

Rats were anesthetized with isoflurane and whole blood was collected via a carotid catheter into syringes containing one-tenth the volume of 0.106 M sodium citrate. Platelet count

was determined with an automatic cell counter (Micros 60 ABX model, Montpellier, France). Blood was centrifuged at 190 g for 10 min at room temperature to obtain platelet-rich plasma (PRP) and then at 1,750 g for 10 min to obtain platelet-poor plasma. PRP was adjusted to 200×10^9 platelets/l by addition of autologous platelet-poor plasma and used for platelet aggregation and thrombin generation. Platelet-free plasma (PFP) was obtained by centrifugation of platelet-poor plasma at 13,000 g for 30 min at 4°C, and frozen at −80°C.

Preparation of Arterial Cryo-Sections

Artery cryo-sections were collected in the cross-sectional orientation and used subsequently for *in situ* gelatin zymography. The descending thoracic aorta was embedded in Optimal Cutting Temperature (OCT) medium and frozen using iso-pentane pre-cooled in liquid N_2 and stored at −80°C until cryo-sectioning. Cryo-sections were cut at a thickness of 5 μm and mounted onto glass slides (Leica, Milton Keynes, UK) and stored at −80°C until use.

Cell Culture

The descending thoracic aorta was excised from rats after isoflurane anesthesia (4.5% in 1.5 l/min dioxygen) and exsanguination. VSMCs were isolated as described previously (Ait Aissa et al., 2015). VSMCs were grown in DMEM/F12 supplemented with 10% fetal bovine serum (Lonza, Basel, Switzerland). For thrombin generation assays, VSMCs at passages 3–5 were seeded (7,500 cells/well) in 96-well tissue culture flat-bottom plates (MICROTEST^{TM}96), grown to subconfluence and washed with HBS before use.

Platelet Aggregation

Blood was centrifuged at 190 g for 4 min followed by 70 s at 1,900 g at room temperature to obtain PRP and then platelets were sedimented by centrifugation at 5,000 g for 4 min. Platelets were re-suspended in Tyrode buffer (5 mM Hepes, 137 mM NaCl, 2.7 mM KCl, 12 mM $NaHCO_3$, 0.4 mM NaH_2PO_4, 2 mM $CaCl_2$, 1 mM $MgCl_2$, 5.5 mM glucose, pH 7.3). Platelet aggregation was measured by turbidimetry at 37°C under stirred conditions. PRP or washed platelets were adjusted to 200×10^9 platelets/l and were stimulated by 5 μg/ml collagen or 5 μM ADP (SD Innovation, Frouard, France). Aggregation was followed for 10 min using a TA-8V aggregometer (SD Innovation).

Thrombin Generation Assay

Calibrated automated thrombinography (CAT) in PRP or PFP was performed in a microtiter plate fluorometer (Fluoroskan Ascent, ThermoLabsystems, Helsinki, Finland) using a dedicated software program (Thrombinoscope BV, Maastricht, The Netherlands) as reported previously (Regnault et al., 2004). All reagents were used at half the ordinary volume as follows: 40 μl PRP or PFP, 10 μl of 5 pM recombinant human tissue factor (TF) (Dade Behring, Marburg, Germany) and phospholipid vesicles (PV) consisted of phosphatidylcholine-serine-ethanolamine (PC/PS/PE) 60/20/20 mole% at a final concentration of 4 μM equivalent PS, 10 μl fluorogenic substrate and calcium. PV were replaced by buffer in PRP and VSMC experiments. Round-bottom 96-well Greiner blue plates were used for PFP and PRP, and MICROTEST^{TM}96 plates for VSMC monolayers. Thrombin generation curves were recorded in triplicate. Thrombin generation was monitored also following supplementing PFP with adiponectin or leptin (BioVision, San Francisco, USA), with fibrinogen (Sigma-Aldrich, St Louis, USA), or with palmitic acid or linoleic acid (Sigma-Aldrich).

Coagulation and Circulating Parameters

Prothrombin and FVIII were measured in PFP samples diluted 1:40–80 in factor diluent (Instrumentation Laboratory, Le Pré Saint Gervais, France). For each assay 50 μl of diluted sample were added to 50 μl of human prothrombin-deficient plasma (Siemens Healthcare Diagnostics SAS, Saint-Denis, France) or FVIII deficient plasma (Dade Behring, Deerfield, USA). After 1 min of incubation at 37°C in a KC10 coagulometer, coagulation was started by addition of 80 μl of Thromborel® S. Calibration curves were generated using the reference plasma Unicalibrator (Diagnostica Stago, Asnières, France). Fibrinogen was measured in PFP samples diluted 1:10–20 in Owren–Koller buffer (Diagnostica Stago, Asnières, France). Unicalibrator was used to generate calibration curves. After 4 min of incubation at 37°C in a KC10 coagulometer, coagulation was started by addition of 100 μl of Fibriquik (Biomérieux-Trinity Biotech, Bray, Ireland). Antithrombin levels were measured with the Coamatic® antithrombin test kit from Chromogenix, and TAT with the Enzygnost® TAT micro (Instumentation Laboratory). TF and TF pathway inhibitor (TFPI) activities were measured in PFP using the Actichrome® tissue factor and Actichrome® TFPI activity assay respectively (American Diagnostica, Stamford, CT). PAI-1 levels were measured with the rat PAI-1 total antigen ELISA kit from Innovative Research, Inc. IL-13 and IL-1β concentrations were measured with the IL-13 and IL-1 beta rat ELISA kits from Invitrogen. MMP-9 levels were measured with the Quantikine rat total MMP-9 immunoassay from R&D Systems. VCAM-1 was assessed with the rat VCAM-1 ELISA kit from Elabscience.

In Vitro Fibrinolytic Test

PFP (20 μl) was diluted by addition of 40 μl buffer containing 5 pM recombinant TF, PV at 4 μM equivalent PS, 5 nM rabbit thrombomodulin (TM) (American Diagnostica, Greenwich, USA) and 4 μg/ml recombinant human tissue Plasminogen Activator (tPA) Actilyse® (Boehringer Ingelheim, Ingelheim am Rhein, Germany). Clot formation was initiated by addition of 10 μl of 100 mM $CaCl_2$. To monitor clot lysis, absorbance was read kinetically at 405 nm using a microplate reader. To standardize the figure, for each sample basal optical density (OD) after lysis was subtracted from each point of the curve. Half lysis time was defined as the time required to reach half-maximal variation in OD.

Microscopy of Fibrin Fiber Ultrastructure

The thrombin generation assay was performed in order to generate fibrin for fixation using the same TF and PV concentrations as in the CAT experiments. This was done using plasma on paper disks and a Rhodamine substrate was used

(Ninivaggi et al., 2012). Immediately after thrombin generation was finished (50 min for each run), the mineral oil was removed from the well and a solution of glutaraldehyde (grade I) in phosphate buffered saline (PBS) (Sorensen's PBS, pH 7.2) was applied. This was put at room temperature for 1 h and then kept at 4°C overnight. The samples were then washed 5 times with PBS and a secondary fixation was performed in OsO_4 (1%) in sodium cacodylate (200 nM, pH 7.4) for 1 h at RT. The samples were then dehydrated with increasing concentrations of ethanol each during 3 min (30, 50, 70, 90, 100%) and the last step (100%) was performed three times. Further dehydration was accomplished by a hexamethyldisilazane (HMDS)/ethanol solution (1:1) for 3 min and HMDS for 10 min. The samples were removed from the wells and left to dry. In order to visualize the samples with a Phenom G2Pro scanning electron microscopy (SEM) (Phenom-World, Eindhoven, the Netherlands), they were put on stubs using carbon tabs and coated with gold.

For each sample, 3–5 pictures were analyzed. Fiber thickness was measured using ImageJ software (version 1.48v). For each picture 100 measurements were performed. The density of the fibers was calculated from the pictures by counting the number of fibers that crossed a line of 26.8 μm (Konings et al., 2011).

Rat Cytokine Antibody Array

The Rat Cytokine Array Panel A (Cat # ARY008) from R&D system (Minneapolis, MN) was used to probe cytokines in PFP from MSZR and LZR by following the procedures recommended by the manufacturer. Bound antibodies were detected by chemiluminescence using the Immobilon™ Western Chemiluminescent HRP Substrate (Millipore, Billerica, MA). This was performed once with a plasma pool from 5 to 6 animals to reduce inter-animal variability in each group.

Phospholipid Procoagulant Activity

The chromogenic assay measuring the phospholipid-related procoagulant activity (PPA) in VSMCs was performed as described previously for plasma (Wagenvoord et al., 1994; Membre et al., 2008). VSMCs cultured in 96 well plates were washed and 50 μl of 50 mM Tris, 175 mM NaCl, pH 7.9 (TBS) containing 2 g/l bovine serum albumin (BSA) were added as well as 50 μl of activated factor X (1.2 nM), activated factor V (2.4 nM), $CaCl_2$ (15 mM) and 50 μl of bovine prothrombin (6 μM) plus Z-Gly-Gly-Arg-AMC substrate (1.25 mM) in 20 mM HEPES pH 7.5 containing 60 g/l BSA. The plate was placed in the Fluoroskan Ascent fluorometer and allowed to warm up to 37°C for 5 min before kinetic readings were taken over 10 min. Phospholipid concentration was estimated from the initial rate of thrombin formation by reference to a standard curve constructed with PV, and expressed as PS equivalents.

Western Blot

Cell extracts were obtained by lysing VSMCs in complete Lysis-M buffer (Roche Diagnostics Corporation, Basel, Switzerland). Detergent-soluble fractions were retained, and protein concentrations in samples were determined using a Bradford protein assay (Bio-Rad, Hercule, USA). Lysates containing 30 μg of protein were electrophoresed on polyacrylamide gels (8% gel), transferred to Hybond-C nitrocellulose membranes (transblot turbo, Bio-Rad, Hercule, USA) and blotted with the following antibodies: α-smooth muscle actin (αSMA), 4/1,000 (Sigma-Aldrich), smooth muscle myosin heavy chain (SM-MHC), 1/1,000 (Abcam; Cambridge, UK); smoothelin, 1/500 (Santa Cruz Biotechnology, USA); integrin α_v, 1/1,000 (Santa Cruz Biotechnology, Dallas Texas); integrin β_3 1/500 (Merck Millipore, Billerica, USA) and tubulin, 2/1,000 (Sigma-Aldrich). After rinsing, incubation with a secondary rabbit antibody 1/1,000 (α_v, β_3, smoothelin, SM-MHC, Sigma-Aldrich) and mouse antibody 1/1000 (αSMA, tubulin, Sigma-Aldrich). Reactions were visualized by the ECL Western Blot Detection Kit (Bio-Rad, Hercule, USA) after incubation with peroxidase conjugates 1/2000 (GE Healthcare, Little Chalfont, UK). Tubulin was used as loading control and the protein expression was normalized to tubulin.

In Situ Gelatin Zymography

In situ gelatin zymography was performed to determine the gelatinase activity across the aortic wall using DQ-gelatin (Life Technologies, Paisley, UK) as described previously (Mook et al., 2003). Fluorescein isothiocyanate (FITC, 1/110), and 4′,6-diamidino-2-phenylindole (DAPI, 1/150) filters were used to visualize the degree of gelatinase activity and the localisation of nuclear tissue by fluorescence microscopy using a x20 optical objective (Keynece, Osaka, Japan). Analysis of average fluorescence was performed for three 20 μm thick profile lines across 3 arterial wall regions for each sample.

Zymography Analysis

VSMCs from LZR or MSZR (passage 4–6) were seeded (50,000 cells/well) in 6-well culture plates in DMEM/F-12 supplemented with 10% fetal bovine serum (life technology Thermo Fisher Scientific, Waltham, USA). Cells were grown to subconfluence and after 16 h in serum-free medium, cells were washed with PBS (Sigma-Aldrich), the medium was changed and cells were incubated for 4, 8, or 20 h at 37°C. Conditioned media were then removed and centrifuged at 500 g for 10 min at room temperature and used for the determination of MMP-2 secretion.

Conditioned media were analyzed for gelatin degradation by electrophoresis under non-reducing conditions on a 10% polyacrylamide-SDS gel containing 0.1% gelatin. Gels were washed for 1 h at room temperature in a 2% triton X-100 solution and incubated overnight at 37°C in 50 mM Tris–HCl/10 mM $CaCl_2$ (pH 7.6) buffer.

Gels were stained in a 0.1% coomassie Blue (G250)/45% methanol/10% acetic acid solution and de-stained in a 10% acetic acid/20% methanol solution. White lysis strips, indicative of gelatinolytic activity, were revealed and scanned (Fujifilm LAS 4000, Life sciences, Branford, USA). Densitometric analysis was made using MultiGauge software (Fuji, Tokyo, Japan). Fetal bovine serum diluted at 1% in serum free medium was used as a positive control.

Statistical Analysis

Results are presented as mean ± standard error of the mean. Data were analyzed by a one-way or two-way ANOVA, followed by a Fisher's test for multiple comparisons to evaluate the influence of age and strain and their interaction on the different variables. In the case of SEM measurements, the differences in fiber thickness were analyzed using the Mann Whitney *U*-test.

RESULTS

Platelet Aggregation, Thrombin Generation, and Fibrinolysis Were All Impaired with the MetS and/or Aging

Platelet count in blood was increased in MSZR at both ages compared to the same aged LZR (**Table 1**). Platelet aggregation using washed platelets and collagen as a strong agonist was not significantly modified as shown by the mean maximum aggregation (**Figure 1A**). For platelet aggregation in PRP using ADP, mean maximum aggregation was increased in 80 week-old MSZR and LZR compared to 25 week-old controls (**Figure 1B**). The F1+2 fragment was analyzed to evaluate the *in vivo* reactivity of the coagulation system. The amount of F1+2 fragment was increased in 25 week-old MSZR compared to the same aged LZR (**Table 1**). Thrombin generation measurement was performed as an integrative *in vitro* phenotype of coagulation. Adult and very old MSZR had a significantly increased endogenous thrombin potential (ETP) compared to same aged LZR. The other thrombin generation parameters (lag time, peak, and velocity) were not changed significantly except for the time to peak which was increased in obese at both ages (**Table 1**; **Figure 1C**). The ratio of thrombin generation in PFP and PRP compared to 25 week-old LZR was made to evaluate the platelet reactivity impact on thrombin generation. Interestingly, thrombin generation was more increased in PRP from MSZR at 25 week of age compared to 80 week-old rats (**Figure 1D**). The coagulation parameters, TF, TFPI, prothrombin and fibrinogen, were all increased in MSZR compared to LZR at both ages. TFPI was decreased and fibrinogen was increased with age in MSZR and prothrombin was increased with age in LZR. FVIII was increased significantly with age and MetS in 80 week-old MSZR. Antithrombin measurements showed no modification in MSZR and LZR rats (**Table 1**). Fibrin clots were characterized by SEM. Computerised analysis of the SEM images showed a decrease of fibrin fiber thickness in MSZR compared to LZR at both ages while fiber density was only increased in 80 week-old LZR (**Figures 1E-G**). Circulating levels of PAI-1 were increased in both 80 week-old LZR and MSZR (**Figure 1H**). In a fibrinolysis test (**Figure 1I**), half-time lysis was increased in MSZR compared to LZR at both ages and aging significantly increased half-time lysis in both groups (**Figure 1J**). Maximal lysis speed was not modified (**Figure 1K**).

Inflammation, Metabolic Factors, and Free Fatty Acids Modified Thrombin Generation

Fibrinogen concentration was correlated highly to ETP ($r = 0.069$) and supplementing plasma with exogenous fibrinogen at concentrations that agreed with the changes between MSZR and LZR gradually increased ETP (**Figures 2A,B**). The 1.2-fold increase in ETP with the 2.5 mg/mL concentration is consistent with the 1.4 increase in plasma fibrinogen in MSZR. We have then tested the effects of addition of exogenous leptin, adiponectin, linoleic acid, and palmitic acid to PFP at concentrations selected to encompass the range previously

TABLE 1 | Blood coagulation parameters and thrombin generation parameters of LZR and MSZR at 25 and 80 weeks of age.

	25 week-old		80 week-old		ANOVA		
	LZR	MSZR	LZR	MSZR	Strain	Age	Interaction
n	9	10	12	9			
Platelets (10^3/mm^3)	574 ± 37	789 ± 34*	633 ± 29	834 ± 63*	≤0.0001	0.009	0.013
F1+2 (pmol/l)	4.1 ± 0.5	7.9 ± 1.0*	5.8 ± 1.2	5.5 ± 0.9	0.009	0.7	0.05
TF (pM)	0.3 ± 0.1	12.2 ± 1.7*	2.0 ± 0.4	9.9 ± 1.5*	≤0.0001	0.8	0.09
TFPI activity (U/ml)	4.9 ± 0.2	11.2 ± 0.2*	5.4 ± 0.2	9.9 ± 0.6*#	≤0.0001	0.3	0.01
FVIII (%)	104 28	190 34	124 28	466 52*#	≤0.0001	0.002	0.001
Prothrombin (%)	94 ± 3	223 ± 19*	155 ± 14#	264 ± 16*	≤0.0001	0.002	0.5
AT (%)	129 ± 2	125 ± 2	127 ± 1	123 ± 3	0.04	0.5	0.9
Fibrinogen (g/l)	2.8 ± 0.1	4.0 ± 0.2*	3.1 ± 0.1	4.9 ± 0.2*#	≤0.0001	0.0003	0.2
n	11	11	10	7			
Lag time (min)	1.5 ± 0.1	1.7 ± 0.1	1.4 ± 0.1	1.5 ± 0.1	0.09	0.4	0.6
Peak (nM)	99 ± 8	121 ± 9	102 ± 10	117 ± 15	0.07	0.98	0.7
Time to peak (min)	4.4 ± 0.1	5.2 ± 0.3*	4.1 ± 0.1	5.3 ± 0.2*	≤0.0001	0.6	0.3
ETP (nM.min)	395 ± 37	549 ± 52*	362 ± 34	553 ± 76*	0.001	0.8	0.8
Velocity (nM/min)	35 ± 3	37 ± 4	40 ± 4	31 ± 4	0.6	0.98	0.2

*Results are mean ± standard error to the mean. *$p < 0.05$, SMZR vs. LZR at the same age; #$p < 0.05$, 80 vs. 25 week-old rats in the same strain. F1+2, fragment 1+2; TF, tissue factor; TFPI, tissue factor pathway inhibitor; AT, antithrombin; ETP, endogenous thrombin potential.*

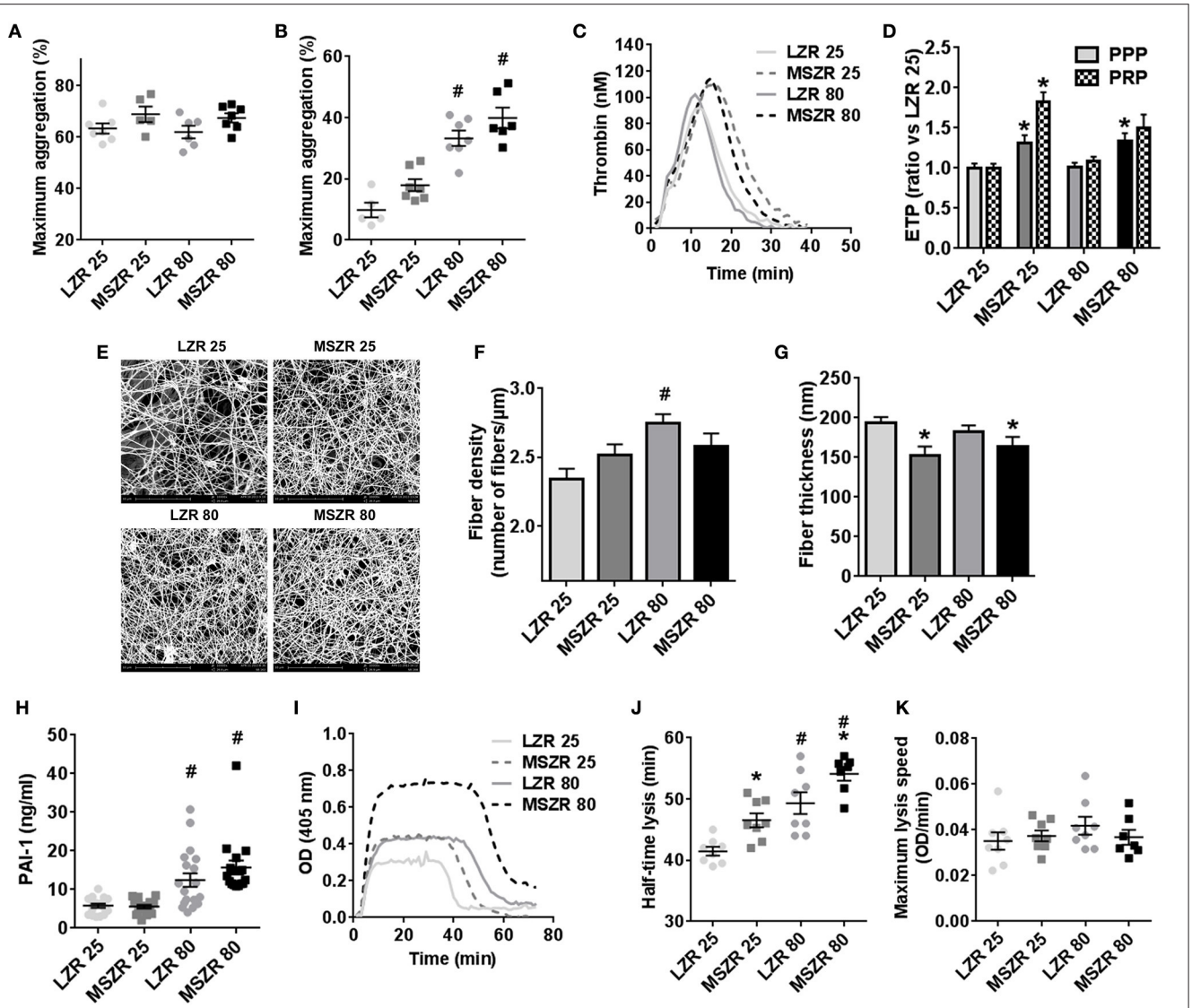

FIGURE 1 | Platelet aggregation, thrombin generation, and fibrinolysis in LZR and MSZR rats**. (A)** Mean maximum aggregation in washed platelets in response to collagen (5 µg/ml) and in **(B)** platelet-rich plasma (PRP) in response to ADP (5 µM), with the platelet count adjusted to 200 × 10^9 platelets/l. **(C)** Calibrated automated thrombinography (CAT) in rat plasma. Mean thrombin generation curves in platelet free plasma (PFP) triggered by 5 pM tissue factor in LZR and MSZR at 25 and 80 weeks of age. **(D)** Endogenous thrombin potential (ETP) in PFP and PRP of 25 and 80 week-old LZR and MSZR, expressed as ratios of values for 25 week-old LZR. **(E)** Ultrastructure of fibrin fibers was visualized by scanning electron microscopy. Pictures were made at 10,000 × magnification. **(F,G)** Fiber thickness and fiber density of fibrin clot in LZR and MSZR. **(H)** ELISA results of PAI-1 measured in PFP (n = 17–19). **(I)** Representative curves of fibrinolytic tests in PFP in LZR and MSZR. **(J,K)** Half-lysis time and maximal lysis speed of fibrinolytic tests in LZR and MSZR. Results are mean ± standard error of the mean (n = 7–11). $^*p < 0.05$ vs. LZR at the same age; $^\#p < 0.05$ vs. 25 week-old rats in the same strain.

reported for each molecule in MSZR (Sloboda et al., 2012; Godin et al., 2013). Addition of leptin or adiponectin elicited similar concentration-dependent changes in ETP whatever the group of rat. The two adipokines had opposite effects on thrombin generation, leptin increased ETP whereas adiponectin decreased it (**Figures 2C,D**). The two lower concentrations of added linoleic acid (0.75 and 1.5 mg/mL) had clear procoagulant effects whereas the higher concentration (3 mg/mL) was less effective in increasing thrombin generation (**Figures 2E,F**). There was a significant increase in thrombin generation for all added concentrations of palmitic acid whatever the group of rat. The results show an additive effect of FFAs on MSZR plasma.

Plasma Cytokines Were Increased Both with MetS and Aging

To explore inflammation in our model we performed a plasma cytokine array of 27 cytokines in order to provide qualitative data that will subsequently be used to quantify cytokines known likely to promote prothrombotic phenotypes (**Figure 3**). Panel

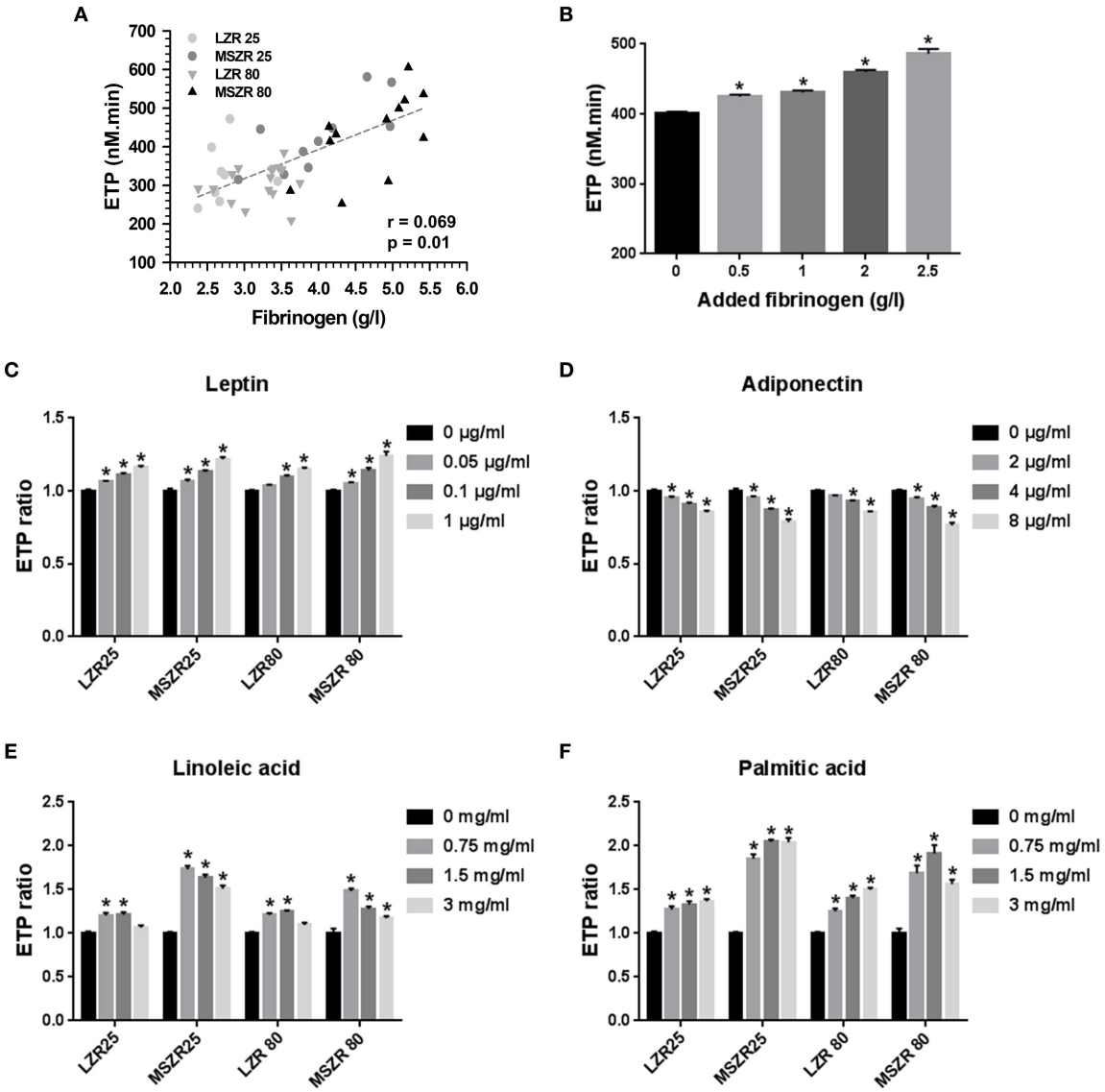

FIGURE 2 | Effect of fibrinogen, adipokines, and free fatty acids on thrombin generation. **(A)** Correlation between ETP and plasma fibrinogen concentration of 25 and 80 week-old LZR and MSZR ($r = 0.069$, $p = 0.01$). **(B)** ETP values in 25 week-old LZR platelet free plasma supplemented with 0.5, 1.0, 2.0, or 2.5 g/l fibrinogen. **(C–F)** ETP values, expressed as ratios of values in presence of adipokines or free fatty acids to those obtained with no addition for each group, in platelet free plasma supplemented with 0.05, 0.1, or 1.0 ng/ml leptin **(C)**, with 2, 4, or 8 µg/ml adiponectin **(D)**, with 0.75, 1.5, or 3 mg/ml of linoleic acid **(E)** or with 0.75 1.5, or 3 mg/ml of palmitic acid **(F)**. Results are mean ± standard error of the mean ($n = 11$–16). *$p < 0.05$ vs. no addition.

A presents pictures of the cytokine array membranes. A 50% variation between two groups was chosen as a threshold to classify cytokines into four groups. The first group of five cytokines showed no modifications (**Figure 3B**), a second group of eight cytokines were increased with MetS (**Figure 3C**), a third group of three cytokines were increased with aging (**Figure 3D**) and a last group of 11 cytokines were increased with both MetS and aging (**Figure 3E**). The highest variation between 25 week-old MSZR and LZR was found for IL-1β (>3,000% variation) and the highest variation between 80 and 25 week-old rats was observed for IL-13 (>400% variation). ELISAs performed with individual rat PFP for IL-1β and IL-13 showed an increase of these cytokine levels in LZR and MSZR with age (**Figures 3F,G**). IL-13 was increased also in 80 week-old MSZR compared to same aged LZR.

MetS and Aging-Induced Inflammation and Haemostasis Impairment Were Related to Alteration of VSMCs

To explore the contribution of VSMCs, thrombin generation was measured at the surface of cultured VSMCs isolated from LZR and MSZR. Thrombin generation with PFP from LZR and MSZR was always increased at the surface of MSZR VSMCs

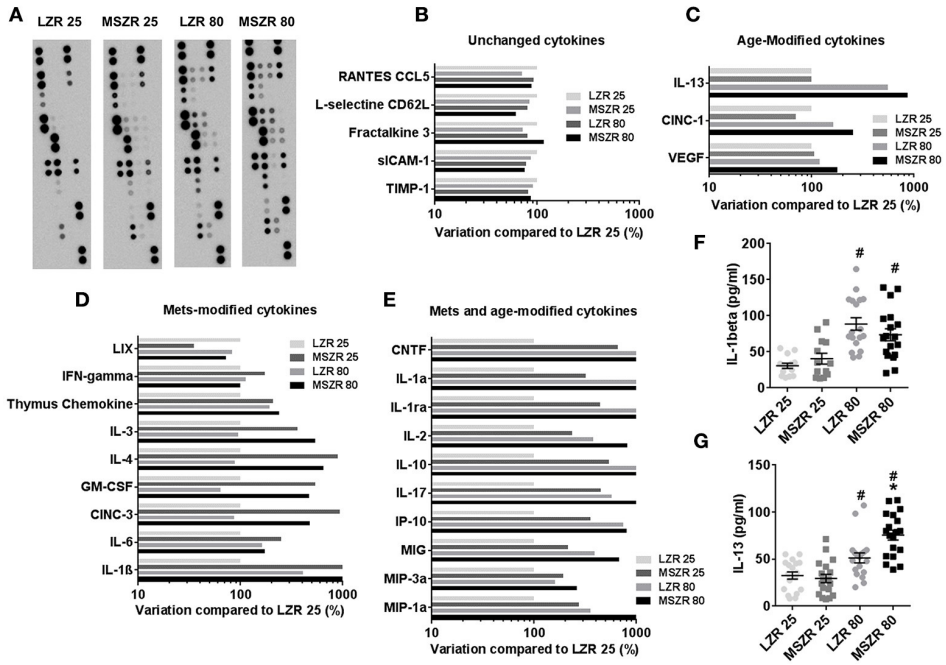

FIGURE 3 | Plasma cytokine array in Zucker rats**. (A)** Cytokine arrays of pooled platelet free plasma from 25 to 80 week-old MSZR and LZR. Relative chemoluminescence compared to 25 week-old LZR was measured. **(B)** Unchanged cytokines, **(C)** cytokines modified with age, **(D)** with MetS, or **(E)** both with MetS and age. ELISAs results for IL-1β **(F)** and IL-13 **(G)** measured in PFP ($n = 14$–18), results are mean ± standard error of the mean, $^{*}p < 0.05$ vs. LZR at the same age; $^{\#}p < 0.05$ vs. 25 week-old rats in the same strain. VEGF, vascular endothelial growth factor; CINC-1, cytokine-induced neutrophil chemoattractant 1; CINC-3, cytokine-induced neutrophil chemoattractant 3; GM-CSF, granulocyte macrophage colony stimulating factor; MIP, Macrophage Inflammatory Protein; MIG, C-X-C motif ligand 9; IP-10, interferon gamma-induced protein 10; CNTF, ciliary neurotrophic factor; INFγ, interferon γ; IL, interleukin.

compared to LZR VSMCs. Remarkably, addition of palmitic acid in LZR VSMCs increased thrombin generation to the level of MSZR independently of the PFP used (**Figure 4A**). MSZR VSMCs displayed increased procoagulant phospholipids at their surface compared to LZR VSMCs (**Figure 4B**). Integrin subunit α_v was increased in MSZR compared to LSZ VSMCs while the β_3 subunit was not modified. VSMC differentiation markers α-SMA, SM-MHC, and smoothelin, interestingly, were all decreased in MSRZ VSMCs compared to LZR VSMCs (**Figures 4C,D**). Thus, *in situ* gelatin zymography was performed to explore MMP activity through gelatinase activity (**Figure 4E**). **Figure 4E** shows representative photographs of *in situ* gelatin zymography in aorta, gelatinase activity is in green. Mean gelatinase activity in the aortic wall was increased in 25 and 80 week-old MSZR compared to age matched LZR aortas (**Figure 4F**). However, age did not modulate gelatinase activity. At the cellular level MSZR VSMCs displayed increased MMP-2 secretion compared to LZR VSMCs (**Figures 4G,H**). Circulating levels of MMP-9 were increased in 80 week-old MSZR whereas VCAM-1 was increased in 25 week-old MSZR compared to same aged LZR and in 80 week-old LZR (**Figures 4I,J**).

DISCUSSION

The aim of the present study was to determine concomitant changes in the haemostasis system and VSMC phenotype and their interplay with FFAs and MMPs during aging in obese rats compared to lean rats of the same age. Our results demonstrated (1) increased thrombin generation in MetS in plasma as early as 25 weeks of age, independently of platelets and at the surface of VSMCs; (2) reinforcement of this hypercoagulability by reduced plasma fibrinolysis; (3) no influence of aging on plasma thrombin generation; (4) an age-related increase in platelet aggregation and clot half lysis time and, (5) contribution of saturated FFAs to the increased thrombin generation both in plasma and at the surface of VSMCs.

Increased thrombotic risk can be attributed to three factors: abnormalities in the vessel wall, in blood flow, and in haemostasis including coagulation and fibrinolysis. We found previously that MSZR presented endothelial dysfunction as shown by increased circulating VWF. This endothelial dysfunction was exacerbated during aging as shown by increases in both VWF and soluble CD146 (Sloboda et al., 2012).

Few studies have used Zucker rats to look at haemostasis and to our knowledge none have been performed in very old Zucker rats. Paul et al. found that 12 week-old diabetic Zucker rats presented unmodified *in vitro* platelet reactivity (Paul et al., 2007). Recently Shang et al. have shown increased thrombosis, increased thrombin generation and decreased fibrinolysis in 7–10 week-old diabetic Zucker rats (Shang et al., 2014). They found also decreased platelet reactivity to collagen and ADP in obese rats in PRP. In PRP, we found increased platelet aggregation using ADP in 80 week-old MSZR and LZR rats compared to

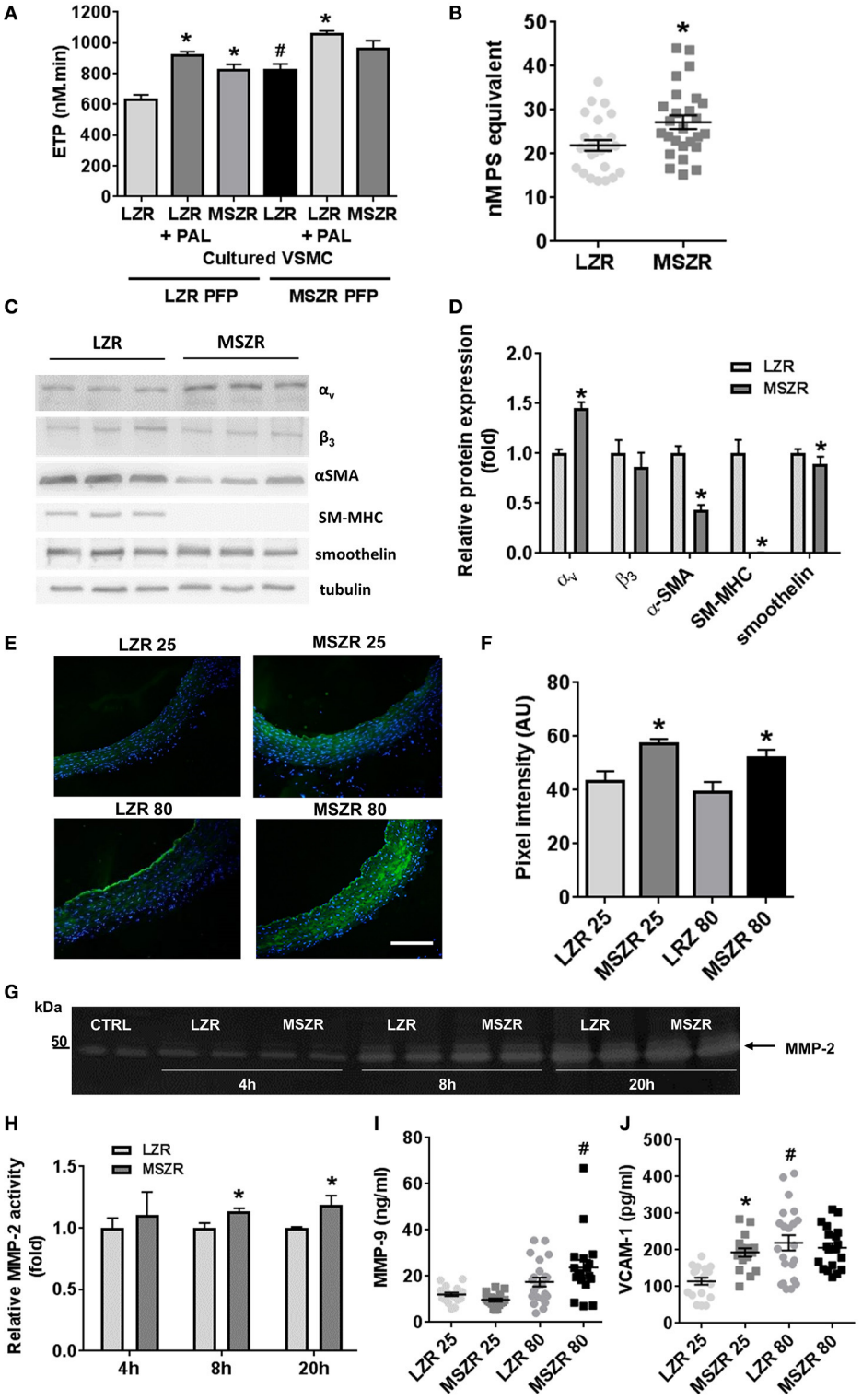

FIGURE 4 | Role of smooth muscle cells in thrombin generation. **(A)** ETP values measured at the surface of vascular smooth muscle cells (VSMCs) from LZR and MSZR, with LZR or MSZR platelet free plasma (PFP), and with or without 1.5 g/l exogenous added palmitic acid (PAL). Results are mean ± standard error of the mean, $n = 3$ with 6 wells per condition per experiment. $^{*}p < 0.05$ vs. LZR VSMC, $^{\#}p < 0.05$ vs. LRZ PFP and LRZ VMSC. **(B)** VSMC associated procoagulant activity reported as phosphatidylserine (PS) equivalent in LRZ and MSZR. Results are mean ± standard error of the mean ($n = 25$). $^{*}p < 0.05$ vs. LZR. **(C)** Typical Western blot and **(D)** quantification analysis of VSMC differentiation markers (αSMA, SM-MHC, and smoothelin) and integrin subunits (α_V and β_3) in cultured VSMCs.

(Continued)

FIGURE 4 | Continued
Results, expressed as fold change vs. VSMCs from LZR, are mean ± standard error of the mean ($n = 6$). *$p < 0.05$, MSZR vs. LZR. **(E)** Representative images of gelatinolytic metalloproteinase activity in the aorta was measured using *in situ* gelatin zymography for each group of Zucker rats. Fluorescence as marker for intra-plaque gelatinolytic activity was quantified. Nuclei were visualized by DAPI staining. **(F)** Average wall fluorescence of the gelatinolytic metalloproteinase activity in the aorta. **(G)** Representative images of zymography gels of LZR and MSZR VSCMCs supernatant at 4, 8, and 20 h. **(H)** Relative MMP-2 activity in LZR and MSZR VSMC supernatant at 4, 8, and 20 h. Results are mean ± standard error of the mean ($n = 5$). *$p < 0.05$, MSZR vs. LZR. ELISAs results of MMP-9 **(I)** and VCAM-1 **(J)** measured in PFP ($n = 17$–22). *$p < 0.05$ vs. LZR at the same age; $^{\#}p < 0.05$ vs. 25 week-old rats in the same strain.

25 week-old controls, but not between rats of the same age. In addition, we were not able to aggregate platelets using collagen. Washed platelets were able to aggregate when triggered with collagen but we did not find any significant changes with obesity or with age. These changes might be related to the metabolic differences existing between rats since they used diabetic Zucker rats while we used obese Zucker rats that only develop diabetes very late with age. Moreover, platelet count was not modified in the diabetic Zucker rats of the Shang et al. study while we found a 25% increased count in MSZR compared to LZR at both ages. Interestingly, platelet-related thrombin generation showed a very important increase in 25 week-old MSZR compared to thrombin generation made with PFP. Altogether, increased platelet aggregation to ADP with age concomitant to increased platelet count in obese Zucker rats is in favor of a prothrombotic state.

To better assess the prothrombotic state in obese and aged rats we investigated *in vivo* thrombin generation by measuring F1+2 fragments, which were increased in MSZR indicating increased *in vivo* formation of thrombin with MetS. As expected, MetS also increased the *in vitro* thrombin generation capacity of plasma, but this ability was not modified with age. This change in the *in vitro* reactivity of the coagulation system points out the role of several components including metabolic factors and the vascular wall. Regarding individual clotting factors it was clear that TF increased in MSZR as well as its inhibitor (TFPI). Increased prothrombin concentration leads to higher thrombin generation and can contribute to the increased ETP in MSZR. Other procoagulant factors such as FVII, FVIII, and VWF are known to be increased with MetS and aging. Metabolic factors such as leptin and adiponectin can participate in haemostasis. Leptin has been suggested previously to represent a link between obesity and atherothrombosis (Petrini et al., 2016). It has been reported that leptin enhanced platelet aggregation while adiponectin reduced it (Konstantinides et al., 2001; Restituto et al., 2010). Adiponectin has been involved also in the endothelium anticoagulation function (Lee et al., 2011) since it increased endothelial TFPI synthesis (Chen et al., 2008). We found in all Zucker rats a strong positive correlation between plasma TPFI and adiponectin concentrations dosed previously (data not shown; Sloboda et al., 2012). Moreover, in our study, we found for the first time that leptin increased ETP and that adiponectin decreased it. Despite it being a modest effect, it argues for a major involvement of adipokines in the regulation of thrombin generation.

Fibrinogen concentration was correlated also to ETP and we confirmed that increased plasma fibrinogen increased ETP (Kumar et al., 1994). Thrombin linked to fibrin can possibly be protected from inhibition by antithrombin, in the same way as it is protected from inhibition when bound to TM (Bourin, 1987). This may participate in explaining the increased time to peak observed in MSZR and increased ETP with no significantly increased peak.

We found that fibrinogen concentration was increased in MSZR and during aging. In favor of the relevance of this result it has been shown that synthesis of fibrinogen is upregulated by inflammatory cytokines such as IL-6 (Morozumi et al., 2009). The consequence of an increased thrombin generation was an increased fibrin network formation in MSZR as shown by thinner fibrin fibers (Wolberg, 2007). The increase in PAI-1 with aging in LZR as well as in MSZR is relevant to human physiology since it is known that during aging PAI-1 is associated with an increased thrombotic risk. In addition, the fibrinogen concentration increased during aging but the mechanisms underlying this association with thrombotic risk are unclear (Cesari et al., 2010). Human fibrinolysis is also impaired in the MetS with a decrease in clot lysis ability linked to increased PAI-1 (Pandolfi et al., 2001). Organization of the fibrin network is likely due to the increased thrombin generation found in MSZR (Wolberg, 2007). Moreover, clots with thinner fibrin fibers are more resistant to lysis than clots with thick fibers (Gabriel et al., 1992). This is supported by the increased half-time lysis found in MSZR and very old Zucker rats. Other factors must be implicated since fiber thickness was unchanged with age in both groups whereas fibrinolysis time increased only during aging indicating the formation of a denser clot. In line with this, adiponectin may act as an anticoagulant molecule. Indeed, full length adiponectin reduces platelet aggregation, inhibits TF and enhances TFPI expression at the surface of endothelial cells (Chen et al., 2008; Restituto et al., 2010). Both adiponectin and IL-13 increase the expression of MMPs which can degrade fibrinogen (Hotary et al., 2002; Wanninger et al., 2011; Firszt et al., 2014). Consistent with this, we found an increase in IL-13 plasmatic concentration with aging and also with the MetS in 80 week-old MSZR which presents the same variations as plasma levels of MMP-9 and FVIII. Whether adiponectin interplays directly with fibrinogen remains an open question. The increase in FVIII with MetS and associated inflammatory stimuli was anticipated in Zucker rats as it is in humans (Begbie et al., 2000; Kotronen et al., 2011).

Inflammation during aging and in the MetS triggers vascular remodeling. Fibrinogen (Lominadze et al., 2010) as well as fibrin and fibrin degradation products have proinflammatory functions that can modify VSMC phenotype (Lu et al., 2011). Cytokines in the plasma, as shown in the array presented here, are increased by the MetS, aging, or both. Our data indicated that the more relevant proinflammatory cytokines such as IL-1α, IL-1β, IL-2, IL-3, and IL-6 were increased early with the MetS while few

anti-inflammatory cytokines were increased with MetS and aging (IL-10, IL-1ra, IL-17). Our cytokine array made with a pool of plasma for each group was checked using ELISA measurements with individual samples for the two main cytokines involved in the regulation of haemostasis (IL-13 and IL-1β). IL-13 changes were confirmed while IL-1β increased only with aging but not with the MetS at 25 weeks of age. This points to a determinant role of age in complex vascular pathologies including several comorbidities. IL-1β has a pleiotropic effect in the development of atherothrombosis through its action on leukocyte adhesion to the vascular wall and induction of procoagulant activity (Libby et al., 1986; Dinarello, 2011). Recently, inhibition of IL-1β and subsequent reduction of inflammation (without modification of lipid levels) in patients with previous episodes of myocardial infarction was found to reduce recurrent cardiovascular events (Ridker et al., 2017). These findings are in line with the increase of circulating IL-1β and increased activity of haemostasis with age we observed in MSZR. Therefore, exploration of haemostasis function in MSZR with inhibition of IL-1β could be of interest.

Other factors related to MetS that can potentiate the modifications we observed in MSZR haemostasis are FFAs. Saturated FFAs such as palmitic acid are known to be associated with ischemic heart disease and increase postprandial concentrations of fibrinogen (Simon et al., 1995; Pacheco et al., 2006). One other mechanism proposed recently to explain the thrombogenic effect of palmitic acid was its ability to induce extracellular release of histones (Shrestha et al., 2013). Histones are known to promote thrombin generation through platelet activation (Semeraro et al., 2011). Additionally, palmitic acid was measured recently in diabetic Zucker rats pointing out a 2.75 times increased concentration in obese rats (0.68 g/l in LZR vs. 1.87 g/l in MSZR) (Godin et al., 2013). A similar increase was observed for a polyunsaturated FFA, linoleic acid. We supplemented 25 week-old LZR PFP with linoleic or palmitic acid to reach MSZR plasma concentrations. We showed for the first time a direct effect of FFAs on thrombin generation confirming the prothrombotic effect of palmitic acid.

All these FFAs, pro-inflammatory cytokines and coagulation factors can have deleterious effects on the vascular wall. We have shown previously the presence of endothelial dysfunction in MSZR (Sloboda et al., 2012). In the present study we studied VSMCs in more detail. Interestingly, thrombin generation measured at the surface of VSMCs from MSZR was increased compared to LZR VSMCs. This increase can be related to the increased procoagulant phospholipids at the surface of MSZR VSMCs. We showed recently that thrombin generation at the surface of VSMC from spontaneously hypertensive rats (SHR) leads to increased ETP and VSMCs were responsible for a prothrombotic phenotype in SHR rats. In the same way as for SHR rats, increased VSMC-supported thrombin generation can be a mechanism implicated in the prothrombotic phenotype we have observed in Zucker rats. In these cellular experiments addition of palmitic acid exacerbated also thrombin generation over MSZR VSMCs.

MMPs are related to FFAs, obesity-related diseases such as type 2 diabetes and overall, inflammation. In our model, mean gelatinase activity, focusing on MMP-2 and-9 activities, was increased in MSZR. These molecules are responsible for the degradation of type IV collagen, elastin, fibronectin, and laminin, among other proteins. It is known that FFAs and insulin lead to hyperactivity of MMP-2 and-9 (Boden et al., 2008). The close relation between MMPs and insulin was demonstrated also in Zucker rats (Zhou et al., 2005). IL-13 was increased in old rats and is known to be an activator of MMPs (Firszt et al., 2014). This increase in aortic MMP activity in the intima with aging has been described in rats and was 2-fold higher in old vs. young non-human primates (Li et al., 1999; Wang et al., 2007). In addition, MMP activity may participate also in age-related vascular remodeling in the aortic media since MMPs accumulate around elastic fibers in the aortic media (Li et al., 1999), which become fragmented with age-associated increases in arterial stiffness which thus increases cardiovascular risk. Interestingly, MMP production can be stimulated through integrin $\alpha_v\beta_3$ (Bendeck et al., 2000). Concerning this pathway, we found an increase of the α_v subunit in MSZR VSMCs and MMP-2 secretion was increased in MSZR compared to LZR. Moreover, we have shown previously that this integrin is responsible for thrombin generation supported by VSMCs and it argues for its role in vascular remodeling (Mao et al., 2012). Very interestingly all VSMC differentiation markers we tested were downregulated in MSZR and even absent concerning SM-MHC. This illustrates a phenotype switch from contractile to secreting VSMCs occurring in vascular diseases such as atherosclerosis (Lacolley et al., 2012).

In conclusion, our study demonstrates in MetS a prothrombotic phenotype of the blood compartment reinforced by procoagulant properties of the vascular wall. Regarding the mechanisms, fibrinogen contributes to this hypercoagulable phenotype in plasma at an early stage of MetS. Leptin and adiponectin exert moderate opposite effects on thrombin generation precluding a major contribution of adipokines. An increase in proinflammatory cytokines likely increased MMP activity inducing a VSMC dedifferentiated phenotype exhibiting procoagulant properties. An increase in FFAs contributes to the increased thrombin generation both in plasma and at the surface of VSMCs. Plasma from MSZR and palmitic acid elicit additive procoagulant effects. The potential benefit of direct thrombin inhibitors should be investigated both on haemostatic balance in blood compartments and on the cellular phenotypic modulation within the vessel wall, and MMP production in MetS and its complications with aging.

AUTHOR CONTRIBUTIONS

JL: performed experiments, analyzed data and wrote the manuscript; AM, MD, and HL: performed experiments and analyzed data; LW, SB, and RA: contributed to the collection, analysis and interpretation of data and writing of the manuscript; BdL, BD, MS, ST, BF, PC, and JKC: contributed to critical writing and revising the intellectual content and final approval of the version of manuscript; PL and VR: designed research and supervised the work, analyzed the data, wrote and reviewed the manuscript.

FUNDING

This work was supported by grants from Institut National de la Santé et de la Recherche Médical, Université de Lorraine, FEDER, and Agence Nationale de la Recherche (ANR-09-GENO-010-GRAF, ANR-13-BSV1-0026, ANR-15-RHU-0004). Jeremy Lagrange was supported by the Région Lorraine and the Communauté Urbaine du Grand Nancy. Lucy Walton was supported by a BBSRC Ph.D. studentship.

ACKNOWLEDGMENTS

We are extremely grateful to Anne-Laure Leblanc for technical assistance, Cecile Lakomy for her help in thrombin generation experiments, Walid Chayouâ and Gideon van der Stelt for their help in the analysis of the SEM pictures, Dr. Xuegen Zhao for his expert assistance with the SAM work and Dr. Abigail Langton for her advice regarding *in situ* gelatin zymography.

REFERENCES

Ait Aissa, K., Lagrange, J., Mohamadi, A., Louis, H., Houppert, B., Challande, P., et al. (2015). Vascular smooth muscle cells are responsible for a prothrombotic phenotype of spontaneously hypertensive rat arteries. *Arterioscler. Thromb. Vasc. Biol.* 35, 930–937. doi: 10.1161/ATVBAHA.115.305377

Alessi, M.-C., and Juhan-Vague, I. (2008). Metabolic syndrome, haemostasis, and thrombosis. *Thromb. Haemost.* 99, 995–1000. doi: 10.1160/TH07-11-0682

Begbie, M., Notley, C., Tinlin, S., Sawyer, L., and Lillicrap, D. (2000). The Factor VIII acute phase response requires the participation of NFκB and C/EBP. *Thromb. Haemost.* 84, 216–222.

Beijers, H. J., Ferreira, I., Spronk, H. M., Bravenboer, B., Dekker, J. M., Nijpels, G., et al. (2010). Body composition as determinant of thrombin generation in plasma: the Hoorn study. *Arterioscler. Thromb. Vasc. Biol.* 30, 2639–2647. doi: 10.1161/ATVBAHA.110.211946

Bendeck, M. P., Irvin, C., Reidy, M., Smith, L., Mulholland, D., Horton, M., et al. (2000). Smooth muscle cell matrix metalloproteinase production is stimulated via $\alpha_v\beta_3$ integrin. *Arterioscler. Thromb. Vasc. Biol.* 20, 1467–1472. doi: 10.1161/01.ATV.20.6.1467

Boden, G., Song, W., Pashko, L., and Kresge, K. (2008). *In vivo* effects of insulin and free fatty acids on matrix metalloproteinases in rat aorta. *Diabetes* 57, 476–483. doi: 10.2337/db07-1261

Bourin, M. C. (1987). [Effect of rabbit thrombomodulin on the inhibition of thrombin by the antithrombin-heparin complex: role of the acid domain of thrombomodulin]. *Comptes Rendus Académie Sci. Sér. III Sci. Vie* 304, 173–176.

Cesari, M., Pahor, M., and Incalzi, R. A. (2010). Plasminogen activator inhibitor-1 (PAI-1): a key factor linking fibrinolysis and age-related subclinical and clinical conditions. *Cardiovasc. Ther.* 28, e72–e91. doi: 10.1111/j.1755-5922.2010.00171.x

Chen, Y.-J., Zhang, L.-Q., Wang, G.-P., Zeng, H., Lü, B., Shen, X.-L., et al. (2008). Adiponectin inhibits tissue factor expression and enhances tissue factor pathway inhibitor expression in human endothelial cells. *Thromb. Haemost.* 100, 291–300. doi: 10.1160/TH08-02-0124

Dandona, P., Aljada, A., Chaudhuri, A., Mohanty, P., and Garg, R. (2005). Metabolic syndrome: a comprehensive perspective based on interactions between obesity, diabetes, and inflammation. *Circulation* 111, 1448–1454. doi: 10.1161/01.CIR.0000158483.13093.9D

Dinarello, C. A. (2011). Interleukin-1 in the pathogenesis and treatment of inflammatory diseases. *Blood* 117, 3720–3732. doi: 10.1182/blood-2010-07-273417

Firszt, R., Francisco, D., Church, T. D., Thomas, J. M., Ingram, J. L., and Kraft, M. (2014). Interleukin-13 induces collagen type-1 expression through matrix metalloproteinase-2 and transforming growth factor-β1 in airway fibroblasts in asthma. *Eur. Respir. J.* 43, 464–473. doi: 10.1183/09031936.00068712

Gabriel, D. A., Muga, K., and Boothroyd, E. M. (1992). The effect of fibrin structure on fibrinolysis. *J. Biol. Chem.* 267, 24259–24263.

Godin, J.-P., Ross, A. B., Cléroux, M., Pouteau, E., Montoliu, I., Moser, M., et al. (2013). Natural carbon isotope abundance of plasma metabolites and liver tissue differs between diabetic and non-diabetic Zucker diabetic fatty rats. *PLoS ONE* 8:e74866. doi: 10.1371/journal.pone.0074866

Halcox, J. P. J., Donald, A. E., Ellins, E., Witte, D. R., Shipley, M. J., Brunner, E. J., et al. (2009). Endothelial function predicts progression of carotid intima-media thickness. *Circulation* 119, 1005–1012. doi: 10.1161/CIRCULATIONAHA.108.765701

Hotary, K. B., Yana, I., Sabeh, F., Li, X.-Y., Holmbeck, K., Birkedal-Hansen, H., et al. (2002). Matrix metalloproteinases (MMPs) regulate fibrin-invasive activity via MT1-MMP-dependent and -independent processes. *J. Exp. Med.* 195, 295–308. doi: 10.1084/jem.20010815

Konings, J., Govers-Riemslag, J. W. P., Philippou, H., Mutch, N. J., Borissoff, J. I., Allan, P., et al. (2011). Factor XIIa regulates the structure of the fibrin clot independently of thrombin generation through direct interaction with fibrin. *Blood* 118, 3942–3951. doi: 10.1182/blood-2011-03-339572

Konstantinides, S., Schäfer, K., Koschnick, S., and Loskutoff, D. J. (2001). Leptin-dependent platelet aggregation and arterial thrombosis suggests a mechanism for atherothrombotic disease in obesity. *J. Clin. Invest.* 108, 1533–1540. doi: 10.1172/JCI13143

Kotronen, A., Joutsi-Korhonen, L., Sevastianova, K., Bergholm, R., Hakkarainen, A., Pietiläinen, K. H., et al. (2011). Increased coagulation factor VIII, IX, XI and XII activities in non-alcoholic fatty liver disease. *Liver Int.* 31, 176–183. doi: 10.1111/j.1478-3231.2010.02375.x

Kumar, R., Béguin, S., and Hemker, H. C. (1994). The influence of fibrinogen and fibrin on thrombin generation–evidence for feedback activation of the clotting system by clot bound thrombin. *Thromb. Haemost.* 72, 713–721.

Lacolley, P., Regnault, V., Nicoletti, A., Li, Z., and Michel, J.-B. (2012). The vascular smooth muscle cell in arterial pathology: a cell that can take on multiple roles. *Cardiovasc. Res.* 95, 194–204. doi: 10.1093/cvr/cvs135

Lee, S., Park, Y., Dellsperger, K. C., and Zhang, C. (2011). Exercise training improves endothelial function via adiponectin-dependent and independent pathways in type 2 diabetic mice. *Am. J. Physiol. Heart Circ. Physiol.* 301, H306–H314. doi: 10.1152/ajpheart.01306.2010

Li, Z., Froehlich, J., Galis, Z. S., and Lakatta, E. G. (1999). Increased expression of matrix metalloproteinase-2 in the thickened intima of aged rats. *Hypertension* 33, 116–123. doi: 10.1161/01.HYP.33.1.116

Libby, P., Ordovas, J. M., Auger, K. R., Robbins, A. H., Birinyi, L. K., and Dinarello, C. A. (1986). Endotoxin and tumor necrosis factor induce interleukin-1 gene expression in adult human vascular endothelial cells. *Am. J. Pathol.* 124, 179–185.

Lim, H. S., Lip, G. Y. H., and Blann, A. D. (2004). Plasma von Willebrand factor and the development of the metabolic syndrome in patients with hypertension. *J. Clin. Endocrinol. Metab.* 89, 5377–5381. doi: 10.1210/jc.2004-0616

Lominadze, D., Dean, W. L., Tyagi, S. C., and Roberts, A. M. (2010). Mechanisms of fibrinogen-induced microvascular dysfunction during cardiovascular disease. *Acta Physiol. Oxf. Engl.* 198, 1–13. doi: 10.1111/j.1748-1716.2009.02037.x

Lu, P., Liu, J., Liu, N., Guo, F., Ji, Y., and Pang, X. (2011). Pro-inflammatory effect of fibrinogen and FDP on vascular smooth muscle cells by IL-6, TNF-α and iNOS. *Life Sci.* 88, 839–845. doi: 10.1016/j.lfs.2011.03.003

Mao, X., Said, R., Louis, H., Max, J.-P., Bourhim, M., Challande, P., et al. (2012). Cyclic stretch-induced thrombin generation by rat vascular smooth muscle cells is mediated by the integrin $\alpha_v\beta_3$ pathway. *Cardiovasc. Res.* 96, 513–523. doi: 10.1093/cvr/cvs274

Matsuzawa, Y., Funahashi, T., Kihara, S., and Shimomura, I. (2004). Adiponectin and metabolic syndrome. *Arterioscler. Thromb. Vasc. Biol.* 24, 29–33. doi: 10.1161/01.ATV.0000099786.99623.EF

Membre, A., Wahl, D., Latger-Cannard, V., Max, J.-P., Lacolley, P., Lecompte, T., et al. (2008). The effect of platelet activation on the hypercoagulability induced by murine monoclonal antiphospholipid antibodies. *Haematologica* 93, 566–573. doi: 10.3324/haematol.12364

Mook, O. R. F., Van Overbeek, C., Ackema, E. G., Van Maldegem, F., and Frederiks, W. M. (2003). *In situ* localization of gelatinolytic activity in the extracellular matrix of metastases of colon cancer in rat liver using quenched fluorogenic DQ-gelatin. *J. Histochem. Cytochem.* 51, 821–829. doi: 10.1177/002215540305100613

Morozumi, T., Sharma, A., and De Nardin, E. (2009). The functional effects of the−455G/A polymorphism on the IL-6-induced expression of the beta-fibrinogen gene may be due to linkage disequilibrium with other functional polymorphisms. *Immunol. Invest.* 38, 311–323. doi: 10.1080/08820130902745153

Ninivaggi, M., Apitz-Castro, R., Dargaud, Y., de Laat, B., Hemker, H. C., and Lindhout, T. (2012). Whole-blood thrombin generation monitored with a calibrated automated thrombogram-based assay. *Clin. Chem.* 58, 1252–1259. doi: 10.1373/clinchem.2012.184077

Pacheco, Y. M., Bermúdez, B., López, S., Abia, R., Villar, J., and Muriana, F. J. G. (2006). Ratio of oleic to palmitic acid is a dietary determinant of thrombogenic and fibrinolytic factors during the postprandial state in men. *Am. J. Clin. Nutr.* 84, 342–349.

Pandolfi, A., Cetrullo, D., Polishuck, R., Alberta, M. M., Calafiore, A., Pellegrini, G., et al. (2001). Plasminogen activator inhibitor type 1 is increased in the arterial wall of type II diabetic subjects. *Arterioscler. Thromb. Vasc. Biol.* 21, 1378–1382. doi: 10.1161/hq0801.093667

Paul, W., Queen, L. R., Page, C. P., and Ferro, A. (2007). Increased platelet aggregation *in vivo* in the Zucker Diabetic Fatty rat: differences from the streptozotocin diabetic rat. *Br. J. Pharmacol.* 150, 105–111. doi: 10.1038/sj.bjp.0706957

Petrini, S., Neri, T., Lombardi, S., Cordazzo, C., Balìa, C., Scalise, V., et al. (2016). Leptin induces the generation of procoagulant, tissue factor bearing microparticles by human peripheral blood mononuclear cells. *Biochim. Biophys. Acta* 1860, 1354–1361. doi: 10.1016/j.bbagen.2016.03.029

Phillips, M. S., Liu, Q., Hammond, H. A., Dugan, V., Hey, P. J., Caskey, C. J., et al. (1996). Leptin receptor missense mutation in the fatty Zucker rat. *Nat. Genet.* 13, 18–19. doi: 10.1038/ng0596-18

Regnault, V., Hemker, H. C., Wahl, D., and Lecompte, T. (2004). Phenotyping the haemostatic system by thrombography–potential for the estimation of thrombotic risk. *Thromb. Res.* 114, 539–545. doi: 10.1016/j.thromres.2004.06.017

Restituto, P., Colina, I., Varo, J. J., and Varo, N. (2010). Adiponectin diminishes platelet aggregation and sCD40L release. Potential role in the metabolic syndrome. *Am. J. Physiol. Endocrinol. Metab.* 298, E1072–E1077. doi: 10.1152/ajpendo.00728.2009

Ridker, P. M., Everett, B. M., Thuren, T., MacFadyen, J. G., Chang, W. H., Ballantyne, C., et al. (2017). Antiinflammatory therapy with canakinumab for atherosclerotic disease. *N. Engl. J. Med.* 377, 1119–1131. doi: 10.1056/NEJMoa1707914

Samad, F., Pandey, M., and Loskutoff, D. J. (2001). Regulation of tissue factor gene expression in obesity. *Blood* 98, 3353–3358. doi: 10.1182/blood.V98.12.3353

Semeraro, F., Ammollo, C. T., Morrissey, J. H., Dale, G. L., Friese, P., Esmon, N. L., et al. (2011). Extracellular histones promote thrombin generation through platelet-dependent mechanisms: involvement of platelet TLR2 and TLR4. *Blood* 118, 1952–1961. doi: 10.1182/blood-2011-03-343061

Shang, J., Chen, Z., Wang, M., Li, Q., Feng, W., Wu, Y., et al. (2014). Zucker diabetic fatty rats exhibit hypercoagulability and accelerated thrombus formation in the Arterio-Venous shunt model of thrombosis. *Thromb. Res.* 134, 433–439. doi: 10.1016/j.thromres.2014.04.008

Shrestha, C., Ito, T., Kawahara, K., Shrestha, B., Yamakuchi, M., Hashiguchi, T., et al. (2013). Saturated fatty acid palmitate induces extracellular release of histone H3: a possible mechanistic basis for high-fat diet-induced inflammation and thrombosis. *Biochem. Biophys. Res. Commun.* 437, 573–578. doi: 10.1016/j.bbrc.2013.06.117

Simon, J. A., Hodgkins, M. L., Browner, W. S., Neuhaus, J. M., Bernert, J. T., and Hulley, S. B. (1995). Serum fatty acids and the risk of coronary heart disease. *Am. J. Epidemiol.* 142, 469–476. doi: 10.1093/oxfordjournals.aje.a117662

Sloboda, N., Fève, B., Thornton, S. N., Nzietchueng, R., Regnault, V., Simon, G., et al. (2012). Fatty acids impair endothelium-dependent vasorelaxation: a link between obesity and arterial stiffness in very old Zucker rats. *J. Gerontol. A Biol. Sci. Med. Sci.* 67, 927–938. doi: 10.1093/gerona/glr236

Sonnenberg, G. E., Krakower, G. R., and Kissebah, A. H. (2004). A novel pathway to the manifestations of metabolic syndrome. *Obes. Res.* 12, 180–186. doi: 10.1038/oby.2004.24

Suehiro, A., Wakabayashi, I., Uchida, K., Yamashita, T., and Yamamoto, J. (2012). Impaired spontaneous thrombolytic activity measured by global thrombosis test in males with metabolic syndrome. *Thromb. Res.* 129, 499–501. doi: 10.1016/j.thromres.2011.06.019

Wagenvoord, R. J., Hendrix, H. H., Kai, H., and Hemker, H. C. (1994). A chromogenic test to determine the procoagulant phospholipids in platelet-rich plasma and whole blood. Thromb. *Haemost.* 72, 582–587.

Wakil, S. J., and Abu-Elheiga, L. A. (2009). Fatty acid metabolism: target for metabolic syndrome. *J. Lipid Res.* 50, S138–S143. doi: 10.1194/jlr.R800079-JLR200

Wang, M. Y., Zhou, Y. T., Newgard, C. B., and Unger, R. H. (1996). A novel leptin receptor isoform in rat. *FEBS Lett.* 392, 87–90. doi: 10.1016/0014-5793(96)00790-9

Wang, M., Zhang, J., Jiang, L.-Q., Spinetti, G., Pintus, G., Monticone, R., et al. (2007). Proinflammatory profile within the grossly normal aged human aortic wall. *Hypertension* 50, 219–227. doi: 10.1161/HYPERTENSIONAHA.107.089409

Wanninger, J., Walter, R., Bauer, S., Eisinger, K., Schäffler, A., Dorn, C., et al. (2011). MMP-9 activity is increased by adiponectin in primary human hepatocytes but even negatively correlates with serum adiponectin in a rodent model of non-alcoholic steatohepatitis. *Exp. Mol. Pathol.* 91, 603–607. doi: 10.1016/j.yexmp.2011.07.001

Weiss, T. W., Arnesen, H., and Seljeflot, I. (2013). Components of the interleukin-6 transsignalling system are associated with the metabolic syndrome, endothelial dysfunction and arterial stiffness. *Metab. Clin. Exp.* 62, 1008–1013. doi: 10.1016/j.metabol.2013.01.019

Wolberg, A. S. (2007). Thrombin generation and fibrin clot structure. *Blood Rev.* 21, 131–142. doi: 10.1016/j.blre.2006.11.001

Zhou, Y.-P., Madjidi, A., Wilson, M. E., Nothhelfer, D. A., Johnson, J. H., Palma, J. F., et al. (2005). Matrix metalloproteinases contribute to insulin insufficiency in Zucker diabetic fatty rats. *Diabetes* 54, 2612–2619. doi: 10.2337/diabetes.54.9.2612

Conflict of Interest Statement: The authors declare that the research was conducted in the absence of any commercial or financial relationships that could be construed as a potential conflict of interest.

Journal of
Clinical Medicine

MDPI

Article

Rivaroxaban Effects Illustrate the Underestimated Importance of Activated Platelets in Thrombin Generation Assessed by Calibrated Automated Thrombography

Stephanie Makhoul [1], Marina Panova-Noeva [1,2], Véronique Regnault [3,4], Wolfram Ruf [1,2,5], Philip Wenzel [1,2,6] and Jeremy Lagrange [1,3,*]

1 Center for Thrombosis and Hemostasis, University Medical Center Mainz, 55131 Mainz, Germany; stephaniemakhoul@live.com (S.M.); Marina.Panova-Noeva@unimedizin-mainz.de (M.P.-N.); ruf@uni-mainz.de (W.R.); wenzelp@uni-mainz.de (P.W.)
2 DZHK (German Center for Cadiovascular Research), Partner Site Rhine Main, University Medical Center Mainz, 55131 Mainz, Germany
3 Université de Lorraine, INSERM U1116, DCAC, 54505 Nancy, France; veronique.regnault@inserm.fr
4 CHRU Nancy, Vandœuvre-lès-Nancy, 54511 Nancy, France
5 Department of Immunology and Microbial Science, The Scripps Research institute, La Jolla, CA 92037, USA
6 Center for Cardiology—Cardiology I, University Medical Center Mainz, 55131 Mainz, Germany
* Correspondence: jeremy.lagrange@inserm.fr

Received: 19 September 2019; Accepted: 12 November 2019; Published: 15 November 2019

Abstract: Background: The direct oral anticoagulant rivaroxaban inhibiting specifically activated factor X (FXa) causes delayed thrombin generation (TG) as measured by calibrated automated thrombography (CAT). The implications of these changes for assessing bleeding or residual prothrombotic risks of patients are unclear in the absence of a better understanding of the underlying mechanism. Methods: We compared platelet rich plasma (PRP) without or with prior collagen-induced platelet aggregation (agPRP) in the CAT assay to better characterize TG in the presence of rivaroxaban. Results: In the presence of rivaroxaban, TG curves in agPRP showed a distinct profile with a rapidly ascending phase followed with a protracted phase. Inhibition of tissue factor pathway inhibitor amplified the first phase of the curve which was also modulated by procoagulant phospholipids. Inhibition of FXIIa-dependent FXI activation revealed that aggregated platelets influenced the first phase by a combination of extrinsic and intrinsic coagulation pathway initiations. Thrombin-dependent amplification of TG (even prior collagen activation) was responsible for the second phase of the TG curve. Conclusions: AgPRP fully includes platelet ability to support TG and reveal distinct TG phases in the presence of direct FXa inhibitors highlighting its potential use in an anticoagulated setting.

Keywords: thrombin; platelets; factor Xa inhibitor; phospholipids

1. Introduction

Direct oral anticoagulants (DOACs) are increasingly used as first line treatment for venous thromboembolism (VTE) and for prevention of ischemic stroke in atrial fibrillation, but regular assessment of their anticoagulant effects remains challenging. The coagulation system leads to the formation of thrombin and fibrin and its polymerization that will form a clot. Most of the thrombin generation (TG) occurs after the clot formation and total TG potential of a plasma can be assessed with calibrated automated thrombography (CAT), which gives a better overview of the coagulation

system than clotting times (prothrombin time or activated partial thromboplastin time) [1–4]. The CAT assay uses a fluorogenic substrate to measure prothrombin conversion to thrombin in a recalcified plasma in the presence of phospholipids (PL). In patients with acute VTE, the use of TG assays becomes challenging once an antithrombotic treatment, including DOACs, has been initiated. It is well established that anticoagulants impair dramatically thrombin generation, making it difficult to monitor the bleeding or residual prothrombotic risk.

The COMPASS study (Cardiovascular Outcomes for Peoples Using Anticoagulant Strategies) included patients with stable atherosclerotic disease treated with rivaroxaban plus aspirin compared to rivaroxaban or aspirin alone and showed a lower risk of cardiovascular death, stroke, myocardial infarction, fatal bleeding, or symptomatic bleeding into a critical organ with dual therapy [5]. However, major bleeding events occurred in 3.1% (rivaroxaban plus aspirin patients) vs. 1.9% (patients under aspirin) pointing out that even if the combination of anticoagulation with antiplatelet therapy on the overall cardiovascular risk is beneficial, stratification needs to be improved.

Current clinical guidelines recommend assessment of bleeding and thrombotic risks when making a decision to start anticoagulation, principally by using the clinical risk scores, such as ABC-bleeding [6], HAS-BLED [7], or CHA2DS2-VASc risk score [8]. In addition to clinical characteristics, biomarkers shown to improve bleeding and/or stroke risk estimates are also part of the clinical scores, such as NT-proBNP, high-sensitivity cardiac troponin T (hsTnT), growth differentiation factor-15 (GDF-15), hemoglobin level and platelet count [6,9]. However, risk scores may present limitations depending on cohort recruitment and follow-up and parameters selected [10]. In addition, to date no hemostatic functional assays are routinely used to estimate patients' bleeding risk. The evaluation of bleeding risk in patients receiving both anticoagulant and antiplatelet agents, e.g., rivaroxaban and aspirin, poses a greater challenge. The reason is that the hemostasis inhibition includes both inhibition of platelets and of coagulation, and most laboratory tests evaluate these processes separately.

The presence of rivaroxaban in plasma can change the appearance of the TG curve with the formation of camel-back shaped instead of normal curves [11]. Endogenous thrombin potential (ETP), representing the total amount of thrombin formed, and the peak height of TG, representing the maximum thrombin formed, are the most widely used parameters to evaluate the thrombin potential of a plasma. However, the presence of DOACs seems to affect more the parameters related to the kinetics of TG such as the lag time, the velocity and the time to peak, often not reported in the literature [12]. Not only the amount (ETP) but also the kinetic of thrombin formation and its inhibition are important for hemostasis. After a systemic review using the words (thrombin generation) and (rivaroxaban) in PubMed, from the 54 publications released over the past 10 years in which the CAT assay was performed only 26 presented curves of TG and no more than 17 of these publications showed camel-back shaped curves. These curves were also described with other Xa inhibitors as apixaban [13]; however, to date this effect has not been clarified. To the best of our knowledge, no specific studies reported on the impact of rivaroxaban on the shape of TG curves.

In the present work, we aimed to explore the origin and determinants of camel-back shaped TG curves in the presence of new oral anticoagulants, in particular rivaroxaban. We took advantage of the use of aggregated platelet rich plasma (PRP/agPRP) in the CAT [14] which fully includes platelet procoagulant activity since modified TG kinetics in particular faster TG could compensate the slow TG often observed after rivaroxaban treatment.

2. Experimental Section

2.1. Blood Sampling and PRP Preparation

Studies using human platelets were approved by the ethics committee of the University Mainz (study no. 837.302.12; 25.07.12). Blood from 16 healthy volunteers (8 women, 8 men, mean age 30 ± 2.6 years) was obtained after informed consent by venipuncture via a 21-gauge needle and collected in S-monovette tubes containing sodium citrate (3.2%) (Sarstedt, Nümbrecht,

Germany). Complete blood counts and hematocrit were determined with a cell counter (KX-21N, Sysmex Corporation, Kobe, Japan). PRP was prepared within 1 h following blood sampling with a centrifugation at 200× *g* for 10 min at 20 °C. The supernatant was removed and the platelet count was adjusted to 200 × 109/L with platelet poor plasma (PPP) prepared with a 10 min centrifugation at 2000× *g* at 20 °C. Platelet free plasma (PFP) was prepared by centrifuging PPP at 13,000× *g* for 30 min at 4 °C. The collected PFP was stored at −80 °C until use.

2.2. Platelet Aggregation

Platelet aggregation was monitored for 10 min by measuring light transmission through stirred PRP at 37 °C using a platelet aggregometer (APACT 4S plus aggregometer, Diasys Greiner, Holzheim, Germany). Platelet aggregation was triggered by 2 µg/mL equine collagen fibrils type I (Chrono-log Corp, Havertown, PA, USA). Aggregated PRP was used directly after aggregation for CAT measurement [14].

2.3. Thrombin Generation Assay

CAT was performed with PRP and agPRP or PFP (Figure S1). CAT in PRP and PFP was performed in a microtiter plate fluorometer (Fluoroskan Ascent, ThermoLabsystems, Helsinki, Finland) using dedicated software (Thrombinoscope BV, Maastricht, The Netherlands) as reported previously [15,16]. All reagents were used as follows: 80 µL PRP, homogenous agPRP or PFP, 20 µL of PRP-Reagent or PPP-Reagent low (Thrombinoscope BV, Maastricht, The Netherlands), and 20 µL of a mix of fluorogenic substrate and calcium (FluCa-Kit reagent). In specific experiments with PRP or agPRP TG was triggered with 0.1 U/mL human thrombin (Roche Diagnostics, Mannheim, Germany) instead of PRP-Reagent. Rivaroxaban, PAR 1 (vorapaxar) and PAR 4 (BMS 986120) inhibitors were purchased from Cayman Chemical (Ann Arbor, MI, USA) and reconstituted in DMSO. Vorapaxar was used at a final concentration of 100 ng/mL following a 10,000-times dilution in HEPES buffer (HEPES 20 mM, NaCl 140 mM, pH 7.35) before an additional 67 times dilution in plasma. BMS 986120 was used at a final concentration of 1 µg/mL following a 1000 times dilution in HEPES buffer before an additional 67 times dilution in plasma. Anti-TFPI antibody was purchased from Loxo (Dossenheim, Germany) and used at a final concentration of 5 µg/mL. An IgG isotype control was purchased from Sigma-Aldrich, St Louis, MO, USA) and used at a final concentration of 5 µg/mL (Figure S2). The 14E11 monoclonal antibody which is directed against the A2 domain of FXI in order to block its activation by FXIIa was provided by A. Gruber and use at a final concentration of 5 µg/mL. The phospholipid vesicles (PV) consisted of phosphatidyl-choline -serine -ethanolamine (PC/PS/PE; Sigma-Aldrich, St Louis, MO, USA) 60/20/20 mol % at final concentrations of respectively 1 µM, 4 µM, and 48 µM equivalent PS were prepared in HEPES buffer sonicated (amplitude 8%) 5 times 5 min on ice bath.

2.4. Statistical Analysis

Normal distribution of the data was tested by D'Agnostino and Pearson test. Data were analyzed with Kruskal–Wallis or Mann–Whitney test. Results are presented as median (min–max).

3. Results

3.1. Addition of Rivaroxaban to agPRP Change the Shape of the TG Curve

TG was performed in PRP and collagen-induced agPRP from healthy volunteers in the absence or presence of rivaroxaban and initiated with 1 pM of tissue factor (TF) (Figure 1A). Addition of rivaroxaban to PRP leads to two-fold increased lag time (8.4 (5.9–13) versus 16 (8.9–26) min) and time to peak (tt peak) (18 (14–25) versus (35 (28–51) min) and decreased peak and velocity of TG (Table 1, Figure 1C,E). ETP is also significantly decreased (Table 1). The use of agPRP spiked with rivaroxaban showed similar modifications (Table 1, Figure 1D,F). Concerning the curve shapes, PRP and agPRP presented normal shaped TG curves (Figure 1A). After addition of rivaroxaban to PRP, small curve

alterations were discernible in a few subjects while clear transformation of the TG curve into a camelback shape was visible when using agPRP.

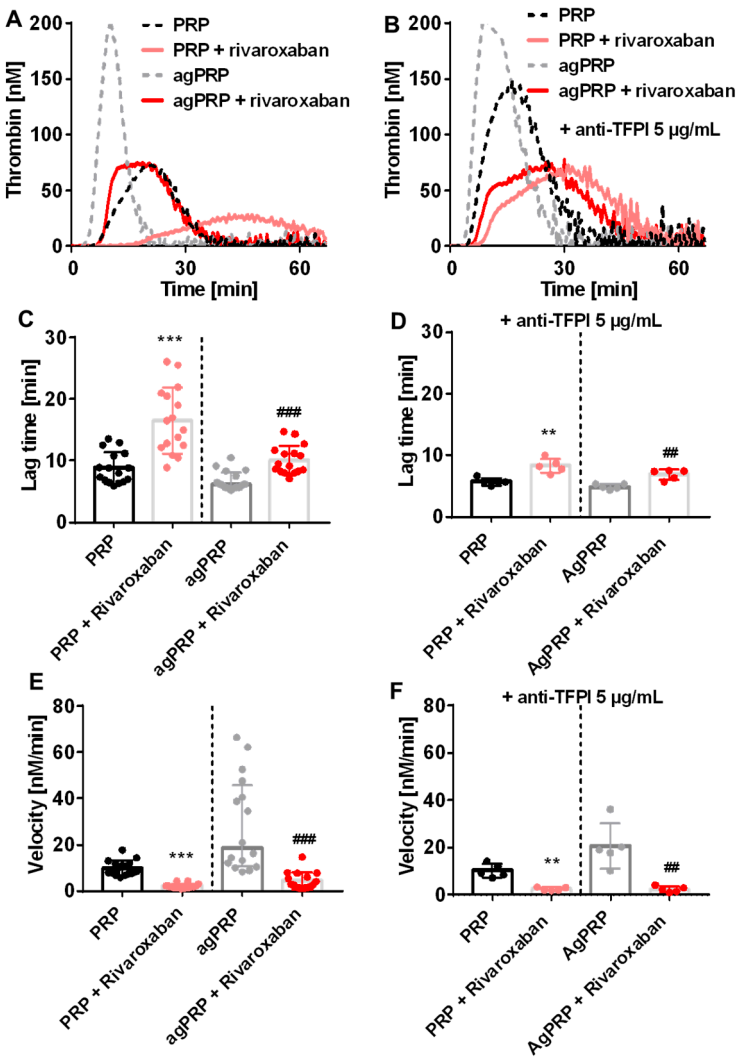

Figure 1. Effect of platelet aggregation with addition of rivaroxaban and anti-tissue factor pathway inhibitor (TFPI) on human platelet rich plasma (PRP) in thrombin generation (TG). Representative TG curves in PRP or PRP after aggregation (agPRP) triggered with 2 µg/mL of collagen with and without addition or 50 ng/mL of rivaroxaban (**A**) and inhibition of TFPI (anti-TFPI 5 µg/mL) (**B**). Lag time of thrombin generation for the different conditions (**C**,**D**). Velocity of thrombin generation under the different conditions (**E**,**F**). Results are presented as median (min-max). ** $p < 0.01$, *** $p < 0.001$, vs. PRP; ## $p < 0.01$, ### $p < 0.001$, vs. agPRP, $n = 16$ per group for left panels and $n = 5$ for right panels.

Table 1. PRP thrombin generation parameters.

	ETP (nM.min)			
	PRP	**PRP + Rivaroxaban**	**agPRP**	**agPRP + Rivaroxaban**
TF	1489 (1231–2185)	1299 (819–1759) **	1680 (1437–2692)	1330 (1016–1915) ###
TF + anti-TFPI	1473 (1231–2185)	1375 (1175–1759)	1579 (1510–2692)	1324 (1016–1915)
TF + Vorapaxar	1348 (1196–1483)	1148 (546–1443)	1911 (1514–2130)	1461 (1220–1621) #
TF + BMS 986120	1332 (1190–1463)	977 (667–1423)	1737 (1481–2078)	1259 (1084–1753)
TF + Vorapaxar + BMS 986120	1414 (1231–1538)	1143 (779–1445)	1864 (1556–2095)	1363 (873–1519) ##
TF + 14E11	1124 (821–1370)	692 (570–1482)	1621 (1375–1727)	917 (719–1304)
Thrombin	1220 (873–1380)	794 (300–1002) *	834 (615–1086)	758 (610–1003)
	Peak (nM)			
	PRP	**PRP + Rivaroxaban**	**agPRP**	**agPRP + Rivaroxaban**
TF	91 (64–152)	35 (22–72) ***	137 (82–270)	48 (26–87) ###
TF + anti-TFPI	85 (64–115)	36 (34–49) **	105 (91–219)	36 (28–66) ##
TF + Vorapaxar	79 (64–106)	38 (24–46) *	182 (140–328)	52 (33–101) ##
TF + BMS 986120	75 (66–98)	28 (26–49) *	168 (110–227)	47 (34–129) #
TF + Vorapaxar + BMS 986120	88 (57–99)	35 (29–58)	199 (171–245)	37 (30–61) ##
TF + 14E11	49 (45–73)	16 (12–29) *	120 (104–183)	29 (15–42)
Thrombin	70 (43–92)	21 (15–38) *	33 (28–56)	13 (11–24) ##
	tt peak (min)			
	PRP	**PRP + Rivaroxaban**	**agPRP**	**agPRP + Rivaroxaban**
TF	18 (14–25)	35 (18–51) ***	14 (9.7–19)	26 (15–40) ###
TF + anti-TFPI	17 (16–18)	35 (30–37)	14 (12–16)	29 (22–31)
TF + Vorapaxar	21 (19–22)	39 (32–72) *	14 (9.0–15)	20 (14–34) #
TF + BMS 986120	22 (1–23)	39 (30–72) *	13 (12–17)	26 (15–33)
TF + Vorapaxar + BMS 986120	21 (19–24)	38 (29–72) *	12 (11–13)	25 (20–32) ##
TF + 14E11	26 (24–28)	49 (47–50) *	16 (15–16)	33 (28–36)
Thrombin	18 (14–21)	30 (26–58) *	15 (12–22)	35 (30–49) ##

Thrombin generation parameters of platelet rich plasma (PRP) and PRP after aggregation (agPRP) triggered with 1 pM of TF or thrombin (0.1 U/mL) with addition of rivaroxaban (50 ng/mL), anti-TFPI (5 µg/mL), vorapaxar (100 ng/mL), BMS 968120 (1 µg/mL), or 14E11 (5 µg/mL). Results are presented as median (min-max). $n = 3–16$, * $p < 0.05$ ** $p < 0.01$ *** $p < 0.001$, vs. PRP, # $p < 0.05$ ## $p < 0.01$ ### $p < 0.001$, vs. agPRP.

3.2. TFPI Modulates the First Phase of the Camelback TG Curves

TG curves in agPRP in the presence of rivaroxaban and initiated with 1 pM TF presented a camelback shape with two peaks. One possible explanation is the ability of TFPI to inhibit both TF-FVIIa and FXa. In order to limit these effects an antibody targeting TFPI was added prior the CAT assay (Figure 1B). In the presence of rivaroxaban, inhibition of TFPI affected lag time and velocity to the same extent as without rivaroxaban but camelback curves were still present (Figure 1D,F). Variation of ETP, peak and tt peak with or without rivaroxaban after collagen-induced agPRP were similar as the variations observed without TFPI inhibition (Table 1). Interestingly, TFPI inhibition exacerbated the first phase of the camelback phase in PRP plus rivaroxaban leading to curves similar to agPRP plus rivaroxaban.

3.3. Phospholipids Modulate the Camelback Shape of TG Curve in Presence of Rivaroxaban

AgPRP can influence TG by the release of coagulation factors such as FV and emission of procoagulant vesicles. It seems unlikely that platelet-derived coagulation factors are implicated since camelback curves are often present when using PFP. To test whether PL could modulate the appearance of camelback curves we used PFP in which we added different concentrations of PV and rising concentrations of rivaroxaban (Figure 2). The addition of PV to PFP mimicked the camelback curves of TG especially when using the usual PV concentration used for the CAT assay (4 µM). PV increased the peak height of the first TG phase of the camelback shaped curve in a concentration-dependent manner. Moreover, a shift in the peak was visible, changing the peak from long and vague at low PV concentration to high and marked at high PV concentration (Figure 2B,C). This effect was visible in the changes of the modifications of the tt peak (Table 2).

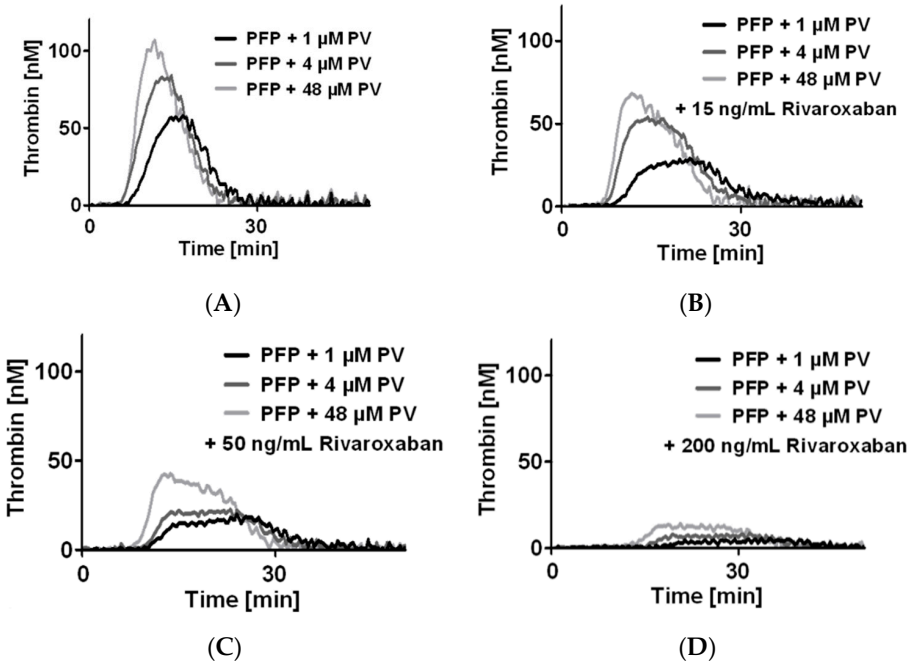

Figure 2. Modulation of camel-back shaped thrombin generation (TG) curve by the addition of phospholipids artificial vesicles. Representative curves of TG in platelet free plasma (PFP) supplemented with increasing concentrations of rivaroxaban: baseline (**A**), 15 ng/mL (**B**), 50 ng/mL (**C**), and 200 ng/mL (**D**). For each concentration, three concentrations of phospholipid vesicles (PV) were tested. PRP: Platelet rich plasma; agPRP with collagen 2 µg/mL, ETP, endogenous thrombin potential, tt peak, time to peak. Results presented as median (min-max). $n = 6$.

Table 2. PFP thrombin generation parameters.

	Lag Time (s)			
	PFP	**PFP + Rivaroxaban 15 ng/mL**	**PFP + Rivaroxaban 50 ng/mL**	**PFP + Rivaroxaban 200 ng/mL**
1 µM PV	8.6 (5.2–14)	10.5 (6.8–15)	12 (7.9–17)	19 (9.6–32) *
4 µM PV	7.1 (4.6–11)	8.9 (5.9–14)	11 (6.8–16)	16 (9.8–26) **
48 µM PV	7.9 (4.6–11)	8.6 (5.9–13)	11 (7.3–19)	15 (10–22) **
	ETP (nM.min)			
	PFP	**PFP + Rivaroxaban 15 ng/mL**	**PFP + Rivaroxaban 50 ng/mL**	**PFP + Rivaroxaban 200 ng/mL**
1 µM PV	572 (387–1837)	426 (322–1150)	300 (184–663)	104 (67–332) *
4 µM VS	687 (457–2035)	616 (409–1527)	320 (210–1021)	163 (111–363) **
48 µM PV	907 (737–1878)	745 (596–1779)	516 (282–1176)	245 (144–483) **
	Peak (nM)			
	PFP	**PFP + Rivaroxaban 15 ng/mL**	**PFP + Rivaroxaban 50 ng/mL**	**PFP + Rivaroxaban 200 ng/mL**
1 µM PV	43 (30–170)	27 (17–70)	12 (10–34) *	4.2 (3.1–16) *
4 µM PV	60 (39–280)	45 (21–121)	16 (11–65)	7 (5.6–19) **
48 µM PV	100 (76–336)	67 (40–201)	29 (18–94) *	12 (9.3–33) ***
	tt peak (s)			
	PFP	**PFP + Rivaroxaban 15 ng/mL**	**PFP + Rivaroxaban 50 ng/mL**	**PFP + Rivaroxaban 200 ng/mL**
1 µM PV	18 (11–21)	21 (17–25)	26 (21–29)	34 (23–48) ***
4 µM PV	14 (11–20)	17 (11–20)	22 (14–25)	29 (20–38) **
48 µM PV	13 (7.9–15)	12.9 (9.9–19)	18 (12–27)	25 (19–32) ***
	Velocity (nM/min)			
	PFP	**PFP + Rivaroxaban 15 ng/mL**	**PFP + Rivaroxaban 50 ng/mL**	**PFP + Rivaroxaban 200 ng/mL**
1 µM PV	5 (3.9–27)	2.3 (1.2–6.7)	1 (0.6–2.6) *	0.3 (0.2–1.1) ***
4 µM PV	8.4 (5–64)	6.3 (2.1–22)	2.3 (0.9–11)	0.6 (0.4–1.8) **
48 µM PV	23 (16–100)	16 (4.2–50)	4.9 (2.3–19)	1.3 (0.8–4.0) ***

Thrombin generation parameters of platelet free plasma (PFP) triggered with 1 pM of TF with addition of rivaroxaban and phospholipid vesicles (PV). Results are presented as median (min-max). $n = 6$, * $p < 0.05$, ** $p < 0.01$, *** $p < 0.001$, vs. PFP.

3.4. A Potential Platelet Secondary Activation Is Not Responsible for the Camelback TG Curves

Another possible explanation of the camelback curves is a secondary activation of platelets by the first amount of thrombin generated during the initiation of TG. In order to inhibit the thrombin effect on platelets we added PAR-1 (vorapaxar) and PAR-4 (BMS-986120) inhibitors or the combination of both prior the CAT assay (Figure 3). In PRP addition of PAR-1 and/or PAR-4 inhibitor prior to CAT tended to lower TG while no changes were visible after aggregation (Table 1). However, inhibition of PAR-1 and/or PAR-4 in the presence of rivaroxaban affected the kinetic parameters (lag time and velocity) to the same extent as without rivaroxaban (Figure 3D–I) and camelback curves were still present (Figure 3A–C).

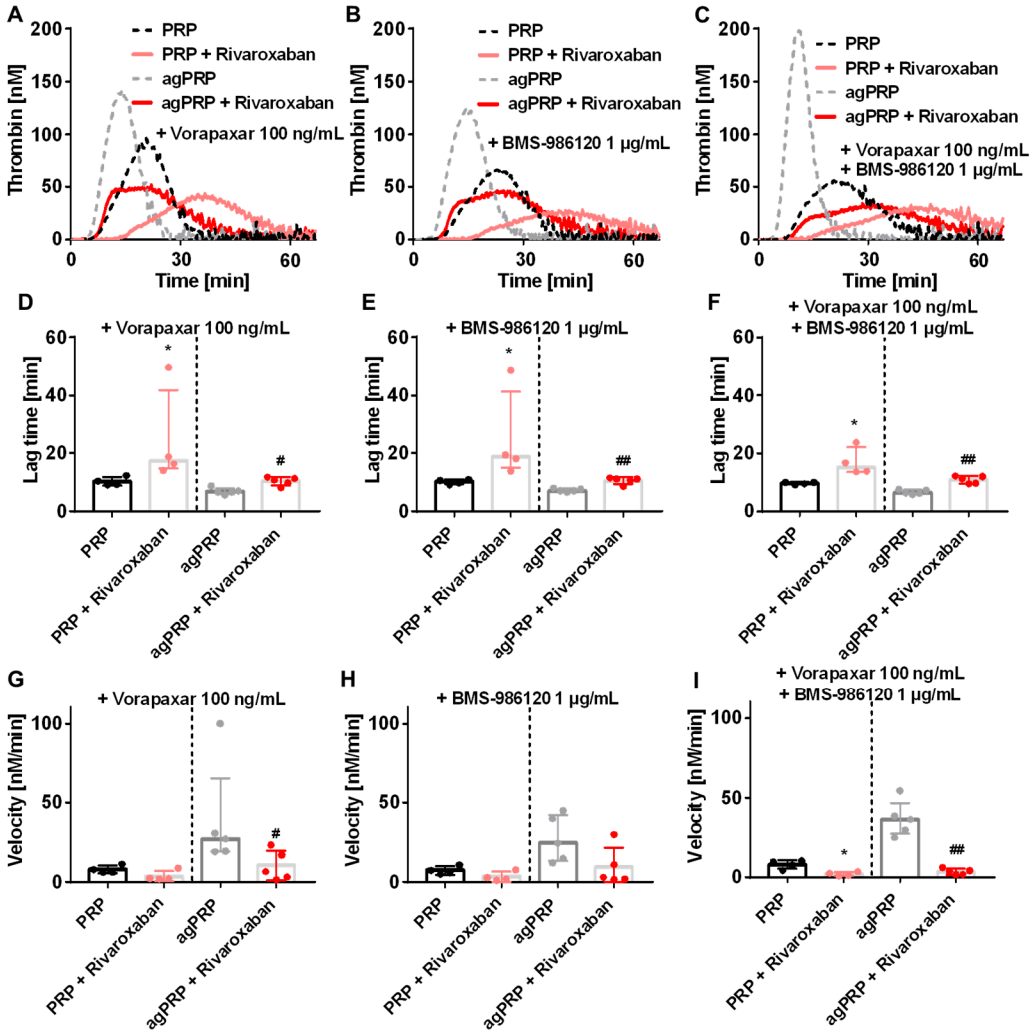

Figure 3. Effect of platelet aggregation with addition of rivaroxaban, PAR-1 and PAR-4 inhibitor to human platelet rich plasma (PRP) in TG. Representative TG curves in PRP or PRP after aggregation (agPRP) triggered with 2 µg/mL of collagen with and without addition or 50 ng/mL of rivaroxaban and inhibition of PAR-1 with vorapaxar (100 ng/mL) (**A**), inhibition of PAR-4 with BMS 896120 (1 µg/mL) (**B**) or a combination of both inhibitor (**C**). Lag time after addition of vorapaxar (**D**) BMS 986120 (**E**) or a combination of both inhibitor (**F**). Velocity after addition of vorapaxar (**G**) BMS 986120 (**H**) or a combination of both inhibitor (**I**). Results are presented as median (min-max). * $p < 0.05$, vs. PRP; # $p < 0.05$, ## $p < 0.01$, vs. agPRP, $n = 4$–5 per group.

3.5. Triggering TG with Thrombin in the Presence of Rivaroxaban Abolished the Camelback Curve

The two phases of the rivaroxaban-derived TG curves could be the result of dissociation between TG amplification related to FVa and propagation phases due to activation of FXIa by thrombin. Indeed, FXa inhibition prolonged TG and could lead to a distinct appearance of those phases, which should normally be fused into the normal shaped TG curve. To test this, we used an antibody blocking specifically FXI activation by FXIIa but not by thrombin (antibody 14E11). In this condition, agPRP plus rivaroxaban still displayed camel-back curves with two phases in the ascending part of the curve (Figure 4A) but a lower first ascending phase compared to agPRP with rivaroxaban must be noted. Rivaroxaban displays similar effects on PRP and agPRP in the presence of 14E11 as in its absence (Table 1, Figure 4C,E). To highlight the thrombin-dependent increase of TG, we used low amounts of thrombin to initiate TG (Figure 4B). This lead to normal shaped curves in PRP as well as in agPRP with or without rivaroxaban despite a flattening of the curves indicating, in concert with the decrease of the first ascending part of TG in agPRP plus rivaroxaban with 14E11, that the first phase is a combination of the activation of both extrinsic and intrinsic pathways, while the latter phase depends on thrombin activation (Figure 4D).

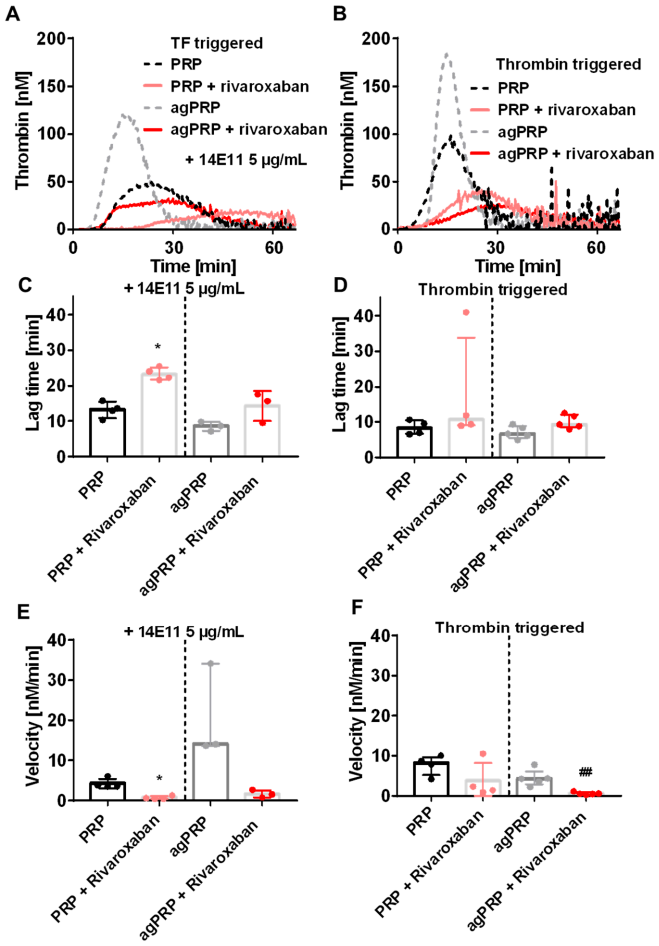

Figure 4. Implication of tissue factor (TF) and thrombin positive feedback pathways in the camel-back shaped TG curve. Representative TG curves in PRP or PRP after aggregation (agPRP) triggered with 2 µg/mL of collagen with an antibody inhibiting FXIIa-dependent activation of FXI without affecting thrombin-dependent activation of FXI (14E11; 5 µg/mL) (**A**). Corresponding lag time and velocity (**B**,**C**). Representative curves of PRP and agPRP triggered with thrombin instead of TF (**D**) and corresponding lag time and velocity (**E**,**F**). Results are presented as median (min-max). * $p < 0.05$, vs. PRP; ## $p < 0.01$, vs. agPRP. n = 3–5 per group.

4. Discussion

Recent studies reported an unexpected interaction between platelet and oral thrombin inhibitors leading to increased platelet aggregation during arterial thrombosis [17,18]. Platelets, especially mean platelet volume and platelet count, are important modulators of TG [19]. Interactions between platelets and the coagulation system are most often not considered in clinical laboratory tests and the use of direct oral anticoagulants presents novel challenge into this analytical gap. Here we explored the determinants of camelback TG curves appearing in the presence of FXa inhibitor. AgPRP was used as we observed that performing platelet aggregation before performing the CAT assay highly accelerates the kinetics of prothrombin conversion compared to PRP. Moreover, the observed changes were different compared to an activation step of platelet prior TG [14]. Thus, using PRP with unstimulated platelets does not fully include their procoagulant activity (induced by the first traces of generated thrombin) and ability to support thrombin generation. The use of agPRP in TG measurement is an advantage in the presence of anticoagulants that flatten TG curves and highly diminish ETP. Indeed, after addition of 50 ng/mL of rivaroxaban, TG curves were still visible when using agPRP and displayed two phases in the ascending part (or very long-lasting peaks). Some publications reported the presence of bell-shaped curves in patients taking rivaroxaban and we reproduced this phenomenon in control persons by adding ex vivo 50 ng/mL rivaroxaban [20–22]. The concentration of 50 ng/mL corresponds to the plasma concentration of rivaroxaban 12 h after administration of 10 mg of rivaroxaban [23]. Under physiological conditions, platelet activation mainly due to exposed collagen follows vascular injury and supports TG while in the CAT assay using PRP, platelets are activated once first traces of thrombin are generated. This can be visible by comparing lag time of TG which is often prolonged in PRP compared to similar conditions in PFP, while the opposite should be expected due to platelet procoagulant function and ability to generate procoagulant large extracellular vesicles and coagulation factors. In our set of experiments, baseline lag time for PRP was 8.9 ± 2.6 min vs. 7.5 ± 2.1 min (mean ± SD) for PFP. This shows that at baseline, platelets are neutral to coagulation and need to be activated to support thrombin generation.

In a comment, Kremers et al. [24] have suggested that TFPI could play a role in the appearance of the camel-back curves. We found that the addition of an antibody against TFPI did not restore normal shaped curves. However, in the presence of anti-TFPI the first phase of the ascending part of the curve in PRP in the presence of rivaroxaban matched the agPRP plus rivaroxaban curve indicating that contrary to the second phase of the camel-back shape the first is highly dependent on TF and FX. Since platelets contain almost half of circulating full length TFPI, which is the main active form, the absence of increased TG in agPRP plus rivaroxaban compared to PRP plus rivaroxaban in the presence of the anti-TFPI is surprising [25,26]. The increase in procoagulant PL may maximize the formation rate of thrombin and TFPI action is not sufficient to inhibit it.

In the presence of rivaroxaban, a secondary activation of platelets by the generated thrombin was a possible explanation for the occurrence of camelback curves once aggregation is completed. It has been already described that PAR-1 is responsible for a second wave of aggregation [27]. In order to test this hypothesis, we added inhibitors of platelet receptors for thrombin PAR-1 and PAR-4. The very first ascending phase of the curve was perceptibly decreased after the use of PAR-4 and in combination of PAR-1 inhibitors. However, these inhibitors—separately or combined—did not abrogated the camelback curves.

In order to test the importance of FXII and FXI in the first phase, we added an antibody (14E11) blocking specifically FXIIa-dependent FXI activation, or initiated TG directly with a small amount of thrombin. Addition of 14E11 did not abolish the first phase of camelback curves although the first phase peak height was lowered compared to identical conditions with no antibody. This result shows that both intrinsic (starting from thrombin-triggered FXI activation) and extrinsic pathways lead to this first burst of thrombin generation. Interestingly, the use of thrombin as a trigger of TG to dissect the importance of thrombin-dependent TG amplification in the presence camelback shape curve reveals that this amplification is not responsible for the presence of camel-back curves. Conversely to

TF-triggered TG in PRP or agPRP, lag time and time to peak were identical when using thrombin as an initiating factor. These results highlight the importance of TF and FXIIa-dependent initiation in enhancing the kinetics of TG. Moreover, triggering PFP (where platelets are replaced by PV) with thrombin leads to no TG emphasizing the role of platelets in TG amplification which could be linked with recent findings pointing out the ability of platelet surface to concentrate procoagulant factors (FIXa, FX, and FXa, FVIII and prothrombin) [28]. This role of platelets is again not visible without prior activation. One remaining question was coming from the important variability observed in the first phase of the camelback shaped curves. Platelet-derived microvesicles are well described to initiate TG in a FXIIa-dependent manner [29]. Antiplatelet agents were shown to lead to two-peaked thrombin generation in PRP due to delayed PL exposure on the platelet surface [30]. Thus, we decided to add increasing concentrations of PV in PFP. The most striking effect of PV in the presence of rivaroxaban was on the first ascending phase of the curve indicating that surfaces, presenting PL such as platelet-derived microvesicles are very important for the first amplification of TG. Here again TG performed with PRP very likely hides the ability of platelets to modulate TG through microvesicle production.

Taken together, our results show that agPRP might be of use in the presence of new oral anticoagulant since TG is well detectable. The relevance of the CAT assay has been established in the occurrence of venous thrombosis, but its use is more controversial concerning the prediction of recurrence [31–34]. The use of agPRP could lead to a better stratification of thrombotic risk in patients by including platelet ability to modulate TG (independently of thrombin induced platelet activation) which is underestimated with the use of unactivated PRP. Taking into account the full procoagulant potential of platelets to TG in the CAT assay was already attempted more than 15 years ago by using frozen-thawed PRP and could be an alternative if agPRP cannot be prepared freshly [35]. Since the shape of the curve is affected, it will be necessary to reevaluate the current parameters of the CAT that were developed for asymmetric bell-shaped curves. Another aspect that deserves to be extensively studied is the intra and inter-individual variability to an identical dose of rivaroxaban which is very important, making the requirement for developing an integrative test to personalize treatment even more attractive [23,36,37].

5. Conclusions

In conclusion, we present evidence that camelback shaped curves in the presence of rivaroxaban result from a protraction of TG duration and dissociation of the amplification phase and the thrombin-dependent propagation phase. In addition, we show that the first phase can be modulated by PL and could potentially be of use for personalized treatment adjustment.

Supplementary Materials: The following are available online at http://www.mdpi.com/2077-0383/8/11/1990/s1, Figure S1: Plasma preparations from human citrated blood samples for CAT assay; Figure S2: IgG isotype control effect on aggregated platelet in TG.

Author Contributions: Conceptualization, J.L.; Methodology, J.L., and W.R.; Experiments J.L. and S.M. Analysis, J.L.; Writing—Original Draft Preparation, J.L.; Writing—Review & Editing, S.M., M.P.-N., V.R., P.W., and W.R.; Supervision, J.L.

Acknowledgments: We thank CTH platform 3 (Platelet Function) (K. Jurk), A. Gruber for providing the 14E11 antibody and T. Lecompte for the scientific discussions.

Conflicts of Interest: The authors state that they have no conflict of interest.

References

1. Van Veen, J.J.; Gatt, A.; Makris, M. Thrombin generation testing in routine clinical practice: Are we there yet? *Br. J. Haematol.* **2008**, *142*, 889–903. [CrossRef]
2. Adams, M. Assessment of thrombin generation: Useful or hype? *Semin. Thromb. Hemost.* **2009**, *35*, 104–110. [CrossRef] [PubMed]

3. Castoldi, E.; Duckers, C.; Radu, C.; Spiezia, L.; Rossetto, V.; Tagariello, G.; Rosing, J.; Simioni, P. Homozygous F5 deep-intronic splicing mutation resulting in severe factor V deficiency and undetectable thrombin generation in platelet-rich plasma. *J. Thromb. Haemost.* **2011**, *9*, 959–968. [CrossRef] [PubMed]
4. Hemker, H.C.; Giesen, P.; AlDieri, R.; Regnault, V.; de Smed, E.; Wagenvoord, R.; Lecompte, T.; Béguin, S. The calibrated automated thrombogram (CAT): A universal routine test for hyper- and hypocoagulability. *Pathophysiol. Haemost. Thromb.* **2002**, *32*, 249–253. [CrossRef] [PubMed]
5. Eikelboom, J.W.; Connolly, S.J.; Bosch, J.; Dagenais, G.R.; Hart, R.G.; Shestakovska, O.; Diaz, R.; Alings, M.; Lonn, E.M.; Anand, S.S.; et al. Rivaroxaban with or without Aspirin in Stable Cardiovascular Disease. *N. Engl. J. Med.* **2017**, *377*, 1319–1330. [CrossRef]
6. Hijazi, Z.; Lindbäck, J.; Alexander, J.H.; Hanna, M.; Held, C.; Hylek, E.M.; Lopes, R.D.; Oldgren, J.; Siegbahn, A.; Stewart, R.A.H.; et al. The ABC (age, biomarkers, clinical history) stroke risk score: A biomarker-based risk score for predicting stroke in atrial fibrillation. *Eur. Heart J.* **2016**, *37*, 1582–1590. [CrossRef]
7. Pisters, R.; Lane, D.A.; Nieuwlaat, R.; de Vos, C.B.; Crijns, H.J.G.M.; Lip, G.Y.H. A novel user-friendly score (HAS-BLED) to assess 1-year risk of major bleeding in patients with atrial fibrillation: The Euro Heart Survey. *Chest* **2010**, *138*, 1093–1100. [CrossRef]
8. Boriani, G.; Botto, G.L.; Padeletti, L.; Santini, M.; Capucci, A.; Gulizia, M.; Ricci, R.; Biffi, M.; De Santo, T.; Corbucci, G.; et al. Improving stroke risk stratification using the CHADS2 and CHA2DS2-VASc risk scores in patients with paroxysmal atrial fibrillation by continuous arrhythmia burden monitoring. *Stroke* **2011**, *42*, 1768–1770. [CrossRef]
9. Hijazi, Z.; Oldgren, J.; Lindbäck, J.; Alexander, J.H.; Connolly, S.J.; Eikelboom, J.W.; Ezekowitz, M.D.; Held, C.; Hylek, E.M.; Lopes, R.D.; et al. The novel biomarker-based ABC (age, biomarkers, clinical history)-bleeding risk score for patients with atrial fibrillation: A derivation and validation study. *Lancet* **2016**, *387*, 2302–2311. [CrossRef]
10. Killu, A.M.; Granger, C.B.; Gersh, B.J. Risk stratification for stroke in atrial fibrillation: A critique. *Eur. Heart J.* **2019**, *40*, 1294–1302. [CrossRef]
11. Freyburger, G.; Macouillard, G.; Labrouche, S.; Sztark, F. Coagulation parameters in patients receiving dabigatran etexilate or rivaroxaban: Two observational studies in patients undergoing total hip or total knee replacement. *Thromb. Res.* **2011**, *127*, 457–465. [CrossRef] [PubMed]
12. Bloemen, S.; Zwaveling, S.; Douxfils, J.; Roest, M.; Kremers, R.; Mullier, F. The anticoagulant effect of dabigatran is reflected in the lag time and time-to-peak, but not in the endogenous thrombin potential or peak, of thrombin generation. *Thromb. Res.* **2018**, *171*, 160–166. [CrossRef] [PubMed]
13. Wong, P.C.; White, A.; Luettgen, J. Inhibitory effect of apixaban compared with rivaroxaban and dabigatran on thrombin generation assay. *Hosp. Pract.* **2013**, *41*, 19–25. [CrossRef] [PubMed]
14. Didelot, M.; Docq, C.; Wahl, D.; Lacolley, P.; Regnault, V.; Lagrange, J. Platelet aggregation impacts thrombin generation assessed by calibrated automated thrombography. *Platelets* **2017**, 1–6. [CrossRef]
15. Hemker, H.C.; Giesen, P.; Al Dieri, R.; Regnault, V.; de Smedt, E.; Wagenvoord, R.; Lecompte, T.; Béguin, S. Calibrated automated thrombin generation measurement in clotting plasma. *Pathophysiol. Haemost. Thromb.* **2003**, *33*, 4–15. [CrossRef]
16. Regnault, V.; Hemker, H.C.; Wahl, D.; Lecompte, T. Phenotyping the haemostatic system by thrombography–potential for the estimation of thrombotic risk. *Thromb. Res.* **2004**, *114*, 539–545. [CrossRef]
17. Petzold, T.; Thienel, M.; Konrad, I.; Schubert, I.; Regenauer, R.; Hoppe, B.; Lorenz, M.; Eckart, A.; Chandraratne, S.; Lennerz, C.; et al. Oral thrombin inhibitor aggravates platelet adhesion and aggregation during arterial thrombosis. *Sci. Transl. Med.* **2016**, *8*, 367ra168. [CrossRef]
18. Trabold, K.; Makhoul, S.; Gambaryan, S.; van Ryn, J.; Walter, U.; Jurk, K. The Direct Thrombin Inhibitors Dabigatran and Lepirudin Inhibit GPIbα-Mediated Platelet Aggregation. *Thromb. Haemost.* **2019**, *119*, 916–929. [CrossRef]
19. Panova-Noeva, M.; Schulz, A.; Spronk, H.M.; Beicht, A.; Laubert-Reh, D.; van Oerle, R.; Arnold, N.; Prochaska, J.H.; Blettner, M.; Beutel, M.; et al. Clinical Determinants of Thrombin Generation Measured in Presence and Absence of Platelets-Results from the Gutenberg Health Study. *Thromb. Haemost.* **2018**, *118*, 873–882.

20. Schultz, N.H.; Tran, H.T.T.; Bjørnsen, S.; Henriksson, C.E.; Sandset, P.M.; Holme, P.A. The reversal effect of prothrombin complex concentrate (PCC), activated PCC and recombinant activated factor VII against anticoagulation of Xa inhibitor. *Thromb. J.* **2017**, *15*, 6. [CrossRef]
21. Rigano, J.; Ng, C.; Nandurkar, H.; Ho, P. Thrombin generation estimates the anticoagulation effect of direct oral anticoagulants with significant interindividual variability observed. *Blood Coagul. Fibrinolysis* **2018**, *29*, 148–154. [CrossRef] [PubMed]
22. Borst, O.; Münzer, P.; Alnaggar, N.; Geue, S.; Tegtmeyer, R.; Rath, D.; Droppa, M.; Seizer, P.; Heitmeier, S.; Heemskerk, J.W.M.; et al. Inhibitory mechanisms of very low-dose rivaroxaban in non-ST-elevation myocardial infarction. *Blood Adv.* **2018**, *2*, 715–730. [CrossRef] [PubMed]
23. Harenberg, J.; Krämer, S.; Du, S.; Zolfaghari, S.; Schulze, A.; Krämer, R.; Weiss, C.; Wehling, M.; Lip, G.Y.H. Measurement of rivaroxaban and apixaban in serum samples of patients. *Eur. J. Clin. Invest.* **2014**, *44*, 743–752. [CrossRef] [PubMed]
24. Kremers, R.M.W.; Wagenvoord, R.J.; Hemker, H.C. Comment on the use of computational models to study the effect of apixaban and rivaroxaban on thrombin generation. *Thromb. Haemost.* **2016**, *115*, 869–870.
25. Maroney, S.A.; Mast, A.E. Expression of tissue factor pathway inhibitor by endothelial cells and platelets. *Transfus. Apher. Sci.* **2008**, *38*, 9–14. [CrossRef]
26. Winckers, K.; Thomassen, S.; ten Cate, H.; Hackeng, T.M. Platelet full length TFPI-α in healthy volunteers is not affected by sex or hormonal use. *PLoS ONE* **2017**, *12*. [CrossRef]
27. Jiang, L.; Xu, C.; Yu, S.; Liu, P.; Luo, D.; Zhou, Q.; Gao, C.; Hu, H. A critical role of thrombin/PAR-1 in ADP-induced platelet secretion and the second wave of aggregation. *J. Thromb. Haemost.* **2013**, *11*, 930–940. [CrossRef]
28. Podoplelova, N.A.; Sveshnikova, A.N.; Kotova, Y.N.; Eckly, A.; Receveur, N.; Nechipurenko, D.Y.; Obydennyi, S.I.; Kireev, I.I.; Gachet, C.; Ataullakhanov, F.I.; et al. Coagulation factors bound to procoagulant platelets concentrate in cap structures to promote clotting. *Blood* **2016**, *128*, 1745–1755. [CrossRef]
29. Van Der Meijden, P.E.J.; Van Schilfgaarde, M.; Van Oerle, R.; Renné, T.; ten Cate, H.; Spronk, H.M.H. Platelet- and erythrocyte-derived microparticles trigger thrombin generation via factor XIIa. *J. Thromb. Haemost.* **2012**, *10*, 1355–1362. [CrossRef]
30. Tarandovskiy, I.D.; Artemenko, E.O.; Panteleev, M.A.; Sinauridze, E.I.; Ataullakhanov, F.I. Antiplatelet agents can promote two-peaked thrombin generation in platelet rich plasma: Mechanism and possible applications. *PLoS ONE* **2013**, *8*, e55688. [CrossRef]
31. Van Hylckama Vlieg, A.; Baglin, C.A.; Luddington, R.; MacDonald, S.; Rosendaal, F.R.; Baglin, T.P. The risk of a first and a recurrent venous thrombosis associated with an elevated D-dimer level and an elevated thrombin potential: Results of the THE-VTE study. *J. Thromb. Haemost.* **2015**, *13*, 1642–1652. [CrossRef] [PubMed]
32. Besser, M.; Baglin, C.; Luddington, R.; van Hylckama Vlieg, A.; Baglin, T. High rate of unprovoked recurrent venous thrombosis is associated with high thrombin-generating potential in a prospective cohort study. *J. Thromb. Haemost.* **2008**, *6*, 1720–1725. [CrossRef] [PubMed]
33. Hron, G.; Kollars, M.; Binder, B.R.; Eichinger, S.; Kyrle, P.A. Identification of patients at low risk for recurrent venous thromboembolism by measuring thrombin generation. *JAMA* **2006**, *296*, 397–402. [CrossRef] [PubMed]
34. Van Hylckama Vlieg, A.; Christiansen, S.C.; Luddington, R.; Cannegieter, S.C.; Rosendaal, F.R.; Baglin, T.P. Elevated endogenous thrombin potential is associated with an increased risk of a first deep venous thrombosis but not with the risk of recurrence. *Br. J. Haematol.* **2007**, *138*, 769–774. [CrossRef] [PubMed]
35. Regnault, V.; Béguin, S.; Lecompte, T. Calibrated automated thrombin generation in frozen-thawed platelet-rich plasma to detect hypercoagulability. *Pathophysiol. Haemost. Thromb.* **2003**, *33*, 23–29. [CrossRef]

36. Gulilat, M.; Tang, A.; Gryn, S.E.; Leong-Sit, P.; Skanes, A.C.; Alfonsi, J.E.; Dresser, G.K.; Henderson, S.L.; Rose, R.V.; Lizotte, D.J.; et al. Interpatient Variation in Rivaroxaban and Apixaban Plasma Concentrations in Routine Care. *Can. J. Cardiol.* **2017**, *33*, 1036–1043. [CrossRef]
37. Siguret, V.; Abdoul, J.; Delavenne, X.; Curis, E.; Carlo, A.; Blanchard, A.; Salem, J.-E.; Gaussem, P.; Funck-Brentano, C.; Azizi, M.; et al. Rivaroxaban pharmacodynamics in healthy volunteers evaluated with thrombin generation and the active protein C system: Modeling and assessing interindividual variability. *J. Thromb. Haemost.* **2019**. [CrossRef]

The VWF/LRP4/$\alpha_v\beta_3$-axis represents a novel pathway regulating proliferation of human vascular smooth muscle cells

Jérémy Lagrange[#1], Morel E. Worou[#1], Jean-Baptiste Michel[2], Alexandre Raoul[1], Mélusine Didelot[1], Vincent Muczynski[3], Paulette Legendre[3], François Plénat[4], Guillaume Gauchotte[5], Marc-Damien Lourenco-Rodrigues[3], Olivier D. Christophe[3], Peter J. Lenting[3], Patrick Lacolley[1], Cécile V. Denis*[3], Véronique Regnault*[1]

[1] INSERM, UMR_S 1116, Vandœuvre-lès-Nancy, France; Université de Lorraine, DCAC, Nancy, France.

[2] INSERM, UMR_S 1148, LVTS, Université de Paris, France

[3] HITh, UMR_S1176, INSERM, Université Paris-Saclay, 94276, Le Kremlin-Bicêtre, France

[4] Université de Lorraine, Nancy, France.

[5] CHRU, Anatomie et cytologie pathologiques, Nancy, France

[#] Jérémy Lagrange and Morel E. Worou participated equally to this work.

* Véronique Regnault and Cécile V. Denis participated equally to this work.

Short title: VWF induces VSMC proliferation

Corresponding author:

Cécile V. Denis, Inserm U1176, 80 rue du Général Leclerc, 94276 Le Kremlin-Bicêtre cedex

cecile.denis@inserm.fr

Category: Vascular Pathophysiology

Abstract count: 286

Word count: 9051

Figures: 7

References: 43

Abstract:

Aims: Von Willebrand factor (VWF) is a plasma glycoprotein involved in primary hemostasis, while also having additional roles beyond hemostasis namely in cancer, inflammation, angiogenesis and potentially in vascular smooth muscle cell (VSMC) proliferation. Here, we addressed how VWF modulates VSMC proliferation and investigated the underlying molecular pathways and the *in vivo* pathophysiological relevance.

Methods and results: VWF induced proliferation of human aortic VSMCs and also promoted VSMC migration. Treatment of cells with a siRNA against α_v integrin or the RGT-peptide blocking $\alpha_v\beta_3$ signaling abolished proliferation. However, VWF did not bind to $\alpha_v\beta_3$ on VSMCs through its RGD-motif. Rather, we identified the VWF A2 domain as the region mediating binding to the cells. We hypothesized the involvement of a member of the LDL-related receptor protein (LRP) family due to their known ability to act as co-receptors. Using the universal LRP-inhibitor receptor-associated protein, we confirmed LRP-mediated VSMC proliferation. siRNA experiments and confocal fluorescence microscopy identified LRP4 as the VWF-counterreceptor on VSMCs. Also co-localization between $\alpha_v\beta_3$ and LRP4 was observed via proximity ligation analysis and immuno-precipitation experiments. The pathophysiological relevance of our data was supported by VWF-deficient mice having significant reduced, if any, hyperplasia in carotid artery ligation and artery femoral denudation models. In wild-type mice, infiltration of VWF in intimal regions enriched in proliferating VSMCs was found. Interestingly, also analysis of human atherosclerotic lesions showed abundant VWF accumulation in VSMC-proliferating rich intimal areas.

Conclusions: VWF mediates VSMC proliferation through a mechanism involving A2 domain binding to the LRP4 receptor and integrin $\alpha_v\beta_3$ signaling. Our findings provide new insights into the mechanisms that drive physiological repair and pathological hyperplasia of the arterial vessel wall. In addition, the VWF/LRP4-axis may represent a novel therapeutic target to modulate VSMC proliferation.

Translational perspective

The mechanisms that drive physiological repair and pathological hyperplasia of the arterial vessel wall are complex and only partially understood. Specifically, the role of subendothelial-matrix proteins remains unclear. Here, we show that the hemostatic protein von Willebrand factor (VWF) accumulates in the vascular wall of atherosclerotic lesions and localizes to areas of vascular smooth muscle cell (VSMC) proliferation. VWF was found to use its A2-domain for binding to the VSMC-receptor LRP4, which in turn triggered outside-in signaling via integrin $\alpha_V\beta_3$, thereby inducing VSMC proliferation. Interfering with A2-domain/LRP4 interactions might offer innovative and additional therapeutical approaches to limit pathological hyperplasia.

1. Introduction

Vascular smooth muscle cells (VSMCs) are crucial to maintain the structure and functions of the arterial wall. Upon vascular injury, however, these cells may start to proliferate and migrate from the media into the intima in an early process of repair called neointima formation or intimal hyperplasia (IH). This process is key in several physiological and pathogenic events, such as atherosclerosis progression and in-stent restenosis[1-3]. The molecular basis of VSMC proliferation is complex and may be provoked by a number of mitogenic agents or growth factors, such as platelet-derived growth factor (PDGF)[4]. A basic requirement for these growth factors to induce VSMC proliferation involves their translocation from circulating blood into the vascular wall. Interestingly, the vascular wall already consists of many matrix proteins, and the mitogenic potential of these matrix proteins has poorly been explored so far.

One protein known to be present constitutively in the subendothelial matrix is von Willebrand factor (VWF). VWF is a multimeric plasma glycoprotein that plays a crucial role in hemostasis, bridging platelets to subendothelial components upon vascular injury, thus contributing to bleeding arrest[5]. Following its biosynthesis by endothelial cells, VWF is directed towards storage organelles, the Weibel-Palade bodies, from where it will be secreted through constitutive or regulated pathways[6]. The constitutive pathway not only releases VWF towards the luminal side but also serves to deposit VWF in the subendothelium, usually into an acellular area[7].

Animal studies from the 1990s suggested that the location and quantity of VWF in the vessel wall can vary in vascular pathologies. Indeed, in a model of cuff-induced neointima formation in the rabbit carotid artery, VWF accumulates in the media after 24h, while at later time-points (7-14 days), VWF deposits were observed in the extracellular space of the neointima between VSMCs[8]. Additional modifications in VWF deposition in the vessel wall, whether in the media or during neointima thickening have been reported in various animal models of atherosclerosis or angioplasty[9-11]. These observations have raised the question of a potential role for VWF in vascular tissue injury responses in general and in modulating VSMC behavior in particular. An attempt to answer this question was undertaken by Qin *et al* who reported decreased IH following carotid artery ligation in a murine strain known to have low VWF levels, the RIIIS/J mice, in comparison to wild-type C57B/6J mice[12]. Additional studies further demonstrated that VWF can interact directly with murine VSMCs, and induces proliferation of these cells[12-15]. The VWF-induced proliferation of murine VSMCs has been proposed to involve a Notch-dependent signaling pathway[13-15].

Apparently, VWF combines its presence in the vascular wall with the potential to modulate VSMC proliferation. However, the molecular basis of VWF-mediated VSMC proliferation remains obscure. We further do not know whether the link between VWF and VSMCs applies to human VSMC patho-physiology as well.

Here, we explored human atherosclerotic tissue at different stages of severity, observing abundant intimal VWF accumulation in aorta, coronary and carotid atherothrombotic lesions. In addition, we demonstrate that human VSMCs are prone to VWF-induced proliferation via a novel and unusual pathway. First, the VWF A2-domain induced proliferation via interactions with low-density lipoprotein receptor-related protein-4 (LRP4), a newly identified receptor for VWF. Second, LRP4 was found to co-localize with integrin $\alpha_V\beta_3$, and VWF binding to LRP4 triggered an outside-in signaling pathway via integrin $\alpha_V\beta_3$.

2. Methods

Additional information on Methods is available in the online Supplementary materials.

2.1 Materials and reagents

A detailed description of resources used in this study (reagents & cells, antibodies, inhibitors) are detailed (name, vendor/source and clone/reference) in the Supplementary materials and methods.

2.2 Animals

8-10 weeks old wild-type (VWF+/+) or VWF-deficient (VWF-/-)[16] male mice on a C57BL/6J background were used for this study. Housing and experiments were conducted in accordance with the French regulations and the experimental guidelines of the European Community (Directive 2010/63/EU). Animals were housed under standard conditions and given free access to standard rodent chow and water. The protocols were approved by the local Animal Ethics Committee of the University of Lorraine, France (#9411-2017032718404787 v4). Anesthesia was induced by isoflurane inhalation at 3.5% in 1L/min oxygen, and then maintained at 1.5% in 1L/min oxygen during the intervention. Mice were euthanized via exsanguination under isoflurane anesthesia (1.5% in 1L/min oxygen).

2.3 Human tissues

Post-mortem human arterial, aortic, carotid and coronary artery walls, including healthy and pathology at different stages of atherosclerotic diseases were collected from the Inserm human CV biobank (BB-0033-00029, U 1148, X. Bichat hospital, Paris), included in the European network BBMRI-ERIC, in accordance with the French regular and ethical rules (BioMedicine Agency convention DC2018-3141) and the principles of the declaration of Helsinki. Approval was obtained from the French Biomedical Agency (ABM, PFS09-007 & PFS17-002) and the Institutional Ethical Review board (SC09-09-66). Tissues were obtained from deceased organ donors for kidney and/or hepatic transplantation, in the absence of therapeutic uses for the aorta and/or the heart. Human arterial tissues were fixed with 4% (w/v) buffered formaldehyde solution prepared by depolymerization of paraformaldehyde and imbedded in paraffin. Serial 5-7 μm thick sections were performed.

2.4 Immunohistochemistry

For VSMC detection in murine tissue sections, representative sections were immunostained with a monoclonal antibody (MoAb) against α Smooth Muscle Actin (α-SMA), a MoAb against VWF or a MoAb against proliferating cell nuclear antigen (PCNA). Briefly, sections were deparaffinized and rehydrated. Endogenous peroxidases were quenched with 3% H_2O_2. The mouse primary antibody was first combined with a secondary antibody (a goat anti-mouse

antibody conjugated to horse-radish peroxidase (HRP)) in a tube and allowed sufficient time to form an antibody complex. Any non-complexed secondary antibody was bound up with mouse serum. The mixture is then applied to the tissue. After washing, sections were successively incubated with a biotinylated secondary antibody for 30 min at RT, washed, and reacted with HRP-streptavidin. Color development from peroxidase antibodies was carried out using 3,3'-diaminobenzidine as the chromogen.

Immunohistochemistry of human arterial tissues were performed using α-SMA and VWF MoAbs and then revealed using 3,3'-diaminobenzidine staining on serial sections.

2.5 Cell culture

Human aortic VSMCs were obtained as cryopreserved ampules from Lonza (cat# CC-2571), containing ≥500,000 cells/ampule with >95% viability and >95% seeding efficiency. All cells were from single individuals aged between 18 and 57 years, and >10 different lots have been used during the study (ratio male/female about 60:40). Human aortic VSMCs were cultured in Smooth Muscle Cell Growth Medium-2 (SmGM-2) containing 5% fetal bovine serum at 37°C with 5% CO_2. Human VSMCs were used between passages 3 and 6.

2.6 Proliferation assay

Human VSMCs were seeded at a density of $5x10^4$ cells/well in SmGM-2 containing 5% fetal bovine serum into a 24-well plate. The next day, cells were synchronized in serum-free medium for 6h (or 24h or 48h for indicated experiments) and treated with various proteins: recombinant human platelet-derived growth factor (PDGF-BB), VWF (0-4 nM) or recombinant VWF-Fc fragments (100 ng/ml) in serum-free medium. After 24h, cell proliferation was evaluated by cell counting using a Neubauer-improved counting chamber (Marienfeld). Alternate methods to assess cell proliferation such as analysis of cellular DNA content by flow cytometry or incorporation of 5-bromo-2'-deoxyuridine (BrdU) were used for some experiments. In indicated groups, cells were pre-incubated with receptor-associated protein (RAP; 1 µM) for 1 min, a cyclic RGDPV peptide (1 mM) or RGT and GRT peptides (250 µM) for 30 min. Some experiments were performed in the presence of antibody LM609 (10 µg/ml). In the control group, VSMCs were cultured without any treatment. For each experiment, triplicate wells were counted.

2.7 Wound-healing and migration assays

Experiments were performed on confluent monolayers of human VSMCs seeded in a 6-well plate. After starving the cells in serum-free medium for 6h, a wound scratch was created with a 200 µl pipette tip. Cells were washed twice with PBS to remove detached cells, and then cultured in a serum-free medium with or without VWF or VWF fragment. The wounded area

was observed and photographed at t=0,16, 24 and 48h after wounding. Using ImageJ Software, VSMC migration and wound repair was evaluated by the number of cells that migrated into the wounded area.

2.8 Western blotting

Cells treated as indicated in individual experiments were harvested, washed twice with PBS and lysed in a cold lysis buffer (Roche Life Sciences, Meylan France) containing proteases and phosphatase inhibitors cocktails (Roche). The lysates were pelleted and the supernatant fractions were collected and examined for protein concentration using a Bradford Protein assay kit (Bio-Rad, Marnes-la-Coquette, France). Proteins were separated by SDS-PAGE and electro-transferred onto a nitrocellulose membrane. After blocking for 1h in 5% non-fat milk dissolved in Tris buffered saline with 0.1% Tween-20, membranes were incubated with indicated specific primary antibodies overnight at 4°C. Membranes were then washed and incubated with appropriate secondary antibodies for 1h at room temperature (RT). The immunoreactive bands were visualized by chemiluminescence (Western ECL substrate, Bio-Rad) using a luminescent image analyzer system (LAS-4000 mini, Fujifilm).

2.9 Immunofluorescence staining of VSMCs

A detailed description of this procedure is presented in the Supplementary materials. VSMCs were grown on glass coverslips, and incubated in the presence or absence of VWF. After formaldehyde fixation, cells were incubated with primary antibodies against VWF, $\alpha_v\beta_3$ integrin, Protease Activated Receptor-2 (PAR2) or LRP4. Nuclei were counterstained with 4',6'-diamidino-2-phenylindole (DAPI). Negative controls were performed by omitting the primary antibody or the VWF treatment. Images were acquired via fluorescent confocal microscopy, and analyzed by Image J software using the plugin *colocalization finder* to calculate the Pearson's coefficient[17].

For the Duolink®- Proximity Ligation Assay (PLA), double immunostaining of human VSMCs (treated or not with VWF) was performed using primary antibodies to LRP4 and $\alpha_v\beta_3$ integrin, the secondary antibodies being replaced by PLA probes. The remainder of the protocol was conducted according to the manufacturer's recommendations. For confocal microscopy, a Nikon C2 microscope with Ti-FL stage and C-HGFi fluorescent bulb was used. Acquisition was performed with the NiS Elements software.

2.10 siRNA transfection

To evaluate the role of LRP4 or $\alpha_v\beta_3$ in VWF-induced human VSMC proliferation, cells were transfected with siRNA directed against LRP4 or α_v or the negative control using a magnet-assisted transfection reagent according to the manufacturer's instructions. siRNA-sequences

are provided in the Supplementary materials. Briefly, for each well of a 24-well plate, 0.25 μg of siRNA was diluted in serum-free Dulbecco's Modified Eagle Medium (DMEM) to an end volume of 50 μl. The diluted siRNA was added to 0.75 μl of MATra-Si Reagent, followed by mixing and incubation at RT for 20 min. The transfection complex siRNA/MATra-Si reagent was added to the cells. The plate was then incubated on a magnetic plate for 15 min at 37°C. The magnetic plate was removed, followed by a 24h resting period in a serum-free medium. Cells were then used for VWF-induced human VSMCs proliferation or migration assays.

2.11 Binding assays

LRP proteins (50 µl, 1 µg/ml) were immobilized on half-well microtiter plates in carbonate buffer pH 9.6 overnight at 4°C. After washing with TBS (Tris 25 mM, NaCl 150 mM, pH 7.4) containing 2.5 mM $CaCl_2$ and 0.1% Tween-20, a post-coat step was applied (30 min at 37°C in the same buffer but with 3% BSA). VWF or VWF fragments diluted in TBS-Ca-Tween/3% BSA were then added to the wells (50 µl) for 2h at 37°C. In one set of experiments, VWF was pre-incubated or not with 1 mg/ml of ristocetin at RT before addition to the wells. After three washes, HRP-coupled antibodies to VWF or to Fc-tag were added (50 µl) for 2h at 37°C. 3,3',5,5'-tetramethylbenzidine was added to reveal bound proteins and the reaction was stopped with H_2SO_4. OD was read at 450 and 570 nm in a multiplate reader (Biotek).

2.12 Statistical analysis

Data are presented as mean±SD, unless specified. Statistical analysis was performed using Graphpad prism 5 software. A two-tailed unpaired Student *t* test was applied for comparisons between two groups. When indicated, multiple t-test was performed. One-way ANOVA followed by Tukey's or Dunnett's multiple comparisons test was performed when comparing multiple groups. $P<0.05$ was considered as statistically significant. For the *in vivo* experiments, an N-1 Chi-square test was performed when comparing the number of mice with or without hyperplasia. When comparing the intima/media ratio or nuclei number, a Mann-Whitney test was applied.

3. Results

3.1 VWF is involved in intimal hyperplasia in vivo

In view of the different mouse strains that were compared for their sensitivity to VWF-dependent hyperplasia formation in previous studies[12], we first set to confirm such an effect in a more appropriate setting using VWF-KO mice and their wild-type littermates. Two distinct models of vascular injury were used: 1) ligation of the common carotid artery and 2) femoral artery denudation. In the carotid artery ligation model, 5 out of 9 VWF+/+ mice had extensive intimal hyperplasia (IH), whereas none of the 8 VWF-/- did (p=0.015; **Supplementary Table S1**). A similar difference in neointima formation was observed in the femoral artery denudation model, with 10 out of 14 VWF+/+ mice developing IH versus 4 out of 13 VWF-/- mice (p=0.038; **Supplementary Table S1 & Fig. S1**). Histological analysis of the ligated and contralateral arteries revealed the presence of neointima selectively in the ligated arteries of VWF+/+ mice (**Fig. 1A**). Importantly, only the neointima of ligated arteries in VWF+/+ mice stained positive for PCNA, a marker for cell proliferation (**Fig. 1B**). Indeed, the intima/media ratio was significantly increased in these mice (p=0.0294), as was the number of nuclei (p=0.0294; **Fig. 1F**). Neointima stained positive for α-SMA, compatible with proliferating cells being VSMCs (**Fig. 1C**). Interestingly, neointima also stained positive for VWF, which was absent in the intima of the contralateral artery, suggesting that VWF is present within the proliferating area (**Fig. D**). This infiltration seemed specific for VWF as no changes were observed for collagen, another sub-endothelial matrix protein (**Fig. 1E**). Thus, these mouse data confirm the link between VWF and VSMC proliferation. However, it does not teach us whether VWF modulates VSMC proliferation in a direct or indirect manner.

3.2 VWF is present in the intima and core of human atherosclerotic lesions

To explore the possibility that VWF could contribute to the pathogenesis of neointima formation in humans, we performed qualitative analyses of rare tissue aortic sections for the presence of VWF in areas enriched in proliferating VSMCs. As expected, VWF is predominantly detected in the most luminal part of healthy human aorta (corresponding to the endothelium), with minor variable subendothelial staining in the α-SMA-positive cell area (**Fig. 2A**). In contrast, clear prominent VWF immunostaining was observed in the intima of human fatty streaks (aorta and coronary artery), largely overlapping with areas of α-SMA-positive cell migration and potential proliferation (**Fig. 2B** & **Supplementary Fig. S2**). Similarly, abundant VWF immunostaining was detected in endothelium and VSMC-rich subendothelium of the cap in human fibrolipidic plaques (**Fig. 2C**). VWF accumulation also predominated in the core of the plaque, an area of high plasma protein insudation (**Fig. 2C**). Another example relates to complex neo-atherosclerotic lesions that are formed following coronary artery stenting. Also in this condition,

VWF accumulates in the VSMC-rich area of the shoulder of a stented segment (**Supplementary Fig. S2**).

Extravascular VWF accumulation was also observed in carotid tissue sections (**Supplementary Fig. S2**). Profuse VWF immunostaining was present in areas of carotid intimal proliferation, involving both endothelial, subendothelial and SMA-positive intima (**Supplementary Fig. S2**). In culprit plaque, VWF appeared in the cap endothelium and in the VSMC-rich cap intimal proliferation area (**Supplementary Fig. S2**). As observed in the fibrolipidic aorta, VWF is also present in the VSMC-poor external part of the lesion, an area corresponding to intraplaque hemorrhage (**Supplementary Fig. S2**). Altogether, we observe an accumulation of VWF in VSMC-rich areas of various pathological arterial tissue sections. It seems conceivable therefore that VWF may be in direct contact with these cells.

3.3 VWF induces human aortic VSMC proliferation and migration

In the remainder of our study, we focused on the potential of VWF to induce proliferation of human VSMCs and its underlying molecular pathway. In a first series of experiments, the mitogenic effect of VWF on VSMCs was compared to that of PDGF-BB. Proliferation in the absence of any mitogenic protein was arbitrarily defined as 1.0. As expected, PDGF-BB induced VSMC proliferation in a dose-dependent manner (**Fig. 3A**). In line with previous studies, the proliferative effect of PDGF-BB followed a bell-shaped curve[18, 19]. A similar dose-dependent and bell-shaped effect was observed for VWF (**Fig. 3A**). Interestingly, similar maximum proliferative index values were obtained for PDGF-BB and VWF (1.8±0.1 for PDGF-BB *vs* 1.8±0.3 for VWF at the peak, $p<0.0005$ *vs* untreated cells). Similar proliferative index values for VWF were obtained when applying other means to quantify cell proliferation: cell cycle analysis by flow cytometry or incorporation of BrdU (**Fig. 3B**). In an alternative approach, we analyzed the effect of VWF on VSMC recolonization in a wound healing scratch assay, which measures both migration and proliferation. Again, VWF was found to stimulate VSMC recolonization of the wound area as indicated by the significantly higher number of cells present after 16, 24 and 48h (**Supplementary Fig. S3**). These data are compatible with VWF having the potential to simulate human VSMC proliferation, akin to PDGF-BB.

3.4 Signaling pathways associated with VWF-induced VSMC-proliferation

We next explored the cellular responses of VSMCs used at passages 3-6, following exposure to VWF. First, quantitative PCR of nine specific VSMC markers was performed at 24h and 48h after exposure to VWF. However, no change in RNA expression for each of these markers was detected compared to cells without VWF exposure (**Fig. 3C**). In accordance with these data, no changes in expression of α-SMA, Smooth Muscle Myosin Heavy Chain (SM-MHC), vimentin, myocardin, and smoothelin upon VWF treatment were observed (**Supplementary**

Fig. S4), indicating the maintenance of a differentiated state of VSMCs, allowing the proliferative status of the cells.

To analyze which signaling pathways were activated by VWF, we quantified phosphorylation of Akt, ERK1/2, p38-Mitogen-activated protein kinases (p38-MAPK), Src and STAT3. No VWF-dependent activation of STAT3 could be detected (**Supplementary Fig. S5**). In contrast, VWF significantly induced Akt phosphorylation at the Thr308 site and ERK1/2 phosphorylation at the Thr202/Tyr204 site with a maximum effect at 15 min (**Fig. 3D-E**). To further elucidate the VWF-dependent signaling pathway upstream of regulators of Akt and ERK1/2, we examined the level of phosphorylation of p38-MAPK and Src, a major intracellular mediator of integrin-dependent functions. Induction of both p38-MAPK phosphorylation at the Thr179/Tyr181 site and Src phosphorylation at the Tyr418 site were increased within 5 to 15 min and the phosphorylation returned to basal levels after 30 min (**Fig. 3F-G**).

3.5 Identification of $\alpha_v\beta_3$ involvement in VWF-induced VSMC proliferation

The $\alpha_v\beta_3$ integrin has previously been reported as a receptor for VWF on VSMCs[15], and we therefore investigated whether VWF co-localized with this integrin at the cellular surface *via* confocal microscopy. VSMCs were incubated in the absence or presence of VWF and co-stained for α_V and VWF (**Fig. 4A**) or, as negative control, PAR2 and VWF (**Fig. 4B**). Confocal images revealed selective co-staining for VSMCs incubated with VWF and co-stained for α_V and VWF, but not in other conditions (**Fig. 4A-B**). Observations were quantified via pixel-analysis of multiple z-stacks, revealing a median Pearson's correlation coefficient of 0.71 for α_V/VWF versus 0.11 for PAR2/VWF (**Fig. 4A-B**). These data confirm that VWF co-localizes with $\alpha_V\beta_3$.

To establish if VWF-induced VSMC proliferation involves $\alpha_v\beta_3$, we used a siRNA-strategy. A specifically designed α_v-targeting siRNA blocked α_v RNA expression by 78% and protein expression by 41%, whereas both remained unchanged in the presence of control siRNA (**Supplementary Fig. S6**). Adding the α_v siRNA and control siRNA to VSMCs induced a 15-20% reduction in cell proliferation in the absence of VWF ($p=0.012$ and $p=0.046$, respectively when comparing to "no VWF no siRNA" condition; **Fig. 4C**), indicating that the siRNA procedure in itself has a minor but significant effect on VSMC proliferation. However, a similar 1.6-fold increase in VSMC proliferation was observed for both control conditions (no siRNA and control siRNA) in the presence of VWF compared to the absence of VWF, showing that this procedure does not interfere with the mitogenic activity of VWF. In contrast, no VWF-induced proliferation was found in the presence of the α_v siRNA (**Fig. 4C**). Apparently, the presence of $\alpha_V\beta_3$ is indispensable for VWF-induced VSMC proliferation.

3.6 The VWF-$\alpha_v\beta_3$ integrin axis in VSMC proliferation

Since VWF comprises an RGD-motif in its C-terminal region, we anticipated that this motif would mediate direct binding of VWF to $\alpha_v\beta_3$. This hypothesis was challenged by analyzing VWF-mediated VSMC proliferation in the absence or presence of a cRGDPV-peptide or the anti-$\alpha_v\beta_3$ integrin antibody LM609, both of which would annihilate the binding of the VWF RGD motif to $\alpha_v\beta_3$ and subsequent VSMC proliferation. In the absence of VWF, we observed that the cRGDPV-peptide alone inhibited basal cell proliferation by 60% (p=0.002 compared to control without any additions), whereas no effect was observed when antibody LM609 was tested in the absence of VWF (**Fig. 4D**). Despite the inhibitory effect of the cRGDPV-peptide on basal VSMC proliferation, a similar VWF-dependent increase in VSMC proliferation was observed in all three conditions: 1.5-fold, 1.6-fold and 1.7-fold for control, the cRGDPV-peptide and antibody LM609, respectively.

We next explored the option whether the observed VWF-dependent effect involves $\alpha_v\beta_3$-mediated signaling. This was tested using a myristoylated RGT-peptide (myr-RGT), which selectively inhibits β_3 outside-in signaling[21]. As control, its myristoylated GRT-control peptide (myr-GRT) was applied[21]. Neither peptide had any influence on basal VSMC proliferation, nor did the myr-GRT-control peptide affect VWF-induced proliferation (**Fig. 4E**). In contrast, the myr-RGT-peptide proved an efficient inhibitor of VWF-enhanced VSMC proliferation (proliferative index 2.1±0.2 without peptide *vs* 0.9±0.2 with peptide, p<0.0001; **Fig. 4E**). We then hypothesized that should the VWF mitogenic effect involves signaling via $\alpha_v\beta_3$, then the down-regulation of $\alpha_v\beta_3$ expression would result in an absence of phosphorylation of downstream kinases. Human VSMCs were therefore treated with α_v siRNA and its effect on Src phosphorylation was evaluated. Whereas VWF induced Src phosphorylation in VSMCs treated with control siRNA, this was completely abolished in cells treated with α_v siRNA (**Supplementary Fig. S7**). Thus, VWF induces an $\alpha_v\beta_3$-dependent signaling pathway that results in phosphorylation of Src-kinase. In contrast, this process proceeds independently of a direct interaction between VWF and the RGD-responsive site in $\alpha_v\beta_3$.

3.7 Identification of a member of the LRP family as crucial determinant for VWF-induced VSMC proliferation

Since $\alpha_v\beta_3$ is seemingly not the primary VWF receptor in our experiments, it is conceivable that a second receptor able to crosstalk with $\alpha_v\beta_3$ is implicated. LRP family members are known co-receptors in different cell types, including VSMCs. Indeed, a cooperation between LRP1 and $\alpha_v\beta_3$ in response to tissue-type plasminogen activator has been reported[22]. We therefore tested whether an LRP receptor was involved, and GST-RAP was used as general inhibitor of the LRP-receptor family. GST-RAP alone had no effect on basal VSMC proliferation (**Fig. 5A**).

However, its presence completely abolished VWF-induced cell proliferation (proliferation index with VWF alone: 2.2±0.2 *vs* 0.7±0.2 with VWF+GST-RAP, p<0.0001; **Fig. 5A**). We also measured proliferation using a combination of both GST-RAP and myr-RGT. Blocking simultaneously $\alpha_v\beta_3$ and LRP had no additional effect and VWF-induced VSMC proliferation was reduced to basal proliferation (**Fig. 5A**), suggesting that both receptors operate in concert. We considered the possibility that the LRP-receptor involved in this VWF-dependent process would be LRP1, previously recognized as receptor for VWF on macrophages, and also known to be expressed on VSMCs[23, 24]. However, for this interaction, VWF requires to adopt an active, platelet-binding conformation, which can be mimicked by pre-incubating VWF with ristocetin[23]. Unexpectedly, pre-treatment of VWF with ristocetin did not further increase the proliferative index at any of the VWF concentrations tested (**Fig. 5B**), suggesting that another LRP family member rather than LRP1 is involved in VWF-dependent VSMC proliferation.

3.8 VWF A2-domain mediates VSMC proliferation

To narrow our search for an LRP family member as potential receptor for VWF on VSMCs, we decided to investigate the molecular determinants on the VWF subunit, necessary to induce VSMC proliferation. To do so, we used purified recombinant VWF domains. The VWF mature subunit with its domain structure is represented on **Fig. 5C**. Among isolated VWF fragments, only the VWF-A2 domain promoted VSMC proliferation. No significant difference with full-length VWF were observed in terms of proliferative index (2.1±0.2 for VWF, 1.7±0.5 for A2-Fc, *p*=0.47; **Fig. 5D**). All other VWF fragments as well as a control Fc-fused unrelated protein (Siglec5-Fc) proved inefficient in promoting cell proliferation. A dimeric D4-CK fragment containing the VWF RGD-motif (within the C4 domain) also did not show any proliferative effect, compatible with the finding that the VWF-mediated effect is independent of its RGD-motif (**Fig. 5D**). In the wound healing scratch assay, VWF-A2 fragment induced VSMC migration, similar to full-length VWF (**Fig. 5E & Supplementary Fig. S8**). Similar to full-length VWF, A2-Fc induced proliferation was completely abolished in the presence of the LRP-inhibitor GST-RAP or the presence of myr-RGT (**Fig. 5F**). In addition, A2-Fc induced similar signaling as full-length VWF, as illustrated by the phosphorylation of Erk1/2 (**Fig. 5G**). Apparently, the A2-Fc protein mimics full-length VWF not only in inducing VSMC proliferation and migration, but also in doing so via an LRP-triggered outside-in signaling pathway involving $\alpha_v\beta_3$.

3.9 VWF binds to LRP4 on VSMCs to induce cell proliferation

Having identified an LRP receptor as counter-receptor for the VWF A2-domain on VSMCs, we next attempted to pinpoint which LRP member was involved. First, we measured VWF binding, in the absence of ristocetin, to different LRP receptors selected on the basis of mRNA

identification in VSMCs (www.proteinatlas.org). In these conditions, no binding of VWF to LRP1, LRP5 or LRP8 was detected. However, VWF displayed strong binding to LRP4 in the absence of ristocetin (**Fig. 6A**). Furthermore, when testing VWF-Fc fragments, we observed a specific interaction between VWF-A2 domain and LRP4 (**Fig. 6B**), thus suggesting that LRP4 could represent a candidate receptor for VWF on VSMCs. Since LRP4 is particularly known for its expression on neurons and skeletal muscle cells rather than VSMCs, we first verified LRP4 expression on VSMCs. To this end, immunofluorescence studies were performed and a strong signal for LRP4 on these cells could be detected (**Fig. 6C**). Moreover, when cells were incubated in the presence of VWF, a clear co-staining between VWF and LRP4 was detected (**Fig. 6D**), suggesting that VWF is able to interact with LRP4 at the cellular surface. Using siRNA against LRP4, we next demonstrated the direct involvement of this receptor in VWF-mediated VSMC proliferation. siRNA directed against LRP4 led to a >90% decrease in mRNA expression and a 40% decrease in protein expression (**Supplementary Fig. S9**). In the proliferation assay, complete inhibition of VWF-induced VSMC proliferation was observed in the presence of the LRP4 siRNA with no significant effect of the control siRNA (proliferative index of 1.7±0.1 with control siRNA *vs* 1.0±0.1 with LRP4 siRNA, $p<0.0001$; **Fig. 6E**). Thus, LRP4 seems to be an essential element in VWF-induced VSMC proliferation.

3.10 LRP4 and $\alpha_v\beta_3$ cooperate to mediate VWF-induced VSMC proliferation

Given the observation that LRP4 and $\alpha_v\beta_3$ seem to mediate VWF-dependent VSMC proliferation in a concerted action (**Fig. 5A**), we explored the option that both receptors would be in close proximity at the cellular surface. To this end, Duolink®-PLA analysis was performed, which detects proteins being located within a range of 40 nm. Whereas negative conditions (single primary with both secondary antibodies) did not reveal any signal, we observed a positive signal in the test conditions, demonstrating that both receptors were within 40 nm of distance, strongly suggesting the existence of an interaction (**Fig. 7A-C**). Indeed, the LRP4/$\alpha_v\beta_3$ complex could be precipitated using anti-α_v antibodies (**Fig. 7D**). Interestingly, while Duolink-PLA analysis suggested reduced interactions between LRP4 and $\alpha_v\beta_3$ in the presence of VWF (**Supplementary Fig. S10**), this was not observed in the immunoprecipitation experiments (**Fig. 7D**). We anticipate that reduced complex formation in the former assay is due to reduced antibody accessibility of the receptors in the presence of VWF.

We also checked whether siRNA against LRP4 abrogated the $\alpha_v\beta_3$-dependent activation of Src phosphorylation by VWF. The LRP4 siRNA completely abolished VWF-induced Src activation compared with the control siRNA (**Fig. 7E-F**). Suppression of Akt, ERK1/2 and p-38 MAPK phosphorylation was also evidenced in the presence of the LRP4 siRNA (**Fig. 7E-F**).

Taken together, we have identified VWF as a mitogenic factor that efficiently induces VSMC proliferation via a previously unrecognized pathway involving the heterologous receptor complex LRP4/ $\alpha_v\beta_3$, which in turn activates a Src-mediated signaling cascade.

4. Discussion

Besides its well-known function in primary hemostasis, VWF is increasingly recognized as a pleiotropic protein involved in processes related to angiogenesis, cancer and inflammation[5]. In the vascular wall, observations that VWF location and quantity may vary in vascular diseases indicate a potential intervention of VWF in tissue remodeling following injury[8-11]. In particular, a role for VWF in modulating murine VSMC proliferating properties has been suggested by Qin et al[12]. In this study, we have now characterized this ability of VWF to induce human VSMC proliferation by identifying the pathways involved. We observed a dose-dependent proliferating effect of VWF on VSMCs, consistent with the previous findings. In addition to inducing cell proliferation, VWF also proved able to mediate cell migration in a wound healing scratch assay, further demonstrating its ability to influence tissue remodeling. VWF-induced proliferation and migration of VSMCs had no effect on their differentiation, in agreement with the current concept that dedifferentiation is not a prerequisite for VSMC proliferation[25, 26]. Finally, involvement of the ERK1/2-MAPK cascade and Akt signaling pathway completed and supported the picture of a proliferating status of the VSMCs in presence of VWF.

Having established this proliferating effect of VWF, our next step consisted in identifying the cellular receptor(s) involved. Based on our knowledge of the receptor repertoire of VSMCs, we first considered $\alpha_v\beta_3$ integrin as a potential candidate. Indeed this integrin is strongly expressed by VSMCs[27], is a known receptor for VWF[28] and is involved in VSMC proliferation and migration[29]. Our initial experiments showing co-localization of $\alpha_v\beta_3$ and VWF at the surface of VSMCs supported this hypothesis. Further confirmation of $\alpha_v\beta_3$ involvement arose from the complete inhibition of the VWF-proliferative effect upon treatment of the cells with siRNA against α_v. Importantly, on VSMCs the α_v subunit is only associated to β_3 and β_3 is only associated to α_v[27]. Blocking $\alpha_v\beta_3$ signaling using the myr-RGT-peptide[21, 30] also completely annihilated VWF-induced cell proliferation. However, the use of inhibitors of $\alpha_v\beta_3$ engagement[31] such as a cyclic RGD peptide or the LM609 antibody did not block VWF-mediated cell proliferation. Altogether, our results emphasize the critical importance of $\alpha_v\beta_3$-dependent signaling in mediating VWF-induced cell proliferation, a process that seems to occur independently of VWF binding to this integrin.

Since members of the LRP family are known to act as co-receptors in a variety of cellular settings, including VSMCs[22], we hypothesized for such a mechanism and indeed, using the LRP-inhibitor GST-RAP, we exposed the importance of an LRP receptor in VWF-induced VSMC proliferation. Among LRP family members, VWF is known to bind LRP1 but this binding involves its A1 domain and requires VWF to be in an active conformation[6, 23]. Our present observations showing a lack of effect of ristocetin, a VWF activator, added to the identification of the A2 domain as the necessary VWF determinant, thus pointed to an LRP member other than LRP1. Our data identified LRP4 as a new receptor for VWF. Indeed, using direct binding

experiments we showed that LRP4 is the only LRP member potentially present on VSMCs that is able to bind VWF without ristocetin. In addition, we showed that the only VWF region able to substitute for full-length VWF in mediating VSMC proliferation and migration, *i.e.* the A2 domain is also able to bind to LRP4. Using immunofluorescence, we confirmed expression of LRP4 by VSMCs and showed colocalization between LRP4 and VWF. And finally, direct evidence of LRP4 involvement came from the use of siRNA against LRP4, which completely blocked VWF-induced proliferation.

Three important and original pieces of information can be highlighted from these experiments. The first one is the involvement of the VWF-A2 domain. Besides its critical role in harboring binding and cleavage sites for ADAMTS13, the enzyme responsible for regulating VWF multimeric size[32], the A2 domain has not been reported to play a major role in mediating VWF interaction with its numerous partners. This is in contrast to its neighboring domains, which contains binding sites for many VWF ligands such as glycoprotein Ib, heparin, sulfatides, collagen VI for the A1 domain [33, 34] and collagens for the A3 domain[35]. However very recently, a study reported an interaction between the VWF A2 domain and extracellular vimentin[36], suggesting that the importance of this domain has not yet been fully investigated. The second original finding relates to LRP4. This member of the LRP family has been first identified in 1998 and is unique among other LRP receptors since it is the only type II transmembrane receptor, with its N-terminal region located within the cytoplasmic side of the plasma membrane[37]. A complete deficiency of LRP4 is incompatible with life in mice[38]. LRP4 has been reported to be involved in multiple functions: on skeletal muscle cells, LRP4 is crucial for the formation of neuromuscular junction[39] while on non-muscle cells, LRP4 plays a role in presynaptic differentiation or in bone-mass homeostasis[40]. Although the main functions of the LRP receptors appear to be related to cargo transport or internalization of macromolecules, LRP4 mostly serves as a signal transducer or modulator. A number of ligands for LRP4 have already been identified and for each of its functions, an original and complex signaling mechanism has been described[39]. Our results appear to be following a similar trend. Indeed, LRP4 appears to be the receptor for VWF at the cell surface and as such, it could potentially signal directly through Ca2+/calmodulin-dependent protein kinase II (CaMKII) to activate ERK1/2, Akt and p38-MAPK. However, in our conditions, an LRP4-mediated outside-in signaling through $\alpha_v\beta_3$ is necessary to induce VSMC proliferation, suggesting cooperation between both receptors, the third important point in our study. Indeed, we were able to show using immunoprecipitation experiments and the Duolink-PLA that LRP4 and $\alpha_v\beta_3$ are co-localizing at the surface of VSMCs. Furthermore, the use of siRNA against one or the other of these receptors completely abrogates the proliferating effect of VWF, highlighting the physiological relevance of this cooperation. It is not unusual for LRP receptors to associate with co-receptors depending on the cellular environment, allowing them to extend their ligand profile, to modulate their cellular

activities and to enable signal transduction[41]. This capacity makes LRP family members very versatile receptors and multifunctional cell-surface proteins. For example, cooperation between LRP1 and $\alpha_v\beta_3$ has been shown to mediate vasocontraction of VSMCs by tissue-type plasminogen activator[22]. Still on VSMCs, LRP1 appears to control PDGF receptor-dependent signaling pathways, controlling cell proliferation and preventing atherosclerosis[24].

Relevant to our findings is of course its physiological context. Our mouse model based on a full deficiency of VWF displayed a strong reduction in neointima formation in two different experimental approaches for intimal hyperplasia, consistent with observations using a mouse with a partial deficiency of VWF[12]. In addition, infiltration of VWF in regions enriched in proliferating VSMCs was detected in wild-type mice. It should be noted that both mouse models are limited in that they do not distinguish between a direct and indirect role of VWF. VWF may affect VSMC proliferation indirectly via several mechanisms. For instance, endothelial cells lack VWF-specific storage organelles (Weibel-Palade bodies) in VWF-/- mice[16], which could negatively impact the release of necessary growth factors or other proteins essential in the process to induce VSMC proliferation. However, Weibel-Palade bodies are normally present in the endothelial cells of the RIIIS/J-mice, which express low levels of VWF[12]. It is unlikely therefore that the lack of neointima formation in the VWF-/- mice is due to the absence of Weibel-Palade bodies. Alternatively, VWF may be necessary for the recruitment of platelets at the site of injury, which can release growth factors contributing to cell proliferation. However, characterization of the model by Roque *et al* revealed an early-stage (1h) accumulation of platelets at the site of injury without the need for VWF[42], arguing for a similar platelet involvement between VWF+/+ and VWF-/- mice. Finally, VWF has recently been reported to contribute to wound healing, acting as a molecular bus to deliver growth factors to wound sites[43]. It is possible that this mechanism contributes to the *in vivo* VWF-mediated VSMC proliferation, existing in parallel to the LRP4-$\alpha_v\beta_3$ mechanism that we describe here.

In view of our findings and the potential mechanism by which VWF contributes to VSMC proliferation, it seems relevant to distinguish between subendothelial VWF and VWF derived from the circulation. The data observed using human atherosclerotic pathology fit well with the hypothesis that VWF is present in the wall proportional to the pathology intensity, mainly in endothelium and intima but also in the core of the lesion. These data suggest that deposition of VWF originates from endothelial cells surrounding the lesion. However, other areas in the atherosclerotic lesion, predominantly in the core of the plaque, are prone to hemorrhages and plasma protein insudation[20]. It is likely that in these plasma-borne atheroma injuries, plasma-derived VWF participates in the arterial cellular responses.

In conclusion, we have observed the combined presence of VWF and VSMCs in the neointima of various pathological arteries, but not healthy vessels. In addition, we found that VWF is an effective mitogenic agent towards VSMCs, and further analysis revealed a novel, previously

unrecognized molecular pathway underlying this mitogenic action. VWF can induce VSMC proliferation, involving cooperation between two receptors, one important for ligand binding (LRP4) and the second for signal transduction ($\alpha_v\beta_3$). Our findings provide new insights into the mechanisms that drive physiological repair and pathological hyperplasia of the arterial vessel wall. The identification of VWF and LRP4 may therefore be of potential interest in prevention and treatment of arterial wall remodeling, and open avenues for novel therapeutical strategies.

6. Acknowledgements

We wish to thank Dr. Huguette Louis and Mrs Kenza Benkirane for expert technical assistance. We are indebted to Dr. Muriel Laffargue for her willingness to share her team's expertise in performing femoral wire injury in mice. We thank the Flow cytometry Core Facility and the Imaging Core Facility (PTIBC) of UMS2008/US40 IBSLor (Université de Lorraine-CNRS-INSERM) for cell cycle analysis and confocal microscopy respectively.

7. Sources of funding

This work was supported by the Investments for the Future program under grant agreement No ANR-15-RHU-0004; the Agence Nationale de la Recherche (ANR-13-BSV1-0026); the Région Grand Est; and the "Fonds européen de développement regional".

8. Conflict of interest

None declared.

9. Author contributions

JL, MEW, MD, VM, AR, PL, FP, GG, MDLR, VR performed experiments and analyzed data.
JBM provided human tissue sections and analyzed histology sections.
ODV, PJL, PL, CVD, VR analyzed data, designed and supervised the study.
PJL, PL, CVD, VR wrote the manuscript.
All authors confirmed the final version of the manuscript.

10. Data availability

The data underlying this article will be shared on reasonable request to the corresponding author.

11. References

1. Dzau VJ, Braun-Dullaeus RC, Sedding DG. Vascular proliferation and atherosclerosis: new perspectives and therapeutic strategies. *Nat Med* 2002;**8**:1249-1256.
2. Schober A. Chemokines in vascular dysfunction and remodeling. *Arterioscler Thromb Vasc Biol* 2008;**28**:1950-1959.
3. Lacolley P, Regnault V, Nicoletti A, Li Z, Michel JB. The vascular smooth muscle cell in arterial pathology: a cell that can take on multiple roles. *Cardiovasc Res* 2012;**95**:194-204.
4. Millette E, Rauch BH, Kenagy RD, Daum G, Clowes AW. Platelet-derived growth factor-BB transactivates the fibroblast growth factor receptor to induce proliferation in human smooth muscle cells. *Trends Cardiovasc Med* 2006;**16**:25-28.
5. Lenting PJ, Casari C, Christophe OD, Denis CV. von Willebrand factor: the old, the new and the unknown. *J Thromb Haemost* 2012;**10**:2428-2437.
6. Lenting PJ, Christophe OD, Denis CV. von Willebrand factor biosynthesis, secretion, and clearance: connecting the far ends. *Blood* 2015;**125**:2019-2028.
7. Sporn LA, Marder VJ, Wagner DD. Differing polarity of the constitutive and regulated secretory pathways for von Willebrand factor in endothelial cells. *J Cell Biol* 1989;**108**:1283-1289.
8. Kockx MM, De Meyer GR, Andries LJ, Bult H, Jacob WA, Herman AG. The endothelium during cuff-induced neointima formation in the rabbit carotid artery. *Arterioscler Thromb* 1993;**13**:1874-1884.
9. Bosmans JM, Kockx MM, Vrints CJ, Bult H, De Meyer GR, Herman AG. Fibrin(ogen) and von Willebrand factor deposition are associated with intimal thickening after balloon angioplasty of the rabbit carotid artery. *Arterioscler Thromb Vasc Biol* 1997;**17**:634-645.
10. De Meyer GR, Hoylaerts MF, Kockx MM, Yamamoto H, Herman AG, Bult H. Intimal deposition of functional von Willebrand factor in atherogenesis. *Arterioscler Thromb Vasc Biol* 1999;**19**:2524-2534.
11. Giddings JC, Banning AP, Ralis H, Lewis MJ. Redistribution of von Willebrand factor in porcine carotid arteries after balloon angioplasty. *Arterioscler Thromb Vasc Biol* 1997;**17**:1872-1878.
12. Qin F, Impeduglia T, Schaffer P, Dardik H. Overexpression of von Willebrand factor is an independent risk factor for pathogenesis of intimal hyperplasia: preliminary studies. *J Vasc Surg* 2003;**37**:433-439.
13. Meng H, Zhang X, Lee SJ, Wang MM. Von Willebrand factor inhibits mature smooth muscle gene expression through impairment of Notch signaling. *PLoS One* 2013;**8**:e75808.
14. Zhang X, Meng H, Blaivas M, Rushing EJ, Moore BE, Schwartz J, Lopes MB, Worrall BB, Wang MM. Von Willebrand Factor permeates small vessels in CADASIL and inhibits smooth muscle gene expression. *Transl Stroke Res* 2012;**3**:138-145.
15. Scheppke L, Murphy EA, Zarpellon A, Hofmann JJ, Merkulova A, Shields DJ, Weis SM, Byzova TV, Ruggeri ZM, Iruela-Arispe ML, Cheresh DA. Notch promotes vascular maturation by inducing integrin-mediated smooth muscle cell adhesion to the endothelial basement membrane. *Blood* 2012;**119**:2149-2158.
16. Denis C, Methia N, Frenette PS, Rayburn H, Ullman-Cullere M, Hynes RO, Wagner DD. A mouse model of severe von Willebrand disease: defects in hemostasis and thrombosis. *Proc Natl Acad Sci U S A* 1998;**95**:9524-9529.
17. French AP, Mills S, Swarup R, Bennett MJ, Pridmore TP. Colocalization of fluorescent markers in confocal microscope images of plant cells. *Nat Protoc* 2008;**3**:619-628.
18. Facchiano A, De Marchis F, Turchetti E, Facchiano F, Guglielmi M, Denaro A, Palumbo R, Scoccianti M, Capogrossi MC. The chemotactic and mitogenic effects of platelet-derived growth factor-BB on rat aorta smooth muscle cells are inhibited by basic fibroblast growth factor. *J Cell Sci* 2000;**113 (Pt 16)**:2855-2863.
19. Li H, Papadopoulos V, Vidic B, Dym M, Culty M. Regulation of rat testis gonocyte proliferation by platelet-derived growth factor and estradiol: identification of signaling mechanisms involved. *Endocrinology* 1997;**138**:1289-1298.

20. Michel JB, Virmani R, Arbustini E, Pasterkamp G. Intraplaque haemorrhages as the trigger of plaque vulnerability. *Eur Heart J* 2011;**32**:1977-1985, 1985a, 1985b, 1985c.
21. Su X, Mi J, Yan J, Flevaris P, Lu Y, Liu H, Ruan Z, Wang X, Kieffer N, Chen S, Du X, Xi X. RGT, a synthetic peptide corresponding to the integrin beta 3 cytoplasmic C-terminal sequence, selectively inhibits outside-in signaling in human platelets by disrupting the interaction of integrin alpha IIb beta 3 with Src kinase. *Blood* 2008;**112**:592-602.
22. Akkawi S, Nassar T, Tarshis M, Cines DB, Higazi AA. LRP and alphavbeta3 mediate tPA activation of smooth muscle cells. *Am J Physiol Heart Circ Physiol* 2006;**291**:H1351-1359.
23. Rastegarlari G, Pegon JN, Casari C, Odouard S, Navarrete AM, Saint-Lu N, van Vlijmen BJ, Legendre P, Christophe OD, Denis CV, Lenting PJ. Macrophage LRP1 contributes to the clearance of von Willebrand factor. *Blood* 2012;**119**:2126-2134.
24. Boucher P, Gotthardt M, Li WP, Anderson RG, Herz J. LRP: role in vascular wall integrity and protection from atherosclerosis. *Science* 2003;**300**:329-332.
25. Owens GK, Kumar MS, Wamhoff BR. Molecular regulation of vascular smooth muscle cell differentiation in development and disease. *Physiol Rev* 2004;**84**:767-801.
26. Michel JB. Phylogenic determinants of cardiovascular frailty, focus on hemodynamics and arterial smooth muscle cells. *Physiol Rev* 2020;**in press, doi: 10.1152/physrev.00022.2019**.
27. Lacolley P, Regnault V, Segers P, Laurent S. Vascular Smooth Muscle Cells and Arterial Stiffening: Relevance in Development, Aging, and Disease. *Physiol Rev* 2017;**97**:1555-1617.
28. Denis C, Williams JA, Lu X, Meyer D, Baruch D. Solid-phase von Willebrand factor contains a conformationally active RGD motif that mediates endothelial cell adhesion through the alpha v beta 3 receptor. *Blood* 1993;**82**:3622-3630.
29. Byzova TV, Rabbani R, D'Souza SE, Plow EF. Role of integrin alpha(v)beta3 in vascular biology. *Thromb Haemost* 1998;**80**:726-734.
30. Xi X, Bodnar RJ, Li Z, Lam SC, Du X. Critical roles for the COOH-terminal NITY and RGT sequences of the integrin beta3 cytoplasmic domain in inside-out and outside-in signaling. *J Cell Biol* 2003;**162**:329-339.
31. Mao X, Said R, Louis H, Max JP, Bourhim M, Challande P, Wahl D, Li Z, Regnault V, Lacolley P. Cyclic stretch-induced thrombin generation by rat vascular smooth muscle cells is mediated by the integrin alphavbeta3 pathway. *Cardiovasc Res* 2012;**96**:513-523.
32. Crawley JT, de Groot R, Xiang Y, Luken BM, Lane DA. Unraveling the scissile bond: how ADAMTS13 recognizes and cleaves von Willebrand factor. *Blood* 2011;**118**:3212-3221.
33. Christophe O, Obert B, Meyer D, Girma JP. The binding domain of von Willebrand factor to sulfatides is distinct from those interacting with glycoprotein Ib, heparin, and collagen and resides between amino acid residues Leu 512 and Lys 673. *Blood* 1991;**78**:2310-2317.
34. Sixma JJ, Schiphorst ME, Verweij CL, Pannekoek H. Effect of deletion of the A1 domain of von Willebrand factor on its binding to heparin, collagen and platelets in the presence of ristocetin. *Eur J Biochem* 1991;**196**:369-375.
35. Kalafatis M, Takahashi Y, Girma JP, Meyer D. Localization of a collagen-interactive domain of human von Willebrand factor between amino acid residues Gly 911 and Glu 1,365. *Blood* 1987;**70**:1577-1583.
36. Fasipe TA, Hong SH, Da Q, Valladolid C, Lahey MT, Richards LM, Dunn AK, Cruz MA, Marrelli SP. Extracellular Vimentin/VWF (von Willebrand Factor) Interaction Contributes to VWF String Formation and Stroke Pathology. *Stroke* 2018;**49**:2536-2540.
37. Tomita Y, Kim DH, Magoori K, Fujino T, Yamamoto TT. A novel low-density lipoprotein receptor-related protein with type II membrane protein-like structure is abundant in heart. *J Biochem* 1998;**124**:784-789.
38. Weatherbee SD, Anderson KV, Niswander LA. LDL-receptor-related protein 4 is crucial for formation of the neuromuscular junction. *Development* 2006;**133**:4993-5000.
39. Shen C, Xiong WC, Mei L. LRP4 in neuromuscular junction and bone development and diseases. *Bone* 2015;**80**:101-108.

40. Xiong L, Jung JU, Wu H, Xia WF, Pan JX, Shen C, Mei L, Xiong WC. Lrp4 in osteoblasts suppresses bone formation and promotes osteoclastogenesis and bone resorption. *Proc Natl Acad Sci U S A* 2015;**112**:3487-3492.
41. Nykjaer A, Willnow TE. The low-density lipoprotein receptor gene family: a cellular Swiss army knife? *Trends Cell Biol* 2002;**12**:273-280.
42. Roque M, Fallon JT, Badimon JJ, Zhang WX, Taubman MB, Reis ED. Mouse model of femoral artery denudation injury associated with the rapid accumulation of adhesion molecules on the luminal surface and recruitment of neutrophils. *Arterioscler Thromb Vasc Biol* 2000;**20**:335-342.
43. Ishihara J, Ishihara A, Starke RD, Peghaire CR, Smith KE, McKinnon TAJ, Tabata Y, Sasaki K, White MJV, Fukunaga K, Laffan MA, Lutolf MP, Randi AM, Hubbell JA. The heparin binding domain of von Willebrand factor binds to growth factors and promotes angiogenesis in wound healing. *Blood* 2019;**133**:2559-2569.

12. Figure legends

Figure 1: Immunostaining of murine arterial tissue sections after carotid ligation.

A-E. Arterial tissue sections obtained 4 weeks post-injury from VWF+/+ and VWF-/- mice were stained using HES (A) or Sirius Red (E) or with antibodies against PCNA (B), α-SMA (C) or VWF (D). M: media; I: intima. Scale bars, 50 μm. **F.** Intima/media ratio and nuclei count in injured carotid arteries (n=9 for VWF+/+ and n=8 for VWF-/-). Statistical analysis was performed using a Mann-Whitney test.

Figure 2: Immunostaining of VWF and α-SMA in different stages of aortic atherosclerosis in human.

A. Detection of VWF in endothelium of healthy human aorta and in the subendothelial layer positive for α-SMA staining. **B**. Fatty streaks showing presence of VWF in the α-SMA-positive neointima. **C**. Subendothelium VWF staining in VSMC-rich fibrocellular cap and VWF accumulation in the acellular lipid core of fibrolipidic plaques. Full morphology of the section (Nanozoomer) were associated with X4 magnification (red boxes) and X20 magnification (black boxes). M, media; I, intima. Scale bars = 2 mm (Nanozoomer), 1 mm (X4 magnification) and 0.2 mm (X20 magnification).

Figure 3: VWF-induced proliferation cultured human VSMCs.

A. Human aortic VSMCs were incubated with VWF or PDGF-BB (0-4 nM) for 24h, and cell proliferation was evaluated. Presented is the proliferative index relative to proliferation with medium alone, which is arbitrarily defined as 1.0. Data represent the mean±SEM of 3 (for PDGF) or 4 experiments (for VWF), each performed in triplicate. **B.** Measure of VWF-induced VSMC proliferation using 3 different methods: incorporation of BrdU (n=7), cell counting (n=4) or analysis of cellular DNA (n=3). Data represent mean±SD. **C.** VSMCs were incubated in the absence or presence of VWF (1 nM) for 24h (grey bars) or 48h (dotted bars). RNA was isolated and quantitative PCR was performed for 9 different markers. Relative changes in RNA expression compared to cells incubated in the absence of VWF are presented. Data are expressed as mean±SD, n=indicated for each condition. **D-G**. Phosphorylation of Akt, ERK1/2, p38-MAPK and Src was assessed after exposing cells to 1 nM VWF for 5 to 60 min. Cell lysates were prepared and phosphorylation of Akt (Thr^{308}), ERK1/2 (Thr^{202}/Tyr^{204}), p38-MAPK (Thr^{179}/Tyr^{181}) or Src (Tyr^{418}) was determined using colorimetric cell-based elisa kits. Data represent mean±SD (n=4), and results are expressed as fold increase relative to unstimulated control. Statistical analysis was performed using one-way Anova with Dunnett's multiple comparison.

Figure 4: Involvement of $\alpha_v\beta_3$ in VWF-mediated VSMC proliferation

A-B: Confocal immunostaining of VWF (red) and $\alpha_v\beta_3$ (panel A; green) or PAR2 (panel B; green) in VSMCs incubated for 24h at 37°C in the absence or presence of VWF (1 nM). Nuclei were counterstained using DAPI. Images were acquired using stacks (1 µm) in sequential for the three channels (488, 555 & 633 nm). Bars represent 25 µm, objective 40x. The Pearson's correlation coefficient was obtained by Image J software using the plugin *colocalization finder*. Data are expressed as mean±SD. N=33 cells for α_V without VWF; n=54 for α_V with VWF; n=64 for PAR2 without VWF and n=42 for PAR with VWF. Statistical analysis involved a Mann-Whitney test. **C**. Proliferative index of human VSMCs transfected with control siRNA or siRNA against α_v and incubated with 1 nM VWF for 24h. **D-E**. Proliferative index of human VSMCs treated with VWF (1 nM) for 24h in the presence the LM609 antibody (10 µg/ml) or after pre-treatment of the cells with a cyclic RGDPV peptide (1 mM; panel D) or synthetic myristoylated RGT/GRT peptides (250 µM; panel E). Experiments were reproduced three times in triplicate (C-E) and statistical analysis was performed using one-way Anova with Tukey's multiple comparison.

Figure 5: Identification of the VWF molecular determinant involved in mediating VSMC proliferation. A. Proliferative index of human VSMCs pretreated with GST-RAP (1 µM) or a mixture of GST-RAP and synthetic myristoylated RGT/GRT peptides (250 µM) prior addition of 1 nM VWF for 24h. Data represent mean±SD; n=6 for No VWF, VWF and GST-RAP; n=3 for VWF+GST-RAP, VWF+RGT-myr+GST-RAP and VWF+GRT-myr+GST-RAP (with each experiment performed in triplicate). **B.** Proliferative response of human VSMCs following incubation with VWF or VWF/ristocetin (0-4 nM). Data represent mean±SEM of 3 independent experiments. **C.** Schematic representation of the domain structure of VWF. **D.** Proliferative index of human VSMCs in response to VWF (1 nM), PDGF (0.2 nM) or various VWF-fragments (100 ng/ml) (mean±SD; n is indicated for each condition). **E.** A wound healing scratch assay was performed on human VSMCs in the absence or presence of VWF-A2/Fc (100 ng/ml). Reappearance of cells in the wounded area was monitored at t=0,16, 24 and 48h and quantified using ImageJ Software. Data represent mean±SD (n=3). **F.** Proliferative index of human VSMCs pretreated with GST-RAP (1 µM) or a mixture of GST-RAP and synthetic myristoylated RGT/GRT peptides (250 µM) prior addition of 100 ng/ml VWF-A2/Fc for 24h. **G.** Phosphorylation of ERK1/2 was assessed after exposing cells to 1 nM VWF for 5 to 60 min. Cell lysates were prepared and phosphorylation of ERK1/2 (Thr^{202}/Tyr^{204}) was determined using colorimetric cell-based elisa. Data represent mean±SD (n=4), and results are expressed as fold increase relative to unstimulated control. Statistical analysis was performed using one-way Anova with Tukey's (panels A, D, F) or Dunnett's (panel G) multiple comparison or using multiple t-test (panel E).

Figure 6: Involvement of LRP4 in VWF-mediated VSMC proliferation

A. Immobilized LRP variants (1 μg/ml) were incubated with VWF (0-7.5 μg/ml) in the absence of VWF activator. Bound-VWF was probed by a peroxidase-coupled polyclonal anti-VWF antibody. Data represent mean±SD (n=3). Closed circles: LRP4; open circles: LRP1; open squares LRP5; closed squares LRP8. **B.** Immobilized LRP4 (1 μg/ml) was incubated with VWF-A2/Fc (closed triangles) or VWF-A3/Fc (open triangles; 0-15 μg/ml). Bound-VWF fragments were probed using peroxidase-coupled polyclonal anti-Fc antibodies. Data represent mean±SD (n=3). **C.** Fluorescent immunostaining of LRP4 on VSCMCs. Nuclei were counterstained using DAPI. Representative images were acquired using confocal microscopy. Bars represent 25 μm for objective 40x or 10 μm for objective 100x. **D.** VSMCs incubated in the presence or absence of VWF were stained using anti-LRP4 (green) and anti-VWF (red) antibodies. Nuclei were counterstained using DAPI. Shown are representative merged images acquired using confocal microscopy. Bars represent 25 μm. **E.** Proliferative index of human VSMCs transfected with control siRNA or siRNA against LRP4 and incubated with 1 nM VWF for 24h. Experiment was reproduced three times in triplicate and statistical analysis was performed using one-way Anova with Tukey's multiple comparison.

Figure 7: Association between $\alpha_v\beta_3$ and LRP4 on VSMCs and effect on MAPK signaling pathways

A-C. Duolink-proximity ligation assay (PLA) analysis of LRP4 and $\alpha_v\beta_3$ expression and colocalization on VSMCs. Panels A-B represents control conditions in the presence of only one primary antibody (A: anti-α_V, B: anti-LRP4) and both secondary antibodies with fluorescent probes. Panel C represents test conditions (both primary and secondary antibodies with fluorescent probes). Red spots appear only when $\alpha_v\beta_3$ and LRP4 are within a distance of ≤40 nm. Nuclei were counterstained with DAPI. Scale bars: 10μm, Objective 63x. **D.** VSMCs incubated in the presence or absence of VWF were lysed, and immunoprecipitated using anti α_V-antibodies or control antibodies. Western blots of lysates were first stained using anti α_V-antibodies and subsequently with anti-LRP4 antibodies. **E-F.** Phosphorylation of Akt, ERK1/2, p38-MAPK and Src was assessed after exposing cells transfected with control or siRNA against LRP4 to 1 nM VWF for 10 min. Cell lysates were prepared and phosphorylation of Akt (Thr^{308}), ERK1/2 (Thr^{202}/Tyr^{204}), p38-MAPK (Thr^{179}/Tyr^{181}) or Src (Tyr^{418}) was determined by Western blotting. Immunoreactive bands were visualized by chemiluminescence and quantified using a luminescent image analyzer system. Data represent mean±SD (n=3) and results are expressed as fold increase relative to unstimulated control. Statistical analysis was performed using t-test.

Figure 1

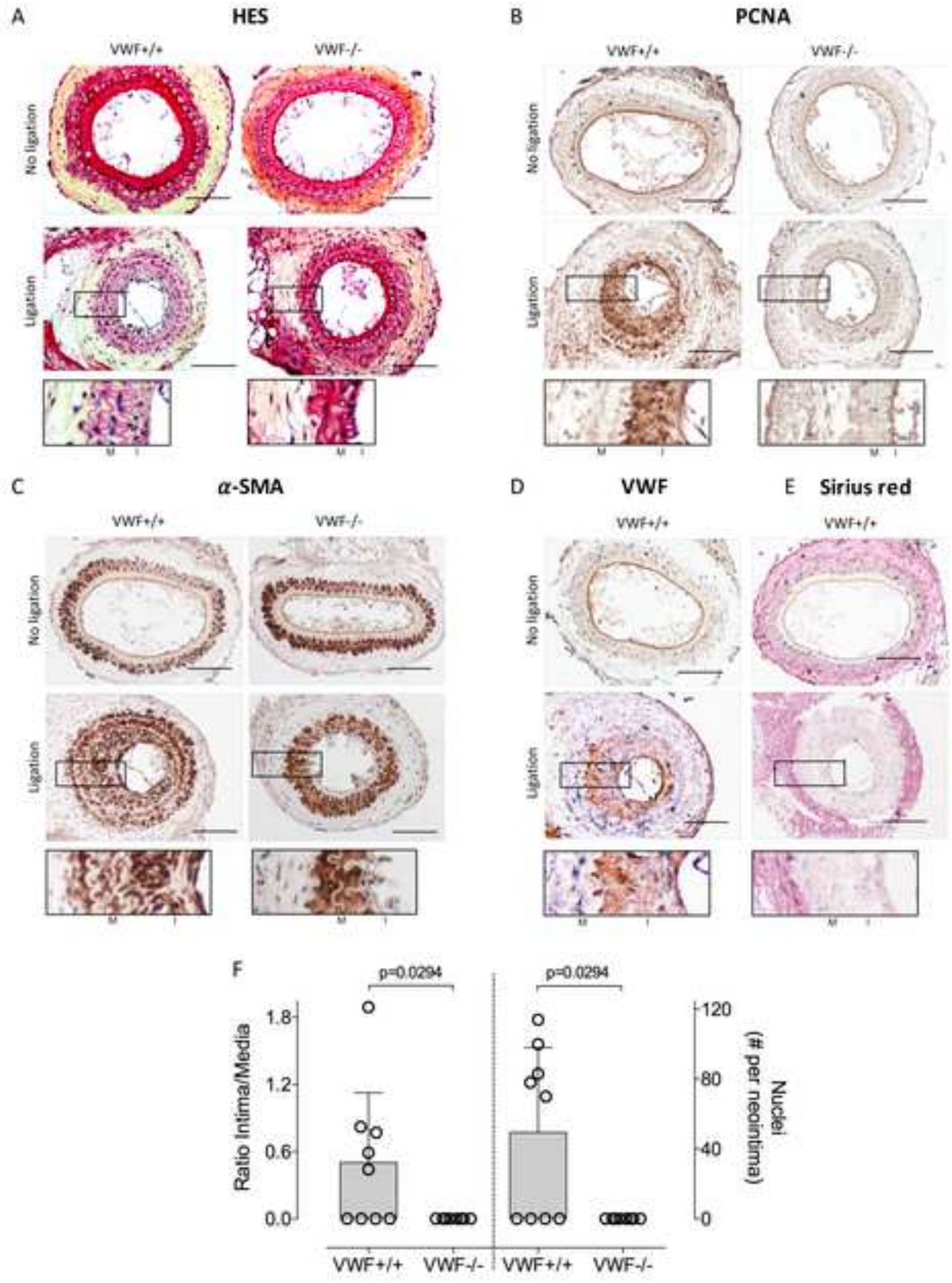

Figure 2

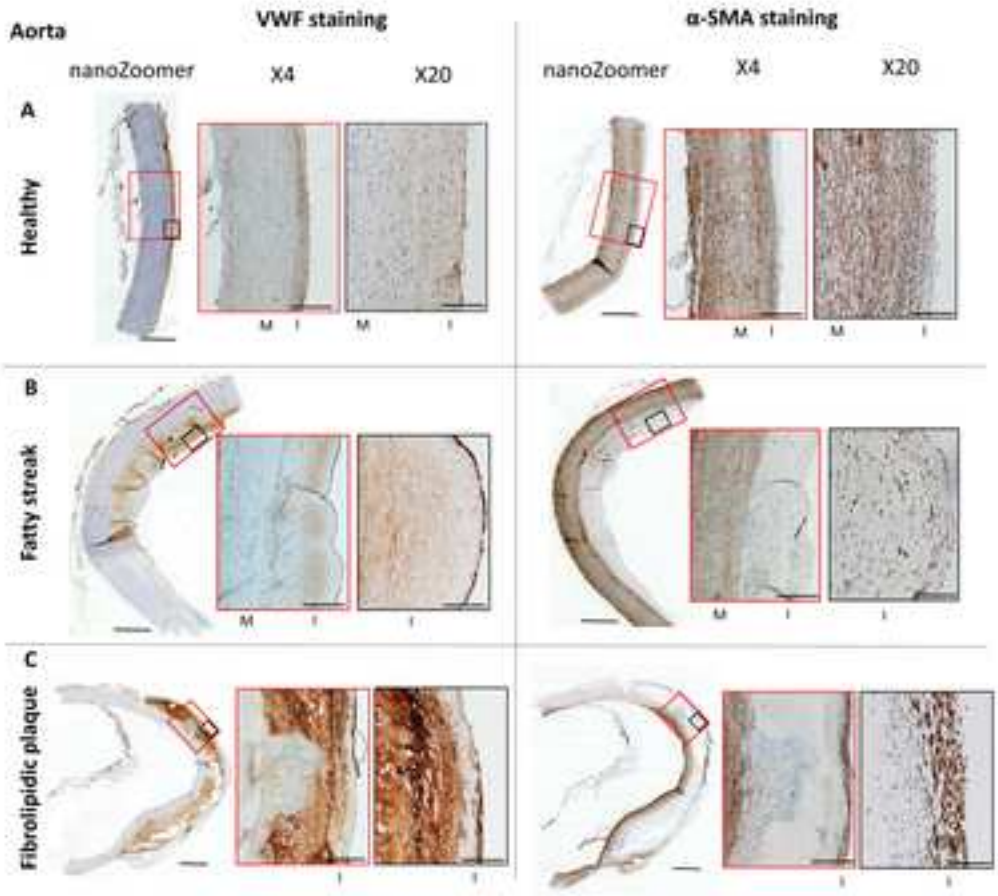

Figure 3

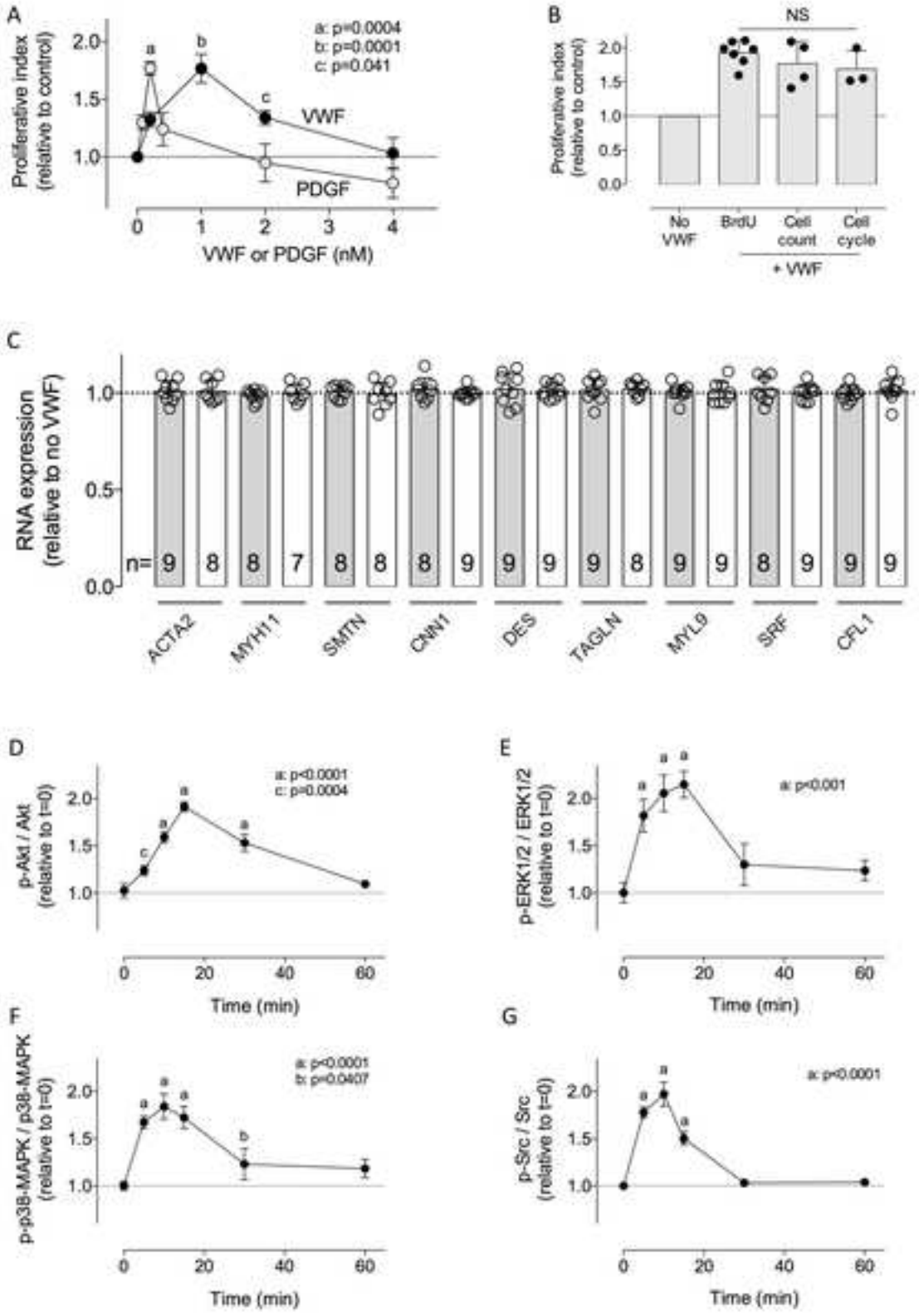

Figure 4

CVR 2020-0707 R2
Lagrange, Worou et al
Fig. 4

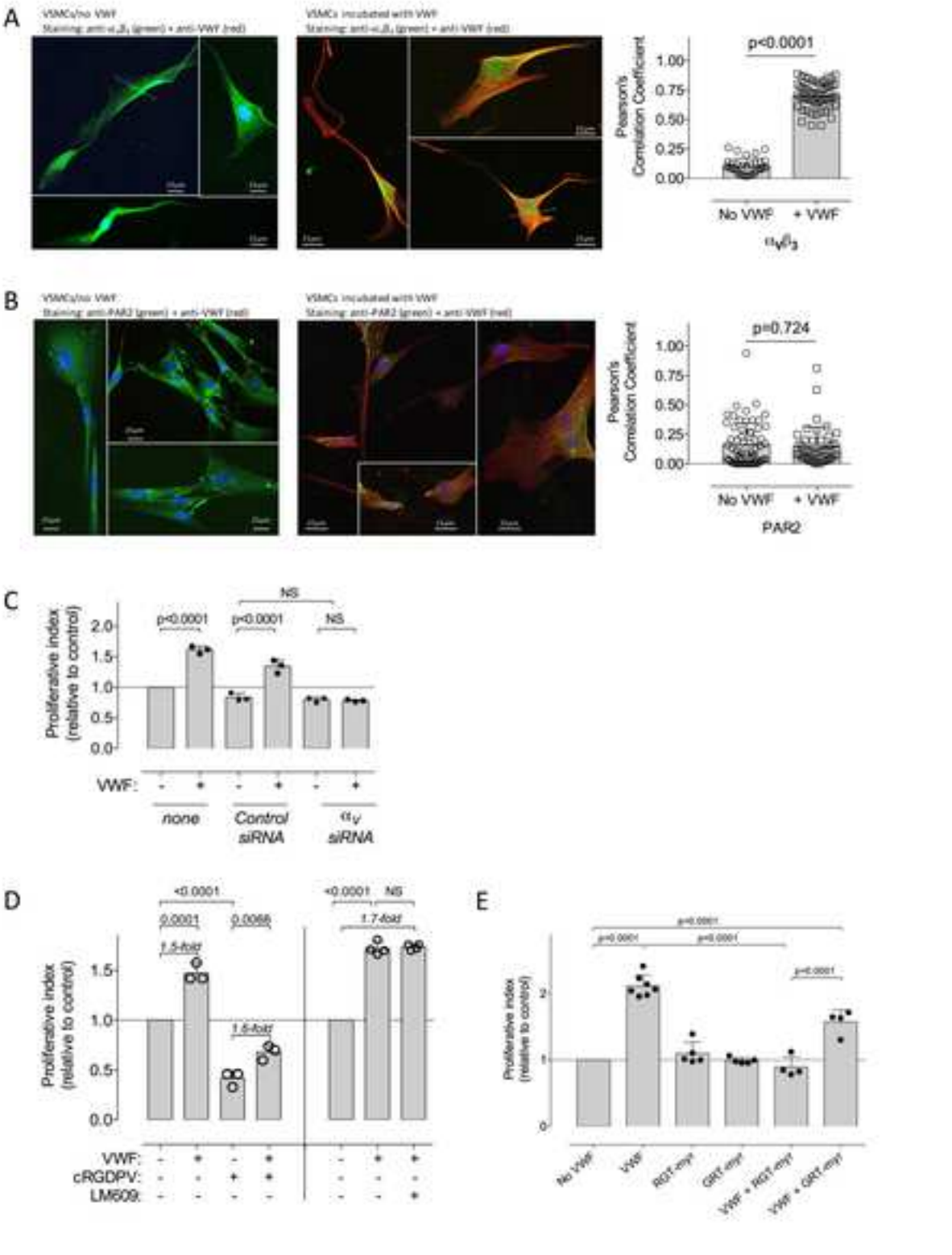

Figure 5

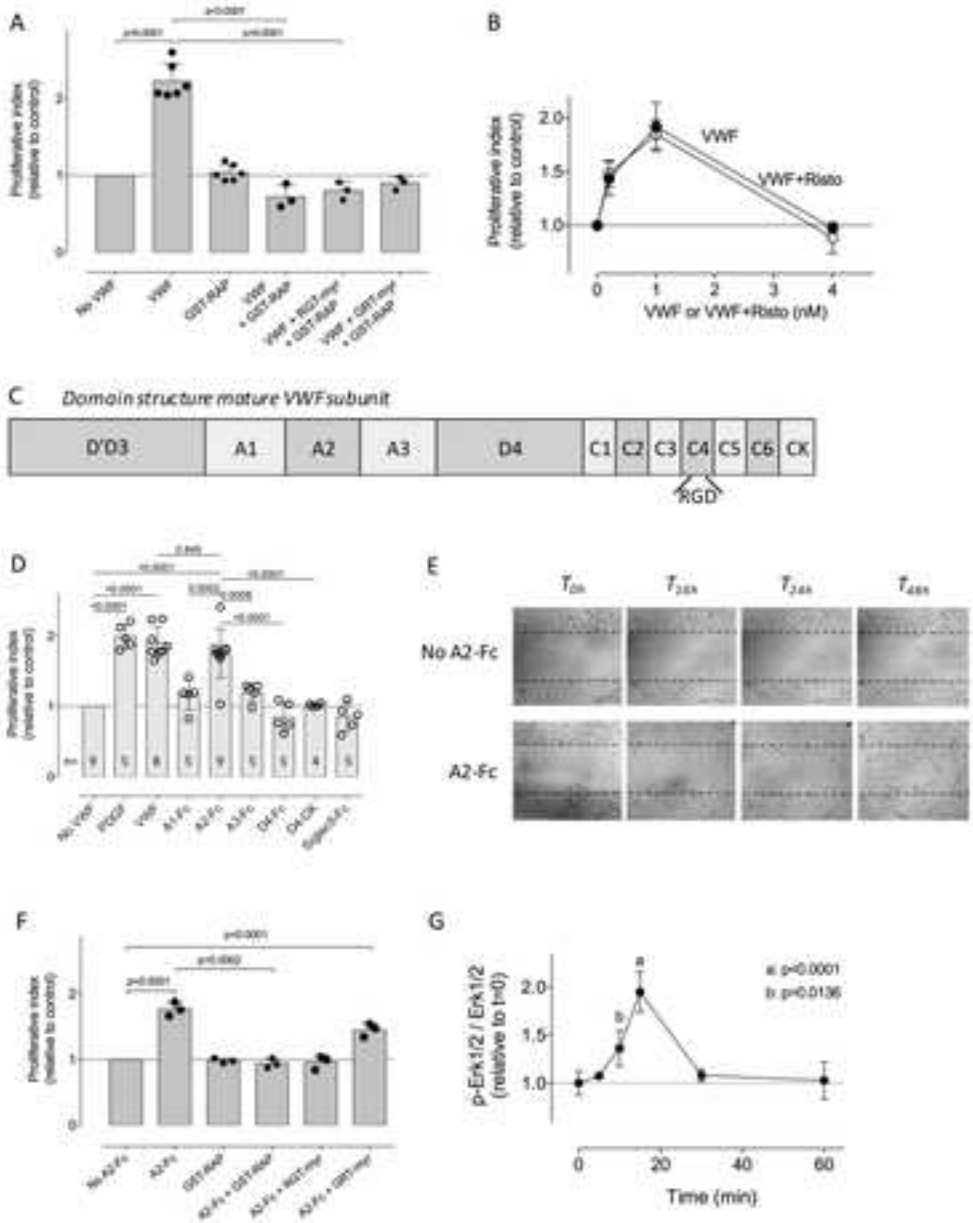

Figure 6

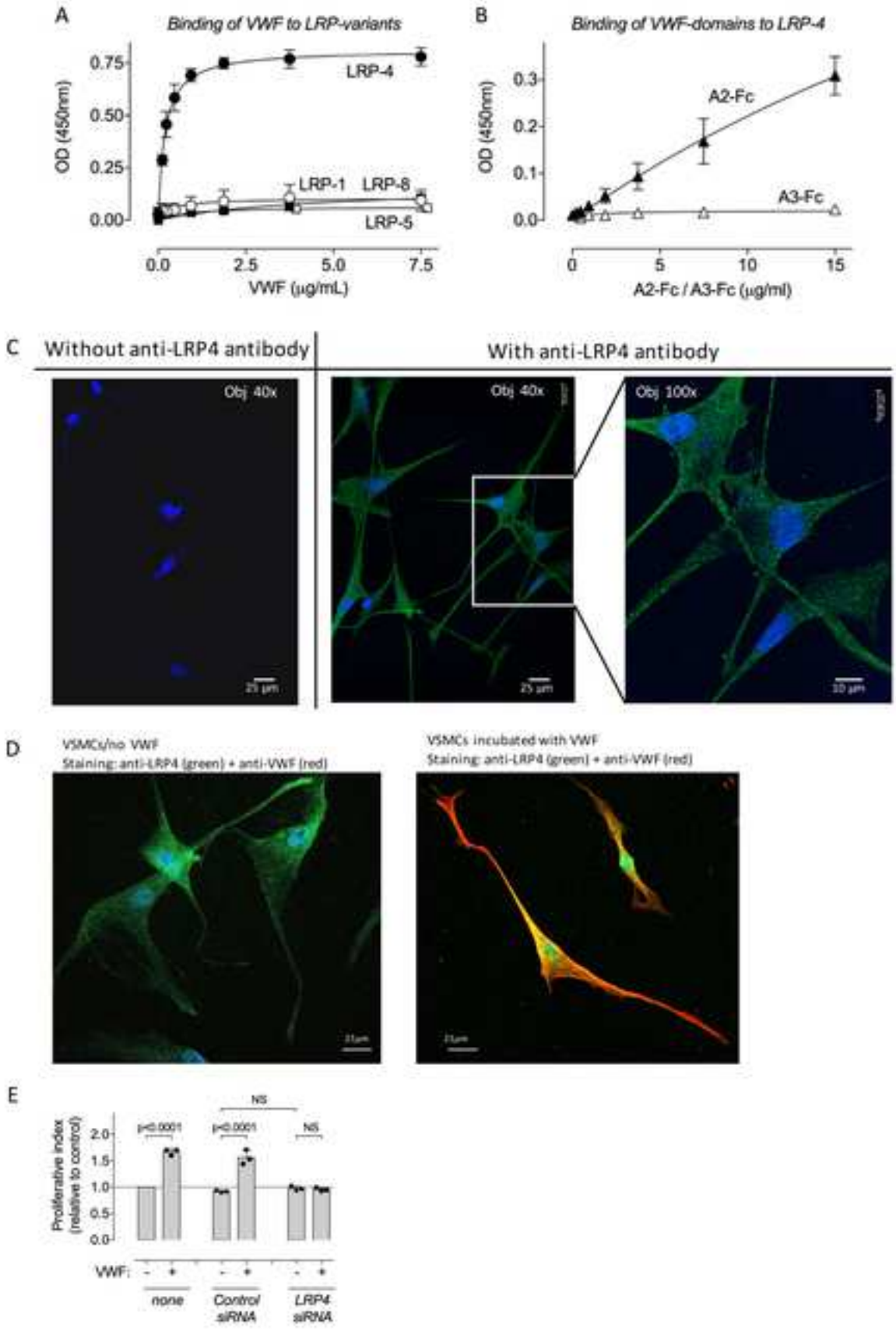

Figure 7

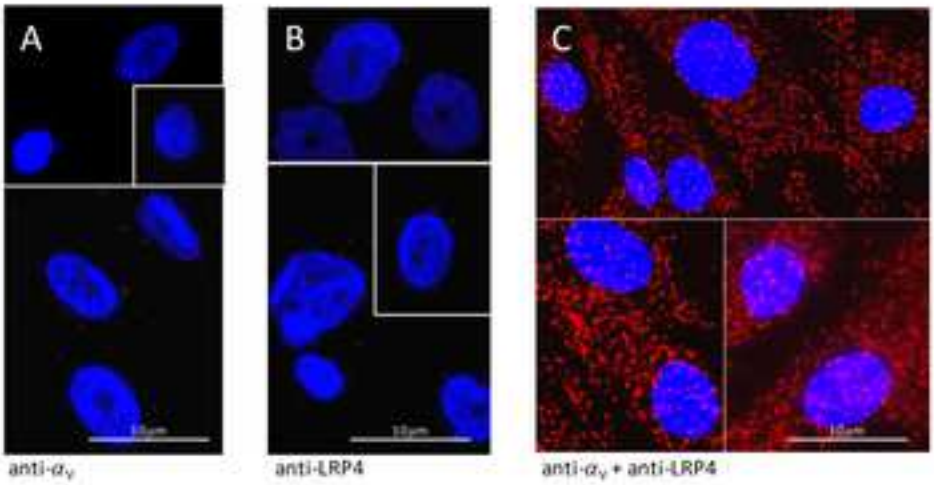

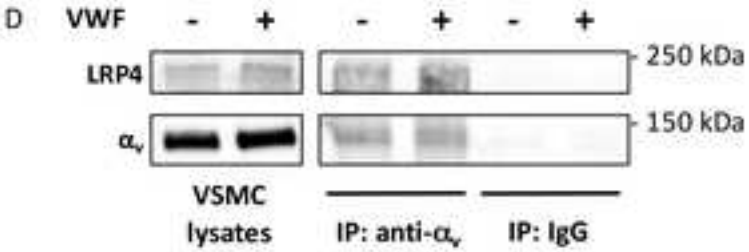

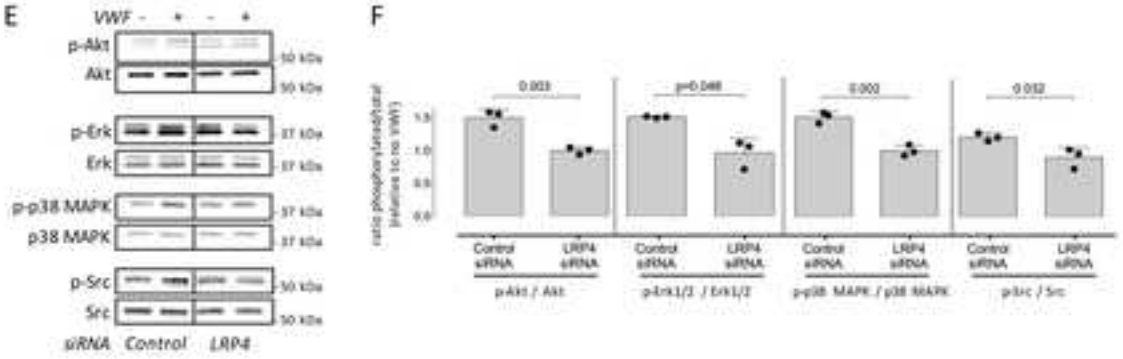

Graphical Abstract

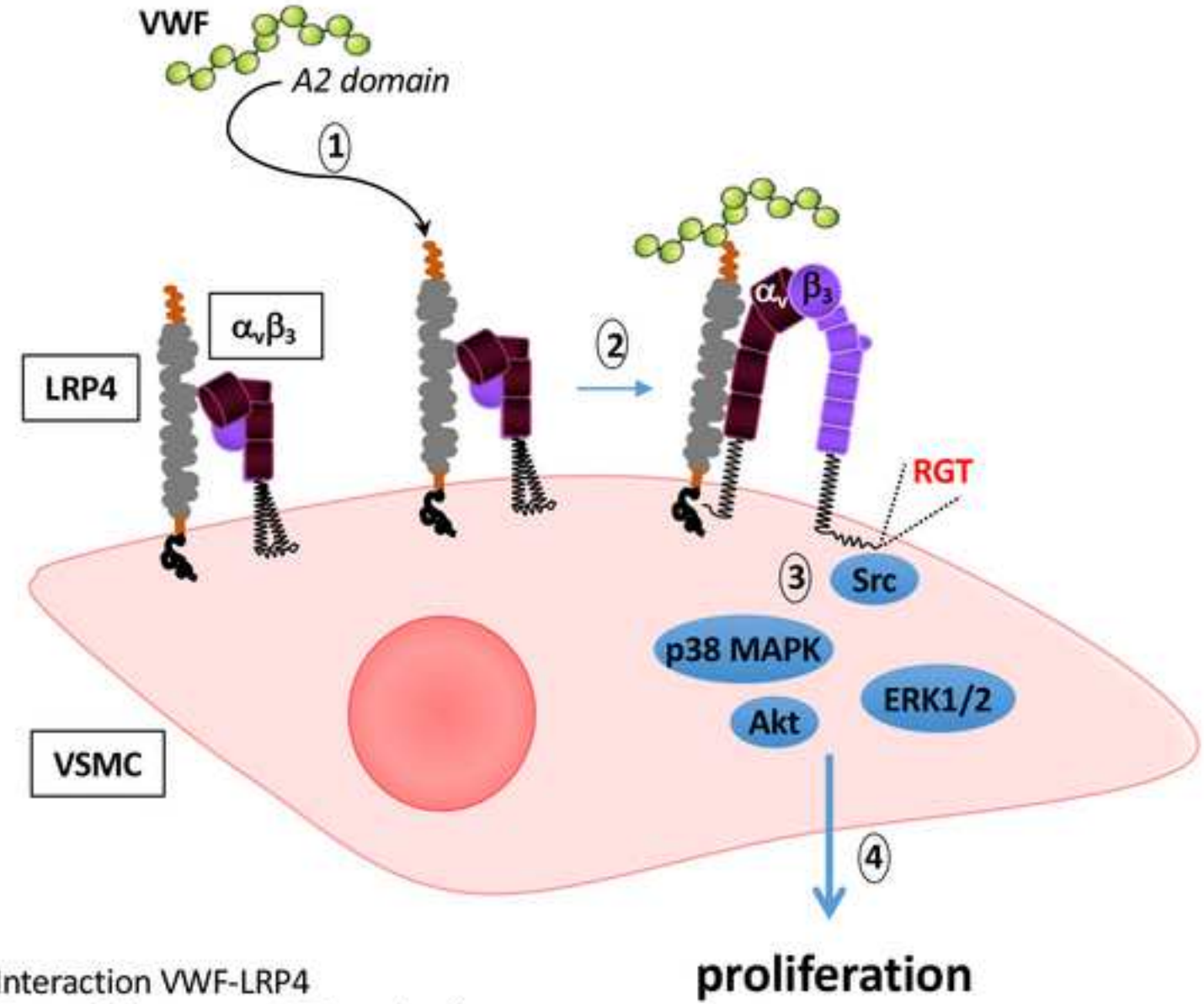

1- Interaction VWF-LRP4
2- Crosstalk between LRP4 and $\alpha_v\beta_3$
3- $\alpha_v\beta_3$-induced signaling via Src
4- VSMC proliferation